Optical studies of organized dye multilayers

Julian Guy Warren

Optical Studies of Organized Dye Multilayers

by

Julian Guy Warren

**A Thesis submitted in partial fulfilment
of the requirements for the degree of
Doctor of Philosophy**

Applied Physics

The University of Durham
1992

Let us go then, you and I,
When the evening is spread out against the sky
Like a patient etherised upon a table;
Let us go, through certain half deserted streets,
The muttering retreats
Of restless nights in one-night cheap hotels
And sawdust restaurants with oyster-shells:
Streets that follow like a tedious argument
Of insidious intent
To lead you to an overwhelming question ...
Oh, do not ask, 'What is it?'
Let us go and make our visit.

(From "The Love Song of J. Alfred Prufrock" by T.S. Eliot)

DECLARATION

I hereby declare that the work carried out in this thesis has not been previously submitted for any degree and is not currently being submitted in candidature for any other degree.

The work in this thesis was carried out by the candidate.

Abstract

The optical studies of organized dye multilayers constructed by the Langmuir-Blodgett technique are described. A number of different organic dye materials are examined; and some warrant special attention. They are S120 a cyanine, the squaraines and perylene. It is shown that these dyes form particularly well ordered films with unique optical properties. S120 forms J-aggregates, Sq1 and Sq3 both squaraines form hypsochromicaly shifted complexes (possibly H-aggregates) and Sq2 another squaraine exhibits band splitting (possibly Davydov). Fluorescence studies of perylene:tricosanoic acid films show that monomer and dimer species exist at room temperature, whilst at low temperature a third emitter is observed (excimer).

Structural studies of perylene:tricosanoic acid films reveal a high degree of order. From the isotherms and polarized absorption spectra it is seen that the molecules are on their edges, tilted with respect to the substrate. RHEED measurements confirm the high degree of structural order.

The dependence of surface plasmon resonance on the overlayers is demonstrated. The silver thickness and history are shown to be important in subsequent surface plasmon resonance measurements. An overlayer containing a dye with a sharp intense absorption band can interact with the surface plasmons to give anomalous dispersion (backbending). Only single backbending is observed for S120 and Sq1, indicating anisotropic films. Good agreement is found between S120 backbending and data reported in the literature.

Acknowledgements

I would like to take this opportunity to express my gratitude to all my friends and colleagues at the University of Durham who have assisted me during my period of study. Firstly, I wish to thank my supervisors Dr Mike Petty and Dr Jonathan Lloyd, for their inestimable help and encouragement and without whom this project would not have been possible.

I would like to thank the following for performing invaluable measurements; the late Dr Graham Russell for the RHEED, Dr Alexei Vithuknovsky and Dr Mike Sluch for the fluorescence spectroscopy and Dr Yuri Lvov for the low angle X-ray diffraction.

A number of pieces of equipment were specially built for this work and I would like to thank Mr Brian Blackburn and the mechanical workshop and Mr Peter Friend and the electronics workshop for always producing first class work. Thanks also for the technical support given by Mr Chris Pearson and Mr Norman Thompson. Special thanks to John Cresswell for disseminating his computing knowledge.

I gratefully acknowledge the financial support given to me by the SERC and Thorn EMI (Central Research Laboratories).

Lastly but not leastly I wish to thank my parents, inlaws, brother and sisters for suffering in silence and most especially my wife, Debbie, for her infinite patience and understanding.

Contents

Chapter I

Introduction

Considerable effort has been expended by the semiconductor industry in its short history to reduce device sizes; this may ultimately require the necessity for molecular scale fabrication. In addition, it has become apparent that organic materials possess properties which enable them to perform functions not possible with inorganic materials; two examples are liquid crystals and tunable dye lasers. They also show promise for some applications such as nonlinear optics and sensing. Sensing is probably the most important area, since, in order for computers to fully realize their potential, they must be able to collect their own data. It was with these thoughts in mind that this project was initiated.

Much work has been done on the properties of dyes in thin film form. The pioneering work in this area was performed by Kuhn[1] and Drexhage[2] who were particularly interested in energy transfer between dye systems. Kuhn and Drexhage utilized fatty acid monolayer assembly techniques to examine the distance dependence of energy transfer. More recently, Fromherz[3], Penner[4], and Leitner[5] have extended this work to include time-resolved fluorescence studies. Such systems provide important models for light-harvesting, photosynthetic processes and may form the basis for artificial molecular information-processing systems.

Recently, physical phenomena which are sensitive monitors of a system have been sought. The surface plasmon resonance (SPR) technique provides a very sensitive method for the investigation of overlayers. It has already been demonstrated by various workers that surface plasmon resonance might form the basis for several types of sensor for example: chemical; gas and bio-sensors[6,7].

An essential component of any sensor is a material whose properties change on exposure to the substance or stimulus to be measured. Since Langmuir-Blodgett (LB) films are composed of organic material they might form an analogue to biomolecular systems. The LB technique offers an elegant method for constructing

thin organic layers of known thickness, which have a unique order. The incorporation of dye chromophores enables oriented, precisely positioned assemblies to be engineered.

Although the SPR technique is very sensitive to changes in the surface conditions of an overlayer, it is non-specific, thus limiting its uses in the application of bio-sensing. In an attempt to overcome these difficulties a technique widely used in microbiology is adopted. The species to be detected is labelled with a chromophore and it is an interaction between the chromophore and the surface plasmon which is measured. Therefore combining the LB and SPR techniques provides us with a method for modelling the structure of a bio-sensor.

The materials used in this work are macrocyclic molecules: porphyrins and phthalocyanines, which are known to have high extinction coefficients, perylene, S120 a cyanine and three squaraine derivatives. Tricosanoic and 22-tricosenoic acids provide an environment for the chromophores.

This thesis reports the formation of novel dye multilayers and the interactions between dyes and surface plasmon polaritons (SPPs).

The principal aims of this project are summarized below:

1) To produce of thin organic dye layers on a variety of substrates.

2) To measure the optical properties of these layers.

3) To study the interactions between dye layers and surface plasmons.

Chapters 2 and 3 contain theory. Chapter 2 introduces the physics of surface plasmon resonance, its origins and production. The properties of organic dyes are discussed in Chapter 3. Particular attention is paid to the effects of aggregation on absorption and fluorescence. The experimental techniques used to produce, characterize and measure film properties are included in Chapter 4. The theory behind each technique is described briefly and then the specific experimental details used in the measurements are discussed. The optical and physical properties of the dye films are reported in Chapter 5. Comparisons are made between dyes in solution, cast films and LB films. The orientation of the chromophores is also investigated. Experimental results and data obtained from a model for surface

plasmon resonance studies are presented in Chapter 6. Finally the experimental results are summarized, suggestions are made for further work and conclusions are drawn in Chapter 7.

1.1 References

1. H. Kuhn *Classical Aspects of Energy Transfer in Molecular Systems* J.Chem. Vol 53 No 1 (1970) pp101-108

2. K. H. Drexhage in *Progress in Optics XII* E. Wolf ed. North-Holland Amsterdam (1974) pp165-232

3. P.Fromherz and G.Reinhold *Energy Transfer Between Fluorescent Dyes Spaced by Multilayers of Cadmium Salts of Fatty Acids* Thin Solid Films Vol 160 (1988) pp347-353

4. T.L.Penner *Energy Transfer between J-Aggregated Dye Monolayers* Thin Solid Films Vol 160 (1988) pp241-250

5. A.Leitner, M.E.Lippitsch, S.Draxler, M.Riegler and F.R.Aussenegg *Energy Transfer of Dyes in L-B Monolayers Studied by Picosecond Time-resolved Fluorimetry* Thin Solid Films Vol 132 (1985) pp55-62

6. B.Liedberg, C.Nylander and I.Lundström *Surface Plasmon Sensing for Gas Detection and Biosensing* Sensors and Actuators Vol 4 (1983) pp299-304

7. S.Baker *Phthalocyanine Langmuir-Blodgett Films and their Associated Devices* Ph.D. Thesis University of Durham (1985)

Chapter II

Surface Plasmons

2.1 Introduction

The object of this chapter is to introduce the physics of surface plasmons. The conditions for their existence are determined and the use of surface plasmon resonance as a sensitive measuring technique is considered. In section 2.2 the concepts of bulk plasma and dielectric function for a metal are defined. Plasmons are then investigated at an interface between two dielectric media and the surface modes that arise are discussed. The problems associated with surface plasmon excitation are explained in section 2.3 and various solutions are considered. One solution to these problems (introduction of a second interface) is described in both theory and practice. The sensitivity of surface plasmon resonance as a technique for detecting changes in surface conditions is demonstrated and the interaction between the surface plasmons and an absorbing layer, which gives rise to anomalous dispersion, is described. Some applications for which surface plasmon resonance has been utilized are outlined in section 2.5. Finally, in section 2.6, a summary is given.

2.2 Surface Plasmon Polaritons

2.2.1 Bulk plasma and dielectric function

The dielectric function of a metal can be modelled as an electron gas. The strong frequency dependence has a significant effect on the physical properties of the solid.

The dielectric function is dependent on frequency and wavevector, that is $\epsilon = \epsilon(\omega, k)$. Ignoring spatial dispersion, $\epsilon(\omega, 0)$ gives rise to the collective oscillations of the electron gas which are described as bulk plasmons. It should be noted that ϵ, of course, is a complex quantity.

The dielectric function is defined as follows

$$\mathbf{D} = \epsilon_0 \mathbf{E} + \mathbf{P} = \epsilon\epsilon_0 \mathbf{E} \tag{2.1}$$

where $\mathbf{D}$ is the dielectric displacement, $\mathbf{E}$ is the electric field, $\mathbf{P}$ is polarization, ϵ_0 is the permittivity of free space and ϵ is the relative permittivity.

The dielectric response $\epsilon(\omega, 0)$ or just $\epsilon(\omega)$ can be obtained from the equation of motion of an electron in an electric field (Kittel[1]).

$$m\frac{d^2x}{dt^2} = -e\mathbf{E} \tag{2.2}$$

where m is the mass of an electron, e is its charge, x is the distance moved by an electron, relative to fixed positive charge, in a field $\mathbf{E}$, where x and $\mathbf{E}$ have a time dependence $e^{-i\omega t}$. Differentiating with respect to t we obtain

$$x = \frac{eE}{m\omega^2} \tag{2.3}$$

the dipole moment, is defined as $p = \triangle q \triangle x$ where q is charge and x is distance. For one electron the dipole moment, relative to fixed positive charges, is

$$-ex = \frac{-e^2 E}{m\omega^2} \tag{2.4}$$

Polarization (dipole moment per unit vol) is given by

$$\mathbf{P} = -nex = \frac{-ne^2}{m\omega^2}\mathbf{E} \tag{2.5}$$

where n is electron concentration.

We now have

$$\epsilon(\omega) = \frac{\mathbf{D}(\omega)}{\epsilon_0 \mathbf{E}(\omega)} = 1 + \frac{\mathbf{P}(\omega)}{\epsilon_0 \mathbf{E}(\omega)} \tag{2.6}$$

and therefore

$$\epsilon(\omega) = 1 - \frac{ne^2}{m\omega^2\epsilon_0} \tag{2.7}$$

The plasma frequency ω_p is defined as the frequency where $\epsilon(\omega)$ is equal to zero. Hence

$$\omega_p^2 = \frac{ne^2}{\epsilon_0 m} \tag{2.8}$$

A plasma is a medium containing equal numbers of positive and negative charges, one of which is mobile. In a metal the negative charges are the free electrons and the positive charges are the ion cores.

We can rewrite the dielectric function in terms of the plasma frequency

$$\epsilon(\omega) = 1 - \frac{\omega_p^2}{\omega^2} \tag{2.9}$$

This is plotted in figure 2.1

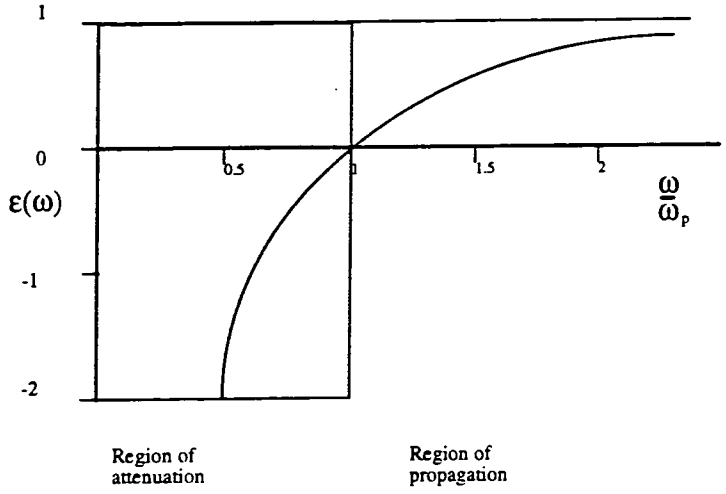

Figure 2.1 The dielectric function $\epsilon(\omega)$ of an electron gas versus the frequency, in units of plasma frequency.

By substituting suitable values for n into equation (2.8) we can obtain values for ω_p for Au and Ag (ω_p=1.3×10^{16} Hz) and for Al (ω_p=2.4×10^{16} Hz), which correspond to the ultra-violet part of the electromagnetic spectrum.

2.2.2 Excitations and polaritons

Many forms of electronic excitation exist in the solid state. Most of these decay rapidly and end in thermal excitation of the lattice. However, some are longer lived and these have been called elementary excitations.

Elementary excitations involving electrons include:

i) quasiparticles like screened electrons, Bloch electrons and polarons;

ii) plasmons, energy quanta of collective electron oscillations; and

iii) excitons (bound state between electron and a hole).

The coupled state formed between a photon and an elementary excitation is called a polariton. Therefore the interaction between a plasma and a photon is known as a plasmon polariton.

2.2.3 Plasmons at the surface (the single interface system)

Figure 2.2 shows the interface between two media of different dielectric constant ϵ_1 and ϵ_2 with z normal to the surface and x and y parallel. All waves are propagating in the z direction.

Only p-polarized fields will be considered, that is electromagnetic fields with a component of $\mathbf{E}$ incident in the (x,z) plane, because only electromagnetic fields with a component of $\mathbf{E}$ normal to the interface can produce surface charge polarization owing to the discontinuity of $\mathbf{E}_z$.

Therefore only the fields $\mathbf{E}_x, \mathbf{E}_z$ and $\mathbf{H}_y$ are of interest.

From Maxwell's equations

$$\nabla.\mathbf{D} = \nabla.(\epsilon\epsilon_0\mathbf{E}) = \epsilon\epsilon_0\nabla.\mathbf{E} = 0 \qquad 2.10$$

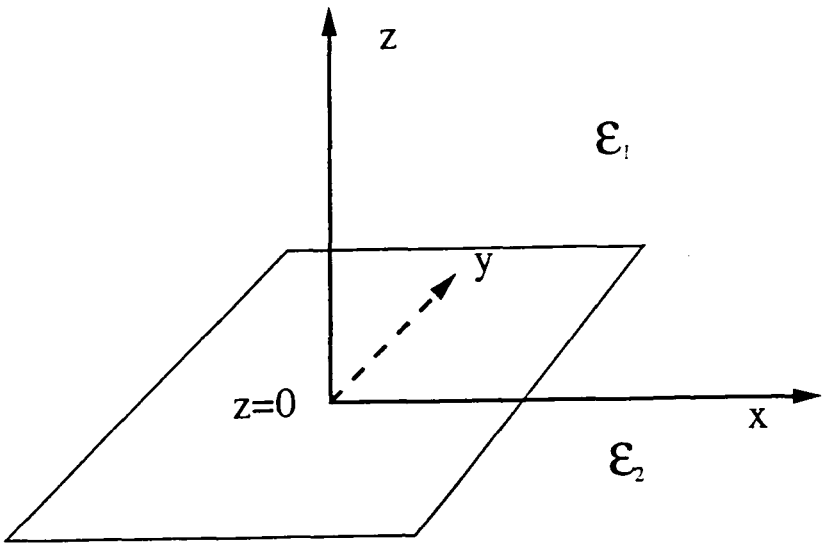

Figure 2.2 The interface at z=0 between two media with different dielectric functions ϵ_1 and ϵ_2. Where z is normal and x and y are parallel to the interfaces.

$$\nabla.\mathbf{B} = \nabla.(\mu\mathbf{H}) = \mu\nabla.\mathbf{H} = 0 \qquad 2.11$$

$$\nabla \times \mathbf{E} = -\frac{\partial \mathbf{B}}{\partial t} = -\mu\frac{\partial \mathbf{H}}{\partial t} \qquad 2.12$$

$$\nabla \times \mathbf{H} = \frac{\partial \mathbf{D}}{\partial t} = \epsilon\epsilon_0\frac{\partial \mathbf{E}}{\partial t} \qquad 2.13$$

The plane wave equation in a nonmagnetic, homogeneous and isotropic dielectric can now be derived.

$$\frac{\partial^2 \mathbf{E}}{\partial z^2} - \mu\epsilon\epsilon_0\frac{\partial^2 \mathbf{E}}{\partial t^2} = 0 \qquad 2.14$$

Assuming a solution of the form

$$\mathbf{E} = \mathbf{E}_1 e^{i(k_x x - \omega t)} e^{ik_z z} \qquad 2.15$$

Substituting (2.15) into equation (2.14) gives

$$k_z = \sqrt{\mu\epsilon\omega^2 - k_x^2} \qquad 2.16$$

From Maxwell's equation a relationship between E_x and H_y can be obtained.

$$H_y = -\epsilon \int \frac{\partial E_x}{\partial t} \partial z \qquad 2.17$$

Assuming that the fields of interest have a phase and time dependence $e^{i(k_x x - \omega t)}$ and are travelling in the z direction, an equation for the electric field $\mathbf{E}$ can be formed and then by using the relationship equation (2.17) an equation for the magnetic field $\mathbf{H}$ can be obtained.

The fields can be written as follows

In medium 1 where $z > 0$

$$\mathbf{E_1} = E_1\left(\frac{k_{z1}}{\sqrt{\epsilon_1}\frac{\omega}{c}}, 0, \frac{k}{\sqrt{\epsilon_1}\frac{\omega}{c}}\right) e^{i(kx-\omega t)} e^{ik_{z1}z} \qquad 2.18a$$

$$\mathbf{H_1} = E_1(0, -\sqrt{\epsilon_1}, 0) e^{i(kx-\omega t)} e^{ik_{z1}z} \qquad 2.18b$$

$$k_{z1} = \pm\sqrt{\epsilon_1 \frac{\omega^2}{c^2} - k^2} \qquad 2.18c$$

In medium 2 where $z < 0$

$$\mathbf{E_2} = E_2\left(-\frac{k_{z2}}{\sqrt{\epsilon_2}\frac{\omega}{c}}, 0, \frac{k}{\sqrt{\epsilon_2}\frac{\omega}{c}}\right) e^{i(kx-\omega t)} e^{-ik_{z2}z} \qquad 2.19a$$

$$\mathbf{H_2} = E_2(0, -\sqrt{\epsilon_2}, 0) e^{i(kx-\omega t)} e^{-ik_{z2}z} \qquad 2.19b$$

$$k_{z2} = \pm\sqrt{\epsilon_2 \frac{\omega^2}{c^2} - k^2} \qquad 2.19c$$

Satisfying the boundary conditions at $z = 0$ that the tangential components of $\mathbf{E}$ and $\mathbf{H}$ are continuous, we have $E_{x2} = E_{x1}$ and $H_{y2} = H_{y1}$

two simultaneous equations can be formed

$$-\frac{k_{z1}}{\sqrt{\epsilon_1}\frac{\omega}{c}}E_1 - \frac{k_{z2}}{\sqrt{\epsilon_2}\frac{\omega}{c}}E_2 = 0 \qquad 2.20a$$

and

$$-\sqrt{\epsilon_1}\mathbf{E}_1 + \sqrt{\epsilon_2}\mathbf{E}_2 = 0 \qquad 2.20b$$

The nontrivial solution of these equations is

$$\frac{\epsilon_2}{\epsilon_1} = -\frac{k_{z2}}{k_{z1}} \qquad 2.21$$

Substituting values for k_{z1} and k_{z2} a familiar dispersion relationship for surface plasmons is obtained.

$$k = \frac{\omega}{c}\sqrt{\frac{\epsilon_2\epsilon_1}{\epsilon_2 + \epsilon_1}} \qquad 2.22$$

2.2.4 Radiative and non-radiative modes

Raether[4] referred to the surface modes as either radiative or non-radiative. Taking the dispersion equation 2.22, if damping is included ϵ_2 and ϵ_1 can become complex, which means that k and ω must also be treated as complex quantities.

$\epsilon_2 = \epsilon_2' + i\epsilon_2''$ and $\epsilon_1 = \epsilon_1' + i\epsilon_1''$

Roots of the equation must be chosen such that (on insertion into field equations (2.18) and (2.19)) they do not produce fields that increase with time or in the direction of propagation.

Let $\epsilon_2 > \epsilon_1$

If ϵ_1 is assumed to be real and positive ($\epsilon_1'' = 0$) and ϵ_2 is also real and positive (corresponding to a lossless dielectric/dielectric interface) then the roots k_{1z} and k_{2z} are real and positive. The resulting radiative surface waves correspond to the Brewster mode.

With ϵ_2 negative and real (lossless dielectric/metal interface) the roots of the equation k_{1z} and k_{2z} are imaginary. The waves decay exponentially away from the interface, this is the non-radiative surface mode called the Fano mode.

A real surface active medium will have a complex dielectric constant. When $\epsilon_2'' \neq 0$ k_{2z} and k_{1z} become complex and waves decay exponentially perpendicular to the interface, k_x is also complex. The wave is therefore bound to the surface and decays as it propagates along the interface, this is called the 'Lossy Fano' mode which is the surface plasmon polariton (SPP). In this case ϵ_2 is the surface active medium and ϵ_1 is the surface inactive medium. The dispersion curves for the Brewster and Fano modes are plotted in figure 2.3.

2.3 Excitation of Non-Radiative Surface Plasmons

2.3.1 Matching momentum (the slow photon)

As mentioned earlier there are two branches of the SPP dispersion curve, the radiative and the non-radiative modes. Direct excitation of the non-radiative (Fano) mode by light on a smooth surface is not possible. However, SPP's can be excited on a statistically rough surface or a metal coated grating with light at grazing incidence, and in thin Al-foils by electron energy loss. It is clear that, on inspection of the dispersion curve (figure 2.3) for a given ω, the component of the light wavevector parallel to the surface will always be smaller than the parallel component k of the SPP wavevector. The conditions for energy (ω) and wavevector (k) conservation cannot be simultaneously satisfied, therefore no coupling occurs. The coupling conditions can also be described in terms of phase velocity; the phase velocity v_{ph} is always smaller than that of light. Otto[2] suggested that a slow photon was required for coupling.

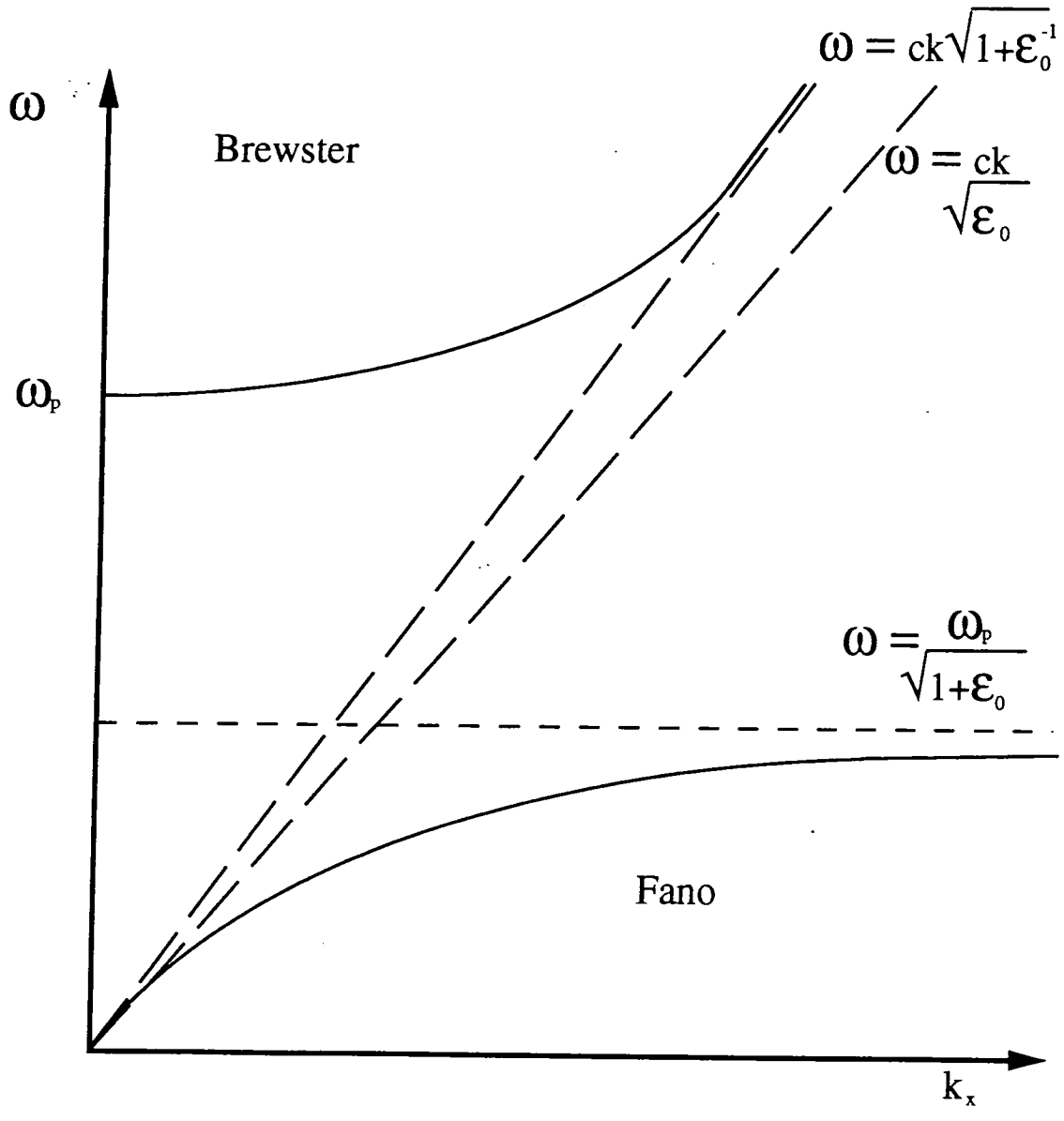

Figure 2.3 The dispersion curve, frequency (ω) versus wavevector (k_x), for electromagnetic waves at a single interface.

2.3.2 Introducing a second interface

The problem of SPP excitation is overcome by the introduction of a second interface (figure 2.4). If a medium with ϵ_3 is introduced at $z = d$ the equations for the electromagnetic fields H_y and E_x in each medium can be written. By including the boundary conditions a more complex dispersion relationship for the system can be produced (Welford[3]).

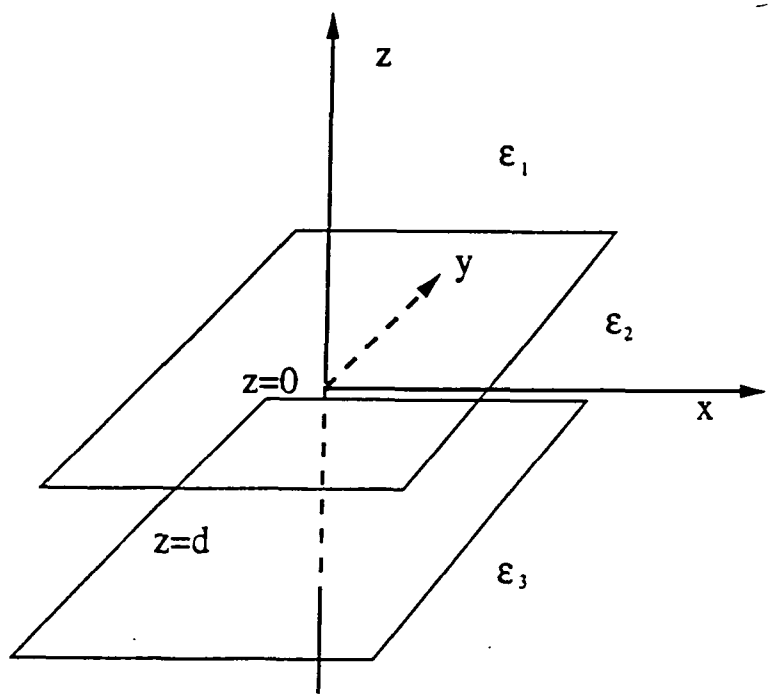

Figure 2.4 The two interface system with a second interface at z=d between media with dielectric functions ϵ_2 and ϵ_3.

$$\frac{\epsilon_3 k_{2z}}{\epsilon_2 k_{3z}} + \frac{(\epsilon_2 k_{1z} + \epsilon_1 k_{2z}) + e^{(2ik_{2z}d)}(\epsilon_1 k_{2z} - \epsilon_2 k_{1z})}{(\epsilon_2 k_{1z} + \epsilon_1 k_{2z}) - e^{(2ik_{2z}d)}(\epsilon_1 k_{2z} - \epsilon_2 k_{1z})} = 0 \qquad 2.23$$

If ϵ_2 is a free electron metal and ϵ_1 and ϵ_3 are real and positive and $\epsilon_1 > \epsilon_3$, the dispersion relationship can be plotted (figure 2.5). There are two branches of the dispersion curve, one for each interface. The light lines $\omega = ck/\sqrt{\epsilon_1}$ and $\omega = ck/\sqrt{\epsilon_3}$ are drawn for media 1 and 3. As k_x tends to 0 these become the asymptotic gradients. They show the maximum k_x for an incident photon travelling parallel to the surface with frequency ω.

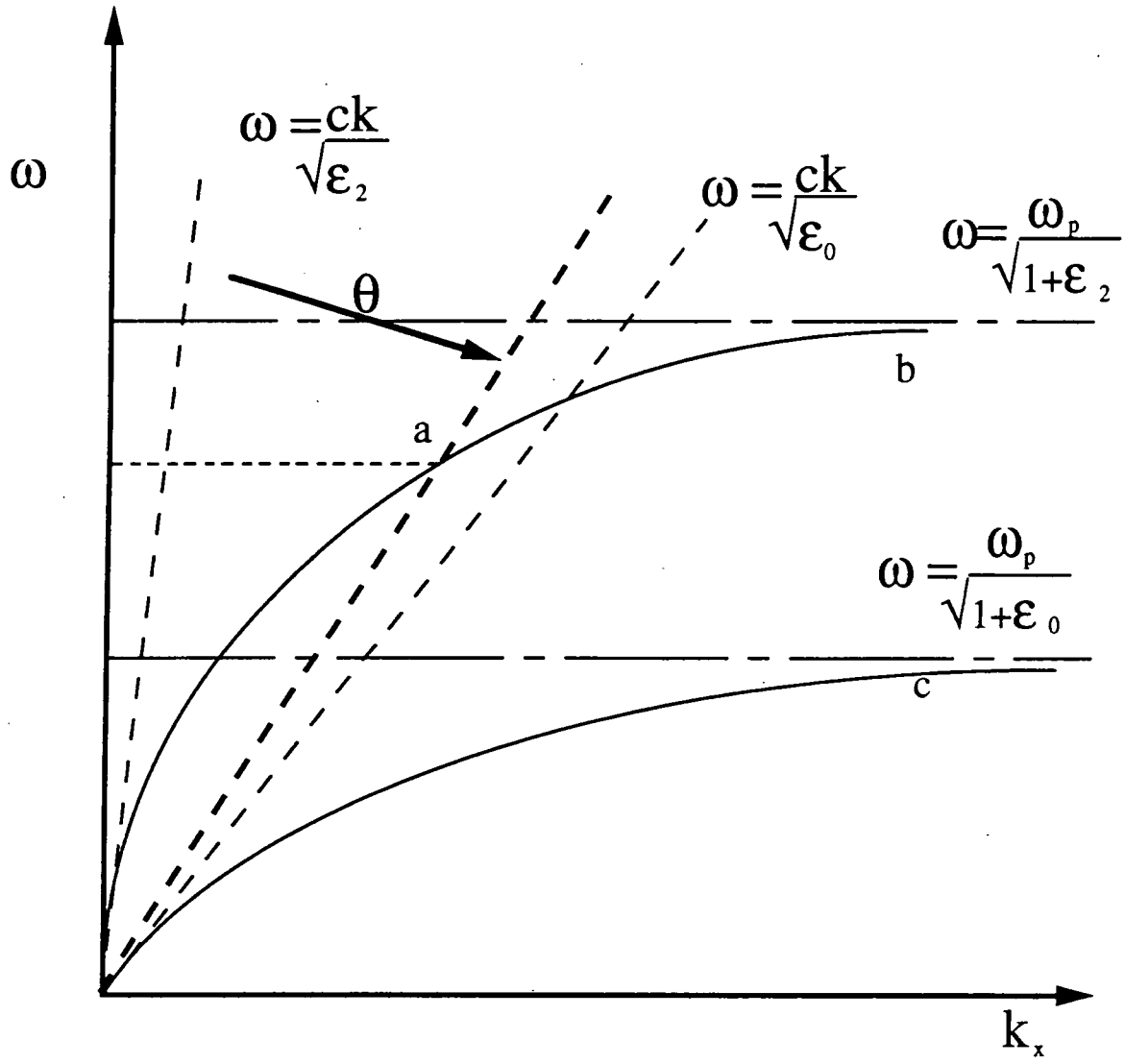

Figure 2.5 The dispersion curves for the two interface system.

Looking at the form of k_{jz} at points b and c of the dispersion curves which both lie in a region where $k_x > \omega\sqrt{\epsilon_1}/c$, The following are obtained

$$k_{1z} = \sqrt{\epsilon_1 \mu_0 \omega^2 - k_x^2} \qquad 2.24a)$$

which is imaginary

$$k_{2z} = \sqrt{\epsilon_2 \mu_0 \omega^2 - k_x^2} \qquad 2.24b)$$

which is imaginary and

$$k_{2z} = \sqrt{\epsilon_3 \mu_0 \omega^2 - k_x^2} \qquad 2.24c)$$

which is also imaginary

These are clearly non-radiative modes which represent coupled Fano modes one at each metal/dielectric boundary.

In the region a (where $\frac{\omega}{c}\sqrt{\epsilon_3} < k_x < \frac{\omega}{c}\sqrt{\epsilon_1}$) k_{2z} and k_{3z} are imaginary and k_{1z} is real. Therefore a photon incident in medium 0 with the correct wavevector can couple into surface plasmon modes at the metal(medium 2)/dielectric(medium 3) interface. At a fixed frequency ω, the wavevector of light parallel to the surface can be made to match that of the surface plasmon by varying the angle of incidence θ. This case is illustrated on the dispersion figure where $\omega = ck/\sqrt{\epsilon_1}\sin\theta$ crosses the curve at a. If the medium 1 is a glass prism and medium 3 is air then as θ increases $k_x > \omega\sqrt{\epsilon_3}/c$ the critical angle is exceeded. Coupling to SPP described by curve a only occurs beyond the critical angle.

2.3.3 Prism coupling (attenuated total internal reflection)

When light is totally internally reflected inside a prism, an evanescent field penetrates approximately an optical wavelength into the air.

Otto[2] (figure 2.6a) brought a silver surface close to a prism base and used the evanescent field to couple p-polarized light into SPP's at the silver surface. Light is totally internally reflected from the prism unless the wavevector parallel to the

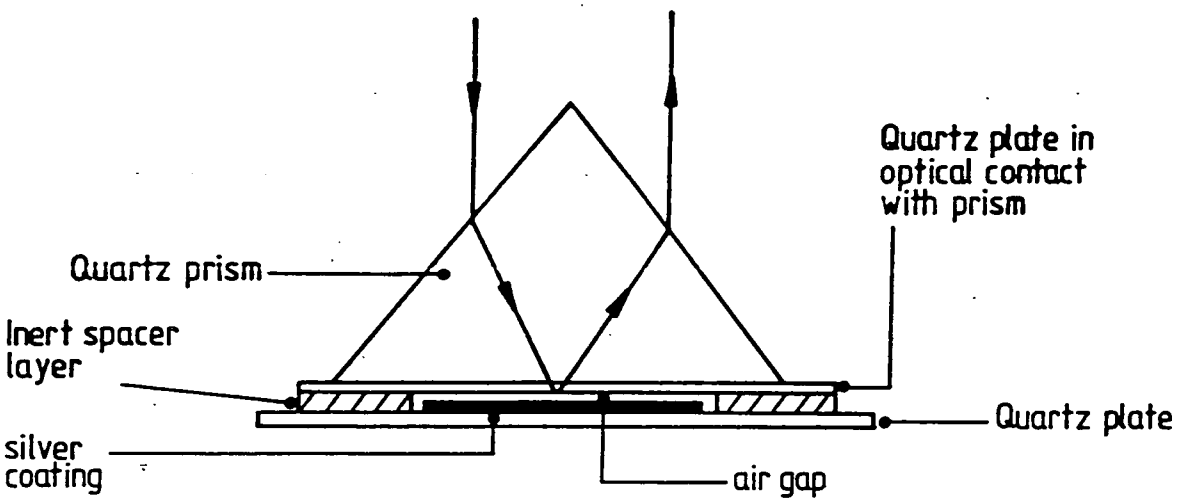

The Otto configuration for SPP excitation

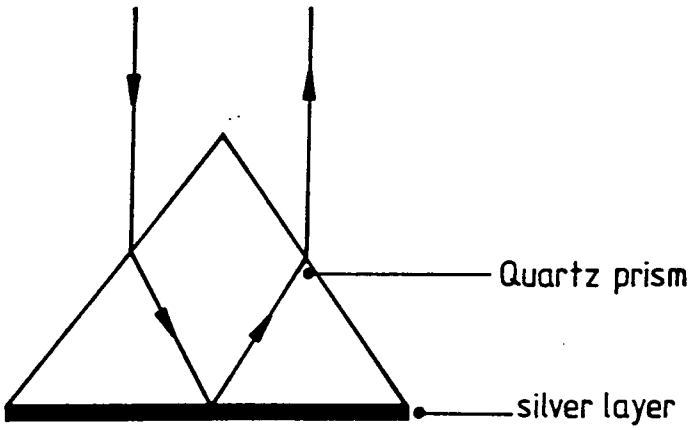

The Kretschman arrangement for SPP excitation

Figure 2.6 a) The Otto and b) the Kretschmann and Raether prism configuration for attenuated total reflection coupling.

surface matches the SPP wavevector. This parallel wavevector can be varied in two ways: by varying the angle of incidence at constant frequency or by fixing the angle and varying the wavelength.

The Otto method has several problems associated with it. There is a difficulty in matching the surfaces closely enough and a method for spacing the silver from the prism surface is required. Kretschmann and Raether[17] (figure 2.6b) overcame these difficulties by evaporating the silver directly onto the prism base. The evanescent field couples through the silver and the SPPs are excited at the silver/air interface.

2.4 Surface Plasmons as Probes of the Surface

2.4.1 Field enhancement

Field enhancements of over 100 times can be achieved close to the surface. Figure 2.7 shows a plot of the Poynting vector against distance through the system at the point of resonance. The incident field is so small that it is not visible, the transmitted field can be seen to decay within a few microns of the surface.

2.4.2 Sensitivity to overlayers

Resonance only occurs when both ω and k satisfy the SPP dispersion relationship. If the dispersion relation is modified by changing superficial conditions, the excitation does not occur for the same values of ω and k.

If there is a transition layer between ϵ_0 and ϵ_2 which is homogeneous, isotropic and has a thickness d_f with a dielectric function $\epsilon_f = \epsilon_f' + i\epsilon_f''$, then the dispersion relationship can be written (Abeles and Lopez-Rios [5])

$$Z_0 + Z_2 = -i(\frac{\omega}{c})d_f[Z_0 Z_2(1 - \frac{S^2}{\epsilon_f}) + \epsilon_f] \qquad 2.25$$

where

$$Z_0 = \frac{\epsilon}{\sqrt{\epsilon - S^2}} \qquad and \qquad Z_2 = \frac{\epsilon_2}{\sqrt{\epsilon_2 - S^2}}$$

Z_0 and Z_2 are optical admittances.

Figure 2.7 The field distribution (Poynting Vector) through the glass silver, silver air interfaces (after Welford).

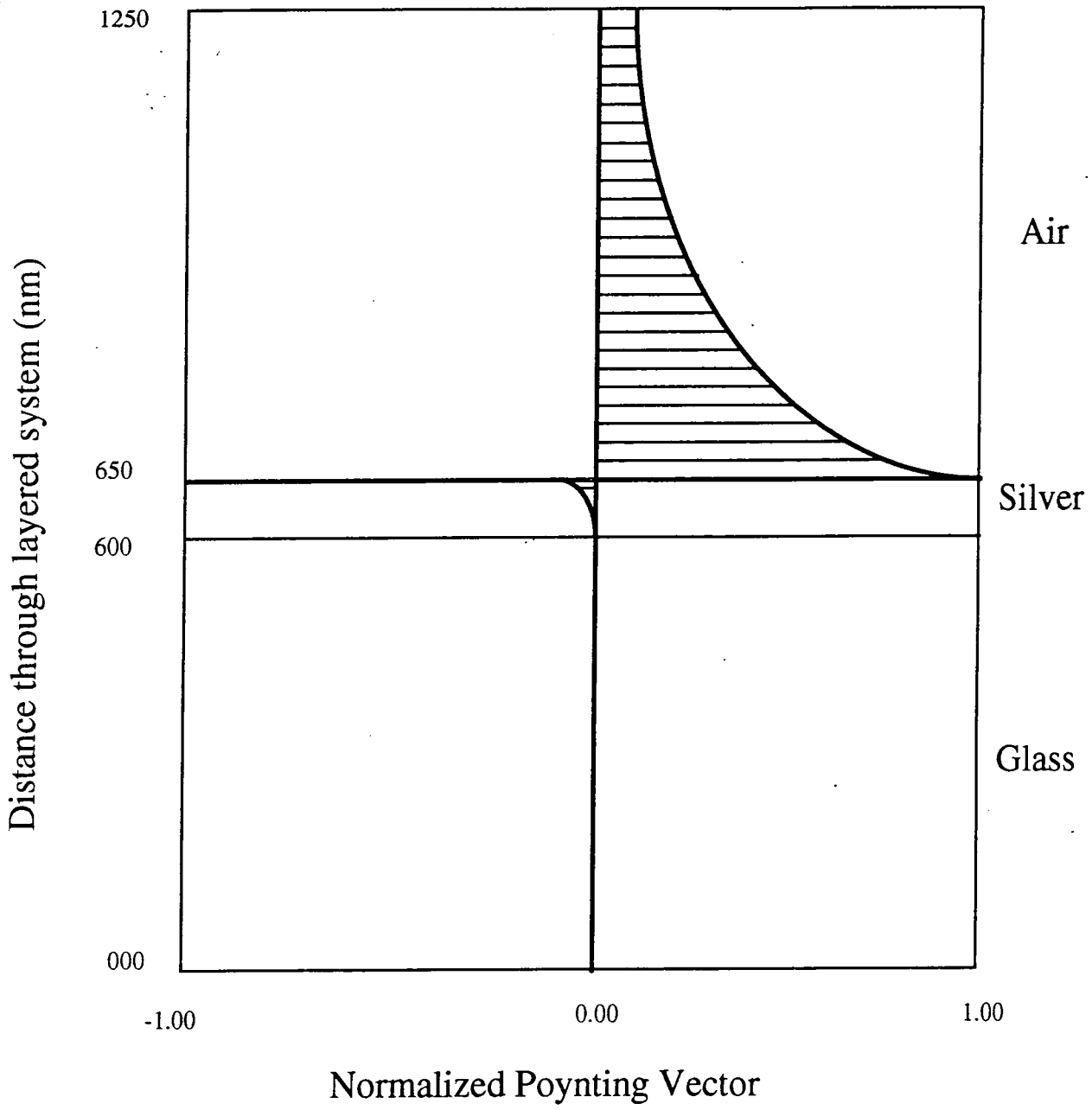

and

$$S^2 = \frac{\epsilon_0 \epsilon_2}{\epsilon_0 + \epsilon_2}$$

S is known as the reduced wavevector.

If ω is constant

$$\partial S = \partial S^r + i\partial S^i = \frac{\sqrt{-\epsilon_0\epsilon_2}}{-\epsilon_2 + \epsilon_0} S^2 \frac{(\epsilon_f - \epsilon_2)(\epsilon_0 - \epsilon_f)}{\epsilon_f(\epsilon_0 + \epsilon_2)} \frac{2\pi}{\lambda} d_f \qquad 2.26$$

It is immediately clear that ∂S is proportional to thickness. If $\epsilon_f = \epsilon_2$ or $\epsilon_f = \epsilon_0$ then $\partial S = 0$

For a highly reflecting substrate the imaginary part of ∂S is strongly related to the absorption of the surface layer. Both broadening and shifting of the resonance curves may be observed for overlayers. The shift in resonance is given by ∂S^r and the broadening by ∂S^i. A change in resonance depth is sometimes seen and this can be related to the absorption of the overlayer ϵ_f^i.

For fixed S and frequency independent ϵ_0

$$\partial\omega = \partial\omega^r - i\partial\omega^i = \frac{2\epsilon_2^2(\epsilon_0 + \epsilon_2 - \epsilon_0\epsilon_2/\epsilon_f - \epsilon_f)}{\sqrt{-(\epsilon_0 + \epsilon_2)}(\epsilon_2 - \epsilon_0)(\partial\epsilon_2/\partial\omega)} \frac{2\pi d_f}{\lambda} \qquad 2.27$$

Again $\partial\omega$ is proportional to d_f and $\partial\omega = 0$ when either $\epsilon_f = \epsilon_0$ or $\epsilon_f = \epsilon_2$

2.4.3 Anomalous dispersion (backbending)

Small changes in the overlayer can affect the characteristics of SPP propagation; this was demonstrated earlier. The SPPs are particularly sensitive to the dielectric constant of the film ϵ_f. A singularity arises when the ϵ_f becomes either infinitely large or small. These two cases can occur for two different frequencies in ionic crystals.

$$\epsilon_f = \epsilon_\infty \frac{(\omega_{LO}^2 - \omega^2)}{(\omega_{TO}^2 - \omega^2)} \qquad 2.28$$

ω_{LO} and ω_{TO} being longitudinal and transverse vibrational frequencies. The reflectivity has singularities for $\omega = \omega_{TO}$ and $\omega = \omega_{LO}$. The latter condition ($\epsilon_f = 0$) also occurs in a free-electron metal at the plasma frequency ω_p.

The interactions between absorbing layers (transition layers) and a surface active layer which can support an electromagnetic surface wave (surface plasmon) have been categorized by Agranovich[10] as either quenched or resonance in nature. A resonance type interaction involves a thin absorbing layer on a surface active material which has a narrow absorption band in the frequency range of the surface plasmon. Quenching involves two surface active materials, one of which is a very thin film where absorption occurs over a wide frequency range. This corresponds to a metal covered by a nanometer thick film of a different metal.

As noted in 2.3.3 surface plasmons can be excited in two ways using the ATR method: either the angle can be fixed and the wavelength varied, or the wavelength fixed and the angle varied. If there is no damping in the superficial layer then the dispersion relationship is the same for both methods and the curve breaks into two branches (figure 2.8a). The modes decouple and tend towards the surface electromagnetic excitations at the two interfaces. However, if damping is present the Brewster and Fano modes are mixed to form a continuous curve (figure 2.8b); this is referred to as anomalous dispersion or 'backbending', allowing the waves to propagate in the forbidden region. In the case of a metal interfacial layer, the backbending and gap in the dispersion curve occurs at the plasmon frequency ω_p (Abeles and Lopez-Rios[5-7]).

Pockrand et al[8,9] studied the resonance type interaction using organic dye layers which have narrow absorption bands. They found that splitting could occur at one or two exciton frequencies depending on the orientation of the dye. For dye transition dipole moments parallel to the surface splitting occured at ω_T and for perpendicular orientation it occurs at ω_L. If the material is isotropic splitting occurs at both frequencies.

2.5 Applications

The large field enhancements and sensitivity to changes in the surface conditions has made the SPR technique of great interest for sensing and the measurement

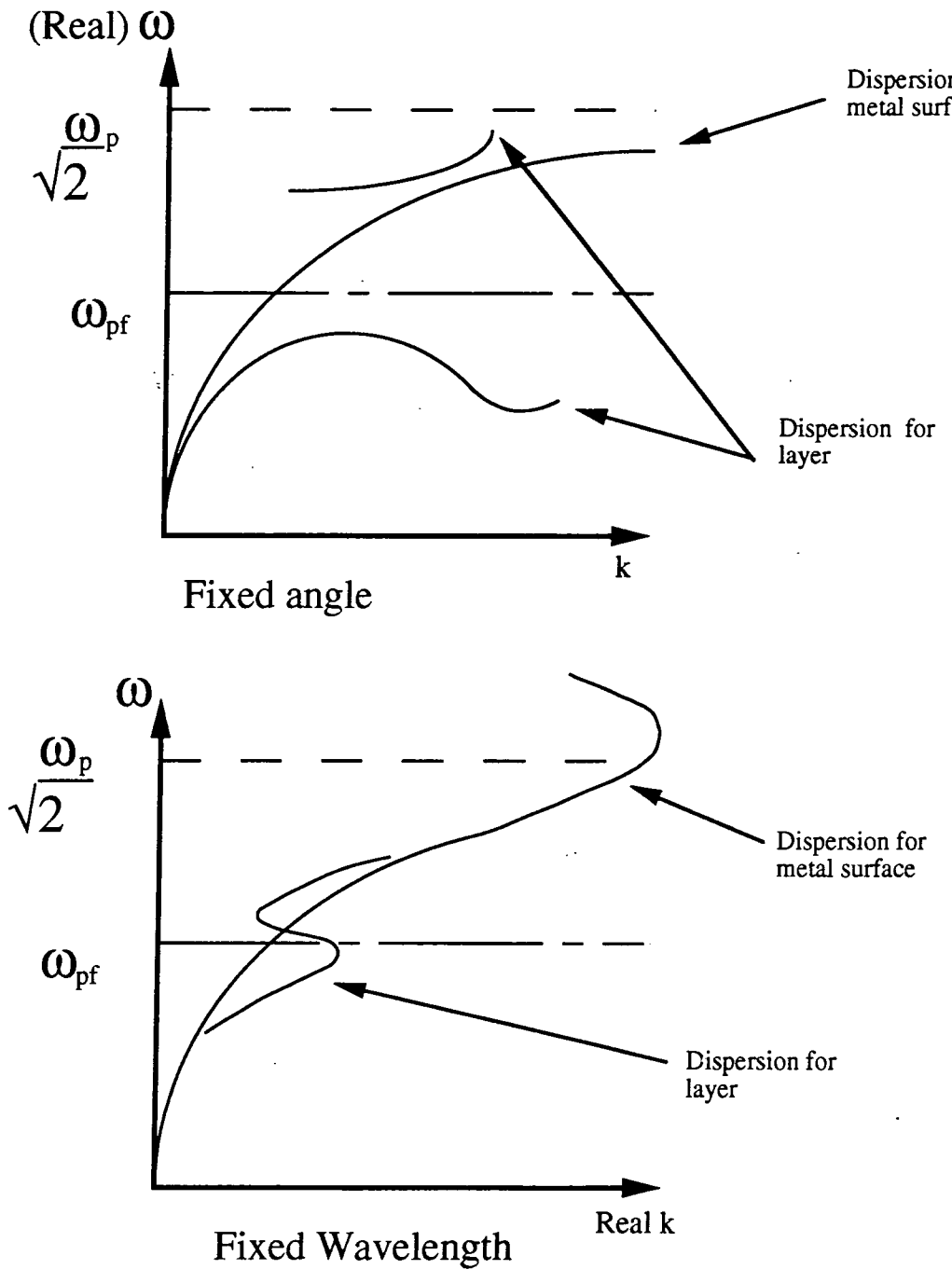

Figure 2.8 Anomalous dispersion curves. a) fixed angle variable wavelength scan b) fixed wavelength variable angle scan (after Abeles and Lopez-Rios).

of thin film parameters.

The dependence of the ω_p on the charge carrier density has been utilized by Evans and Hall[11] to construct a modulator using a silicon Schottky diode with a surface grating formed in the epitaxial layer prior to the evaporation of a silver film. Surface plasmons generated by light of λ=1.3μm exist at the silver/air interface and the silver/silicon interface. The latter are strongly perturbed by the carrier density in the epitaxial layer causing a shift in the resonance angle.

The sensitivity of the surface plasmon resonance to changes in overlayer permittivity have been exploited by Liedberg et al[12] as the basis of gas detection and biosensing. These workers showed that if a thin film of gas-absorbing organic material was deposited onto a silver film, small changes in the refractive index of the organic material on the absorption of gas could be detected by a shift in angle of the surface plasmon resonance. They also demonstrated that surface plasmon resonance measurements could be made at the metal/water interface. This enabled them to measure antibodies forming a single monolayer on the silver surface from a solution. The introduction of an antigen resulted in antigen-antibody binding which could be detected by SPR. The relationship between the overlayer permittivity and the resonance conditions enabled Pockrand et al[16] to determine the optical properties of dye layers. They referred to this technique as surface plasmon spectroscopy. This technique was extended by Cross et al[15] to measure the linear Pockels effect by modulating the dielectric properties of a thin film through the application of a perpendicular electric field and detecting changes in the coupling angle for SPP excitation. This method may be used to quantify the second order nonlinear properties of organic films.

It is possible to image the surface of a patterned film deposited onto the silver film in an SPR arrangement if the sample is illuminated over a large area with an expanded laser beam. Yeatman et al[13] and Rothenhäusler et al[14] have demonstrated that this might form the basis of surface plasmon microscopy.

2.6 Summary

The origins of bulk plasma in a semi-infinite medium have been outlined and the special situation at the boundary of a different medium has been investigated

in detail. These provided the conditions for the non-radiative surface modes or surface plasmon polaritons. The difficulties associated with the generation of these modes have been described and the practical solutions were presented, particularly the prism coupling method which is the simplest experimentally. The sensitivity of surface plasmon resonance to surface conditions has been shown and the special case of anomalous dispersion was expanded on. Finally a few of the applications for SPR have been described.

2.7 References

1. C.Kittel *Introduction to Solid State Physics* Wiley New York

2. A. Otto *Excitation of Nonradiative Surface Plasma Waves in Silver by the Method of Frustrated Total Reflection* Zeitschrift für Physik Vol 216 (1968) pp398-410

3. K. Welford in *Surface Plasmon Polaritons* IOP Short Meetings Series No 9

4. H. Raether *Surface Plasma Oscillations and their Applications* in G. Hass, M. Francombe and R. Hoffman (Eds) Physics of Thin Films (Academic Press New York 1977) Vol 9 pp145-261

5. F. Abeles and T. Lopez-Rios *Surface Polaritons at Metal Surfaces and Interfaces* in V.M. Agranovich and D.L. Mills (Eds) Surface Polaritons pp239-274

6. T. Lopez-Rios *Modification of the Dispersion Relations for Surface Plasmons by Very Thin Surface Films in the Vicinity of their Plasma Frequency* Optics Communications Vol 17 pp342-345

7. T. Lopez-Rios, F. Abeles and G. Vuye *Splitting of the Al Surface Plasmon Dispersion Curves by Ag Surface Layers* Le Journal Physique Vol 39 (1978) pp645-650

8. I. Pockrand, J.D. Swalen, J.G. Gordon and M.R. Philpott *Exciton-Surface Plasmon Interactions* J.Chem.Phys. Vol 70 (1979) pp3401-3408

9. I. Pockrand, A. Brillante and D. Möbius *Exciton-Surface Plasmon Coupling: An Experimental Investigation* J.Chem.Phys. Vol 77 (1982) pp6289-6295

10. V.M. Agranovich *Crystal Optics of Surface Polaritons and the Properties of Surfaces* Sov.Phys.Usp. Vol 18 (1975) pp99-117

11. A.F. Evans and D.G. Hall *Measurement of the Electrically Induced Refractive Index Change in Silicon for Wavelength* $\lambda = 1.3\mu m$ *Using a Schottky Diode* App.Phys.Lett Vol 56 (1990) pp212-214

12. B. Liedberg, C. Nylander and I. Lundström *Surface Plasmon Sensing for Gas Detection and Biosensing* Sensors and Actuators Vol 4 (1983) pp299-304

13. E. Yeatman and E.A. Ash *Surface Plasmon Microscopy* Electronics Letts. Vol 20 (1987) pp1091-1092

14. B. Rothenhäusler and W. Knoll *Surface Plasmon Interferometry in the Visible* Appl.Phys.Lett. Vol 52 No 19 (1988) pp1554-1556

15. G. Cross, I.R. Girling, I.R. Peterson and N.A. Cade *Linear Pockels Response of a Monolayer Langmuir-Blodgett Film* Elec.Lett. Vol 22 (1986) pp1111-1112

16. I. Pockrand, J.D. Swalen, R. Santo, A. Brillante and M.R. Philpott *Optical Properties of Organic Dye Monolayers by Surface Plasmon Spectroscopy* J.Chem.Phys. Vol 69 (1978) pp4001-4011

17. E. Kretschmann *Die Bestimmung optischer Konstanten von Metallen durch Anregung von Oberflächenplasmaschwigungen* Z.Physik Vol 216 (1968) pp398-410

Chapter III

Organic Dyes

3.1 Introduction

This chapter is intended to provide some background detail on the origins of the spectroscopic properties associated with organic dye molecules. In section 3.2 the structural features which make an organic compound a dye are outlined. The absorption process is described in section 3.3 and the factors which determine the observed spectra are discussed. Emission from dye molecules is explained in section 3.4, with special attention paid to the types of emission and the effects of aggregation. Finally in section 3.5 there is a brief summary.

3.2 Structure

3.2.1 Definition of an organic dye

Organic dyes are composed predominantly of carbon and hydrogen, but may also contain oxygen, nitrogen, phosphorous, sulphur and, in some macrocyclic molecules, metal atoms. These can be subdivided into saturated and unsaturated systems, the latter characterized by containing double or triple bonds. Double bonds profoundly affect the chemical reactivity and influence the spectroscopic properties. Organic compounds without double or triple bonds absorb below 160 nm. When two double bonds are separated by a single bond they are said to be conjugated. Compounds containing conjugated double bonds absorb light at wavelengths above 200 nm. All dyes in the proper sense of the word (i.e. compounds absorbing in the visible part of the spectrum) possess several conjugated bonds.

3.2.2 Bonding

Bonding in organic molecules is generally covalent in nature. Interactions between two 1s atomic orbitals give rise to a molecular orbital which is cylindrically symmetrical about the internuclear axis. An electron in such a molecular orbital

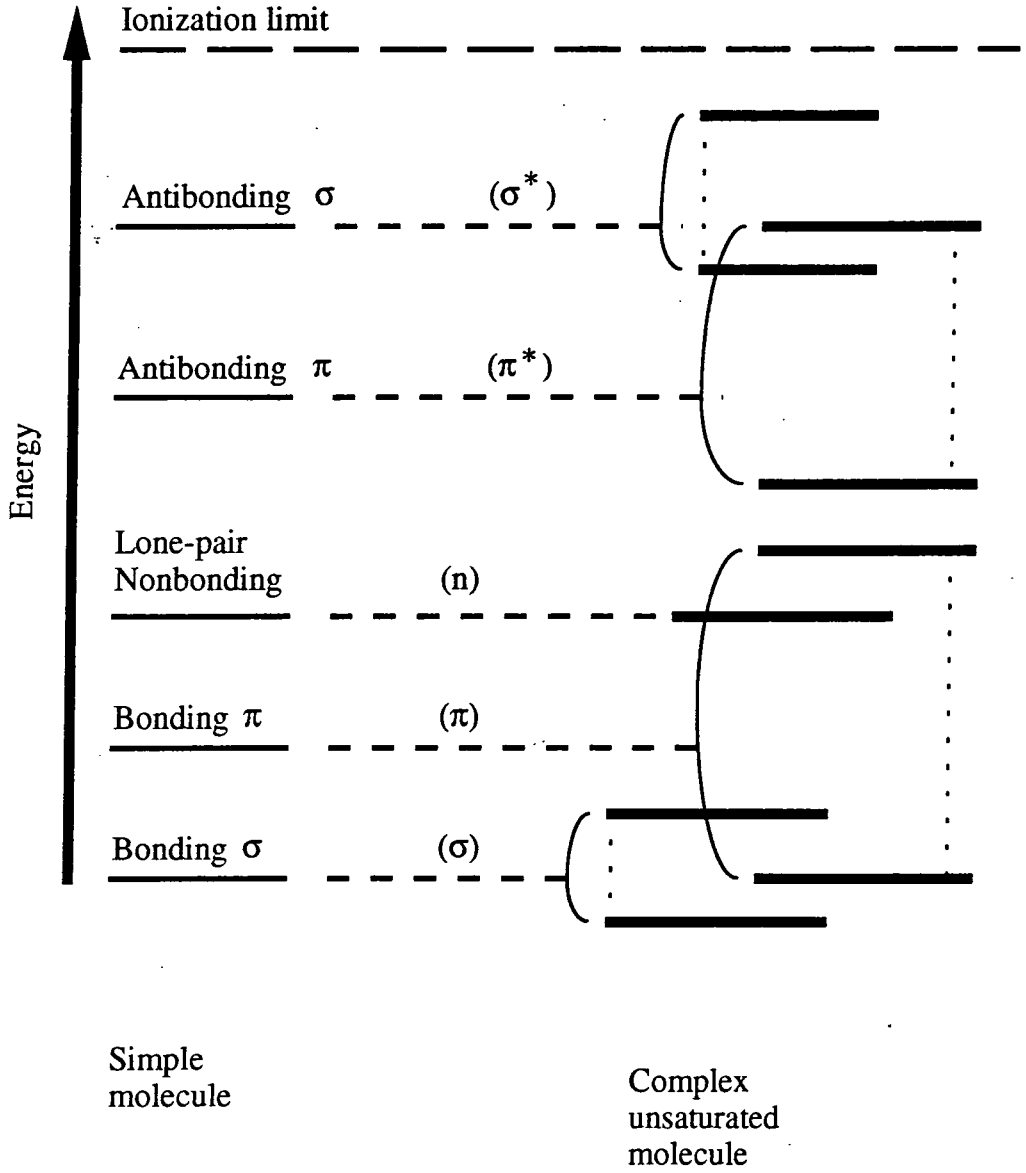

Figure 3.1 The bond energies associated with a simple molecule and unsaturated complex molecule.

has a high probability of being located between the nuclei. Such a molecular orbital forms a σ bond and the antibonding orbital σ^*. The sigma bond is usually associated with single bonds in organic molecules eg covalent bonds which have tightly bound electrons. Atoms held together by σ bonds may also possess p-atomic orbitals whose axes are perpendicular to the axis of the sigma bond. Side to side interactions of the p-orbitals results in the formation of bonding π molecular orbitals and the antibonding molecular orbitals π^*. The multiple bonds formed in organic molecules arise from a combination of a σ bond and one or two π bonds. The relative binding energies of these bonds are illustrated in the energy diagram figure 3.1. Non-bonding n electrons are formed from inner or lone pair electrons. Absorption due to $\sigma \rightarrow \sigma^*$ transitions is usually in the ultra-violet whilst $\pi \rightarrow \pi^*$ and $n \rightarrow \pi^*$ transitions are at longer wavelengths. In dye molecules (large unsaturated systems) there are as many π levels as there are conjugated bonds.

3.2.3 Delocalization and resonance hybrids

Electron pairs may contribute to the bonding of more than two nuclei. Such electrons occupy a volume larger than that implied by their common structural formulas, and are said to be delocalized. Delocalization of electrons is most often associated with molecules containing conjugated double bonds. An example of this is in the benzene cyclic conjugated system where the p orbitals (cyclic π orbitals) overlap above and below the plane of the benzene ring, see figure 3.2. The bond length of the C-C bond is somewhere between that of ethylene and ethane, and cannot be accurately represented by covalent bonds. Resonance theory or mesomerism is used to describe the system; it is said to be a resonance hybrid of the classical structures, see figure 3.2. Electron-delocalized species (resonance hybrids) are energetically more favourable than any contributing resonance structures. Ground and excited states become possible owing to resonance.

3.2.4 Chromophores

A particular group of atoms, with an electronic transition at a specific wavelength, which is transferable from one molecule to another is referred to as a chromophore. The term chromophore is often used when discussing dye compounds as

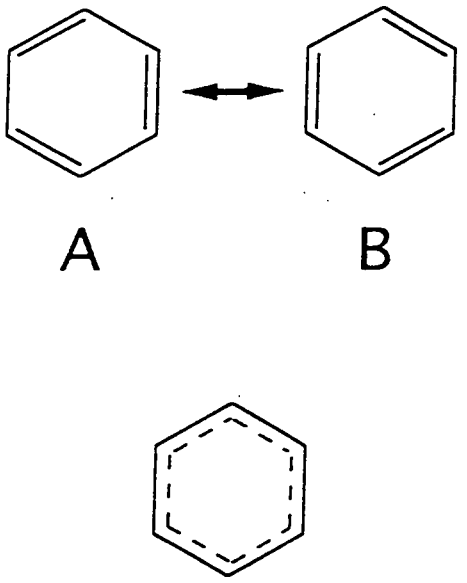

Figure 3.2 Mesomerism of a Benzene ring and resonance hybrid.

it refers to the active part of the molecule and the area of interest. A group can only act as a chromophore if it is not conjugated to another π electron system.

3.3 Absorption of Light

3.3.1 Transition dipole moment

The promotion of an electron from a lower energy level to a higher energy level does not produce a permanent dipole moment. However, at some intermediate, transient stage in the transition, a lack of symmetry in the electron density distribution exists. The transition dipole moment which results enables light absorption to take place. The most intense absorption bands are those associated with an electric-dipole transition moment produced by a linear charge displacement in the absorption process.

The transition dipole moment is a vector quantity, and therefore has direction as well as magnitude. Light will not be absorbed completely unless the oscillating electric field is parallel to the transition moment. The transition moment is fixed relative to the molecular structure, as for instance in ethylene where the $\pi \rightarrow \pi^*$ electronic transition, which is associated with the C-C bond, has the transition mo-

ment polarized along the bond. When the radiation is isotropic and the molecules are randomly oriented, as in a solution, absorption occurs with a high degree of probability. Conversely, when plane-polarized light is incident on a dye in the form of a single molecular crystal, the probability of absorption depends on the angle of incidence[1]. Complex molecules may have more than one transition moment. Anthracene, for example, has two transition moments, the long-wavelength absorption band is associated with the transition moment which lies along the short axis of the molecule and the short-wavelength absorption band is associated with the long axis ($S_0 \rightarrow S_2$ transition), see figure 3.3.

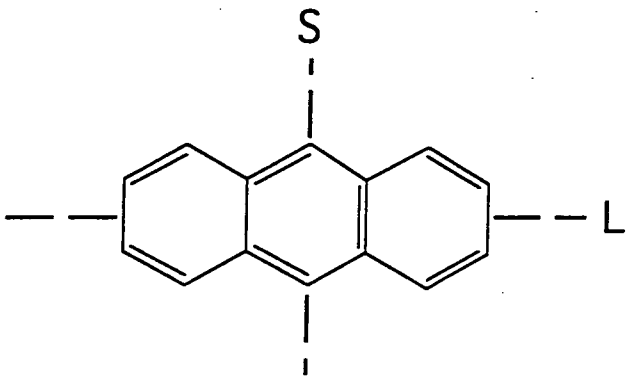

Figure 3.3 The two electronic transition moments for anthracene, polarized along the long (L) and short (S) axes of the molecule.

3.3.2 Energy levels

The energies available to a molecule can be conveniently illustrated by a simple energy level diagram, see figure 3.4. Each electronic level is divided into vibrational levels and each one of these in turn is subdivided into rotational levels. The energy gap between electronic levels can range from 0.4-3.0 eV; between vibrational levels from 0.04-0.4 eV and between rotational levels from 0.001-0.04 eV. The visible spectrum ranges from 1.6-3.1 eV, so it is the electronic levels that account for

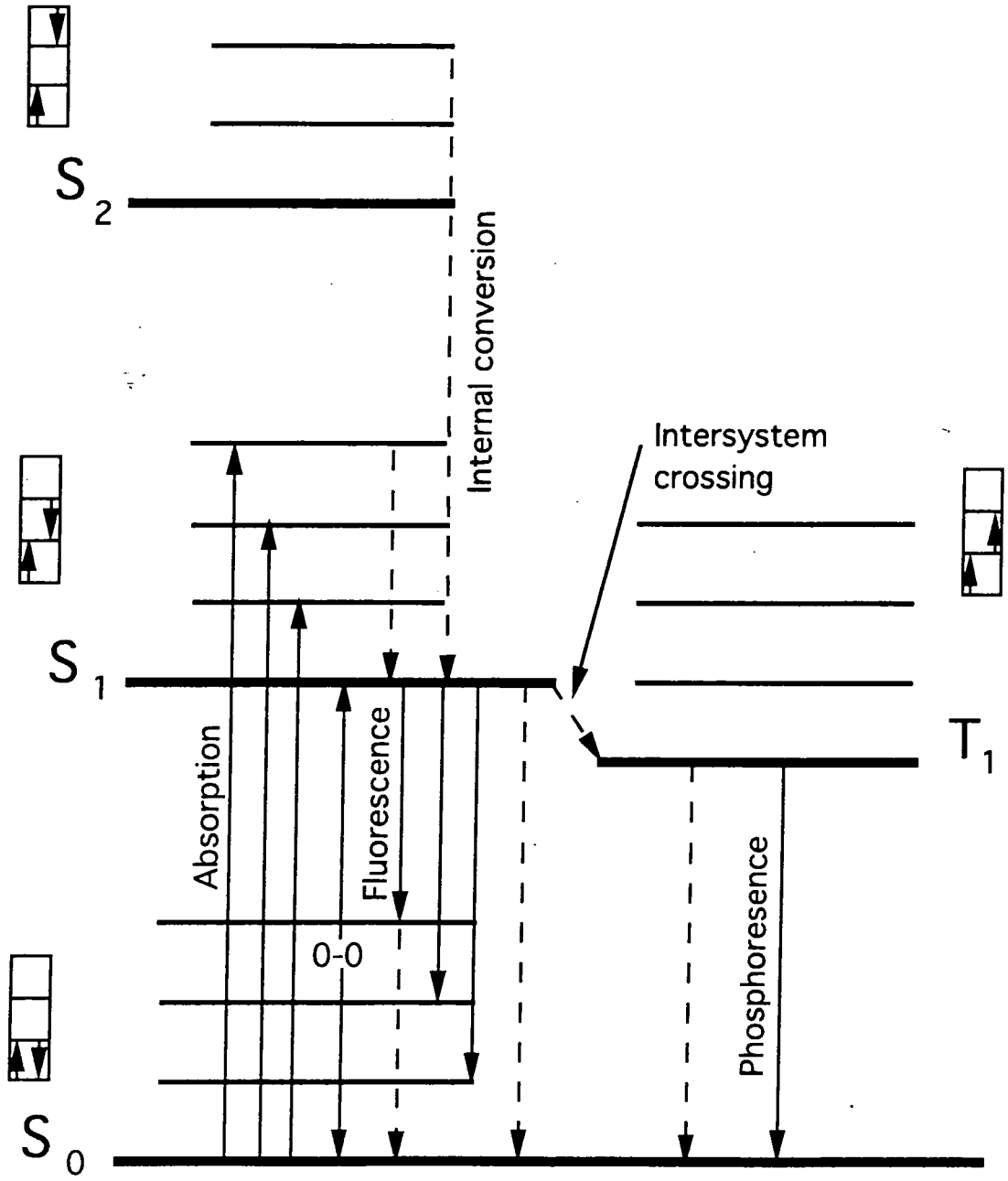

Figure 3.4 The energy levels of a molecule. The light absorption and emission processes are solid lines and the non-radiative transitions are broken lines.

light absorption. Nearly all molecules have an even number of electrons except for free radicals, and in the ground state the electrons occupy the orbitals in pairs. The singlet states S_0,S_1 etc result from electron configurations where all spins are paired so that the molecule has zero net spin, a multiplicity of 1. Triplet states T_1,T_2 etc have an unpaired electron and can have three possible values for their spin quantum number, hence a multiplicity of 3. The ground state for most molecules is a singlet; an important exception to this is molecular oxygen which is a triplet. For every singlet state other than the ground, there is a corresponding triplet state. Absorption occurs between the zero vibrational level of the ground singlet state and the higher vibrational levels of the excited singlet states S_1, S_2 etc . A transition between the zero vibrational levels of the ground and upper electronic states is often referred to as the 0-0 transition. The origin of this labeling system is explained in the next section. Absorption also occurs between the first two triplet states $T_1 \rightarrow T_2$ but is only observed by flash photolysis. Transitions between $S_0 \rightarrow T_1$ are not allowed, however, very weak absorption can take place.

3.3.3 The shape of absorption bands

On the absorption of light in molecules, transitions take place between the lowest vibrational level of the ground electronic state to a higher state depending on the energy of the radiation. For all molecules in solution the rotational levels are so closely spaced that they cannot be distinguished spectroscopically and the vibrational levels are represented as bands containing rotational levels. It might be assumed that each electronic transition in organic molecules would be sharp, as in atomic spectra, but this is not the case. Some molecules have a simple pattern of vibrational levels and these appear in the absorption spectrum as a series of well separated maxima (structured bands). However, in other more complex molecules the pattern of vibrational levels is so complex it leads to one broad unstructured absorption band.

The shape of the absorption bands can be explained by reference to Morse curves. A Morse curve is a plot of potential energy as a function of the nuclear distance r. In figure 3.5a the horizontal lines represent the vibrational levels and each one of these has a vibrational quantum number associated with it j=0,1,2...n. An electronically excited diatomic molecule is represented by a second similar

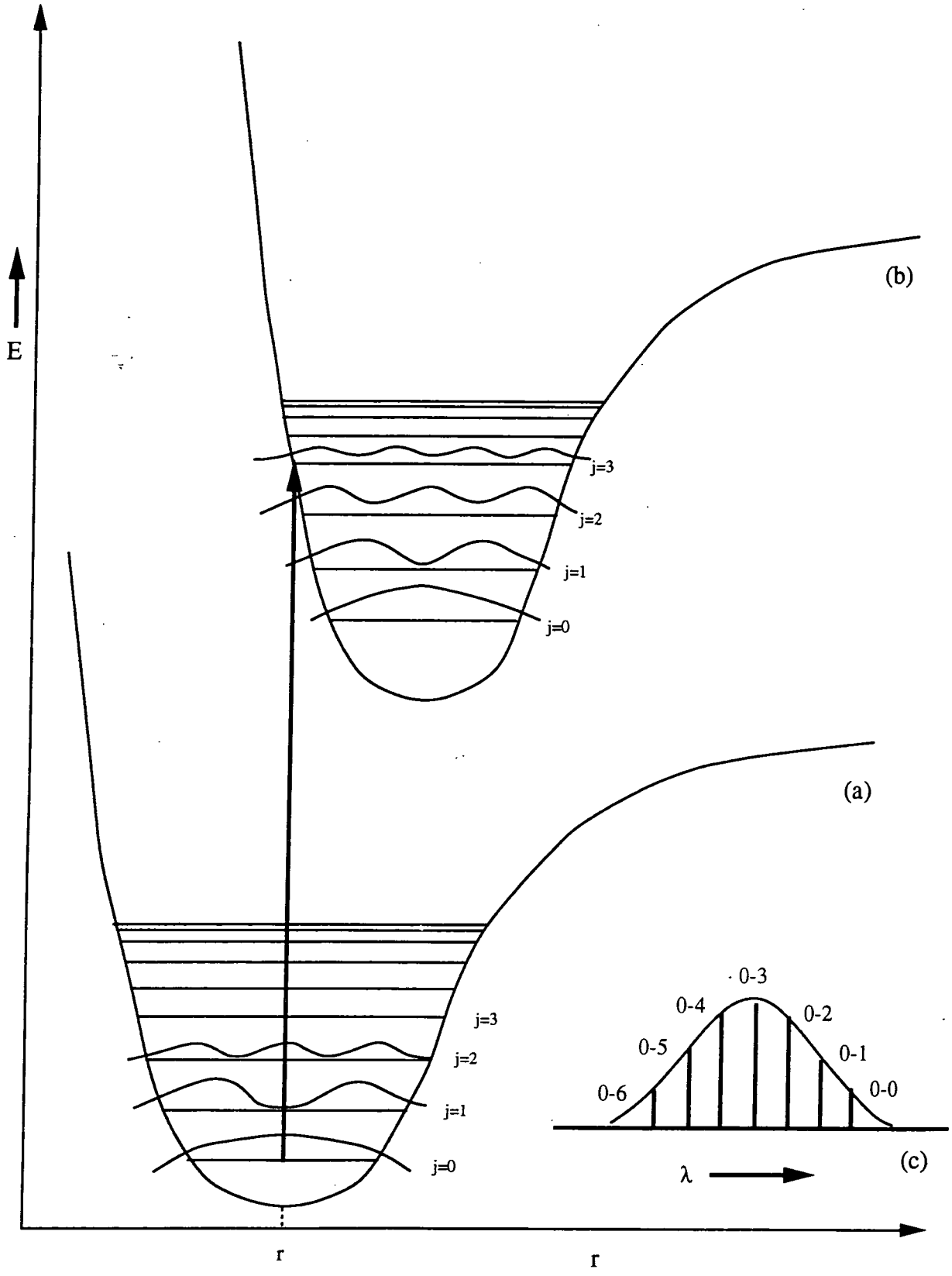

Figure 3.5 Morse curves for a molecule showing the origin of the band shape.

Morse curve which is displaced vertically (higher energy) and horizontally (due to vibration-increased bond length). The Franck-Condon principle imposes limitations on the intensities of the vibronic transitions and also accounts for the characteristic symmetrical shape of the bands. Electronic transitions occur much more rapidly than vibrational transitions, which means that the nuclei have nearly the same position and velocity before and after the transition. Electronic transitions are therefore represented on the Morse curve by vertical lines, since the internuclear distance does not change during the transition, drawn from the j=0 level of the ground state to all possible levels of the excited state. This results in absorption bands rather than single sharp absorption lines.

The probability and thus the intensity of a vibronic transition will be greatest for a line drawn from the centre of the j=0 level of the ground state which intercepts a region of high probability in a vibrational level of the excited state. As the Morse curve is shifted, see figure 3.5b, the transition of maximum probability will not occur between the j=0 and j=0 levels but will take place between the j=0 and a higher energy level in the excited state, this corresponds to λ_{max} for the band, and on either side of this the intensities will decrease to zero producing the familiar bell shaped absorption band 3.5c. In polyatomic molecules the Morse curves are replaced by polydimensional surfaces and the allowed vibronic transitions will become very large and absorption bands become smooth curves. In some cases vibrational fine structure can still be seen.

3.3.4 Beer-Lambert law

A relationship between the absorption and wavelength of materials is given by the Beer-Lambert law. Lambert's law states that the relationship between incident and absorbed radiation at a given wavelength is as follows

$$I = I_0 e^{-kd} \tag{3.1}$$

where I_0 is the intensity of incident light, I is the intensity of transmitted light, k is absorption constant and d is the thickness. The above applies to a transparent coloured substance of thickness d.

For solutions of coloured substances in a solvent, which has negligible absorption, the Beer-Lambert law is used.

$$A = \ln \frac{I_0}{I} = \varepsilon ct \tag{3.2}$$

where A is the absorbance, ε is the molecular extinction coefficient, c is the concentration in moles per litre and t is the thickness of the solution in cm. It is important to note that although Lambert's law is universal, Beer's law (which states that the light absorbed is proportional to the number of molecules of the absorbing material through which it passes) is not valid when there is an interaction between the dye molecules (association) or between dye and solvent (solvatochromism).

3.3.5 Association of dye molecules

As noted in the previous section, organic dyes in solution do not always obey Beer's law, and the absorption spectra of dyes in films can be significantly different. These deviations are attributed to the association of dye molecules, by a process not involving their primary valencies, into dimers and higher aggregates. Aggregation is favoured by certain dye structural features and matrix compositions, and is particularly common in symmetrical cyanines and carbocyanines[2]. Aggregation of dyes was thought to be due to Van der Waals' forces but these are too weak to account for the dimerization energies. However, according to London[3] the mutual potential energy of two identical molecules possessing a single long-wavelength electronic absorption band λ is, to a first approximation, proportional to $f^2\lambda^3$ where f is a measure of the excitation probability (oscillator strength). This force is very large for dyes owing to their high absorption (oscillator strength). The London force is additive and can account for the existence of higher aggregates. Dimers and higher aggregates form a new light absorbing system with absorption properties which can be quite different from the monomer. The effects arise from the co-operative absorption of light by both dye molecules in the dimer. The two equivalent dye molecules A and B have ground state wavefunctions ϕ_a and ϕ_b and excited state wavefunctions ϕ_a' and ϕ_b' . The ground stationary state of the dimer AB can be expressed as $\chi_0 = \phi_a\phi_b$. However, there are two possible excited state configurations $\phi_a{}'\phi_b$ and $\phi_a\phi_b{}'$; a true stationary state must contain both, as the molecules each have an equal probability of absorbing light and becoming excited.

Two stationary states χ_+ and χ_- are possible, an in-phase and an out-of-phase solution.

$$\chi_\pm = \frac{(\phi_a{}'\phi_b \pm \phi_a\phi_b{}')}{\sqrt{2}} \tag{3.3}$$

In the excited state both molecules carry averaged excitation energy and the energy is rapidly interchanged between them. The energies of the χ_+ and χ_- differ from each other and from the excited monomer $\phi_a{}'$ owing to the transition dipole interaction. The interaction is attractive for one dimer excited state, lowering the transition energy; and repulsive for the other, increasing the frequency of the photon required for the transition. These interactions are determined by the geometrical configuration of the dimer.

In the case of cyanines in aqueous solution, as the concentration of the dye increases the position of the absorption band is progressively shifted to shorter wavelength relative to the monomeric dye band. This is termed hypsochromic or metachromic and the aggregates are called 'H'. Shifts occurring toward the long-wavelength side are less progressive and are termed bathochromic they are more uncommon and are designated Scheibe or 'J' aggregates (after Jelley[4]); and are said to exhibit co-operative excitonic absorption. They were first observed in cyanines[5–10] but have recently been reported in squarylium[11]. It was proposed by Bucher and Kuhn[12] that J aggregates had a brickwork like structure and that they consisted of many thousands of molecules. According to Herz[13] these super-aggregates consist of a group of 4 molecules (tetramer) which is repeated.

There are three distinct geometrical configurations of the dimers, according to Kasha[14], each giving rise to a specific change in the absorption band; these are: parallel or sandwich, head-to-tail and oblique dimers, see figure 3.6.

In the sandwich dimer the transition dipoles of the lower energy dimer are antiparallel and therefore cancel so that the absorption $\chi_0 \rightarrow \chi_-$ is negligible. Conversely the transition dipoles are parallel in the higher energy dimer and give a large vector sum, the absorption $\chi_0 \rightarrow \chi_+$ therefore occurs with high intensity. The absorption band is blue shifted (hypsochromic) due to the increase in energy of the allowed transition $\chi_0 \rightarrow \chi_+$, see figure 3.6a.

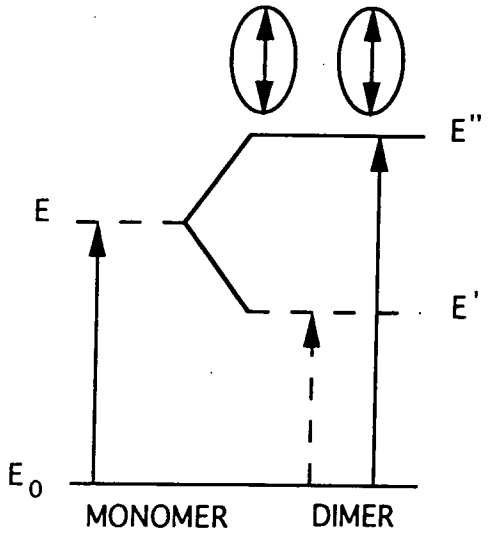

BLUE-SHIFT
(Hypsochromic)

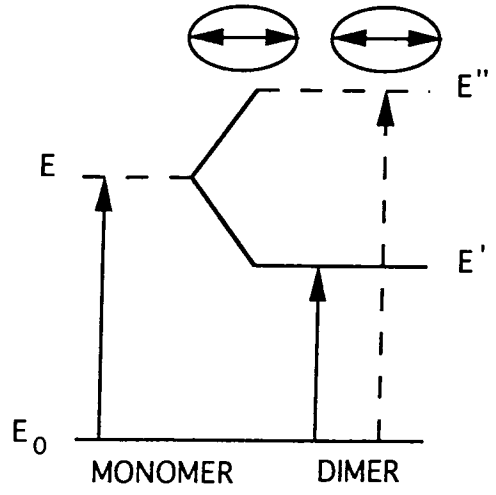

RED-SHIFT
(Bathochromic)

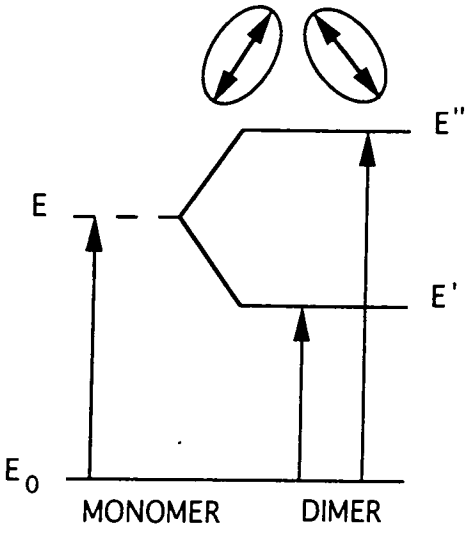

BAND-SPLITTING
(Davydov splitting)

Figure 3.6 Three geometrical configurations of dimers showing the splitting of the energy levels and the allowed transitions.

In head-to-tail dimers the $\chi_0 \rightarrow \chi_-$ transition is forbidden since the transition dipoles are opposed and cancel. In the lower energy dimer where the transition dipoles are head-to-tail they reinforce and the $\chi_0 \rightarrow \chi_+$ transition is allowed. The absorption band is red shifted (bathochromic) because of the lower energy of the allowed transition, see figure 3.6b.

The third configuration is that of oblique transition dipoles, where both excited states are allowed and the intensities will depend on the angular relationship between them, see figure 3.6c. The result is that a split in the band occurs corresponding to "Davydov splitting", as observed in molecular crystals and recently in LB films[15] .

It should be pointed out that these three configurations are limiting cases and that in general the molecules are noncoplanar, both electronic transitions are allowed, and the dimer is potentially optically active.

3.3.6 Solvent effects

Solvent-solute interactions can influence greatly the absorption spectrum; position and intensity of bands may vary as well as band width and in some cases the vibrational structure can appear and disappear. Interactions between solvent and solute molecules are greatest for polar solvents which contain a strong permanent dipole, and are less pronounced for non-polar solvents. The effect is also large if the solute molecules possess a permanent dipole and the solvent molecules arrange themselves around the solute to minimize the energy. This results in the stabilization of the ground state solute molecules. When the solute molecule absorbs radiation, the excited state is produced so rapidly that the solvent cage does not have time to rearrange itself. If the excited state is less polar than the ground state, the solvent cage is unable to stabilize the excited state effectively. This results in the solvent lowering the ground state energy more than the excited state; a hypsochromic (blue) shift of the spectrum takes place. If the ground state is less polar than the excited state the solvent tends to stabilize the excited state more than the ground state. The energy of the excited state is reduced more than the ground state; and a bathochromic (red) shift of the spectrum occurs.

3.3.7 Solution spectra

Solution spectra are generally structured in nature, although exceptions exist due to solvent type and solute concentration. The factors governing these have been discussed in some detail in previous sections.

3.3.8 Crystal spectra

Although the forces between molecules in crystals are weak and short range (Van der Waals'), and the overlap between orbitals of adjacent molecules in the lattice is small, there is still a substantial difference between the electronic spectra of molecular crystals and free molecules. Some of these differences are caused by interactions between the electronic states of molecules in the vicinity; others are due to crystal lattice properties. Crystal spectra have absorption bands which are broader than those in solution because the molecular interactions are affected by thermal vibrations as well as relative orientation of the molecules. Bands are often shifted and split (Davydov splitting[16]) when compared to solution.

3.3.9 LB film spectra

Film spectra exhibit features which are somewhere between those of solution and crystal spectra. Bands are generally broader than in solution, with the exception of J aggregates, and they lose any vibrational fine structure. The spectrum of a dye layer deposited onto another non-absorbing LB layer can be affected by the properties of the two layers; for example, Lehmann[6] and Hada[17] found that the aggregation of cyanine dyes was determined by the charges of the two layers. When an optically passive material is mixed with a dye it acts as a matrix, orienting and aggregating the dye. The degree to which these effects occur is determined by the concentration of the dye. Aggregation is the major factor affecting the spectra and has been covered in some detail in a preceding section.

3.4 Fluorescence

3.4.1 Emission spectra

A molecule raised to an upper vibrational level of any excited state rapidly loses its excess vibrational energy through collisions with other molecules. Almost

all molecules raised to an electronic state higher than the first undergo a process called internal conversion. A molecule passes from a low vibrational level of an upper excited state to a high vibrational level of a lower excited state which has the same energy. Then through collision with solvent molecules it rapidly loses its excess vibrational energy. In such a way molecules which are raised to excited states higher than the first, rapidly fall to the lowest vibrational level of S_1. The net result of this is that emission from the upper excited levels are very rare due to the competing decay processes. Internal conversion from S_1 is a slow process so light emission can easily take place.

Emission generally occurs at longer wavelength (lower energy) than absorption (Stokes' law) but in rare cases very weak fluorescence can be observed at a shorter wavelength, and is referred to as anti-Stokes fluorescence.

Emission bands often appear to be an approximate mirror image of the absorption bands, see figure 3.7, and attempts have been made to derive a formula to account for this[18]. A simple explanation is that the vibronic levels in the ground and first excited state are very similar and in the case of the 0-0 transition the levels are the same; hence the emission and absorption band associated with this transition should occur at the same wavelength (energy). There is often a difference between the emission and absorption 0-0 transitions in solution, which is due to the solvent effects discussed earlier. The relative intensities of emission bands are determined by the Franck-Condon principle, as they are in absorption spectra.

3.4.2 Fluorescence efficiency

Fluorescence efficiency is governed by the competition between radiative and nonradiative processes. The fluorescence efficiency or quantum yield is defined as the fraction of excited molecules which emit light. The fluorescence efficiency, ϕ_f, is given by

$$\phi_f(\lambda_{ex}) = \frac{n_{em}}{n_{ex}} \tag{3.4}$$

λ_{ex} excitation wavelength, n_{em} number emitting per second, n_{ex} number excited per second.

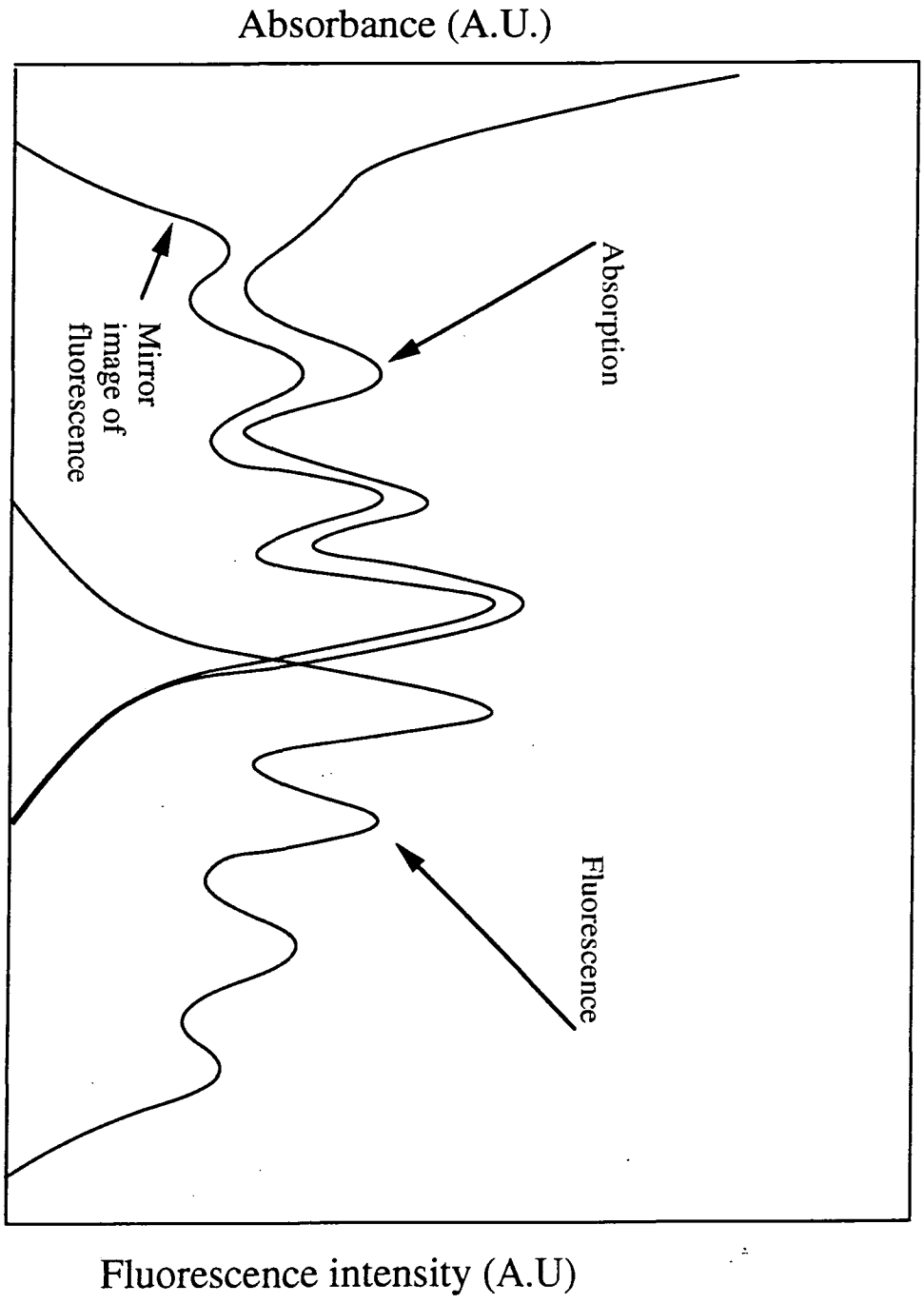

Figure 3.7 The mirror image relationship for anthracene.

3.4.3 Types of emission

The radiative transitions $S_1 \rightarrow S_0$ and $T_1 \rightarrow S_0$ give characteristic emission spectra. Fluorescence is defined as the $S_1 \rightarrow S_0$ transition and phosphorescence is defined as the $T_1 \rightarrow S_0$ transition. Fluorescence spectra occur immediately to the long-wavelength side of the first absorption band and, as noted above, are frequently the mirror image of it. Phosphorescence occurs at longer wavelengths because the triplet state has a lower energy than the first excited state. There are several ways for the S_1 state to be populated and these give rise to different types of fluorescence.

i) Molecules which are excited directly to the S_1 state, with an average lifetime of 10^{-8} , which then make the radiative transition $S_1 \rightarrow S_0$, are said to exhibit prompt fluorescence.

ii) Molecules can be excited to the T_1 state, then decay to the S_1 state and finally result in a radiative transition $S_1 \rightarrow S_0$. The lifetime is much longer than the usual S_1 state and the emission is therefore called delayed fluorescence. Two forms of delayed fluorescence have been observed, E-type and P-type, and are classified according to the mechanism by which the $T_1 \rightarrow S_1$ transition occurs.

E-type, or eosin type (first observed in eosin), delayed fluorescence was studied by many workers but it was Parker and Hatchard[19] who determined the mechanism involved. The transition from $T_1 \rightarrow S_1$ occurs due to thermal activation.

In P-type, or pyrene type, delayed fluorescence, the intensity was found by Parker and Hatchard[20] to be proportional to the square of the rate of absorption of exciting light. This showed that the delayed fluorescence was produced by the transfer of energy between two triplet molecules, one molecule raised to the excited singlet state emitting delayed fluorescence that decayed at a rate equal to twice the rate of the triplet decay.

$$ {}^3A^* + {}^3A^* \rightarrow ({}^1A_2^*) \rightarrow {}^1A^* + {}^1A + h\nu \qquad (3.5) $$

where ${}^3A$ is a triplet, ${}^1A$ is a singlet and * indicates an excited state.

3.4.4 Emission from aggregates

Dimers, which are responsible for the changes in the absorption bands with concentration, are often nonfluorescent. The stability of a dimer is related to the free energy of formation, total heat energy or (enthalpy) $-\Delta H$. The reversible combination of unexcited monomers results in the formation of a ground state dimer $A + A \Leftrightarrow (AA)$. Excitation of such a dimer will produce an excited dimer $(AA)^*$ which can be assumed to be a combination of A and A^*, forming A^*A. If the heat of formation is $(-\Delta H^*) < RT$ then dissociation is rapid.

$$(AA)^* \rightarrow A^* + A \tag{3.6}$$

If $-\Delta H^*$ is large enough to allow the formation of stable excited dimer and if $-\Delta H$ for the ground state dimer is zero or negative, the ground state dimer is unstable; the dimer formed in the excited state is termed an excimer[21].

Excimer fluorescence results in a broad, unstructured band which is red shifted compared to the monomer[22] and does not correspond to a mirror image of any absorption band.

Dimer fluorescence is generally weak and unstructured, and is the mirror image of an absorption band. However, the exact nature of the dimer fluorescence depends on the geometrical configuration of dimers as described earlier. In the case of parallel (sandwich) dimers, no radiative transition exists between χ_+ and χ_0, therefore fluorescence only occurs between χ_- and χ_0. χ_- has a long lifetime and fluorescence is red shifted and weak . However, in the case of head-to-tail dimers, the lifetime of the lowest excited state, χ_+, is almost half that of the monomer resulting in less quenching and far greater fluorescence efficiency. Emission from J aggregates generally coincides with absorption and is very sharp, and is referred to as resonance fluorescence.

3.5 Summary

In the preceding sections the absorption and emission of organic dyes in solution, crystal and films have been discussed. Particular attention has been paid to the effect of aggregation, as this becomes very important in LB films.

3.6 References

1. K. Fuke, K. Kaya, T. Kajiwara and S. Nagakura *The polarized reflection and absorption spectra of perylene crystals in monomeric and dimeric forms* J.Mol.Spec. Vol 63 (1976) pp98-107

2. D.M. Sturmer in A. Weissberger and E. Taylor *The chemistry of heterocyclic compounds* Vol 30 Wiley New York (1977) pp441

3. E. Rabinowitch and L.E. Epstein *Polymerization of dyestuffs in solution* J.Am.Chem.Soc. Vol 63 (1941) pp69-78

4. E.E. Jelley *Molecular, nematic and crystal states of 1:1-Diethyl-χ-Cyanine Chloride* Nature (London) Vol 139 (1937) pp631-2

5. U. Lehmann *Aggregation of cyanine dyes at Langmuir-Blodgett monolayers* Thin Solid Films Vol 160 (1988) 257-269

6. H.J. Nolte *A model of the optically active Scheibe-aggregate of pseudoisocyanine* Chem.Phys.Lett. Vol 31 (1975) pp134-139

7. T.L. Penner and D. Möbius *The formation of mixed J aggregates of cyanine dyes in Langmuir-Blodgett monolayers* Thin Solid Films Vol 132 (1985) pp 134-139

8. D.F. O'Brien *J aggregation in monomolecular layers of cyanine dyes* Photo.Sc. and Eng. Vol 18 (1974) pp16-21

9. G. Biesmans, M.Van der Auweraer and F.C. DeSchryver *Influence of deposition circumstances on the spectroscopic properties of mixed monolayers of dioctadecyloxacarbocyanine and arachidic acid* Langmuir Vol 6 (1990) pp277-285

10. S. De Boer and D.A. Wiersma *Dephasing-induced damping of superradiant emission in J aggregates* Chem.Phys.Lett. Vol 165 (1990) 45-53

11. S. Kim, M. Furuki, L.S. Pu, H. Nakahara and K. Fukuda *Multiplied monolayer assembly of J aggregates of squarylium dye with short alkyl chains* Thin Solid Films Vol 159 (1988) pp337-344

12. H. Bücher and H. Kuhn *Scheibe aggregate formation of cyanine dyes in monolayers* Chem.Phys.Lett. Vol 6 (1970) pp183-185

13. A.H. Herz *Dye-dye interactions of cyanines in solution and at AgBr surfaces* Photo.Sc. and Eng. Vol 18 (1974) pp323-335

14. M. Kasha in B. DiBartolo (ed) *Spectroscopy of the excited state* Plenum New York (1976) pp337-363

15. K. Saito, K. Ikegami, S. Kuroda, M. Saito, Y. Tabe and M. Sugi *Davydov splitting in arachidic acid cyanine dye complex Langmuir-Blodgett films* J.Appl.Phys. Vol 68 (1990) pp1968-1974

16. A.S. Davydov *Theory of molecular excitons* Mc Graw-Hill Book Co, New York (1962) and Plenum, New York (1971)

17. H. Hada, R. Hanawa, A. Haraguchi and Y. Yonezawa *Preparation of the J aggregate of cyanine dyes by means of the Langmuir-Blodgett technique* J.Phys. Chem. Vol 89 (1985) pp560-572

18. J.B. Birks and D.J. Dyson *The relationship between the fluorescence and absorption properties of organic molecules* Proc.Roy.Soc. A275 (1963) pp135-148

19. G.N. Lewis and M. Kasha *Phosphorescence and the triplet state* J.Am.Chem. Soc. Vol 66 (1944) pp2100-2116

20. C.A. Parker and P. Hatchard *Delayed fluorescence from solutions of Anthracene and Phenanthrene* Proc.Roy.Soc. (London) A269 (1962) pp574-584

21. Th. Förster and K. Kasper *Ein Kozentrationsumschlag der Fluoreszenz* Z.Phys. Chem. Vol 1 (1954) pp275-278

22. J. Ferguson *Absorption and emission spectra of the perylene dimer* J.Chem.Phys. Vol 44 (1966) pp2677-2683

Chapter IV

Experimental Methods

4.1 Introduction

This chapter contains descriptions of the methods employed to prepare samples for optical and structural characterization, and surface plasmon resonance studies. Particular attention has been paid to the Langmuir-Blodgett technique (section 4.2), which was used to produce the thin organic films. Methods used to prepare substrates for film deposition are described in section 4.3. An explanation is given of the techniques used to characterize the materials for their structural and optical properties in section 4.4; details are also given of any special procedures adopted. The experimental set-up used for surface plasmon resonance studies is described in some detail in section 4.4.7 along with the measuring procedures adopted.

4.2 The Langmuir-Blodgett Technique

4.2.1 The Langmuir-Blodgett trough

The trough used to prepare all the samples investigated was a bobbin and tape type trough, first described by Zilversmitt[1], and was very similar to those used by Blight et al[2] and Roberts et al [3]; a schematic of the trough is shown in figure 4.1. The barrier was a continuous PTFE coated glass fibre tape which was looped around the six PTFE bobbins. The bobbins were connected to two carriages which were driven back and forth by an electric motor via a toothed drive belt. The motion of the carriages was halted when they came into contact with micro-switches which were located at the maximum and minimum areas. The trough which held the water was constructed from three pieces of glass: one piece was curved to form the base and the two long sides, whilst the other two pieces were flat and formed the short sides which were clamped to the ends and sealed with PTFE tape. The trough rested on a platform which could be raised or lowered by means of a jacking system. With the trough positioned under the

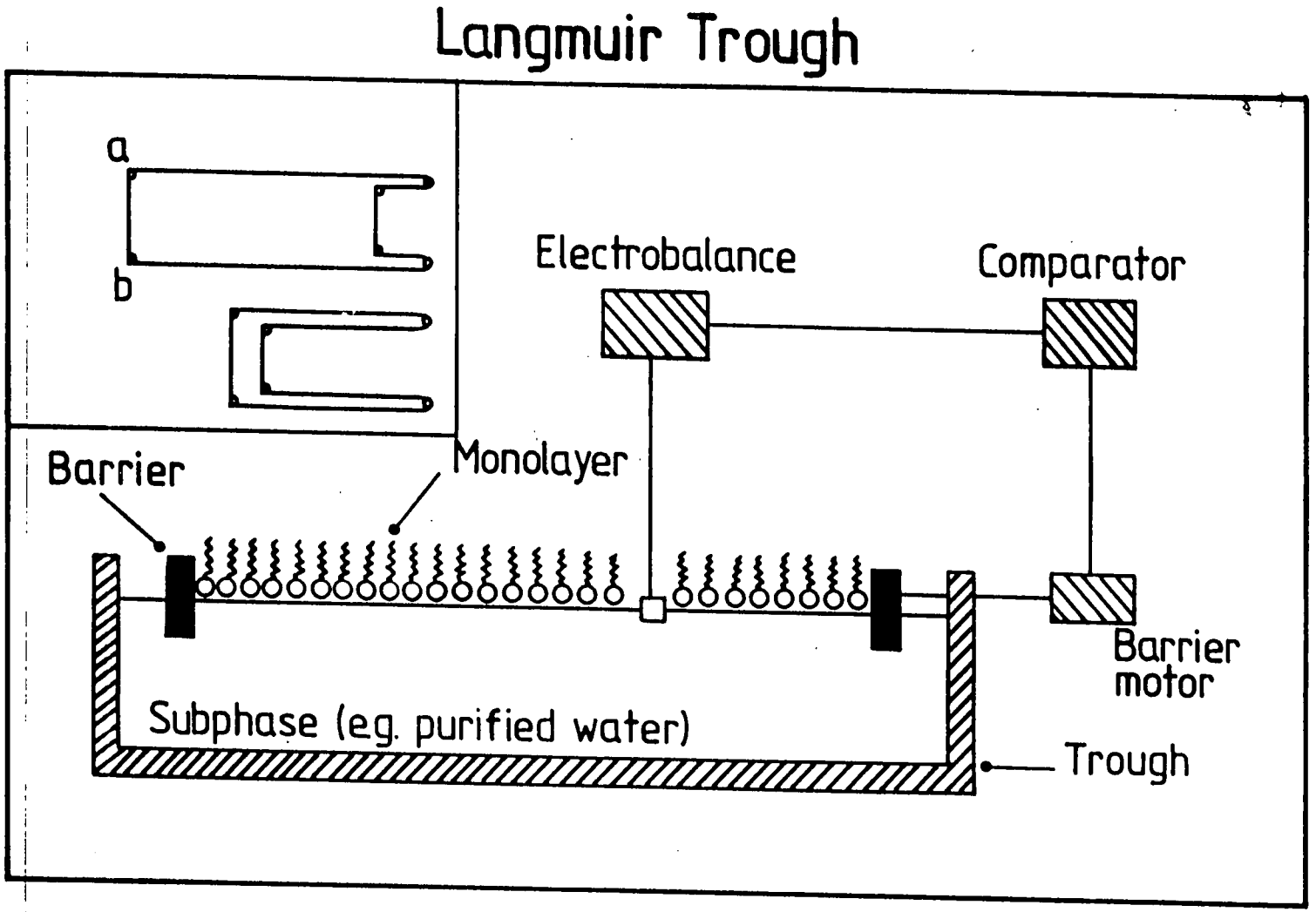

Figure 4.1 A schematic of an Langmuir-Blodgett trough.

barrier system, its height could be adjusted so that the correct water level on the barriers was achieved. This arrangement enabled the trough to be lowered until it was clear of the barriers to facilitate removal for cleaning. The subphase used in the trough was ultra-pure water, essential when manipulating molecules on the surface. It was supplied by an Elga reverse osmosis and deionization system, fitted with a UV sterilizer. The water, typically, had a total organic carbon content of 10 ppb and a resistivity of 17 megohms cm measured by an Anatel water analyser. The water was constantly circulated through the filtration system via a reservoir tank. The troughs were regularly emptied of water (about once a week or when a new type of material was being used) and cleaned in a fume cupboard, firstly with propan-2-ol, then with chloroform and finally with pure water. The bobbins and tape were also cleaned by wiping with propan-2-ol and then refluxing in propan-2-ol vapour. The surface pressure was measured by means of a Wilhelmy plate, which consisted of a piece of chromatography paper cut to about 3cm length and 1cm width; this was hung on a hook which was suspended by a piece of thread from one arm of a modified CI microbalance. The paper formed a contact angle of zero with the surface, and any change in the surface energy was translated into an upward or downward force on the Wilhelmy plate. The microbalance output was connected to the control electronics. A desired surface pressure could be selected on the control box, the electronics would then close the barriers to achieve the set pressure and the feedback system would maintain it. The film was an integral part of the feedback loop and the control of the film was critically dependent on certain properties of the film. The surface was cleaned by the use of a pipette tube connected to an aspirator pump, the tip of the pipette being positioned so that the surface layer could be sucked off in a 'hoover-type' action. The surface was judged to be clean when the barriers could be compressed and the surface pressure changed by less than 0.5 mNm^{-1}. The surface pressure could be zeroed by the use of a potentiometer on the control electronics for fine adjustment, or, for coarse adjustment, by varying the water level.

To spread a film, the surface was cleaned as described previously; the surface pressure was then zeroed and typically 100 μl (the volume depended on the material and concentration of the solution) of material (dissolved in Aristar chloroform) was dispensed using a Kloehn microlitre syringe by gently dropping the solution onto the water surface. The chloroform was allowed to evaporate, aided by the use of

an electric fan which was built into the trough cabinet. After a few minutes, the film could be compressed to the set point pressure. This was achieved by setting the electronics to control with the gain at minimum and then increasing the gain gradually to reach the required pressure. The barrier position and surface pressure were recorded using an Y-t chart recorder.

The substrate was clamped into a holder which was mounted onto the dipping head; this consisted of a micrometer driven by an electric motor. The speed of the dipping motion and the upper and lower limits were adjusted by means of the potentiometers on the control electronics. This enabled a predefined area of the substrate to be passed through the film on the water surface.

4.2.2 Pressure versus area isotherms

A pressure versus area isotherm measurement can be used to determine properties of the floating monolayer; many isotherm studies were made by Gaines[7]. A film spread on the surface was compressed at a slow, constant speed and the surface area was then plotted against the surface pressure. The resulting curve is shown in figure 4.2. There is an increase in surface pressure as the surface area decreases, the exact nature of this curve varies from material to material. Classic LB materials such as stearic acid were thought to show just three distinct phases in their isotherms. These were referred to as a) the quasi gas b) the quasi liquid and c) the quasi solid phases. However, work by Stenhagen[38] and recently Bibo et al[39] reveals some systems to be much more complex with many phases existing. These can be related to the disorder of the molecules on the water surface . Isotherms are good indicators of a material suitability for LB deposition; a steep isotherm is generally desirable for good film control and transfer. Isotherms fall into two main catagories: the condensed isotherm where distinct phases are discernable, such as the curve for a fatty acid shown in fig 4.2a, and the expanded isotherm, where there is a smooth increase in pressure with area, as shown in fig 4.2b. If the area is decreased too far, collapse of the monolayer may occur. For some materials the surface pressure may reach a constant value (plateau) before continuing to increase; this may be attributed to some reordering in the film. If the film has not been compressed beyond its collapse pressure, the area can be increased and the film compressed again. This can be repeated several times to obtain information

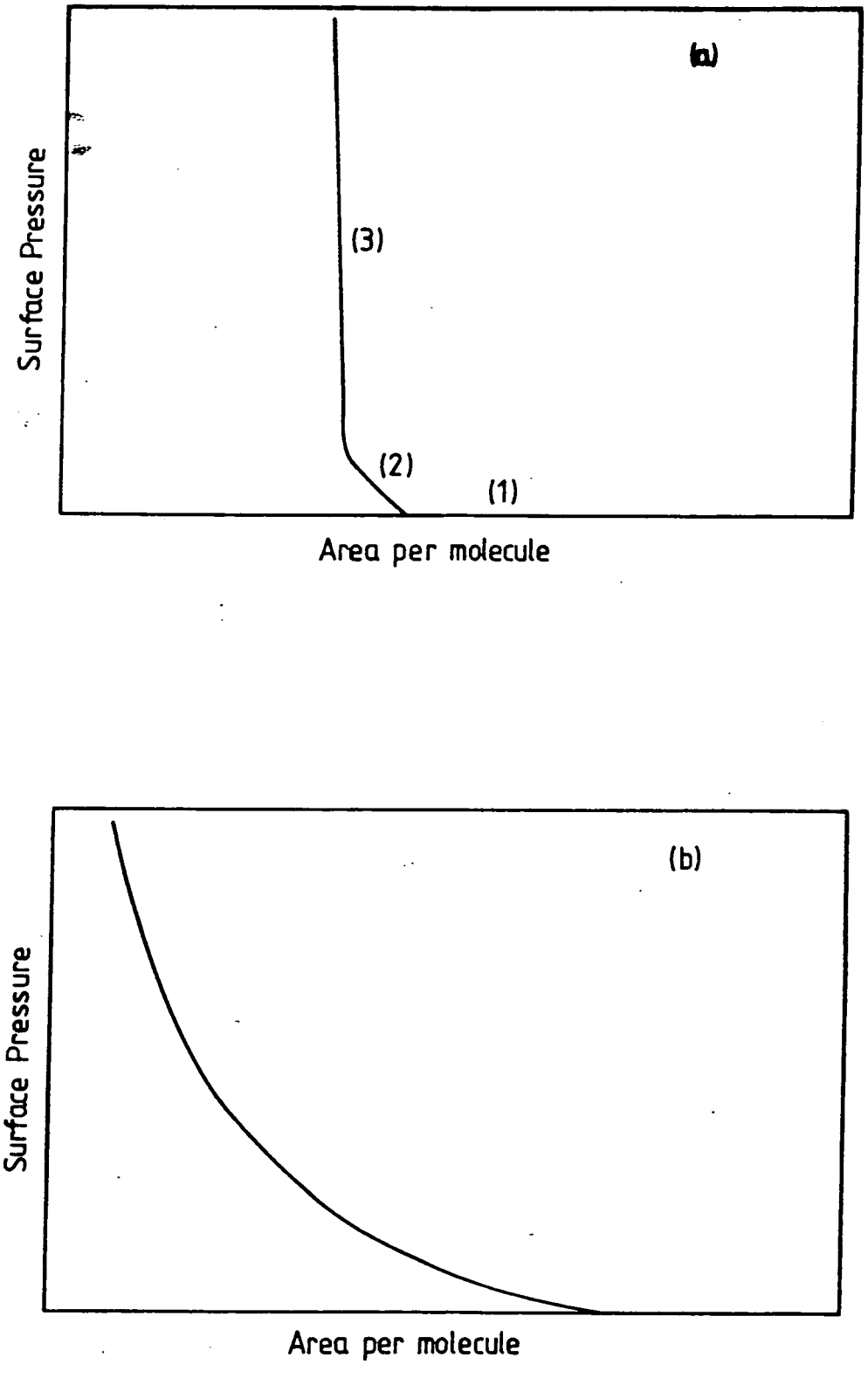

Figure 4.2 Typical pressure area isotherms a) condensed type b) expanded type.

on possible reordering of the molecules in the film. It is also possible to determine the average area occupied by a molecule on the water surface, provided the concentration, volume and molecular weight of the solution spread are known.

4.2.3 Film lifetime and stability

Another important method for determining the film quality was to compress the film to a predetermined surface pressure and control at that set point, monitoring the change in surface area. Many materials do not maintain a steady surface area at constant pressure. This may be due to reordering of molecules, dissolution of molecules into the subphase or collapse of the film. For deposition, film stability is necessary in order that the film could be transferred successfully. A visual inspection of the floating monolayer was a useful way of judging quality; however, most films were so thin that it was impossible to see them on the water surface when viewed from above. Some materials formed islands that were probably many monolayers thick and these could be clearly seen. If a material formed such islands, deposition would not be good, as a patchy film would be transferred. With the source of illumination from above, the floating monolayer became more clearly visible. An important requirement of the film is that it flowed easily on the surface so that when molecules were removed they were replaced immediately. The fluidity of the film could be determined by compression to a set surface pressure and the removal of some film by using the suction pump. The response of the barriers indicated the stiffness and rigidity of the film. For an ideal material, the barriers closed rapidly to compensate for the removal of the floating monolayer. For an inferior material, the barriers moved perceptibly slower and for an unsatisfactory material there was no change in the barriers position and a hole in the monolayer was quite often clearly visible.

4.2.4 Film deposition

Having determined the correct surface pressure for a particular material from an isotherm plot, the compressed film could then be transferred to a suitable substrate. For high quality, films it was essential to have a well prepared substrate; this is mentioned later. There are various methods for transferring the film to a substrate: touching[4], lifting[5], horizontal dipping[6] and vertical dipping. All the

films produced in this work were made using the conventional vertical dipping method illustrated in figure 4.3. Three types of transfer were possible depending on the material and the substrate used. These were named by Blodgett[8] as X,Y and Z-type and are shown in figure 4.3. In X-type deposition the material is transferred on the downstroke only so that the hydrophobic part of the material is in contact with the substrate and the hydrophilic region is away from the surface. All subsequent layers had the same orientation. When film is transferred on both the upstroke and the downstroke the deposition is called Y-type. Transfer only on the upstroke is called Z-type deposition.

4.3 Substrate Preparation

4.3.1 Glass

Microscope slides were the most convenient source of precut glass available. These were obtained from Chance Propper, Warley, West Midlands. These possessed a refractive index of approximately 1.52 and measured 76mm by 26mm, 1.0mm - 1.2mm thick. The first procedure used to clean the slides consisted of rubbing in a surface active cleaning agent (Decon 90 supplied by Decon Laboratories Ltd, Hove) and water solution with gloved hands to remove any large pieces of dirt or grease. The slides were ultrasonically agitated in a beaker containing Decon 90 solution for approximately 10 minutes and then rinsed in ultra-pure water for a further 10 minutes in the ultrasonic bath. Two methods were employed to clean the slides further, depending on the type of surface required. If a hydrophilic surface was needed, the glass slide was placed in a Soxhlet tube and refluxed with boiling propan-2-ol (Analar BDH) for approximately 4 hours; finally it was removed and blow dried with dry, Millipore filtered nitrogen dispensed from an air gun. A second technique was to use a chromic acid etch; this treatment left the surface slightly hydrophobic. The slides were cleaned mechanically, as before, and then immersed overnight in the chromic acid. They were then rinsed thoroughly in ultra-pure water and were finally blow dried using the air gun.

4.3.2 Silvered glass

Glass slides, cleaned by one of the methods described above were mounted in a holder in the evaporator, three slides at a time, at a distance of 170 mm

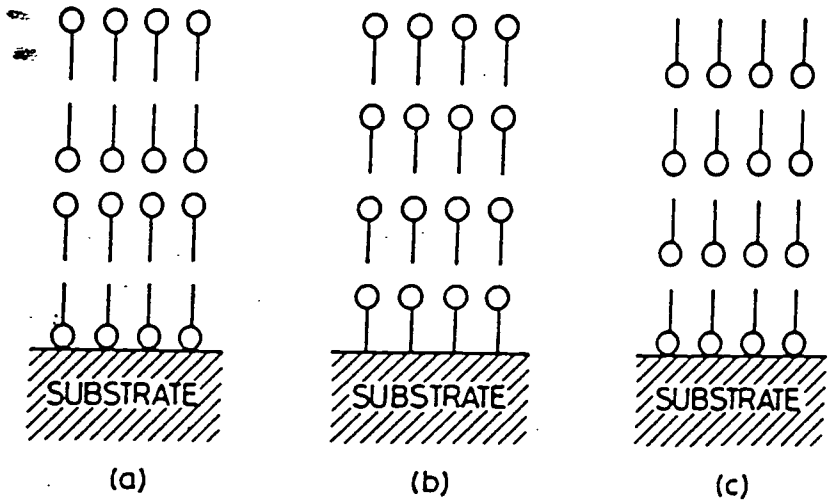

Modes of LB film deposition: (a) Y type, (b) X type, (c) Z type.

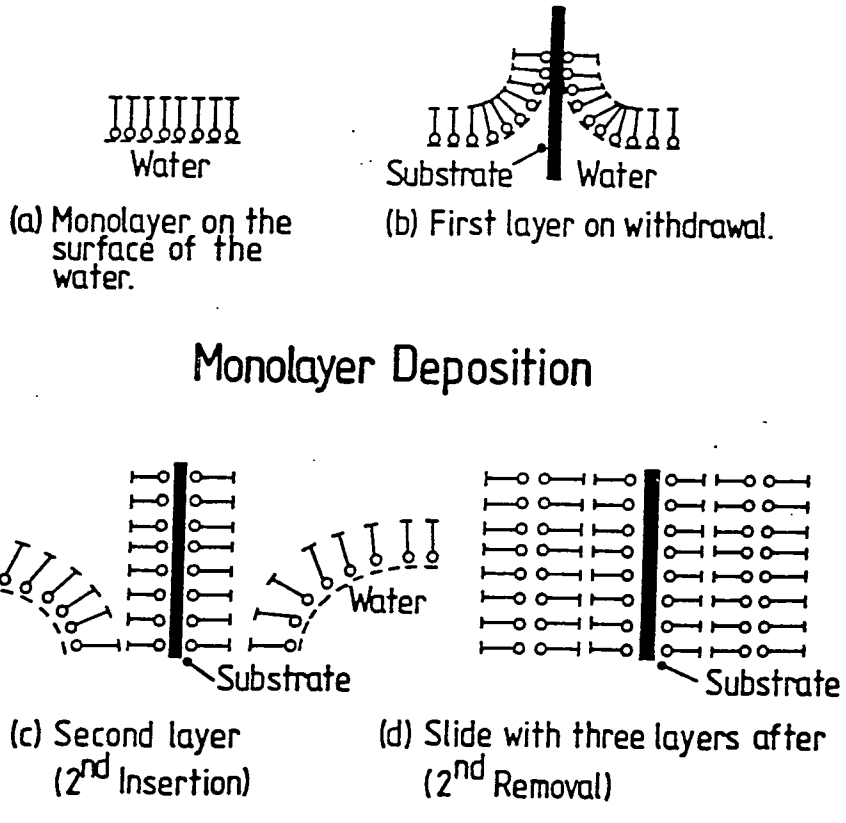

Figure 4.3 A schematic of Y-type deposition onto a hydrophilic substrate and the three modes of deposition.

from the source. The evaporator was an Edwards model E306A with the shutter automatically controlled by a thickness monitor gauge FTM4. The silver was resistively heated in a tungsten boat. Evaporations were performed at a pressure of 10^{-7} torr at a deposition rate of 1.5 nm s^{-1}, with a current of 62A passing through the boat. Approximately 50 nm of silver was evaporated with the aid of the thickness monitor. Occasionally a thin layer of chromium was evaporated first to ensure good silver adhesion (approximately 0.7 nm from a separate boat[9]).

4.3.3 Quartz plates

Quartz was first cleaned by wiping with Decon 90 and water solution as described above; then rinsed in ultra-pure water, and finally refluxed in boiling propan-2-ol for 3 hours.

4.3.4 Silicon

Suitably sized pieces of silicon were cut from a wafer. These wafers were obtained from Dynamit Noble; they were 76.2 mm diameter, polished, (111) orientated, and phosphorus doped. They were cut using a diamond scribe into rectangular pieces approximately 1×4 cm^3. Firstly they were wiped with Decon 90 solution, rinsed in ultra-pure water and finally refluxed in propan-2-ol for approximately 3 hours.

4.3.5 Hydrophobic substrates

Although glass slides became slightly hydrophobic when treated with chromic acid, they were not sufficiently hydrophobic for most purposes. In order to obtain a more hydrophobic surface on glass, quartz or silicon, it was necessary to treat the substrate with a silanizing solution 111-trichloroethane with 5% dichlorodimethylsilane. The substrate was placed in a covered beaker with a small amount of the silanizing solution and left for 30 minutes; it was occassionally turned over and agitated to ensure that the whole surface was treated. The hydroxide groups on the silicon surface react with the chlorine on the dichlorodimethylsilane to produce water and HCl, the silicon is then free to bond to the surface. The result is a surface covered in methyl groups which is very hydrophobic. On removal from the silanizing solution, the substrates were rinsed immediately in ultra-pure water

to wash HCl from the surface. It was often necessary to rinse the substrates with chloroform to remove drying marks.

4.4 Optical and Structural Characterization Techniques

4.4.1 Absorption spectroscopy

Absorption spectroscopy not only gives information on the position and intensity of absorption bands but, from analysis of the spectra, details of the electronic transitions within the molecules and the aggregation of molecules into dimers and trimers can be obtained. Many absorption studies have been made on floating monolayers[10] and deposited LB films[11,13].

The absorption spectra were recorded on a Cary Varian model 2300 UV-Vis-NIR scanning dual beam spectrophotometer, with a spectral range from 3152nm to 185nm and also on the Perkin Elmer Lambda 19. The spectrophotometer was designed to measure the spectra of materials in solution and was therefore fitted with sample holders which held small cuvettes. Special sample holders enabled film spectra to be recorded. These were designed so that a standard microscope slide could be mounted normal to the beam.

Before a solution spectrum could be taken, the cuvettes were rinsed out with Aristar chloroform; they were then filled with chloroform and a baseline was recorded over the range of wavelengths required. The sample cuvette was then removed and filled with the dye solution, which was diluted several times until the shape of the recorded spectrum became reproducible.

Film spectra were recorded in a similar way to solution spectra. A baseline was recorded with two clean substrates of the same type as the sample. One of these was removed and the sample inserted in its place the other remained as a reference. Care was taken to make sure that the beam was incident on the area of the slide covered with film.

4.4.2 Dichroism

The electronic transition dipoles giving rise to optical absorption spectra in dye chromophores have a fixed orientation relative to the molecular structure.

Polarized absorption (dichroism) measurements coupled with knowledge of the transition dipoles in the chromophore can be used to obtain information about the orientation of the chromophores in the film and the degree of preferred order present. This extension of absorption spectroscopy has been used by workers studying multilayer assemblies[14–18]. An illustration of this technique is shown in figure 4.4.

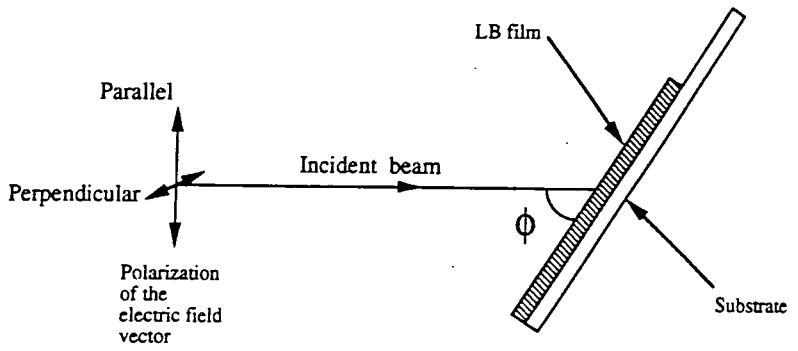

Figure 4.4 The experimental configuration for polarized absorption spectroscopy.

Dichroism measurements were made using the slightly modified Cary 2300 UV-Vis spectrophotometer. Matching polarizers were mounted in front of the two beams before they were incident on the sample and references slides. Each polarizer could be rotated so as to change the plane of polarization. The sample slide was mounted in a special holder so that the angle of the slide relative to the incident beam could be changed. Only six angles of incidence ϕ could be selected: 90°, 80°, 70°, 60°, 50° and 45°.

Samples were prepared in the same way as those used in the absorption spectroscopy measurements. The procedure for taking a measurement was similar to that used for absorption spectra, but with one difference - it was neccessary to

record a new baseline each time the sample was rotated or the plane of polarization was changed. The polarizers were only ever used parallel and perpendicular to the dipping direction.

4.4.3 Fluorescence spectroscopy

Fluorescence spectra give the emission wavelengths and relative intensities of emitters present. Fluorescence decay rates used in conjunction with spectra can reveal information about the type and number of fluorescing species present[19–21].

The fluorescence spectra and decay of samples were measured by Dr A. Vitukhnovsky and Dr M. I. Sluch at the P. N. Lebedev Physical Institute, Moscow. Fluorescence spectra were measured with an optical multichannel analyser OMA-2 with nitrogen laser LG-21 excitation 337 nm and 50 Hz. The fluorescence decay curves were measured with an Edinburgh Instruments spectrofluorimeter using a Philips photomultiplier tube XP2020Q and a flashlamp at 380 nm with a repetition rate of 20 Hz and a single pulse duration of 1.1 ns (fwhm). A schematic of the experimental set-up is shown in figure 4.5. The fluorescence decay curves were analyzed using a nonlinear, least-squares iterative convolution method.

Samples were prepared on glass and quartz plates, cleaned by the methods mentioned earlier. However, glass proved to be unsatisfactory due to its intense fluorescence at 420 nm, close to the region of interest.

4.4.4 Ellipsometry

Ellipsometry provides a convenient method of accurately measuring the thickness of LB films[22–25]. An ellipsometer uses collimated, monochromated light of a known polarization to measure the change in polarization of a reflected beam from the surface of a substance. A measurement involves the irradiation of a surface at a fixed angle (70°) with a collimated monochromated beam which has a variable but known polarization, and comparing the states of polarization of the reflected and incident beams. From these differences it is possible to determine various properties of the surface such as refractive index, absorption coefficient and thickness of overlayers.

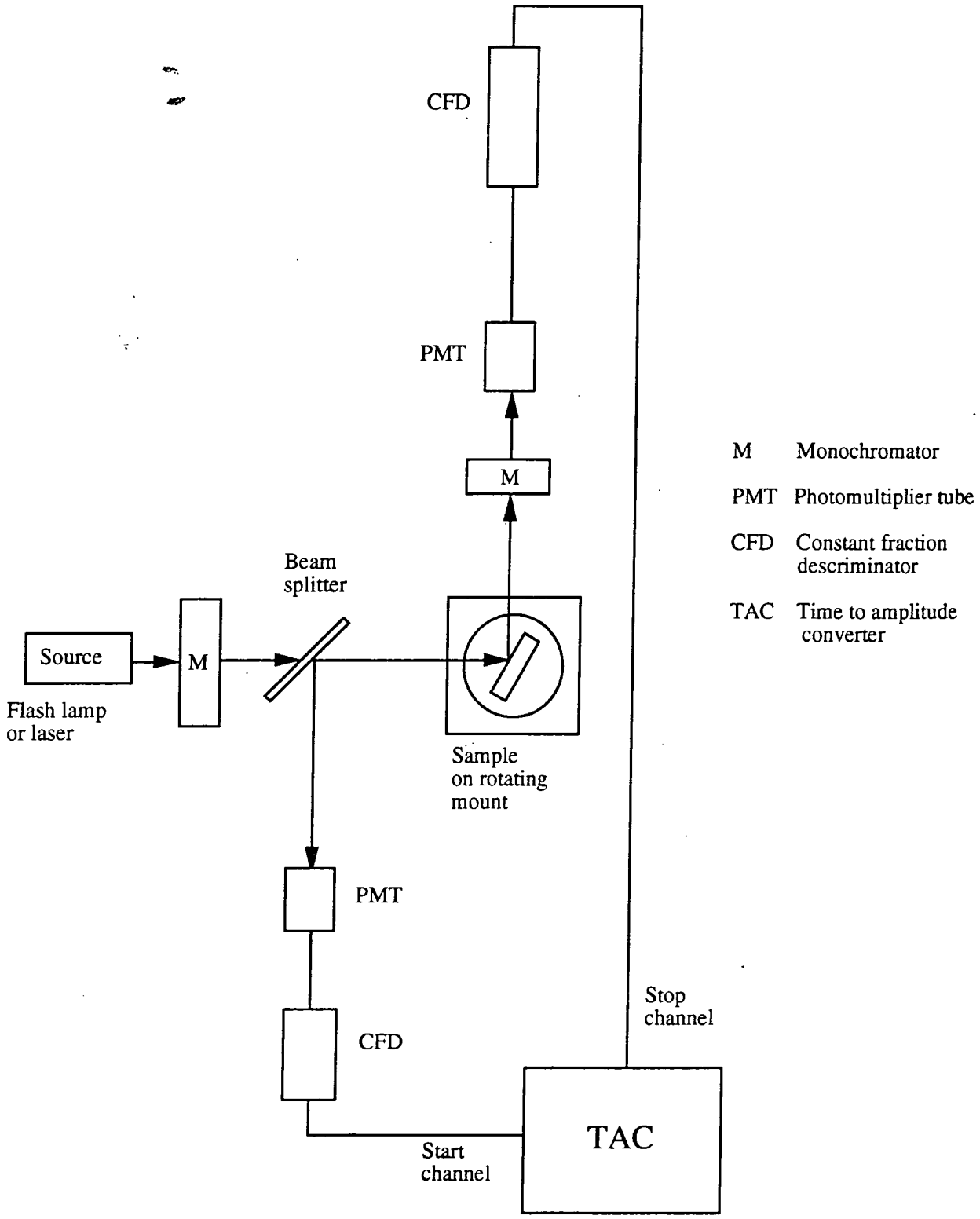

Figure 4.5 The experimental arrangement used for fluorescence spectroscopy.

The instrument used for all the measurements was a Rudolph Auto EL nulling type ellipsometer. Nulling can eliminate undesirable effects due to intensity fluctuations in the incident beam and variations in the total reflectance of the sample. It could be operated at three wavelengths: 632.8, 546.1 and 405.0 nm.

The normal procedure for measuring film thickness was to deposit films onto silicon substrates cleaned by the method stated earlier. In order to obtain an accurate measure of the film thickness a number of layers were deposited in steps on the same substrate, e.g. 20,40 and 60 layers, leaving a portion of silicon uncoated. Before a measurement of thickness could be made it was neccessary to know the substrate refractive index and absorption coefficient. These values were then used in the calculation program used to find the thickness of the overlayer.

4.4.5 Reflection high energy electron diffraction

Reflection high energy electron diffraction (RHEED) is a powerful technique for studying the surface order and arrangement of materials. The first use of electron diffraction to study a surface film was described by Davisson and Germer[26]. It was later used successfully to study LB films and has now become a standard technique[26–29]. Although it does not give as much structural information as transmission electron diffraction (TED), it has several advantages over the latter. In TED the sample and support must be thin enough for the electrons to pass through. However, films for RHEED studies may be deposited onto either glass coated with a thin metal film or silicon subsrates. It is important that the substrate is conducting as this reduces the charging of the LB layers by the electron beam. Silicon is preferred because it has a polished surface. The substrate was mounted onto the goniometer head using silver paste to create a conducting bond.

A beam of high-energy electrons incident on a surface at a grazing angle produce a diffraction pattern which is characteristic of the atomic arrangement of the surface because the component of the electrons momentum is small and is only able to penetrate a small distance. At high-energy, typically 100 KeV, the electron wavelength is small (λ=0.0037 nm), much smaller than the interplanar spacing of LB films, which is typically 6 nm, therefore no diffraction will occur. However, the long-chain fatty acid molecules are composed of C_2H_4 repeat units. Diffraction

occurs from planes of C_2H_4 subcells and gives information on close-packing of the chain.

RHEED studies were performed using a JEM 120 transmission electron microscope operated at 100 kV with the sample stage located at the top of the projection chamber. Film anisotropy could be investigated by rotating the sample so that the incident beam was parallel or perpendicular to the dipping direction.

4.4.6 Small angle X-ray diffraction

The X-ray measurements were all made by Dr.Y.Lvov at the Institute of Crystallography in Moscow. The diffractometer used was a purpose built small angle position-sensitive type (Moglievsky and Dembo 1983). The Cu Kα X-ray radiation (λ=0.154nm) was nickel filtered and collimated by a three slit collimator. Both the incident and reflected rays passed through a vacuum. The samples were slowly rotated at a speed of about 20° h^{-1} and the diffraction pattern located with the use of a position sensitive detector. The sample to detector distance was 74.0 cm giving a good angular resolution. The detector sensitivity was 0.1 mm (equivalent to an angular resolution of approximately 0.001°; assuming the diameter of the X-ray beam to be 0.04°). The measurements on one sample took approximately 4 hours (because several scans were summed). The wavelength of the Kα line is 0.15 nm so X-rays will be diffracted fom the polar planes of the fatty acids rather than the C_2H_4 subcells. The (001) reflection will have a Bragg angle $\theta < 1°$, hence the need for low-angle. The θ and ultimately the d-spacings of planes parallel to the surface can be calculated. The interplanar spacings enable the thickness of individual monolayers to be determined[30–32].

4.4.7 Surface plasmon resonance

As already explained in Chapter 2, the surface plasmons extend only a few microns from the metal surface and therefore only the immediate environment is probed. Many studies have been made on the effect of surface layers on the surface plasmons[33–36].

There are two experimental configurations which use prism coupling to create surface plasmons: the Kretschmann-Raether and the Otto, both of which have

been fully discussed in the chapter 2. All measurements made for this work used the Kretschmann-Raether configuration. The prism with sample mounted is shown in figure 4.6.

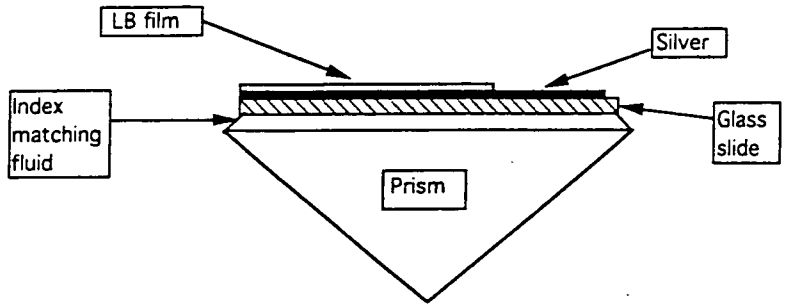

Figure 4.6 The sample arrangement for SPR using the Kretschmann-Raether configuration.

Two sets of experimental arrangements were built each with a different type of source and detector. The initial setup used a HeNe laser PMS model LSTP10 as a source, which was tunable between four wavelengths 632.8, 611.9, 594.1 and 543.5 nm. The laser was plane-polarized and had to be rotated so that the plane of polarization was parallel to the optical bench (p-polarized with respect to the prism face, E-field in the plane of incidence). The laser output was found to be sufficiently stable, thus no reference beam splitting was neccessary. All the optics were mounted on a Micro-Control optical bench and were housed in a light-tight cabinet. The rotation stage on which the prism was mounted was designed and built in Durham. The stage incorporated a detector mount driven by gearing so that it rotated by 2θ. The rotation stage was driven by a Berger Lahr 5 phase stepping motor which was reduced by a gear box (90:1) to give a minimum step of 0.008°. The stepper motor was controlled by a BBC Master computer via a

Berger Lahr D380 RDM 564/50 drive card. The detector used was a 100 mm^2 silicon photodiode with a response from 350 to 1150 nm, used in the photovoltaic mode and connected via an op-amp to a Fluke 8840A multimeter. The intelligent multimeter was connected via an IEEE interface to the BBC Master. Data obtained from this set up were transferred from floppy disc to the mainframe for plotting and analysis.

In order to study the SPR in greater detail, a second experimental setup was designed with a monochromated white light source; a schematic is shown in figure 4.7. Because of the low light levels, a chopped light system using a photo multiplier tube (PMT) had to be used. The white light source was an Oriel lamp fitted with a 100W quartz halogen bulb which was air cooled by an electric fan. The output intensity from the lamp was variable by use of a constant current supply. An Oriel 7155 filter monochromator was attached to the front of the lamp. The monochromator had a wavelength range of 400 - 700 nm, in 20 nm steps, and slit widths of 1, 2, 4 and 6 mm. The slit width was always set at 1 mm to give the greatest wavelength resolution: 10 nm (fwhm) at 400 nm; 11.4 nm (fwhm) at 550 nm; and 15 nm (fwhm) at 700 nm. The monochromated light was chopped at 1 kHz with a Rofin Sinar chopper; it then passed through some collimating optics, a polarizer to give p-polarized light and finally an aperture to give the required spot size. The prism and rotation stage were the same as before. The detector was a Hamamatsu IP28A photomultiplier tube with an extended red response and an operating range from 185 to 700 nm. The signal was converted by a current to voltage transformer and then input to an Ortec Brookdeal Lock-in-amplifier model 9501E synchronized to the chopper. The right-angled prism used measured 40 $\times$40 mm^2 with a refractive index of 1.517 (BK 7 glass), obtained from Ealing Optics. Samples consisting of LB films on silver-coated glass slides had a small drop of index matching fluid (Cargille type B) put on their unsilvered side and were brought up to the base of the prism until the immersion oil came into contact with it; the oil was then allowed to spread drawing the slide onto the prism. No clamp was used to hold the sample in position. It was just supported from beneath so that it did not slip off the prism. Before an SPR curve could be measured it was necessary to calibrate the rotation stage. The prism was cleaned with an acetone soaked tissue and with the use of the cursor controls on the keyboard, the prism was rotated so that the critical angle was roughly located. The critical angle was

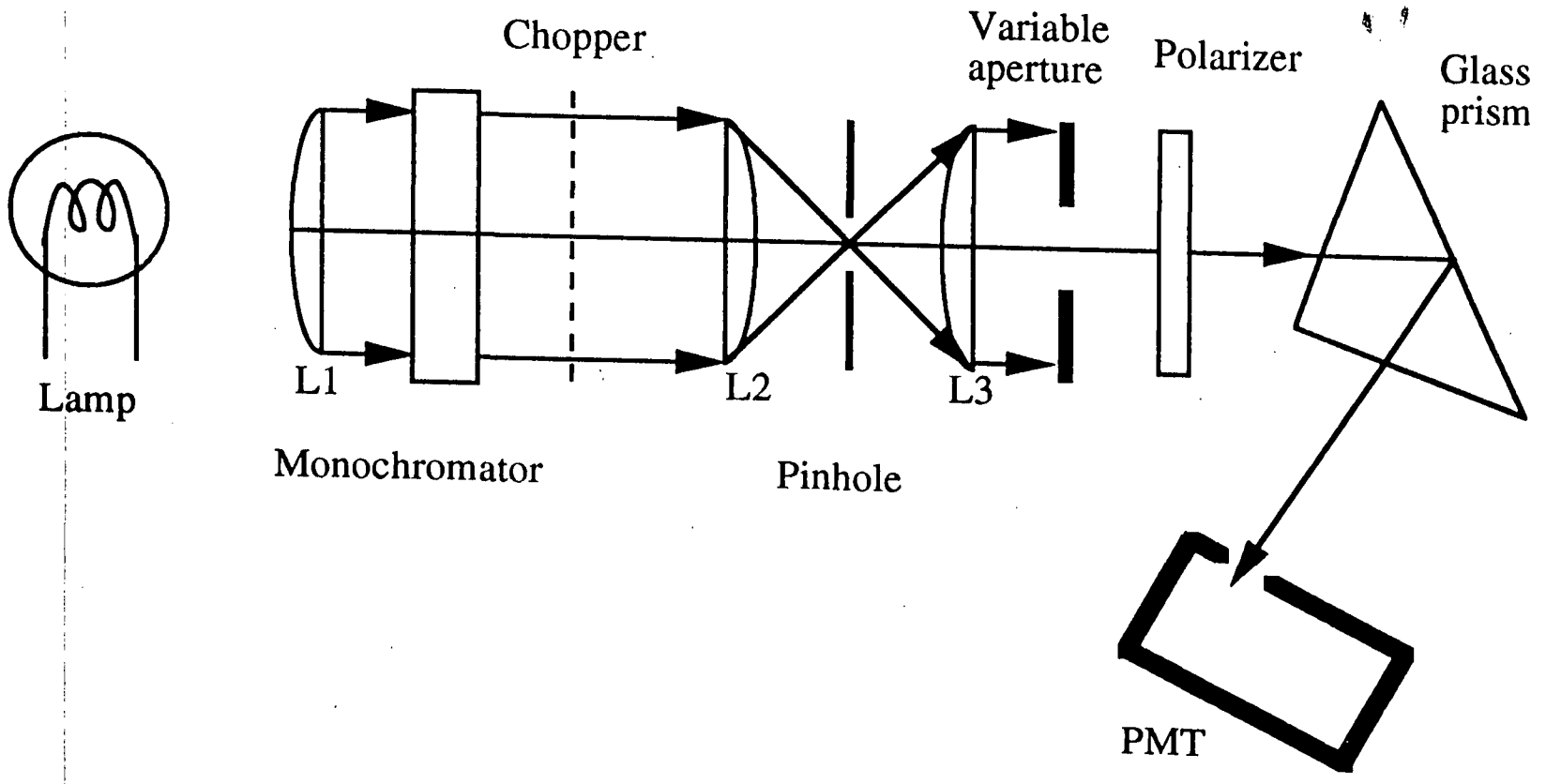

Figure 4.7 The optical set up for surface plasmon resonance wavelength scans.

then found more precisely by the program[37], which scanned an angle range to find the point where the gradient of the reflectivity dropped significantly. This position was then used as the calibration point for the angle values. The sample was then mounted and an SPR scan could be made over the angular region required. An example of this scan can be seen in figure 4.8.

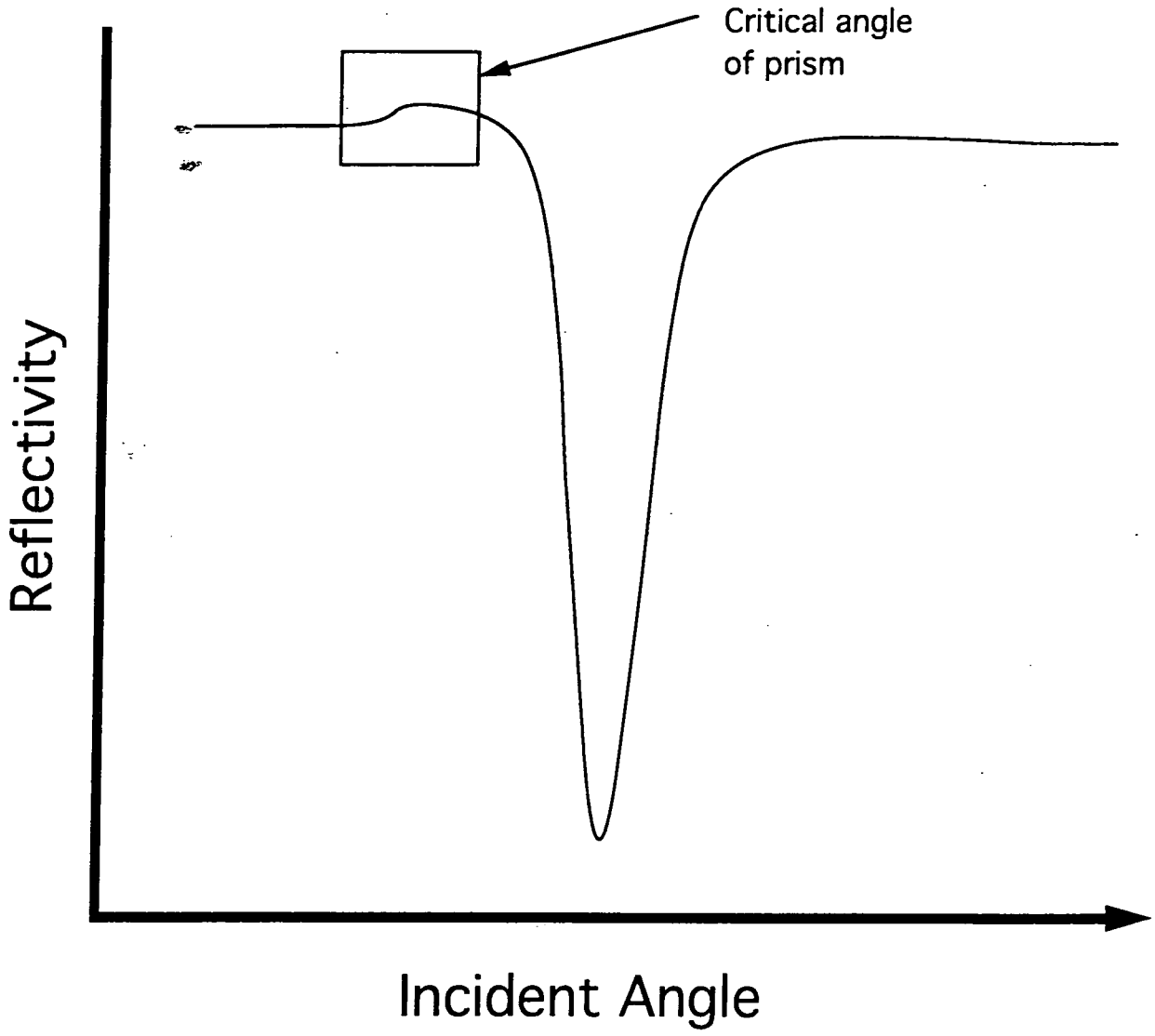

Figure 4.8 A typical surface plasmon resonance curve with the critcal angle of the prism highlighted.

4.5 References

1. D.B. Zilversmit *A method for compressing monomolecular films at oil-water interfaces* J.Colloid.Sci. Vol 18 (1963) pp794-798

2. L. Blight, C.W.N. Cumper and V. Kyte *Manipulation of insoluble films at an oil/water interface* J.Colloid.Sci. Vol 20 (1965) pp393-399

3. G.G. Roberts, W.A. Barlow and P.S. Vincett *Technological applications of Langmuir-Blodgett films* Phys. in Tech. Vol 12c (1981) pp69-74

4. J.H. Schulman, R.B. Waterhouse and J.A. Spink *Adhesion of amphiphathic molecules to solid surfaces* Kolloid Z. Vol 146 (1956) pp77-95

5. I. Langmuir and V.J Schaefer *Activities of urease and pepsin monolayers* J.Am. Chem.Soc. Vol 60 (1938) pp1351-1360

6. D. Day and J.B. Lando *Morphology of crystalline diacetylene monolayers polymerized at the gas water interface* Macromolecules Vol 13 (1980) pp1478-1483

7. G.L. Gaines *Insoluble monolayers at liquid-gas interfaces* Interscience New York (1966)

8. K.B. Blodgett *Films built by depositing successive monomolecular layers on a solid surface* J.Am.Chem.Soc. Vol 57 (1935) pp1007

9. D.S. Campbell *Mechanical properties of thin films* in *Handbook of thin film technology* Maisel L.I. and Glang R., eds. McGraw-Hill, New York, 1970 pp129

10. M. Orrit, D. Möbius, U. Lehmann and H. Meyer *Reflection and transmission of light by dye monolayers* J.Chem.Phys. Vol 85 No 9 (1986) pp4966-4979

11. H. Kuhn, D. Möbius and H. Bücher in *Physical Methods of Chemistry* edited by A. Weissberger and B. Rossiter (Wiley New York 1972) Vol 1 Part III B pp577

12. T.L. Penner and D. Möbius *The formation of mixed J-aggregates of cyanine dyes in Langmuir-Blodgett monolayers* Thin Solid Films Vol 132 (1985) pp185-192

13. T.L. Penner *Energy transfer between J-aggregate dye monolayers* Thin Solid Films Vol 160 (1988) pp241-250

14. K. Matsuki, Y. Nagahira and H. Fukutome *The absorbtion spectra of fat-soluble vitamins and the orientations of their chromophores* Bull.Chem.Soc.Jpn. Vol 53 (1980) pp1817-1824

15. J. Breton, M. Michel-Villaz, G. Paillotin and M. Vandevyerer *Application of linear dichroism to the study of the distribution of pigments in monomolecular layers* Thin Solid Films Vol 13 (1972) pp351-357

16. H. Kuhn, D. Möbius and H. Bücher in *Physical Methods of Chemistry* edited by A. Weisberger and B. Rossiter (Wiley New York 1972) Vol 1 Part III B p588

17. K. Saito, K. Ikegami, S. Kuroda, M. Saito, Y. Tabe, and M. Sugi *Davydov splitting in arachidic acid-cyanine dye complex Langmuir-Blodgett films* J.Appl.Phys. Vol 68 (1990) pp1968-1974

18. H. Bücher, K.H. Drexhage, M. Fleck, H. Kuhn, D. Möbius, F.P. Schäfer, J. Sondermann, W. Sperling, P. Tillmann and J. Wiegand *Controlled transfer of excitation energy through thin layers* Molecular Crystals Vol 2 (1967) pp199-230

19. T. Yamazaki, N. Tamai and I. Yamazaki *Molecular association of pyrene in Langmuir-Blodgett monolayer film: analysis of picosecond time-resolved fluorescence spectra* Chem.Phys.Lett. Vol 124 (1986) pp326-330

20. M. Van der Auweraer, B. Vershuere and F.C. Schryver *Absorption and fluorescence properties of Rhodamine B derivatives forming Langmuir-Blodgett films* Langmuir 4 (1988) pp583-588

21. A. Leitner, M.E. Lippitsch, S. Draxler, M. Riegler and F.R. Aussenegg *Energy transfer of dyes in Langmuir-Blodgett monolayers studied by picosecond time-resolved fluorimetry* Thin Solid Films Vol 132 (1985) pp55-62

22. D. den Engelsen *Ellipsometry of anisotropic films* J.Opt.Soc.Am. Vol 61 (1971) pp1460-1466

23. I.R. Peterson, J.D. Earls, W.L. Barnes and I.R. Girling *Orientational inhomogeneity and scattering in Langmuir-Blodgett films of 22-tricosenoic acid* J.Phys.D:Applied.Phys Vol 21 pp (1988) pp773-779

24. H. Arwin and D.E. Aspnes *Determination of optical properties of thin organic films by spectroellipsometry* Thin Solid Films Vol 138 (1986) pp195-207

25. R. Steiger *Studies of oriented monolayers on solid surfaces by ellipsometry* Helvetica Chimica Acta Vol 54 (1971) pp282-283

26. L.H. Germer and K.H. Storks. *Arrangement of molecules in a single layer and in multiple layers* J.Chem.Phys. Vol 6 (1938) pp280-293

27. C.A. Jones, G.J. Russell, M.C. Petty and G.G. Roberts *A reflection high-energy electron diffraction study of ultra-thin Langmuir-Blodgett films of ω-tricosenoic acid* Phil.Mag.B Vol 54 No 3 (1986) L89-L94

28. A. Bonnerot, P.A. Chollet, H. Frisby and M. Hoclet *Infrared and electron diffraction studies of transient stages in very thin Langmuir-Blodgett films* Chem.Phys. Vol 97 (1985) pp365-377

29. D.B. Neal, G.J. Russell, M.C. Petty, G.G. Roberts, M.M. Ahmed and W.J. Feast *A highly ordered Langmuir-Blodgett monolayer of an amido nitrostilbene* J.Mol.Elec. Vol 2 (1986) pp135-138

30. Y.M. Lvov, D. Svergun, L.A. Feigin, C. Pearson and M.C. Petty *Small angle X-ray analysis of alternate-layer Langmuir-Blodgett films* Phil.Mag.Lett. Vol 59 (1989) pp317-323

31. M. Pomerantz and A. Segmüller *High resolution X-ray diffraction from small numbers of Langmuir-Blodgett layers of manganese stearate* Thin Solid Films Vol 68 (1980) pp33-45

32. B. Belbeoch, M. Roulliay and M. Tournarie *Evidence of chain interdigitation in Langmuir-Blodgett films* Thin Solid Films Vol 134 (1985) pp89-99

33. B. Liedberg, C. Nylander and I. Lundström *Surface plasmon resonance for gas detection and biosensing* Sensors and Actuators Vol 4 (1983) pp299-304

34. G. Wähling, H. Raether and D. Möbius *Studies of organic monolayers on thin silver films using the attenuated total reflection method* Thin Solid Films 58 (1979) pp391-395

35. I. Pockrand, A. Brillante and D. Möbius *Nonradiative decay of excited molecules near a metal surface* Chem. Phys. Lett. Vol 69 pp499-504

36. J.G. Gordon and J.D. Swalen *The effect of thin organic films on the surface plasma resonance on gold* Optics Communications Vol 22 pp374-376

37. N. Kalita *The Pockels Effect in Langmuir Blodgett Films* Ph.D. Thesis (1991) University of Durham

38. A.M. Bibo, C.M. Knobler and I.R. Peterson *A monolayer phase miscibility comparison of long-chain fatty acids and their ethyl esters* J.Phys.Chem. Vol 95 (1991) pp5591-5599

Chapter V

Structural and Optical Properties of Organic Dyes in Langmuir-Blodgett Films

5.1 Introduction

A variety of dye materials are studied in this chapter and a brief description of the different compounds is given in section 5.2. Their ability to form LB films is determined from pressure versus area isotherm measurements in section 5.3 and their possible orientation on the surface is discussed. The optical absorption of the dyes in solution, cast and LB film form (section 5.4) are also examined. The fluorescence spectrum of perylene is investigated in section 5.6. Polarized absorption spectroscopy is used in section 5.5 to find if there is any preferential orientation of chromophores in the films. Ellipsometry (section 5.7) and X-ray low angle diffraction (section 5.8) measurements provide further information on this aspect of the films. Electron diffraction studies described in section 5.9 are used to show the crystalline nature of films. Finally a summary of this work is made in section 5.10.

5.2 Materials

5.2.1 Requirements of a material

Since the object of this work is to look at the interactions between organic dye molecules deposited by the LB technique and surface plasmons, materials were selected using several criteria. Firstly, they had to form a good floating layer on the subphase and readily deposit onto a variety of substrates forming multilayer assemblies of high quality; it was also necessary for them to have absorption bands in the visible which were sharp and intense. Materials with strong fluorescence were also selected.

Many dyes have been studied in the form of thin films. For example: phthalocyanines[1,2]; porphyrins[3,4]; aromatic hydrocarbons[5,6]; cyanines[7,8] and squaraines[9,10].

These have been produced by evaporation, polymer doping and by the LB technique.

The materials studied here can be divided into four groups

i) Phthalocyanines and porphyrins - macrocyclic molecules

ii) Perylene - an aromatic hydrocarbon

iii) Sq materials - derivatives of squaraine

iv) S120 - a cyanine dye

5.2.2 Phthalocyanines and porphyrins

These two groups of macrocyclic molecules have been the subject of much interest (in particular the phthalocyanines) owing to their stability. They have some of the highest extinction coefficients and are extensively used in the dye industry. Many biological substances, such as haemoglobin and chlorophyll have porphyrin structures.

The materials studied were provided by Dr Alexei Vitukhnovsky of the P.N. Lebedev Physical Institute, Academy of Sciences of Russia. Materials similar to these have been shown to form good LB films. Furthermore, these are stable dyes with strong absorption in the visible.

The compounds studied (shown in figure 5.1) are as follows:-

PP1 Protoporphyrin

PP3 Tetra-phenyl-porphyrin

PP4 Zn-tetra-phenyl-porphyrin

PP6 Ga-tetra-4-tert-butyl-phthalocyanine

PP7 Ho-tetra-4-tert-butyl-phthalocyanine

5.2.3 Squaraine materials

Squaraine is the generic name for 1,3-derivatives of squaric acid. They can be

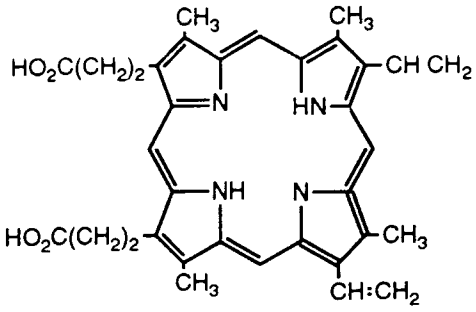

Proto Porphyrin

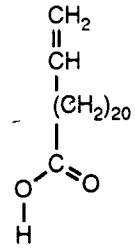

22TA

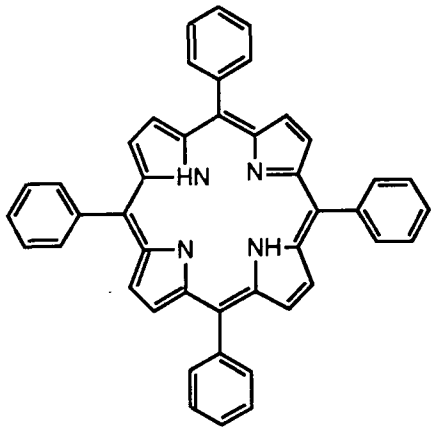

5,10,15,20-Tetra-Phenyl-Porphyrin

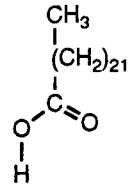

TA

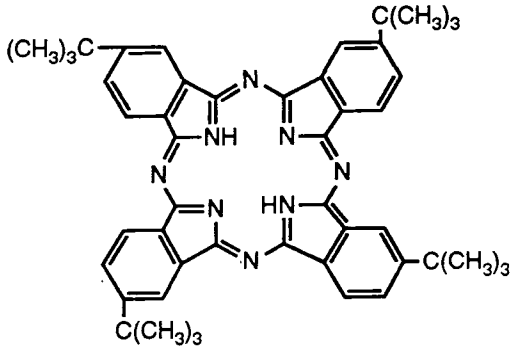

Phthalocyanine

Figure 5.1 The molecular structure of macrocyclic molecules and TA and 22TA.

broadly divided into two groups, depending on the nature of the 1,3-substituents, to form symmetrical or unsymmetrical squaraines. There are many publications concerning evaporated (and some on LB deposited) films of squaraines for electrographic processes[38], solar-cells[39,40], photovoltaic cells[41] and optical storage[10].

The dyes are strong absorbers in the visible, with oscillator strengths in excess of unity and readily form aggregates. The sharp absorption bands in solution are usually in the region 620-670 nm. One report has been made of them forming J-aggregates in LB films[26]. The squaraine compounds structures are shown in figure 5.2. The materials Sq1 and bis 4-(4-chlorophenylmethyl)methylaminophenyl squaraine (referred to here as Sq2) were obtained from J.Sharp and R.Burt from the Xerox Corporation, Canada and (4-(3-(4-(N-Ethyl-N-octadecylamino)-2-hydroxyl phenyl) -2-hydroxy-4-oxo-2-cyclobutene-1-ylidene)-3-hydroxy-2, 5-cyclohexadiene-1-ylidene)-N-ethyl-N-octadecylammonium hydroxide (referred to here as Sq3) was purchased from Japanese Research Institute for Photosensitizing Dyes Co. Ltd. Sq1 and Sq3 are unsymmetrical squaraines whilst Sq2 is symmetrical. All the squaraine materials were used as bought, without any further purification.

5.2.4 Perylene

Very few publications exist concerning perylene in LB films[11,12], although some optical and structural studies have been made of vacuum-evaporated perylene films[13,14] and the spectroscopic properties of solutions[15], solvent glasses[16] and solids[17,18] have been extensively reported. The structure of perylene is shown in figure 5.2. Perylene fluoresces very strongly under white light and was the first dye to be selected for use in dye lasers. However, it was found to be unsatisfactory owing to its triplet-triplet quenching. The material used in this work was obtained from the Aldrich Chemical Company and was used without further treatment.

5.2.5 S120

Extensive studies have been made on cyanine dyes and they have been found to form a number of different aggregates for example: Scheibe or J aggregates, H and H* aggregates[19,20]. The material used in this work 1-octadecyl-1′-methyl-2,2′ cyanine perchlorate referred to as S120, and was obtained from Dr Dietmar

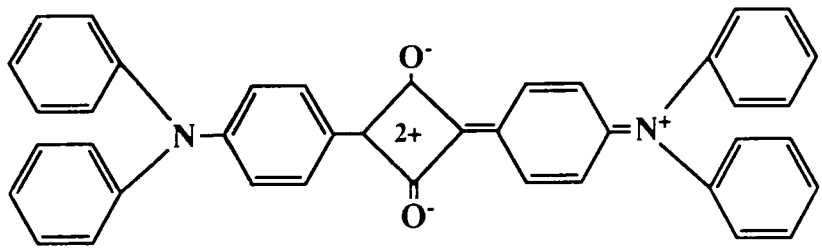

Sq1

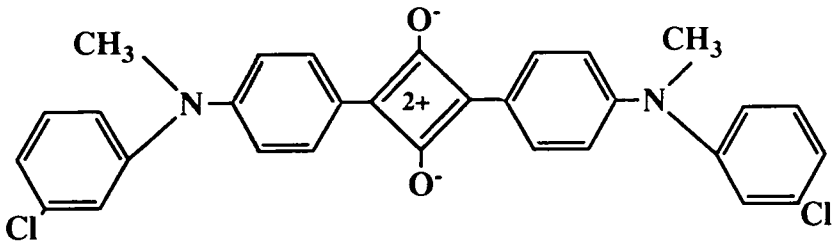

Sq2

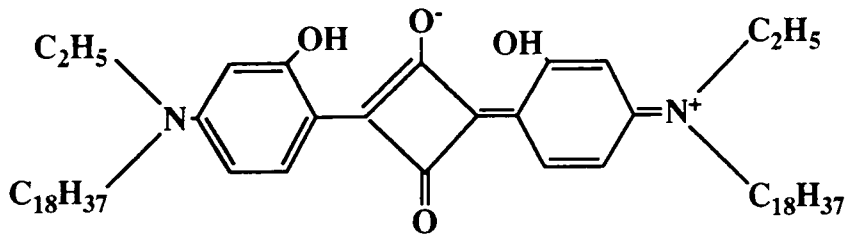

Sq3

S120

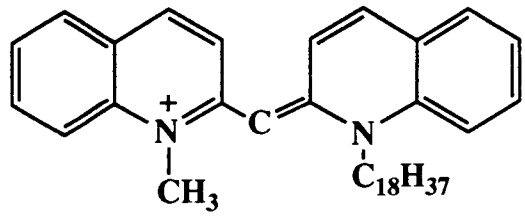

Perylene

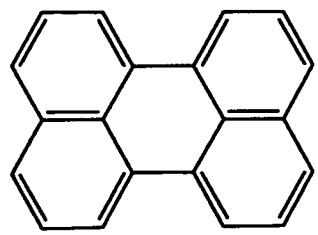

Figure 5.2 The molecular structure of S120, perylene and squaraines.

Möbius, Max-Planck-Instituit für Biophysikalishe Chemie, Göttingen, Germany. The structure of S120 is shown in figure 5.2.

5.3 Isotherms and Film Deposition

The area per molecule can be used to indicate the possible orientation of molecules on the water surface and hence the ability of a material to form a monolayer. The area per molecule can be determined at different points of the pressure versus area isotherm. The two areas which are most often quoted are at the point of collapse a_m^c and the area determined by extrapolating back to zero pressure from the steepest part of the isotherm a_m^0; the latter is the most commonly quoted and will be the only one referred to in this work.

Errors in the average area per molecule are due to many causes: inaccuracies in the concentration of material, quantity of material spread on the surface and area of the surface.

5.3.1 Porphyrins and phthalocyanines

The isotherms of these materials (figure 5.3) were relatively condensed and did not exhibit any distinct phase changes. The a_m^0 calculated for each material are shown in table 5.1.

Material	a_m^0 (nm^2)	Comments
PP1	0.480	
PP3	0.038	Islands Formed
PP4	0.190	Yellow Islands Formed
PP6	0.500	No Islands
PP7	0.476	No Islands

Table 5.1 Area per molecule for phthalocyanines and porphyrins.

The values obtained for PP3 and PP4 were much smaller than expected from known dimensions of similar molecules which suggests that these materials do not form monolayers. For example, the dimensions for substituted Si phthalocyanine were reported by Hua et al[21] to be 1.38 nm×1.38 nm× 0.45 nm, giving the edge

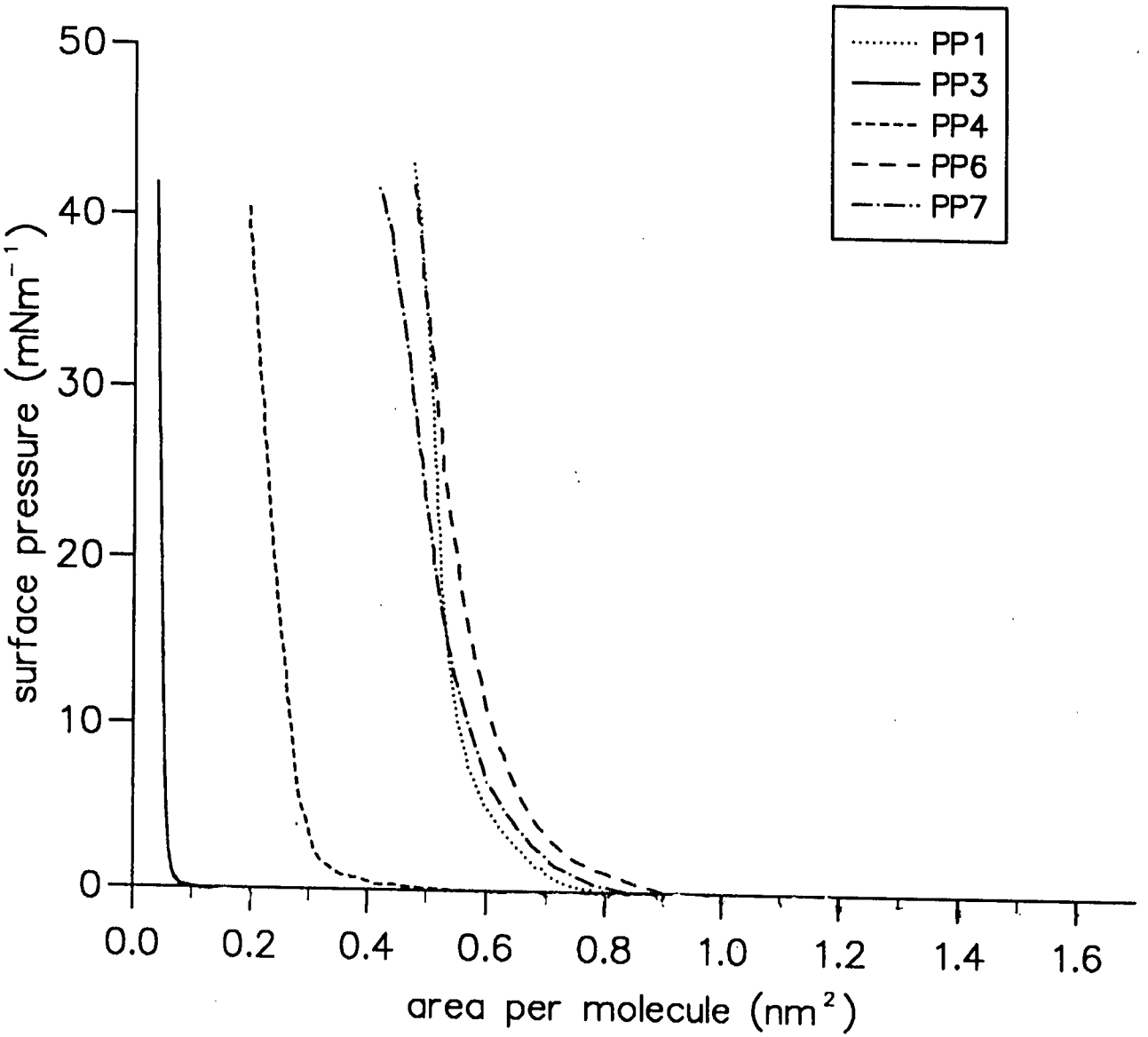

Figure 5.3 Pressure area isotherms of porphyrin and phthalocyanine materials: PP1, PP3, PP4, PP6 and PP7.

of the molecule an area of 0.62 nm^2 and the face an area of 1.9 nm^2. This would suggest that if monolayers were formed, the only orientation of the molecules possible would be on their edges. Visual inspection of the spread films revealed the presence of islands of material, confirming the assumption that monolayers were not formed. It is therefore likely that bilayers or multilayers occur as has been reported by Baker[1]. All the floating layers were stable; however, some became rigid and could not be transferred onto a substrate.

5.3.2 Perylene

A solution of perylene in chloroform formed a film on the surface which had islands. On compression, a steep expanded type isotherm (figure 5.4a) was recorded. The a_m^0 is found to be 0.021 nm^2, which is less than any areas obtained from a space filling model, therefore a monolayer is not formed. If the material was compressed and controlled, it was found not to be stable and collapse occurred. Thus the perylene is either dissolving into the subphase or it piling up on the water surface (i.e. forming multilayers). The latter is the most likely since perylene crystals are found to be insoluble in water.

In order to obtain a stable film that could be transferred to substrates, perylene was mixed with tricosanoic acid (TA) to form films with steep condensed isotherms. The molar mixing ratio of perylene to tricosanoic acid was varied and a series of isotherms were obtained (figures 5.4a and 5.4b). All the isotherms are steep and some exhibit the phase changes characteristic of TA. The a_m^0 was obtained by extrapolation from the pressure area isotherm for each mixture. It was assumed that all the TA molecules were in contact with the subphase and occupied the same a_m^0 that they would if it was a pure TA film, i.e. 0.20 nm^2. Using the equation

$$a_m^0(mixture) = \frac{a_m^0(TA) \times N_{ta} + a_m^0(dye) \times N_{dye}}{N_{ta} + N_{dye}}$$

where N_{dye} and N_{ta} are the numbers of each molecule on the surface, the a_m^0 was calculated for perylene only and the values for different mixtures are shown in table 5.2. A similar procedure was adopted by Neal[22] and Matsumoto et al[23] to determine the area per molecule in a mixed film.

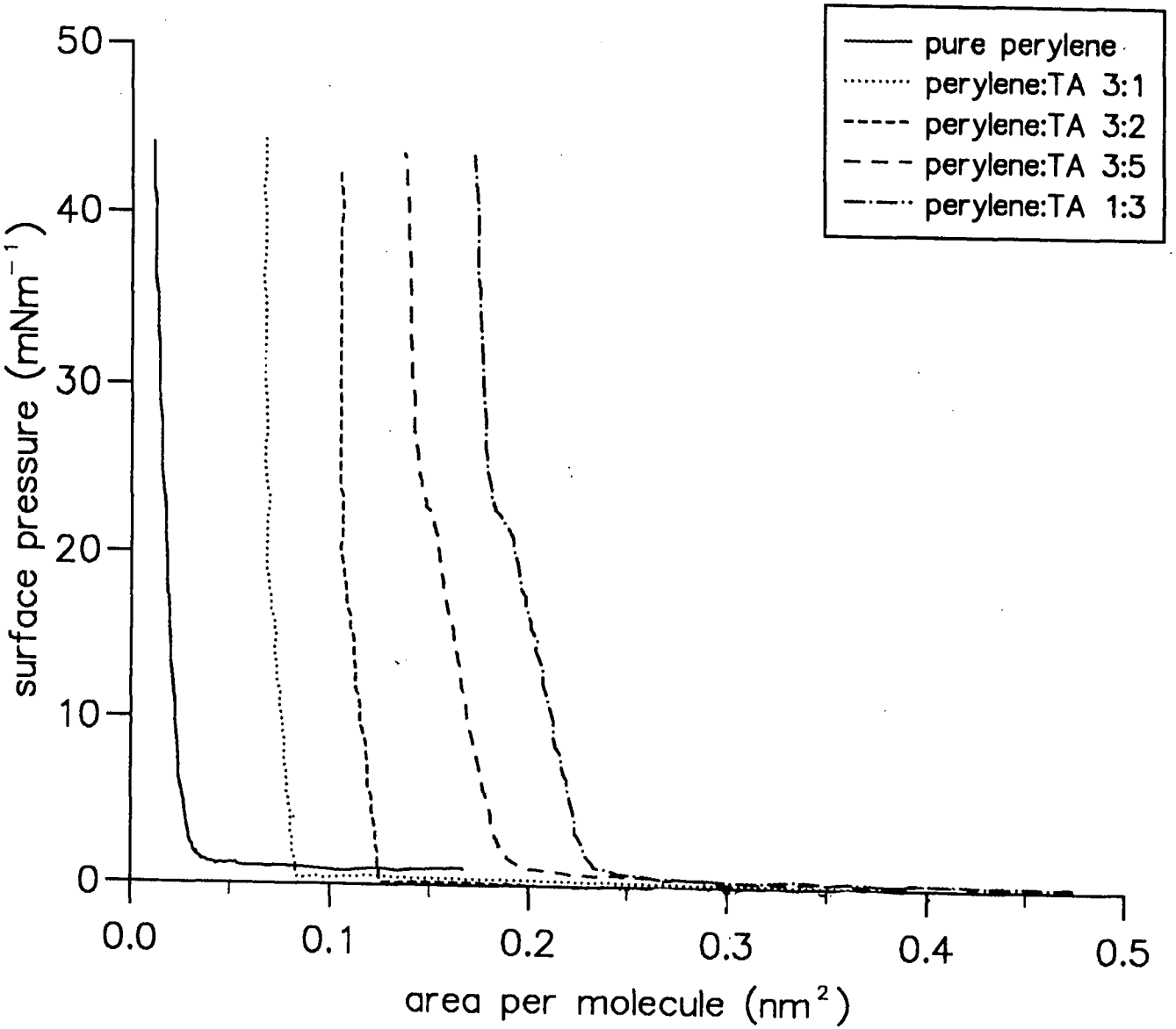

Figure 5.4a Pressure area isotherms of perylene mixed with TA, at different molar ratios.

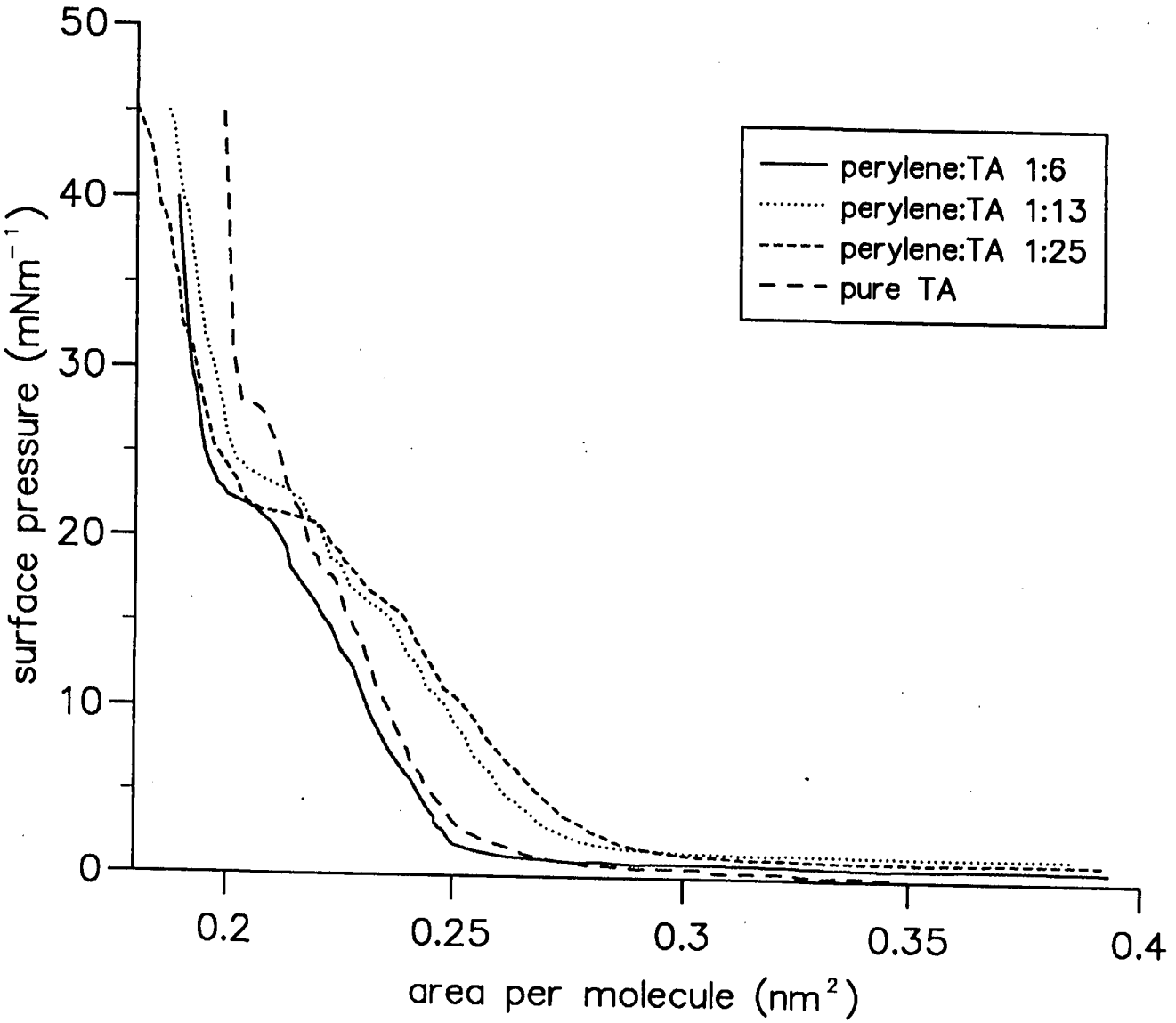

Figure 5.4b Pressure area isotherms of perylene mixed with TA at different molar ratios.

Molar ratio of perylene:TA	a_m^0 (nm^2) of mixture	a_m^0 (nm^2) of perylene
1:25	0.210	0.210
1:13	0.210	0.210
1:6	0.200	0.135
1:3	0.184	0.101
3:4	0.150	0.072
3:2	0.100	0.029
3:1	0.067	0.021
pure	0.021	0.021

Table 5.2 a_m^0 for perylene:TA and perylene only.

From the space filling model a value of 0.29 nm^2 was obtained for the area of the shortest edge. It was therefore conceivable that at molar ratios of 1:13 and 1:26 the perylene molecules stand on their shortest edge of the perylene molecule. The results show that, on increasing the molar ratio of perylene, the area occupied per molecule decreases. The inference is that the perylene molecules become stacked, possibly on top of the TA monolayer. The a_m^0 for perylene at a ratio of 3:1 is the same as in the pure film; this may imply that islands of pure dye are formed. It is very difficult to elucidate the exact orientation of the perylene in the film from isotherm measurements alone. However, it seems clear that some of the molecules are in contact with the surface and are not squeezed out as reported by Steiger[11], who found that on mixing perylene with arachidic acid (AA), the value of a_m^0 for the mixture to be the same as that for AA. A 'squeezing out' mechanism has also been proposed by Matsumoto et al[23] to account for the behaviour of a squaraine in a mixed film.

5.3.3 S120

The isotherm obtained for S120 (figure 5.5) was steep but no phase changes were evident. The average area per molecule was calculated to be 0.68 nm^2. The dimensions reported by Bücher and Kuhn[24] for a similar cyanine molecule are 1.55 nm× 0.6 nm×0.4 nm, which gives a value of 0.62 nm^2 for the area of the long

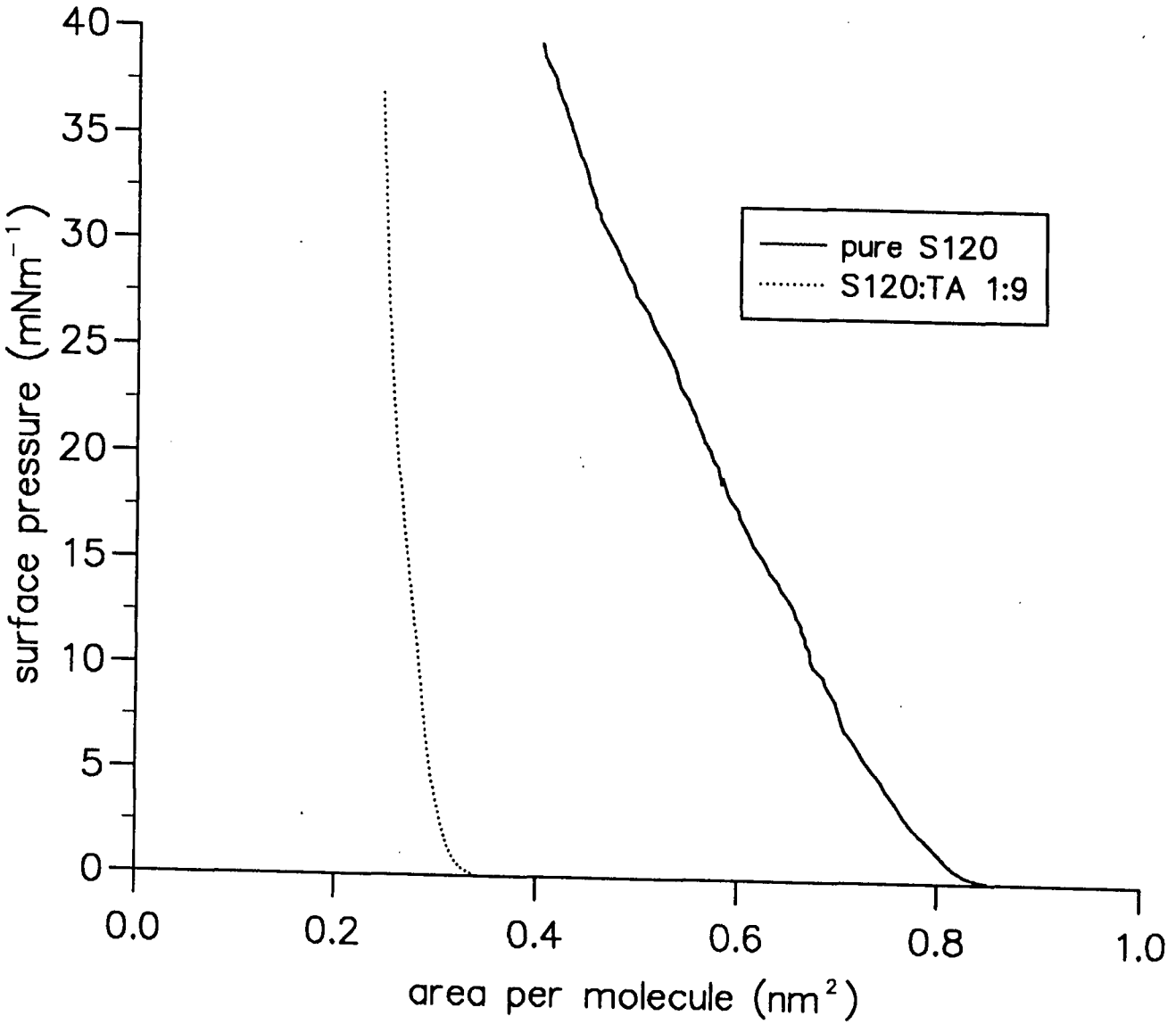

Figure 5.5 Pressure area isotherms of S120 pure and mixed with TA.

edge of the molecule. The value of 0.68 nm^2, from the isotherm, could therefore correspond to the molecules being arranged on their longest edges on the water surface. This would be consistent with reports of a "brickstone work" structure, as suggested by Bücher and Kuhn[24], and Nolte[25] to describe the J-aggregates formed by some cyanine dyes.

S120 was mixed with TA to a molar ratio of 1:9. The isotherm (figure 5.5) was very similar to that for pure S120. However, the characteristic phase changes of the TA were visible. The average area per dye molecule was calculated to be 0.69 nm^2, not very different from that for pure dye, and indicating that the inclusion of TA has little effect on the orientation of the S120 molecules.

5.3.4 Squaraine materials

Figure 5.6 shows a series of Sq1 isotherms for different molar mixtures of Sq1 and TA. The isotherm of pure Sq1 has some interesting features. On compression a condensed region is obtained below 10 mNm^{-1}, but compressing beyond this point results in an apparent collapse of the film, with the surface pressure dropping to approximately 7.5 mNm^{-1}. Further compression results in the gradual increase in surface pressure and a second condensed region is attained beyond 10 mNm^{-1}.

Similar behaviour has been reported for a variety of squaraine derivatives by Kim et al[26] (with a transition pressure at 20 mNm^{-1}), Matsumoto et al[23] (30 mNm^{-1}) and Law and Chen[27] (10 mNm^{-1}).

The average area per molecule, calculated from the limiting area in the first condensed region, is 1.2 nm^2 whilst above 10 mNm^{-1}, in the second condensed region, the area per molecule is 0.58 nm^2. The molecules are assumed to be rectangular in shape and the dimensions for similar squaraine molecules from the literature range from 1.7 nm× 0.7 nm×0.35 nm (Law and Chen[27]) to 1.9 nm× 0.8 nm×0.4 nm (Kim et al[26]); using these dimensions areas can be calculated for the face of the molecules to give 1.2 nm^2 or 1.52 nm^2 and for the long edge 0.59 nm^2 or 0.76 nm^2. It is possible that the a_m^0 of 1.2 nm^2 corresponds to the largest face of the molecule and the a_m^0 of 0.59 nm^2 to the edge. The molecule could therefore lie with its face on the subphase initially and on compression might rotate onto its edge. However, the a_m^0, which is assumed to correspond to an 'edge' area, is also

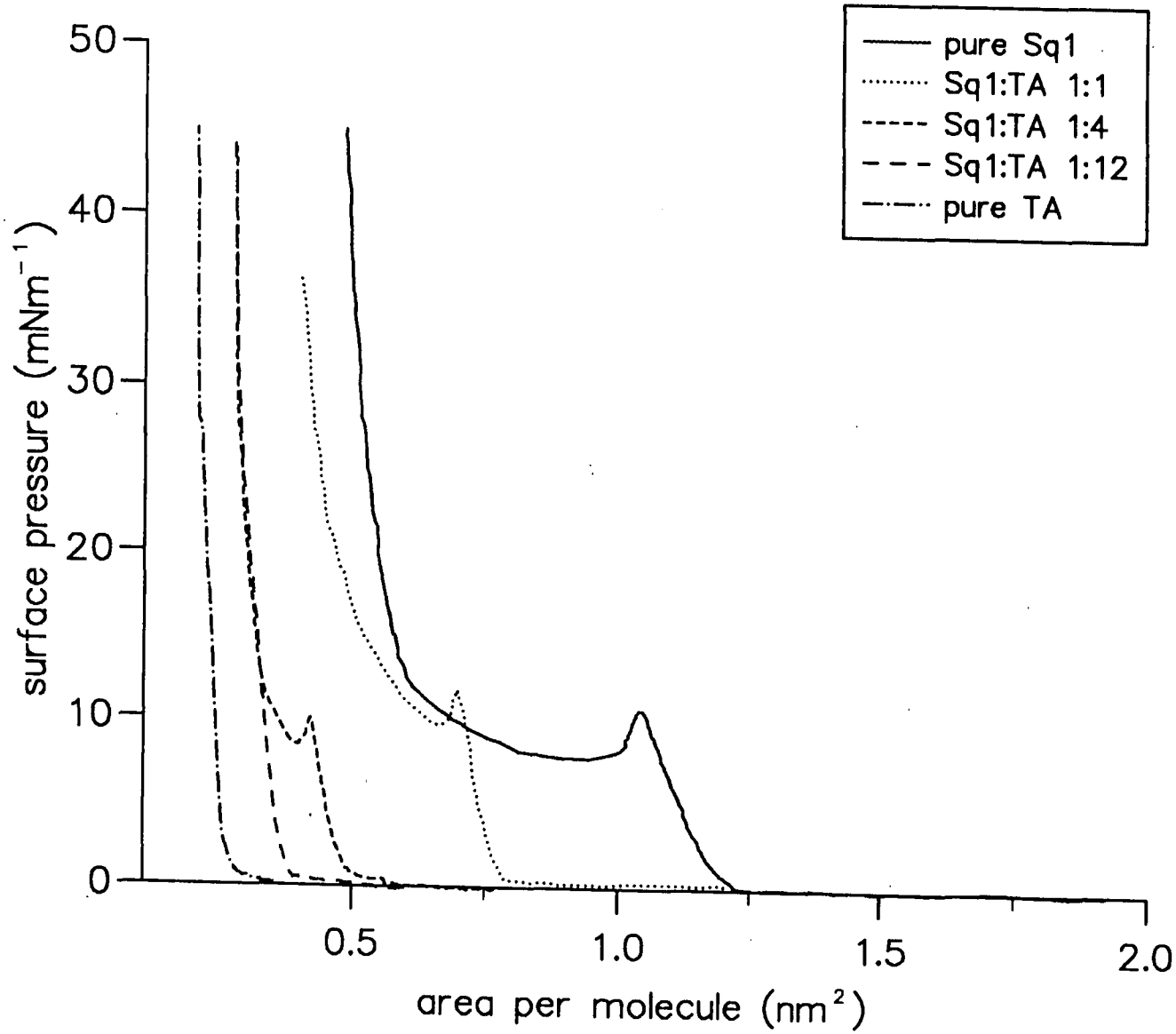

Figure 5.6 Pressure area isotherms of Sq1 pure and mixed with TA.

half that of a face area; therefore it is equally possible that the molecules slip onto each other to form a bilayer. Kim et al[26] and Matsumoto et al[23] suggested that initially the molecules were on their edges. On compression, the former workers reported stacking within the fatty acid matrix whilst the latter group proposed that the squaraine molecules were squeezed out onto the surface of the fatty acid layers. Law and Chen[27] reported a squaraine derivative (TSSQ) which initially lay flat on the surface and beyond the transition pressure it tilted or stacked.

On mixing with TA similar isotherms were obtained for 1:1 and 1:4 ratios; however, the a_m^0 values obtained are different (table 5.3) . These may be due to errors in the calculations or slightly different tilting of the molecules. When the dye concentration was decreased to 1:12 no phase change was observed in the pressure versus area isotherm and the a_m^0 is 1.14 nm^2; this implies that no rearrangement of the dye molecules takes place in the film. There is no evidence to suggest that squeezing out is taking place in these mixed films.

Mixture of Sq1:TA	a_m^0 (nm^2) low pressure region	a_m^0 (nm^2) high pressure region
1:1	1.32	0.71
1:4	1.56	0.56
1:12		1.14

Table 5.3 Sq1 a_m^0 in mixed film.

Isotherms of Sq2 (figure 5.7) show none of the features of Sq1 and the a_m^0 is 0.24 nm^2. This value is very small and could conceivably correspond to the end face of the molecule. However, the existence of islands when the material was spread would seem to preclude the formation of a monolayer. Mixing with TA to a ratio of 1:3 Sq2:TA yields an a_m^0 of 0.25 nm^2. The molecules may be end on or piled into a multilayer on the surface. Increasing the amount of TA in the mixture did not change the area per molecule of the Sq2, indicating that the orientation of the dye molecules does not alter.

The isotherm of pure Sq3 in figure 5.8 exhibits similar features to Sq1. However, the phase change occurs at a higher pressure (24 mNm^{-1}) and only falls to 23 mNm^{-1}. The a_m^0 below the transition pressure is 1.21 nm^2 and 0.68 nm^2

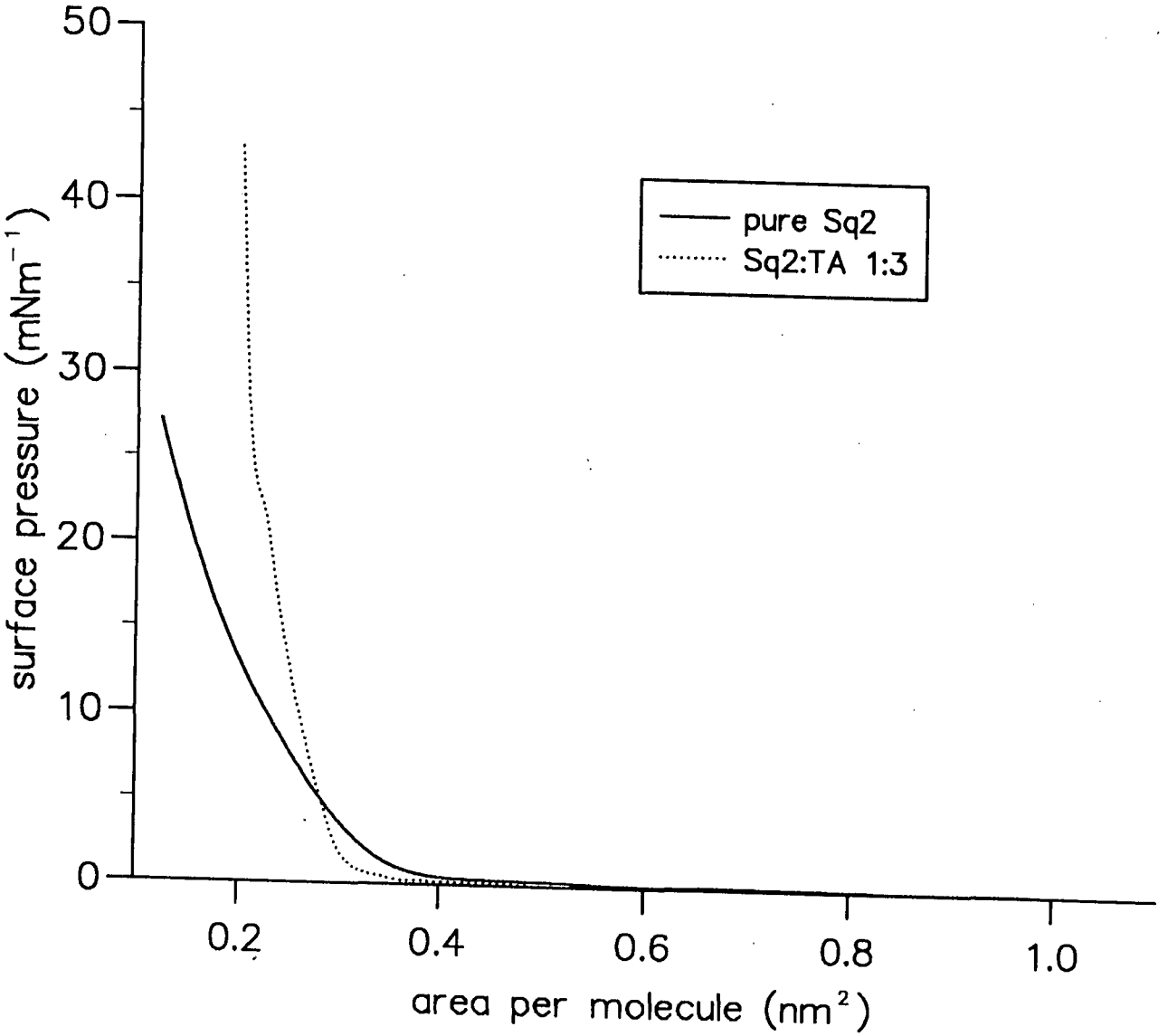

Figure 5.7 Pressure area isotherms of Sq2 pure and mixed with TA.

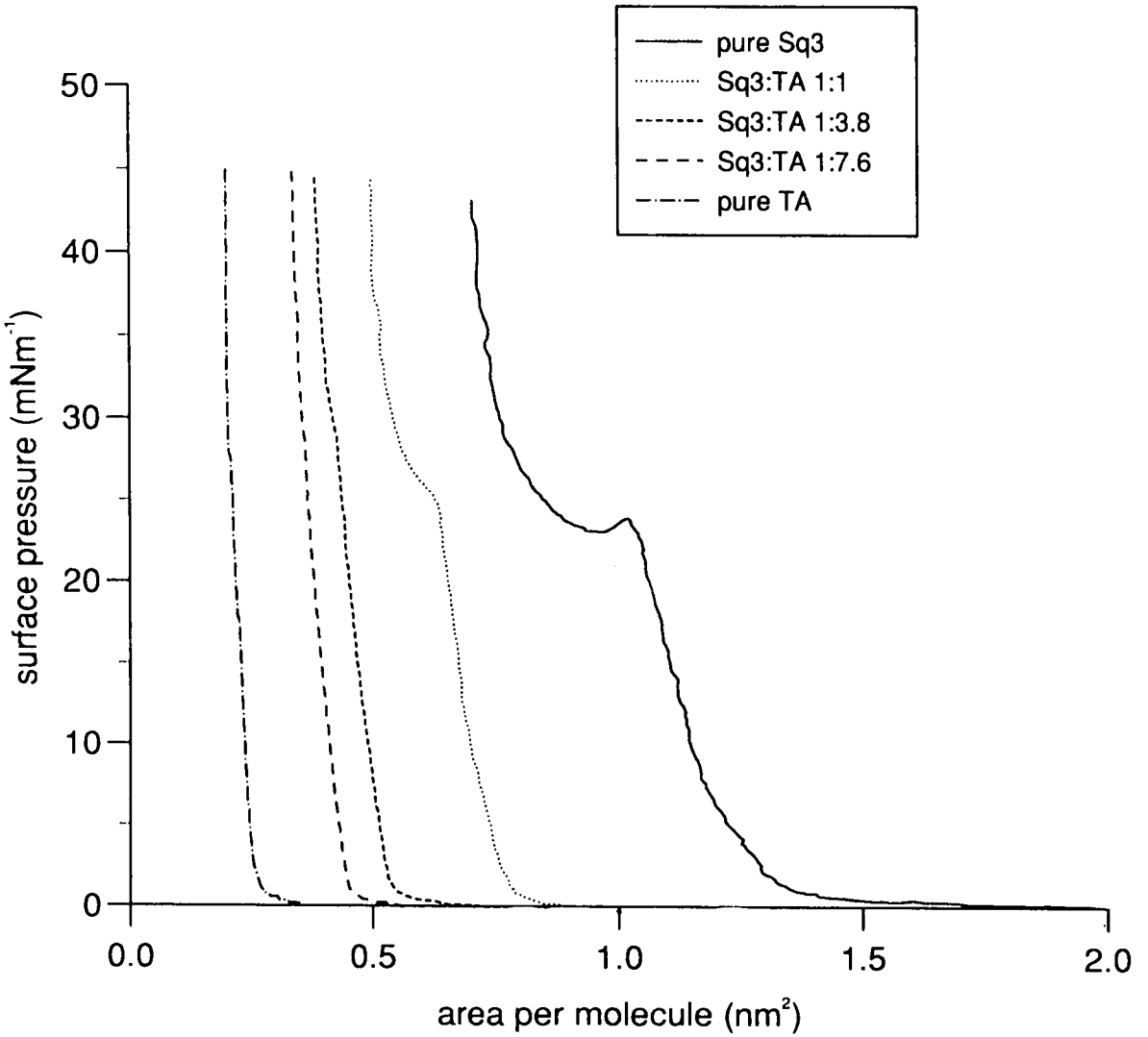

Figure 5.8 Pressure area isotherms of Sq3 pure and mixed with TA.

above. These values are very similar to those obtained for Sq1 and imply that a similar rearrangement of the molecules on the surface is occurring. Although both molecules are unsymmetrical squaraines, Sq3 has long alkyl chains attached which one would expect to reduce the mobility of the molecules. This difference may account for the high transition pressure (24 mNm^{-1}) observed for the Sq3 molecules.

Mixing with TA to a ratio of 1:1 gives an isotherm with a less pronounced phase change at 25 mNm^{-1}, the a_m^0 values for the two condensed regions are 1.25 nm^2 and 0.83 nm^2. Further dilution of the Sq3 results in a loss of the inflexion at 25 mNm^{-1}. At a ratio of 1:3.8 Sq3:TA, the a_m^0 is 1.2 nm^2, increasing to 1.38 nm^2 for a molar ratio of 1:7.6 Sq3:TA. Since a value for the area per molecule is obtained which corresponds to one of the faces of Sq3, it can be assumed that squeezing out is not occurring, but it is difficult to ascertain exactly how the molecules are organized. The a_m^0 in the first condensed region of the pure and 1:1 films of 1.25 nm^2 may correspond to the face of the molecule as for Sq1 and compression might result in tilting or stacking. Mixing with TA has a very noticeable effect on this rearrangement. When the molar ratio of Sq3:TA becomes small, the phase change vanishes, indicating that the dye molecules become separated and can no longer interact. It is assumed that the Sq molecules remain rigid and do not bend or twist.

5.4 Optical Absorption of Solution, Cast and LB Films

All the materials were found to be readily soluble in chloroform and solutions of the materials were made in 10 ml flasks. These solutions typically had to be diluted a thousand times (10^{-6} molar) in order for the absorption to be measured in the spectrophotometer. Concentrated solutions were also spread with a syringe onto an hydrophilic slide to form a cast film.

Materials were deposited both as pure films and mixed with TA onto glass or quartz slides.

5.4.1 Porphyrins and phthalocyanines

Solution spectra for these materials are shown in figures 5.9-5.11. The por-

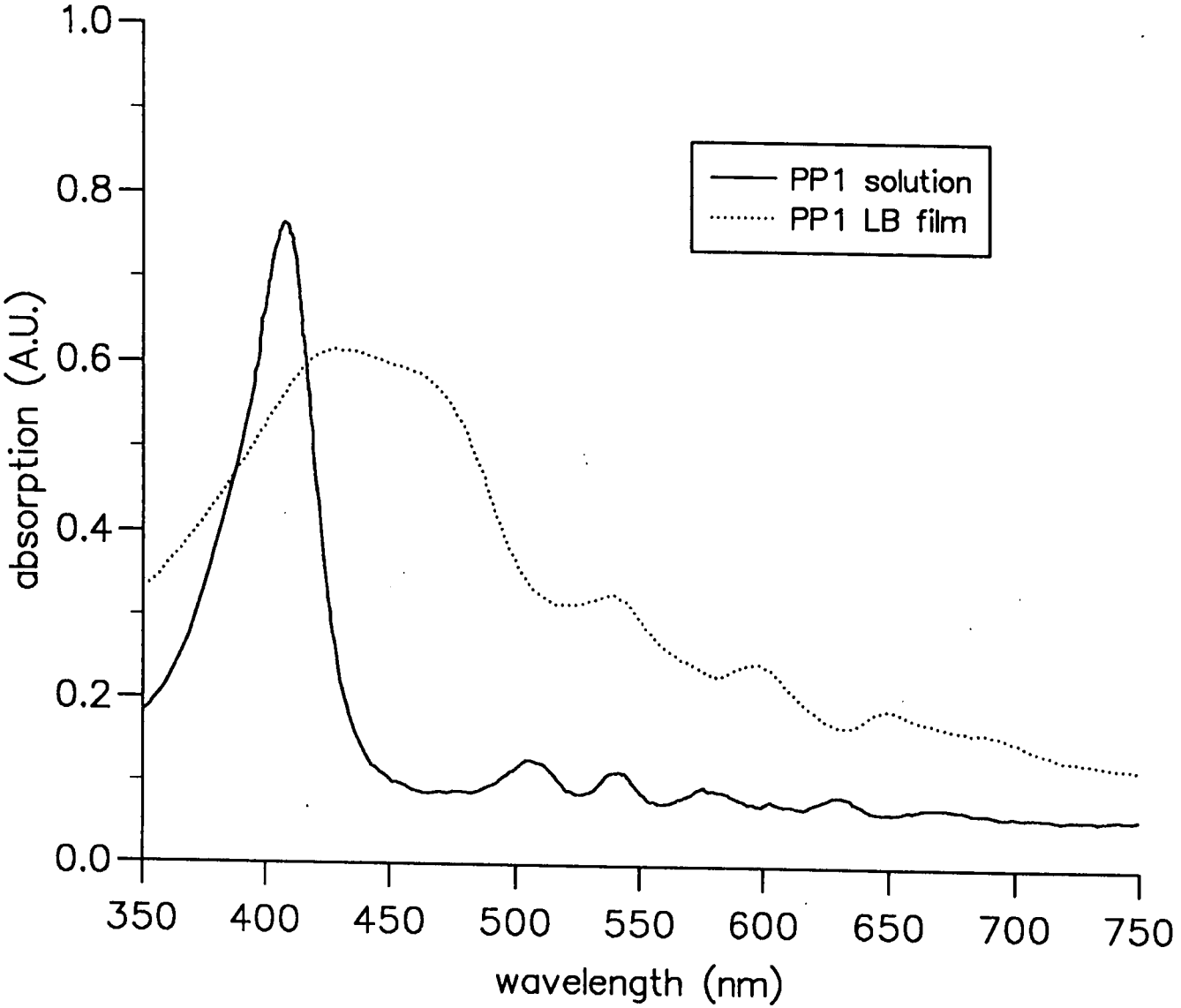

Figure 5.9 Solution and 30 LB layers, absorption spectra of PP1.

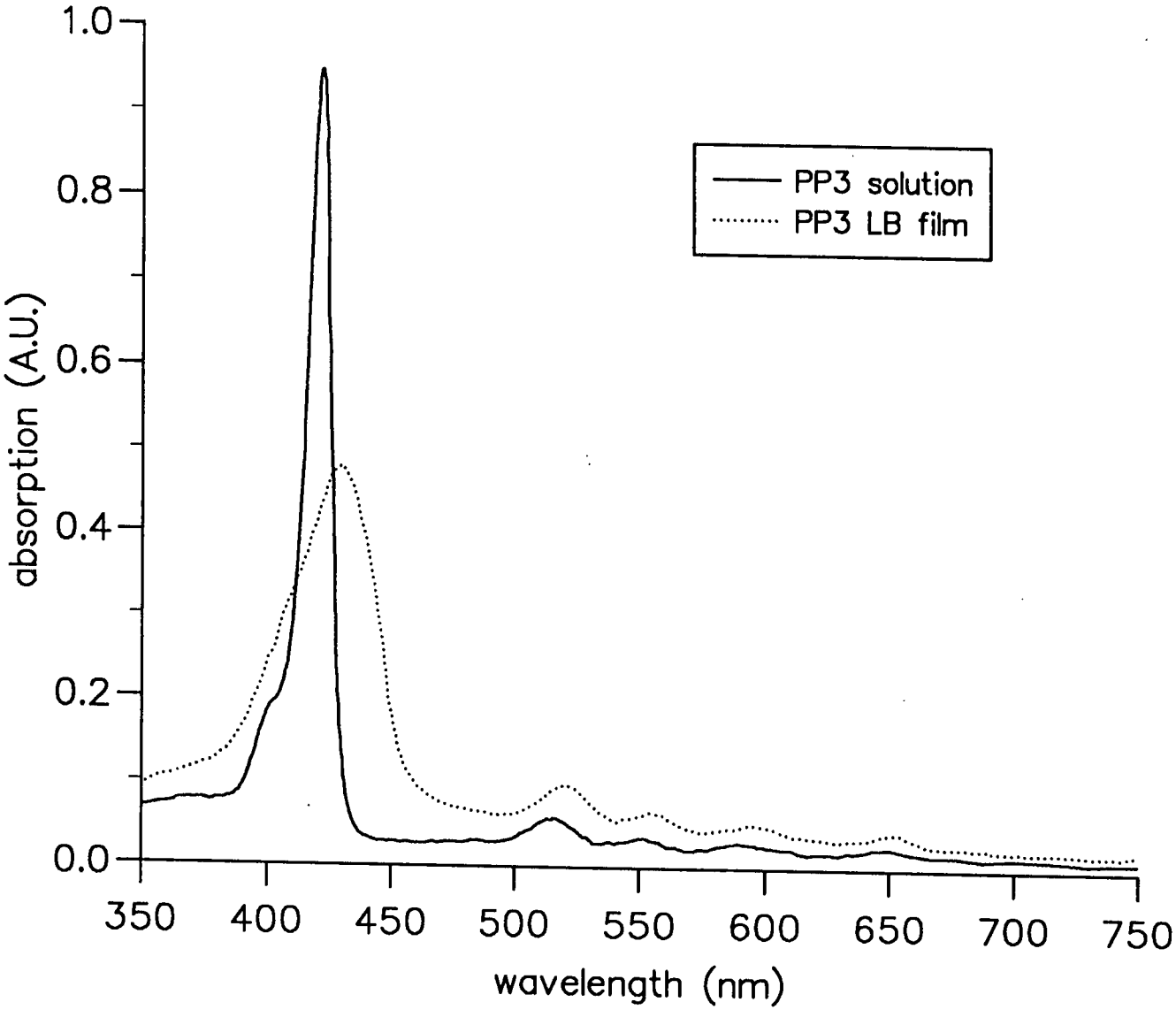

Figure 5.10a Solution and 30 LB layers, absorption spectra of PP3.

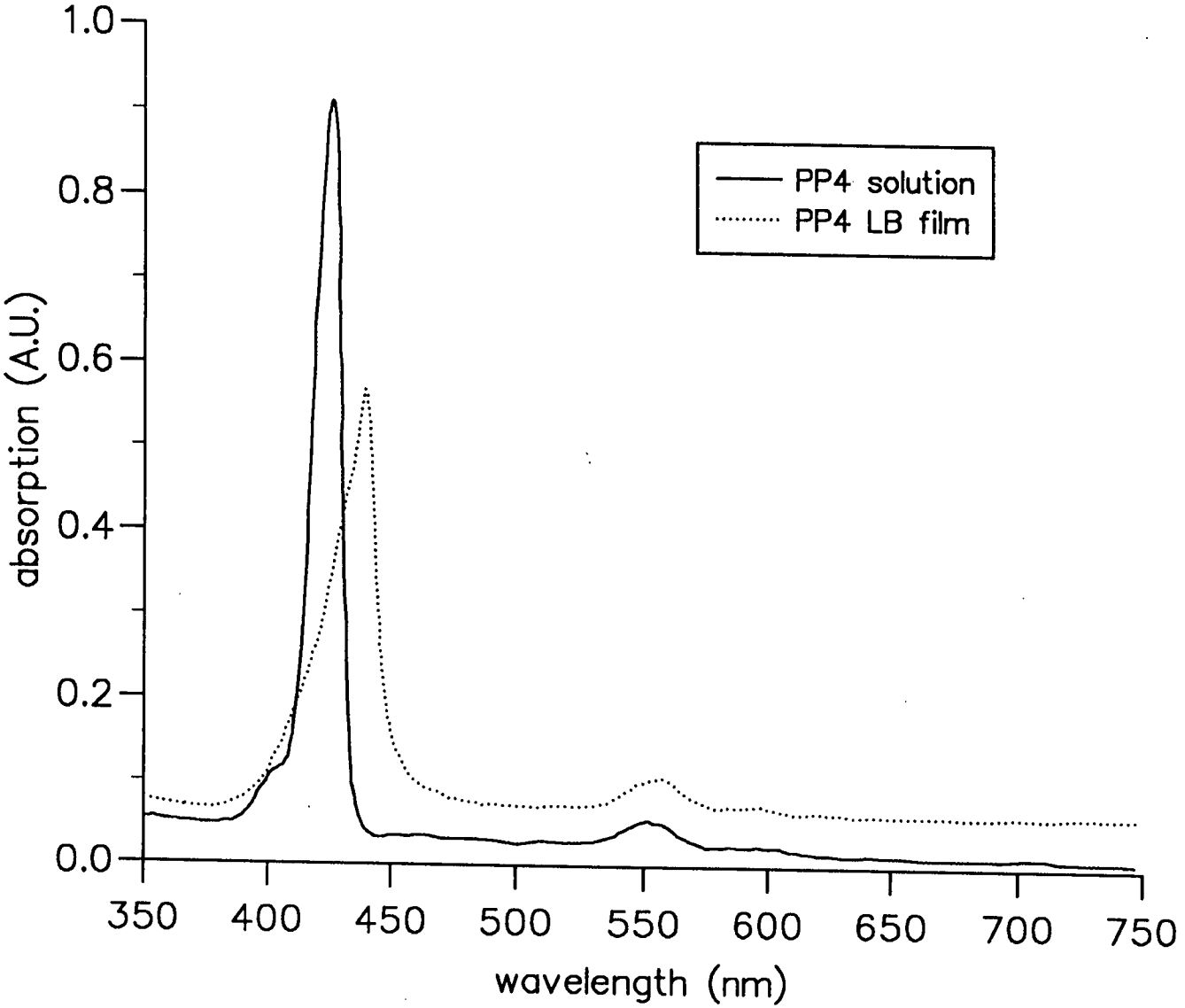

Figure 5.10b Solution and 30 LB layers, absorption spectra of PP4.

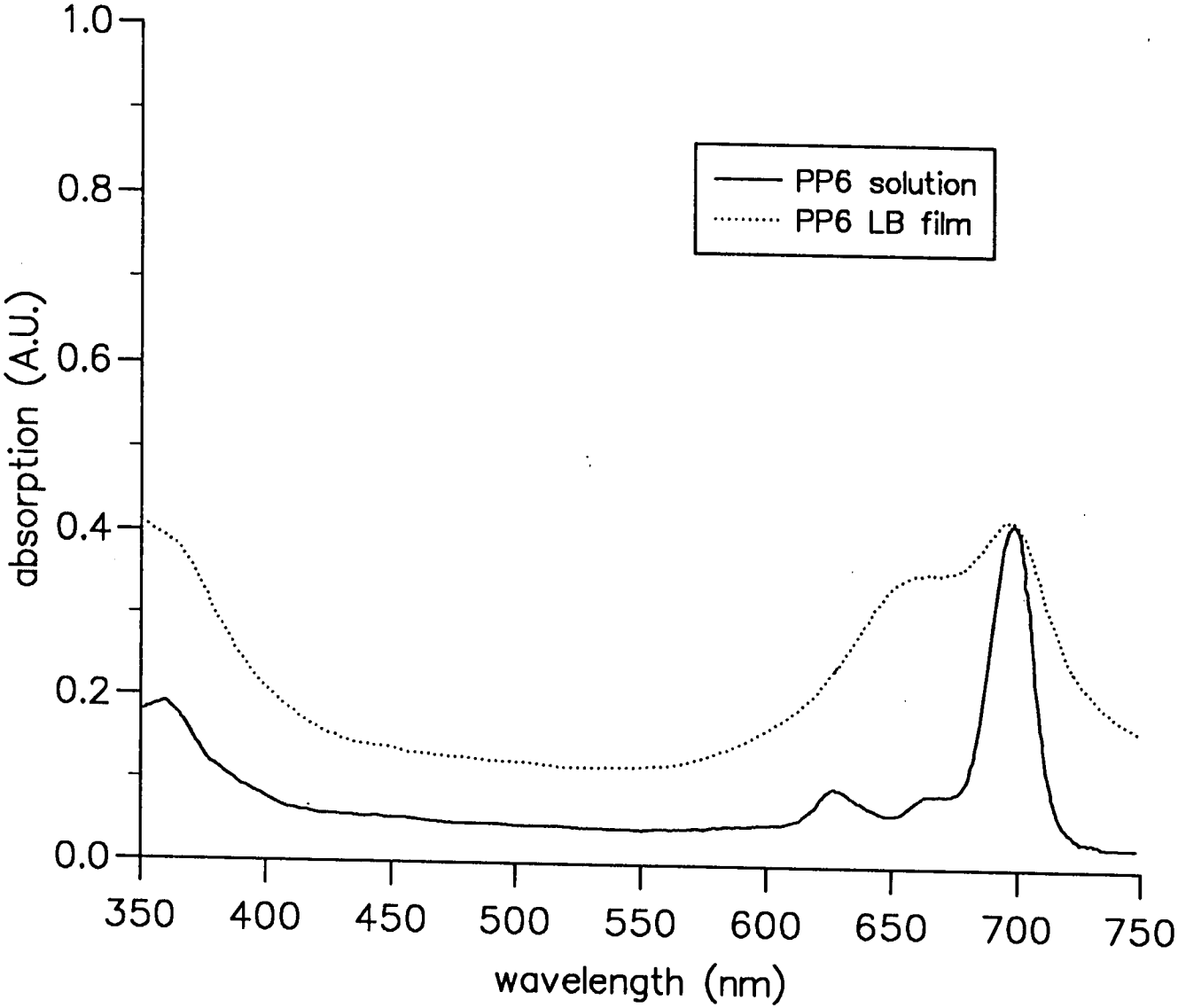

Figure 5.11a Solution and 30 LB layers, absorption spectra of PP6.

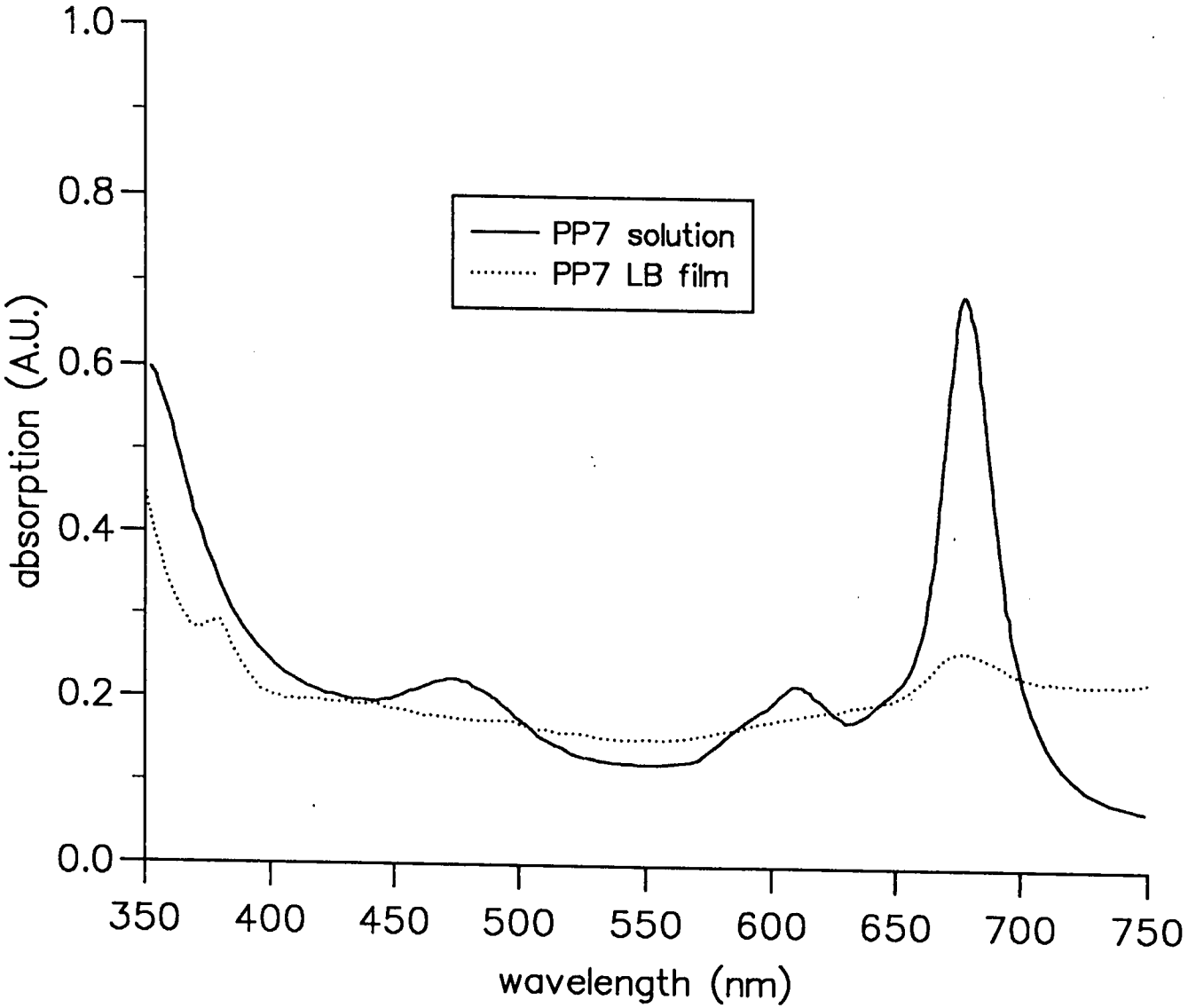

Figure 5.11b Solution and 30 LB layers, absorption spectra of PP7.

phyrins have very intense singlet transitions with shoulders in the blue region of the visible and vibronic peaks towards the red. The phthalocyanines have an intense band associated with the singlet transition 0-0 (explained in chapter 3) in the red region of the visible and minor peaks towards the blue. Extinction coefficients are calculated for the most intense band (0-0) of each material and are shown in table 5.4. The materials have very high extinction coefficients, a typical value for phthalocyanine[1] is $\sim 10^5$.

The absorption spectra of these LB films are shown in figures 5.9-5.11 together with the solution spectra. It is immediately obvious that the LB film absorption spectra are all broader than those in solution. The porphyrins' LB spectra are red shifted relative to the solution by ~10 nm. Phthalocyanine LB spectra of PP6 and PP7 are slightly blue shifted compared to the solution. This effect was observed by Baker[1]. Fujiki and Tabei[30] have attributed such a shift to the formation of aggregates composed of a one-dimensional linear stack of phthalocyanine molecules.

Material	Absorption Band (nm)	ε (extinction coefficient)
PP1	408	1.7×10^5
PP3	420	2.3×10^5
PP4	422	6.2×10^5
PP6	695	1.8×10^5
PP7	677	3.5×10^5

Table 5.4 Extinction coefficients for phthalocyanines and porphyrins

5.4.2 Perylene

The solution spectrum in figure 5.12 is structured in nature and is typical of the monomer and is identical to that reported by Ferguson[16]. The singlet vibronic transitions, in decreasing intensity, are 0-0 at 445 nm , 0-1 at 415 , 0-2 at 390 nm and 0-3 which forms a shoulder at 365 nm. The extinction coefficient for the 0-0 transition is shown in table 5.5. The spectrum of the cast film is much broader than that of the solution: much of the structure is lost and it is bathochromically shifted (red-shifted); this is combined with a change in the relative intensity of

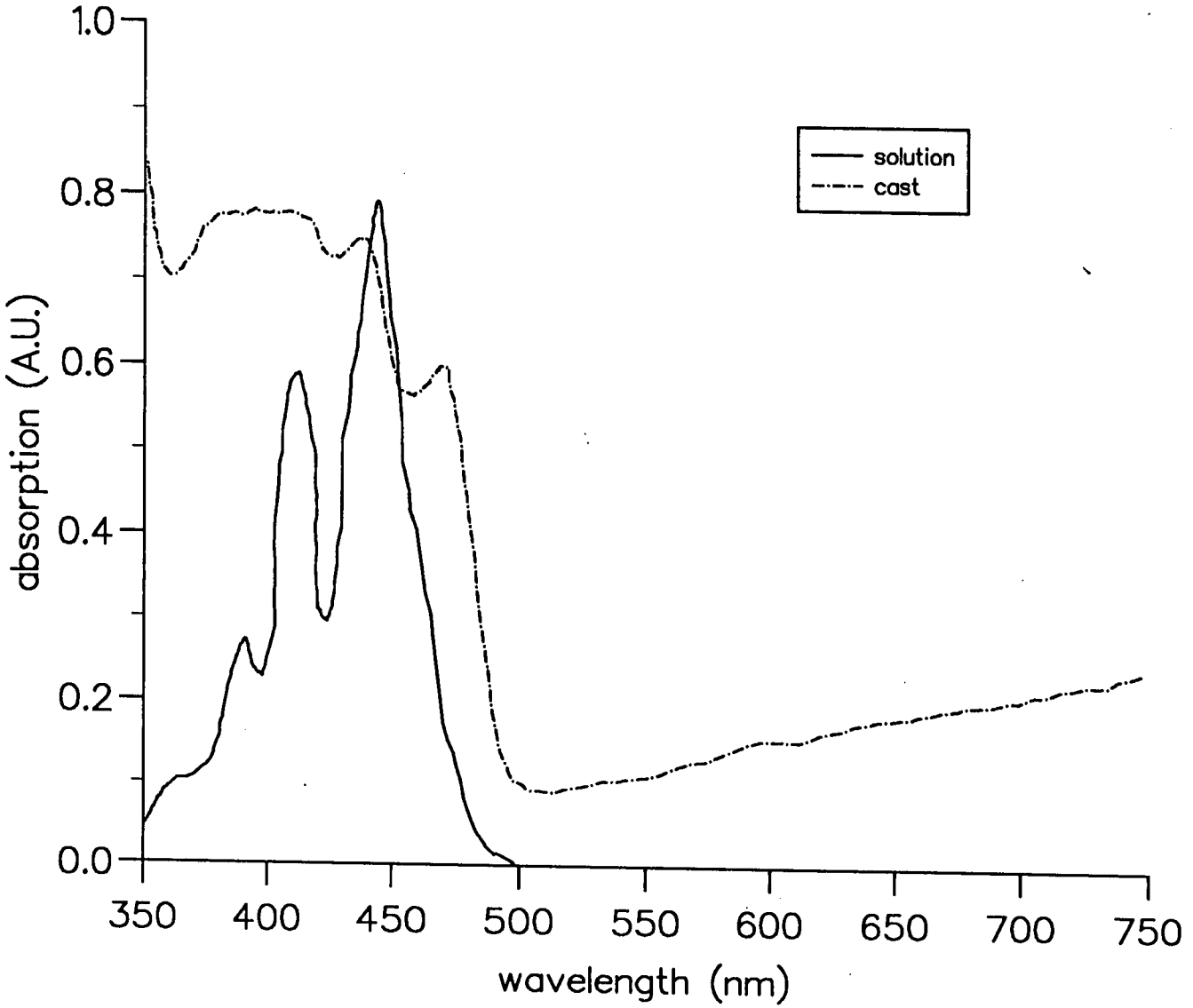

Figure 5.12 Absorption spectra of 10^{-5} M perylene in chloroform and a syringe cast film.

the bands. The 0-0 and 0-1 transitions are still visible at 470 nm and 440 nm, a shift of 25 nm. Transitions 0-2 and 0-3 merge to form a band at 395 nm which is the most intense. This cast film spectrum is very similar to the crystal spectrum polarized parallel to the a crystallographic axis reported by Hochstrasser[17]. These changes can probably be attributed to an interaction between molecules in the microcrystals making up the cast film.

Material	Absorption Band (nm)	ε (extinction coefficient)
Sq1	648	7.1×10^5
Sq2	628	4.1×10^5
Sq3	646	3.2×10^5
perylene	440	3.7×10^5

Table 5.5 Extinction coefficients for squaraines and perylene.

The LB film absorption spectrum of perylene (figure 5.19) is broad and red-shifted relative to the solution spectrum with the most intense band at 390 nm and shoulders implying bands at 430 nm and 465 nm. It is very similar to that of the cast film; however, shoulders have replaced the clearly defined peaks observed in the cast film spectrum.

5.4.3 S120

The solution spectrum (figure 5.13), at 3.9×10^{-6} molar, is fairly broad and has two maxima at 525 nm (0-0 transition) and 495 nm (0-1 transition). The short-wavelength maximum has a shoulder at 470 nm implying the existence of another band, possibly the 0-2 transition. Increasing the concentration to 3.9×10^{-5} molar results in the 0-0 band becoming flatter on the top, but there is no change in the band at 495 nm confirming that this band is not due to a dimer. The cast film spectrum is featureless extending from 425 nm to 600 nm slightly broader than the solution, and shifted equally on both sides.

Pure S120 did not transfer well onto glass but excellent films were produced on TA coated glass slides. A further 2 layers of TA were also deposited on top of the dye to form a "sandwich" structure - this improved the lifetime of the films.

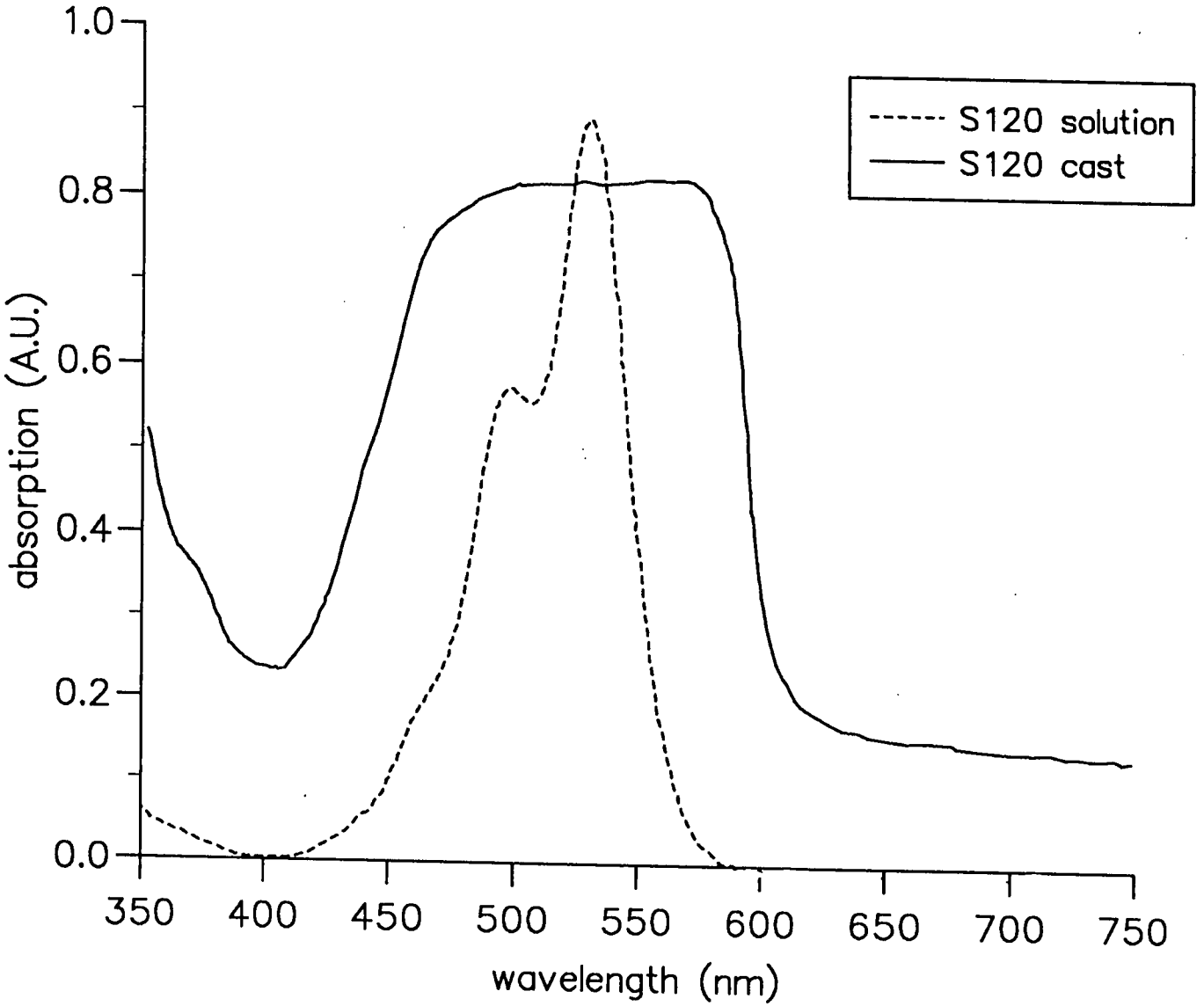

Figure 5.13 Absorption spectra of 10^{-5} M S120 in chloroform and a syringe cast film.

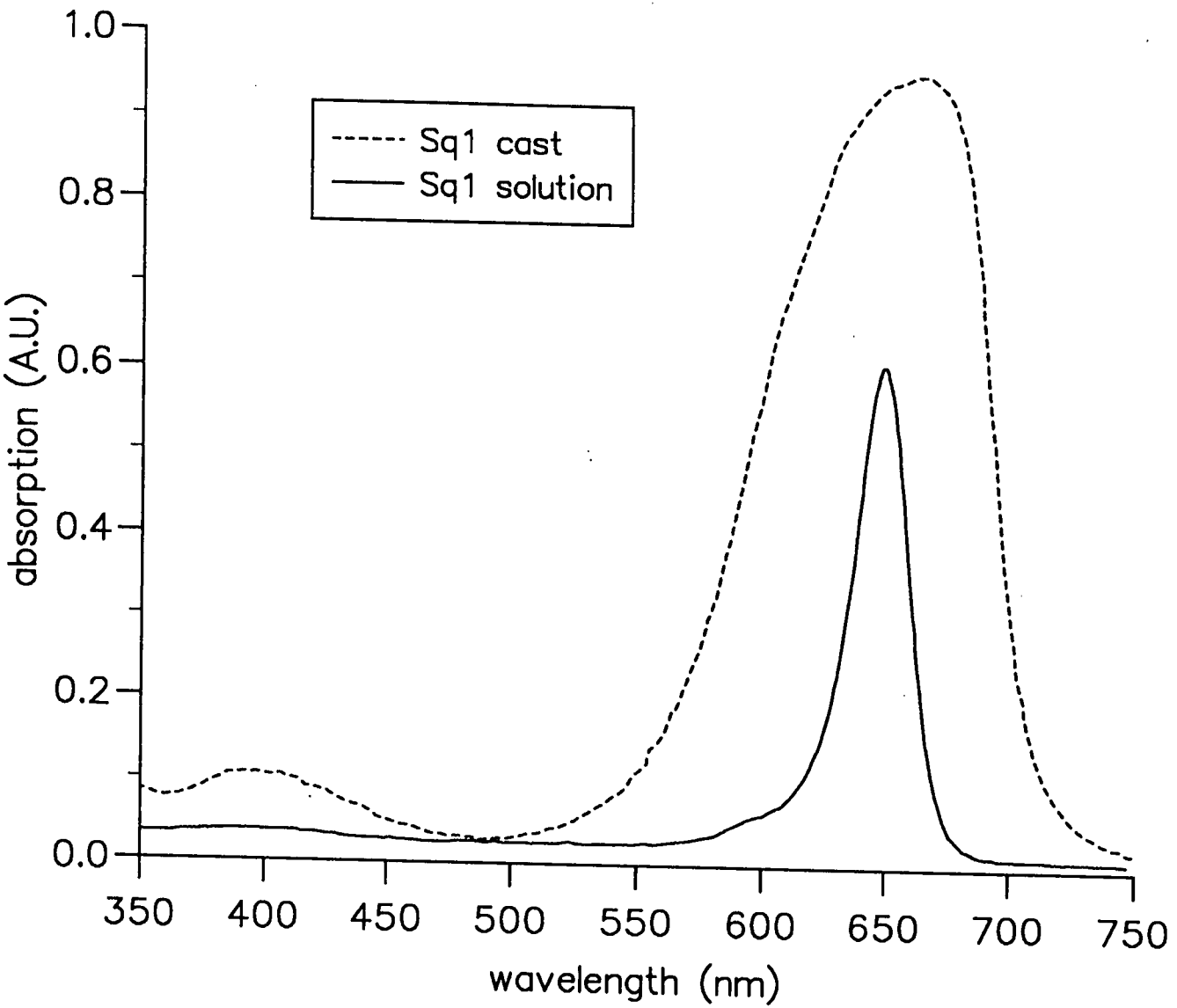

Figure 5.14 Absorption spectra of 10^{-5} M Sq1 in chloroform and a syringe cast film.

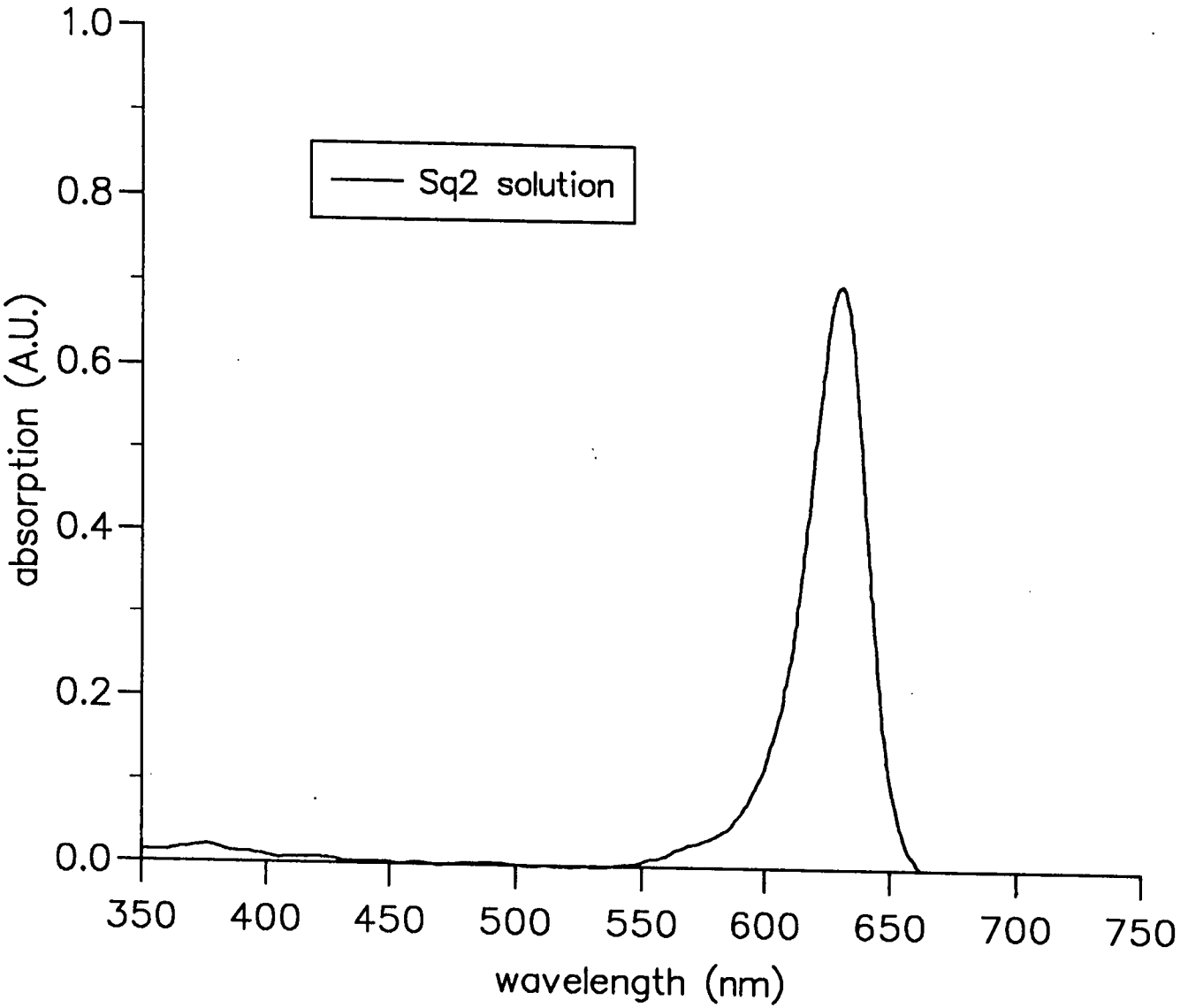

Figure 5.15 Absorption spectrum of 10^{-5} M Sq2 in chloroform.

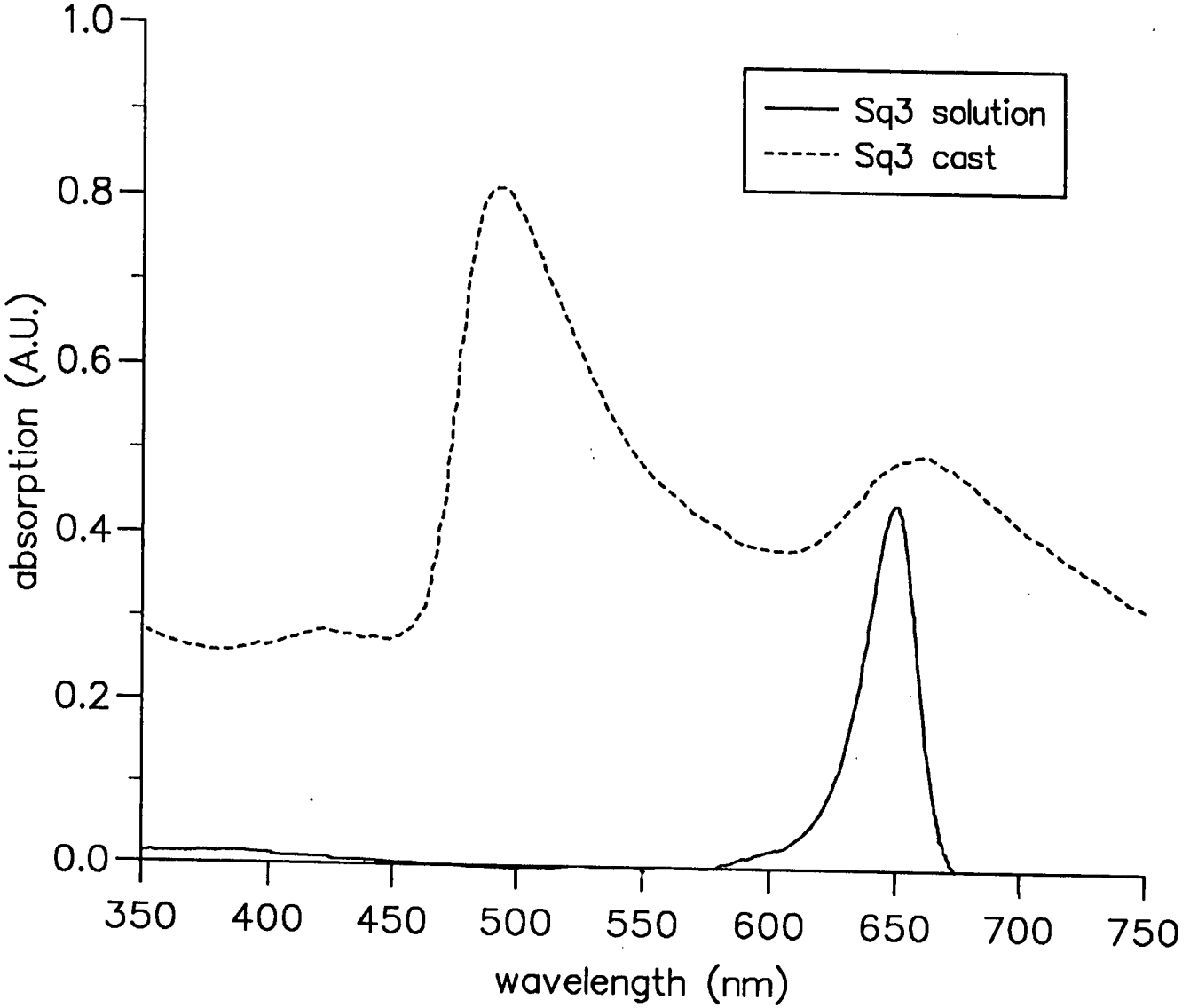

Figure 5.16 Absorption spectra of 10^{-5} M Sq3 in chloroform and a syringe cast film.

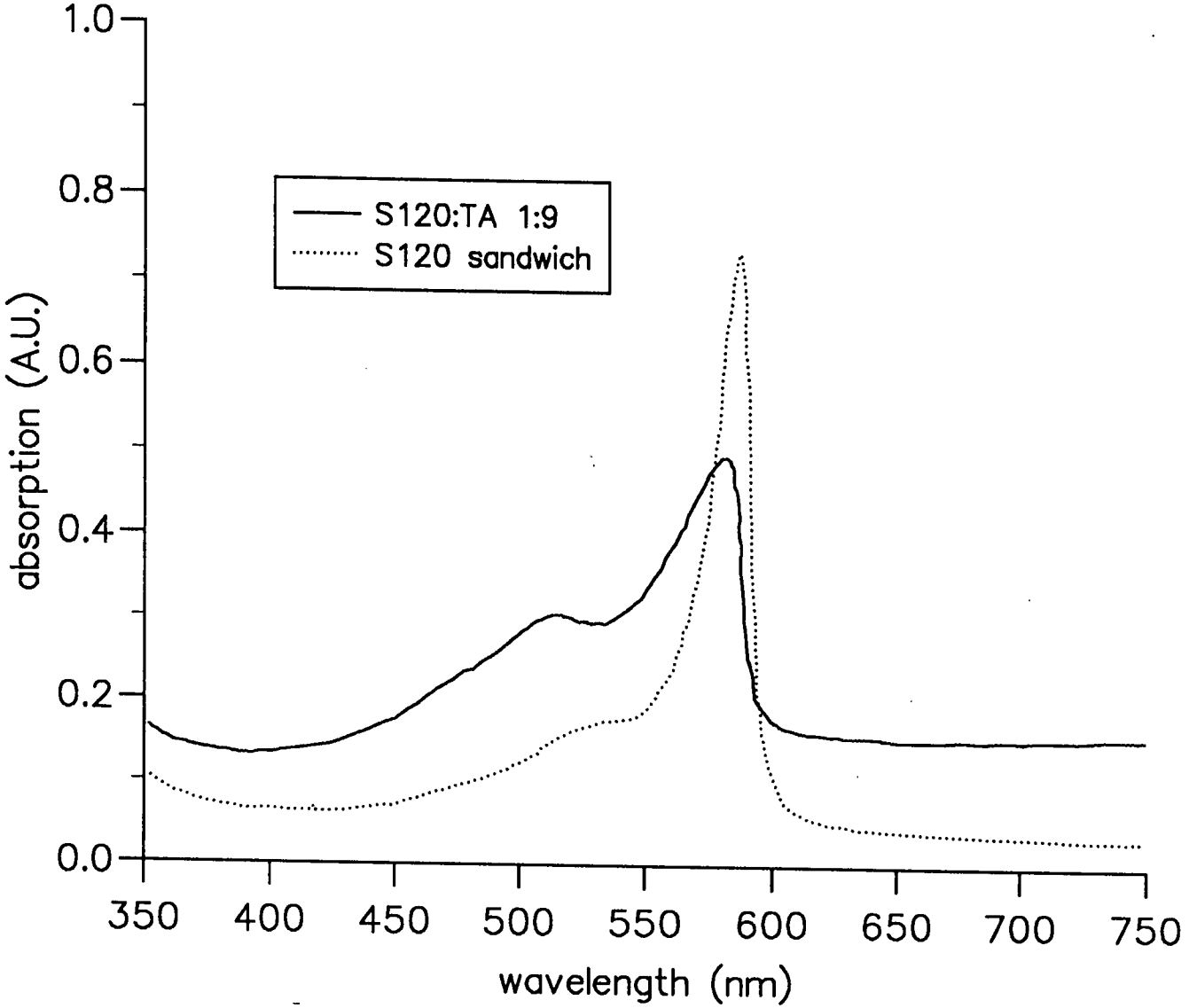

Figure 5.17 Absorption spectra of 3 layers of S120:TA 1:9 and 2 layers of pure S120 between 2 bilayers of TA.

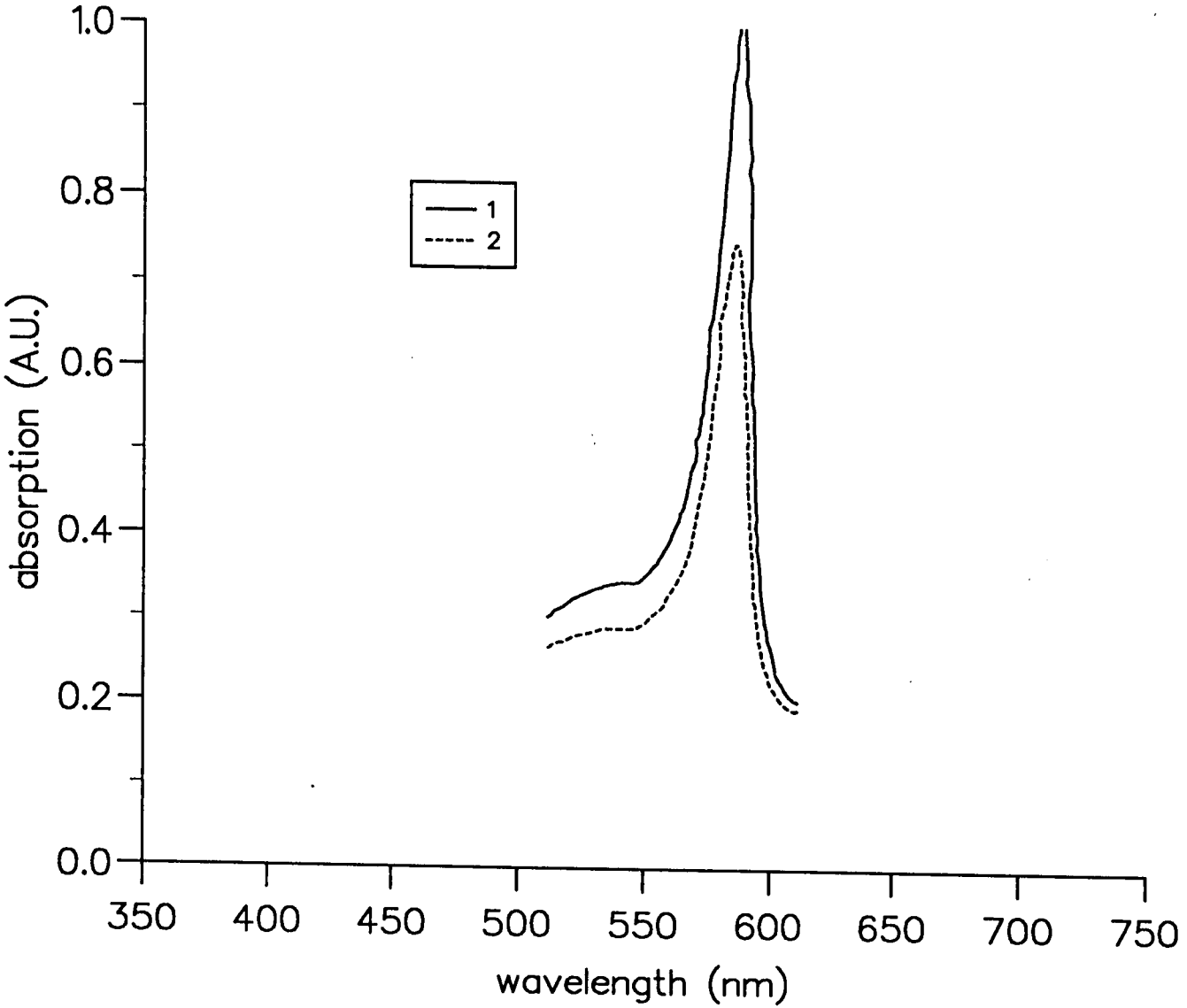

Figure 5.18 Absorption spectra of S120 sandwich structure before (1) and immediately after (2) exposure to light.

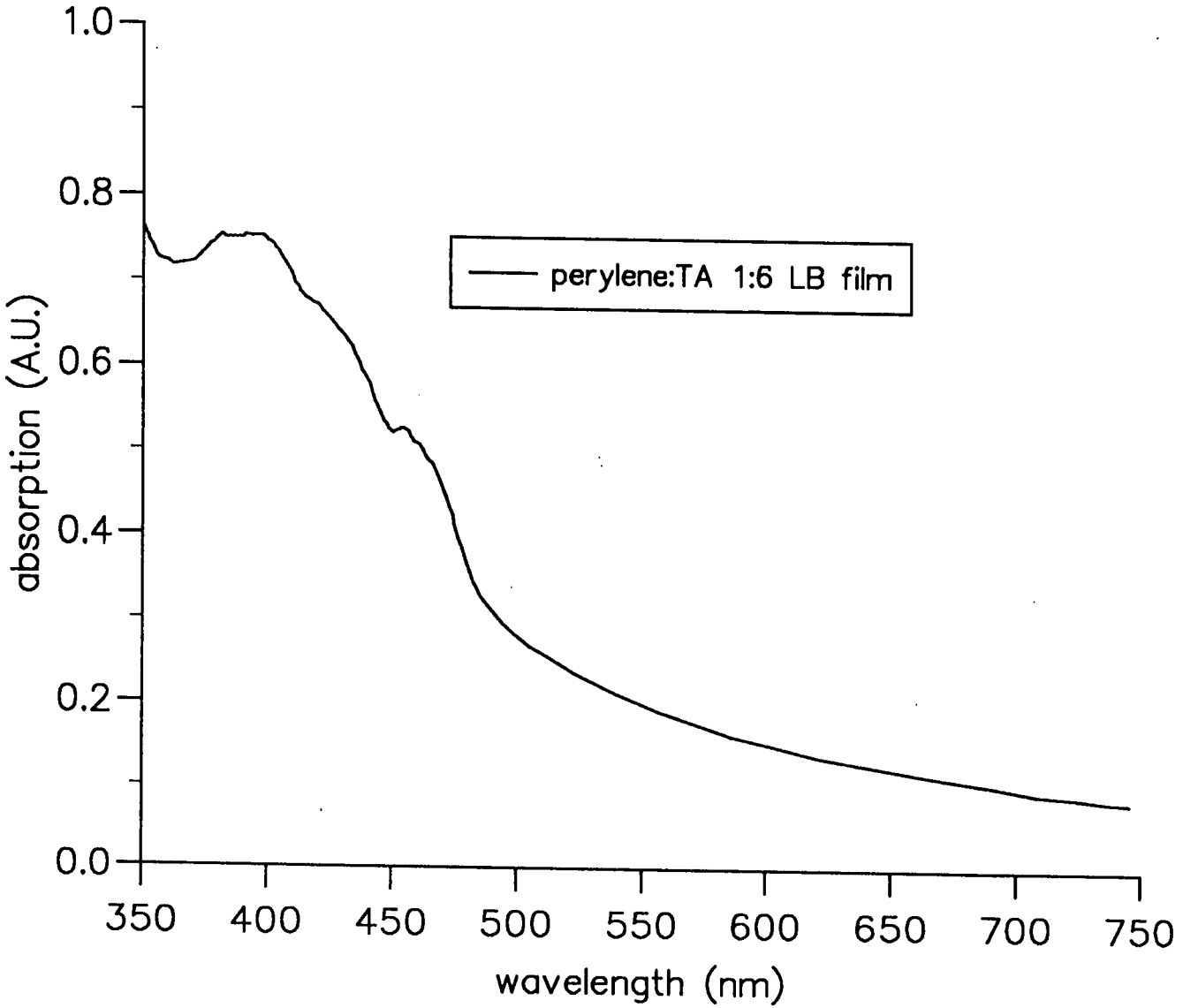

Figure 5.19 Absorption spectrum of 30 layers of perylene:TA 1:6.

Absorption spectra of these films revealed a very sharp, intense band at 580 nm which was red-shifted compared to solution; a shoulder was also evident at 530 nm (figure 5.17). This intense bathochromically shifted band has been assigned by Pockrand et al[31] to J-aggregates (referred to in Chapter 3).

The absorption spectrum of S120 mixed with TA to a molar ratio of 1:9 S120:TA (figure 5.17) was much broader and slightly red-shifted with a maximum at 580 nm and a band at 515 nm. It more closely resembles the solution spectrum in form. The narrowing and increase in intensity of the absorption might therefore result from an interaction between dye molecules. Mixing the dye with TA clearly affects this interaction in some way, possibly by inhibiting the ordering of the dye molecules. This would appear to contradict the results in section 5.3.3 which suggest that there is no change in the orientation of the molecules in the mixed film. However, in section 3.3.5, J-aggregates were shown to be formed from four molecules, so although the S120 molecules are in the correct orientation on the surface, the TA molecules probably prevent them from coalescing to form sufficiently large aggregates.

Figure 5.18 shows the change in intensity of the J-aggregate band with time, the solid line is the initial absorption spectrum, which took approximately 4 minutes to record, the dashed line was recorded 10 minutes later. The material has clearly become photo-bleached.

5.4.4 Squaraines

The 10^{-6} molar solutions of Sq1, Sq2 and Sq3 showed a single absorption band in the visible region which was sharp and intense, typical of a singlet 0-0 transition, at 648 nm, 628 nm and 646 nm, respectively. This is characteristic of a monomer absorption (figures 5.14-5.16). Each of the bands has a small shoulder on the short-wavelength side: at 600 nm for Sq1 and Sq3, and at 575 nm for Sq2. No change in these shoulders was observed when the concentration was increased to 10^{-5} molar, indicating that they are not the result of dimers. The only changes that did occur in the spectra were a flattening of the maxima, probably due to some concentration quenching effect. The extinction coefficients calculated are very high and are listed in table 5.4. These compare favourably with a value of $\sim 3 \times 10^5$ at 638 nm reported by Loufty et al[28] and Law et al[29] for similar squaraines.

Films were cast of Sq1 and Sq3, but it was not possible to cast a film of Sq2. The cast film spectrum of Sq1 is broad and asymmetric, with a maxima at 660 nm, it is bathochromically shifted $\sim$ 20 nm relative to the solution spectrum. Loufty et al reported the solution and solid state absorption spectra of a number of squaraines. Some of their spectra are very similar to that observed for Sq1; they attribute these to weak interaction between molecules in the crystal.

In contrast, the spectrum of Sq3 is very different. Two absorption bands were observed at 655 nm and 494 nm: one was bathochromically shifted relative to the solution spectrum by $\sim$12 nm, whilst the other was hypsochromically shifted (blue-shifted) by $\sim$160 nm. Loufty et al attributed this behaviour to a strong interaction between molecules in aggregates in the film.

Materials were deposited onto glass or quartz both as pure films and mixed with TA.

Pure Sq3 was dipped in both the first and second condensed region of the pressure area isotherm. Both spectra (figure 5.21) have two bands. One occurs at approximately 652 nm, which corresponds to a slightly bathochromically shifted monomer band (628 nm as in solution). The other short wavelength band is more intense and is slightly different for each spectrum: for the first condensed region it is at 504 nm and was symmetric in form, whilst for the second condensed region spectrum it is at 492 nm and is noticeably asymmetric, suggesting the presence of more than one band. The films were stable and there was no significant change in the spectra with time. This is in contrast to data reported by Law and Chen[27].

Pure Sq1 was also dipped in both condensed regions. Both spectra (figure 5.20) are similar, possessing a sharp absorption band at 530-535 nm and a very pronounced shoulder at 650 nm, which corresponds to the monomer band in solution.

Sq1 was mixed with TA in a variety of molar ratios and was dipped at 30 mNm^{-1}. The absorption spectra for the films of 1:1 and 1:4 Sq1:TA mole ratios (figure 5.22) are similar in shape; both have an intense band at 535 nm as was found to be the case for the first condensed region spectrum. Both 1:1 and 1:4

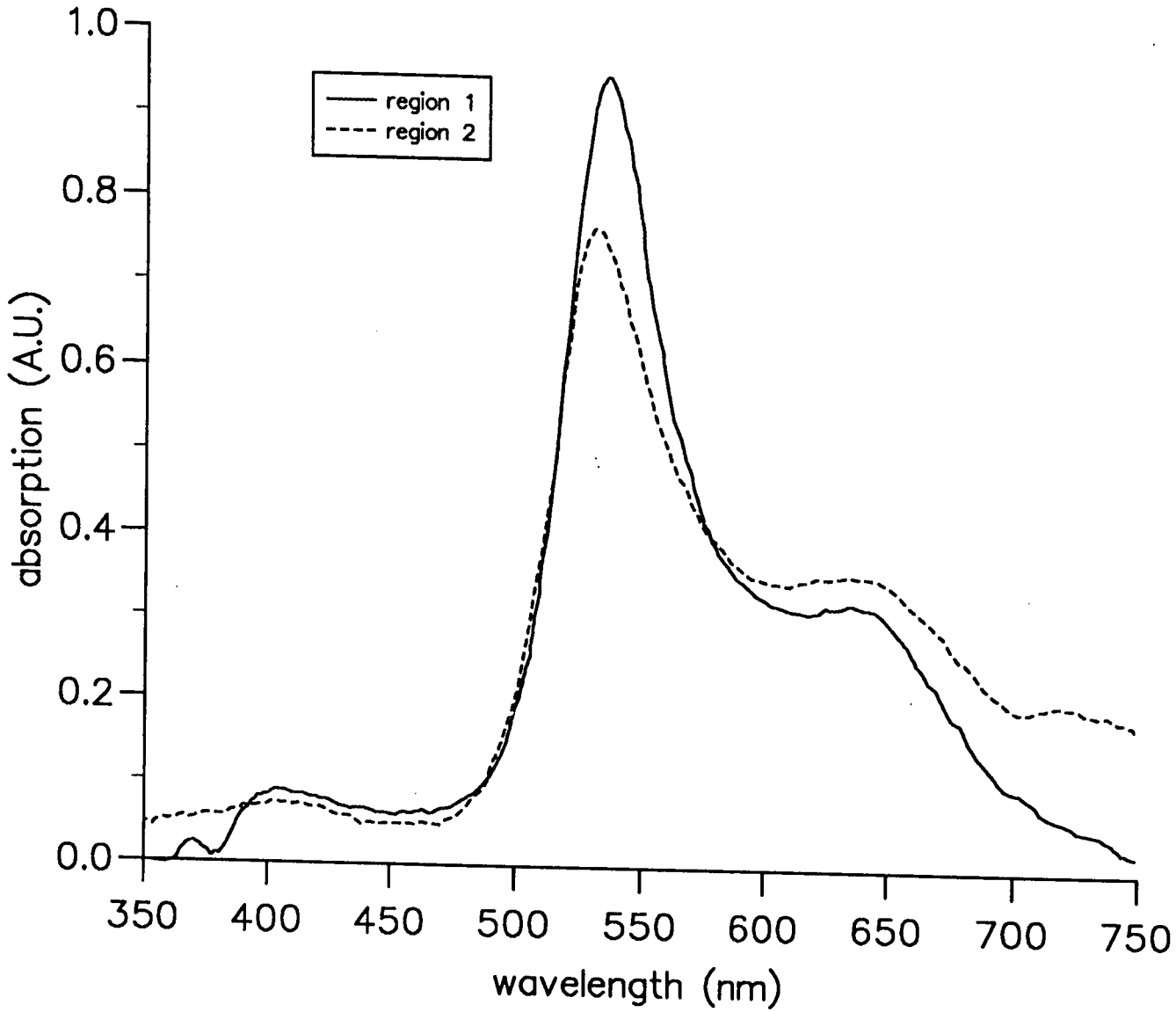

Figure 5.20 Absorption spectra of 2 layers of Sq1 dipped in regions 1 and 2 onto 2 layers of TA.

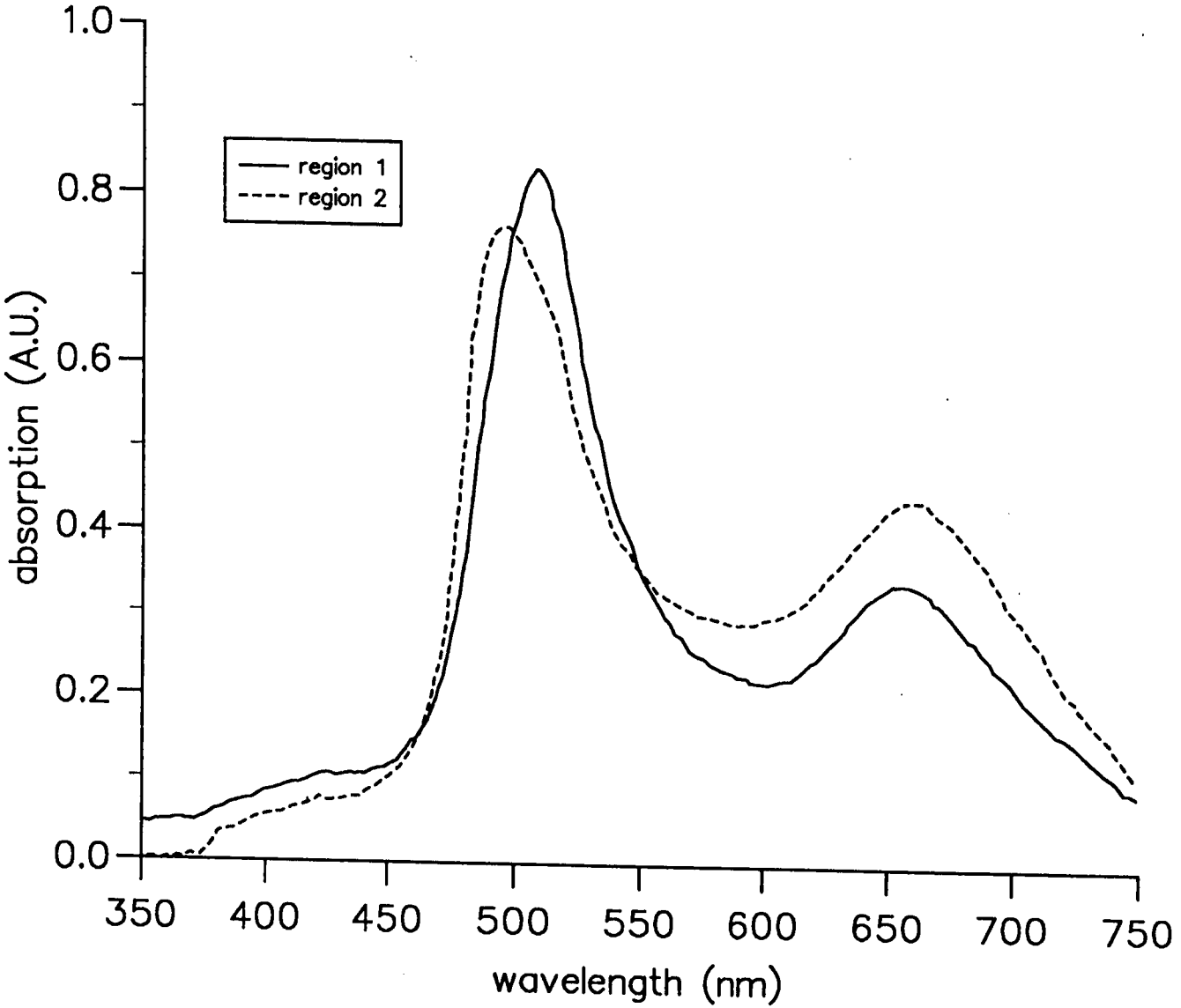

Figure 5.21 Absorption spectra of 2 layers of Sq3 dipped in regions 1 and 2 onto 2 layers of TA.

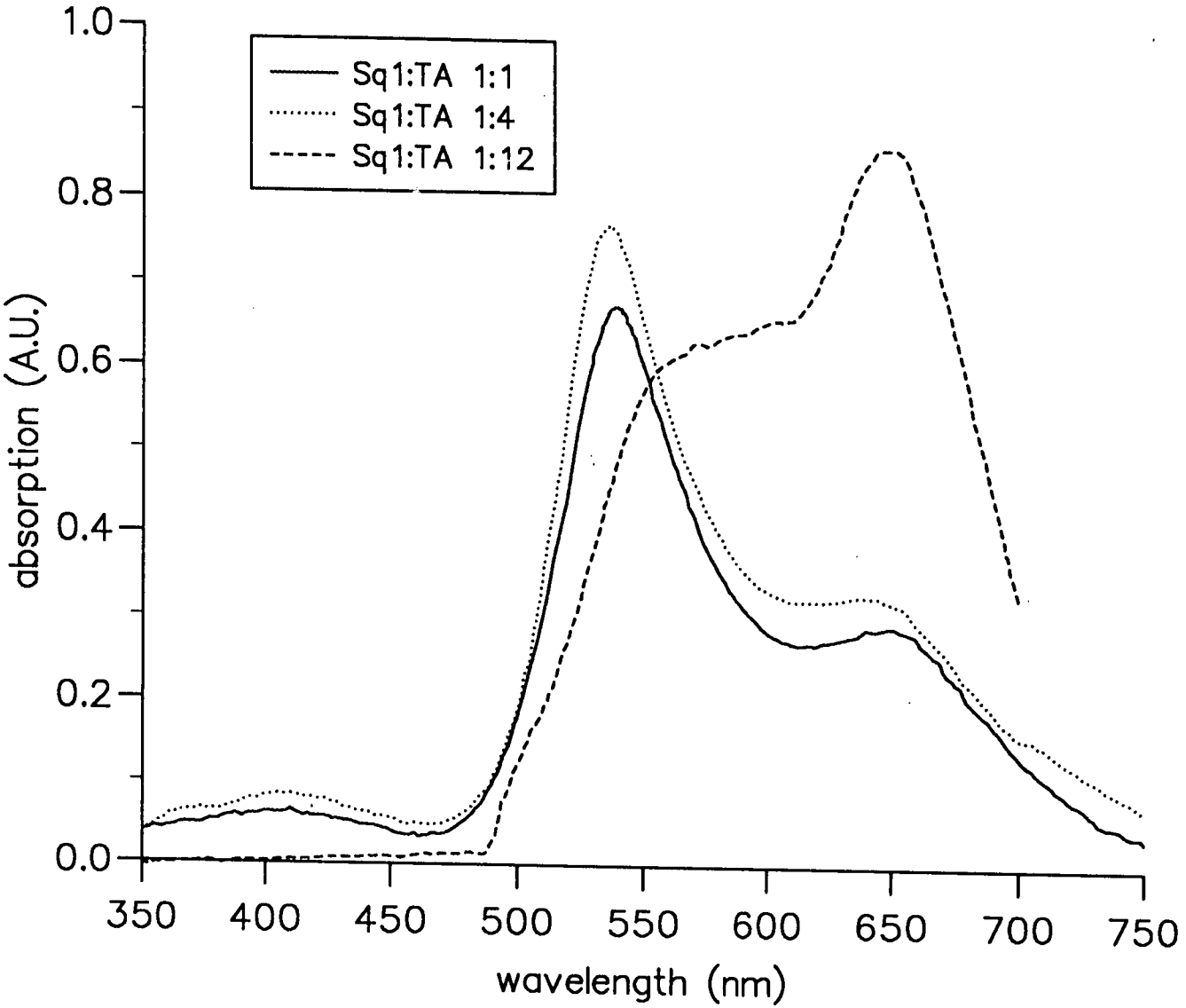

Figure 5.22 Absorption spectra of multilayers of Sq1 pure and Sq1:TA 1:1, 1:4 and 1:12.

spectra possess a shoulder at the long-wavelength side of the main band but these are subtly different in shape .

The absorption spectrum recorded for the 1:12 Sq1:TA film (figure 5.22) is significantly different from those for 1:1 and 1:4 mole ratio films: there is no maximum at 535 nm, an intense band occurs at 650 nm and short-wavelength shoulder is evident between 600 nm and 550 nm. The change in the spectrum towards that of the solution suggests that less aggregation occurs owing to the dispersion of the dye molecules throughout the TA matrix.

The pressure-area isotherm of Sq2 does not have two condensed regions characteristic of Sq1 and Sq3, so the pure dye was dipped at only one surface pressure 30 mNm^{-1}. The absorption spectrum (figure 5.23) of the resulting film is also different in character to those of Sq1 and Sq3; it is very broad with a maximum at 550 nm, another possible band at 650 nm and a shoulder at 750 nm. However, it is likely that this spectrum is composed of more than these three bands.

On mixing with TA there was no change in the spectrum until a ratio of 1:7 Sq2:TA was reached. The spectrum for a film with this composition appeared to possess two main peaks at 550 nm and 750 nm, with a shoulder at 670 nm. The absorption at 550 nm has a flat top suggesting that it is composed of several bands. Comparison between the solution spectra and the mixed LB film spectrum reveals that one maximum is red-shifted ($\sim$100 nm) whilst the other is blue-shifted ($\sim$90 nm) and may indicate that a strong dipole-dipole interaction is taking place (possibly Davydov splitting).

The Sq3 was mixed with TA to different molar ratios and dipped in the second condensed region (above 60 mNm^{-1}). For a molar mixing ratio of 1:1 Sq3:TA the spectrum (figure 5.24) is almost identical to that of the pure dye dipped in the second condensed region.

A ratio of 1:3.8 Sq3:TA has a spectrum (figure 5.24) in which the relative intensity of the two bands is different: the long-wavelength band becomes more intense and the short-wavelength band is slightly red shifted to 496 nm, towards that of the band observed in the first condensed region. There is also a shoulder at 550 nm which is not visible in the spectrum of the 1:1 molar ratio film.

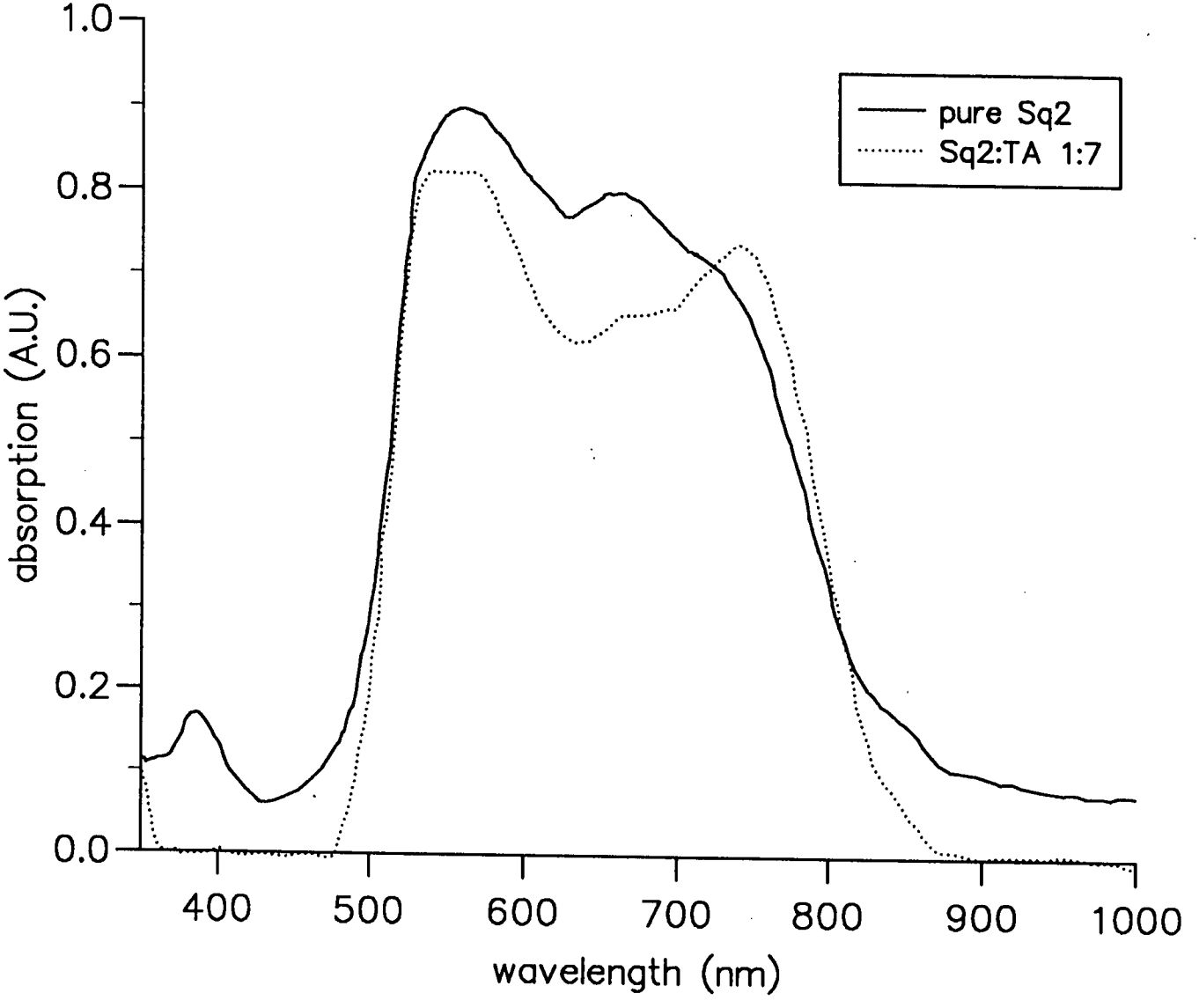

Figure 5.23 Absorption spectra of multilayers of Sq2 pure and Sq2:TA 1:7.

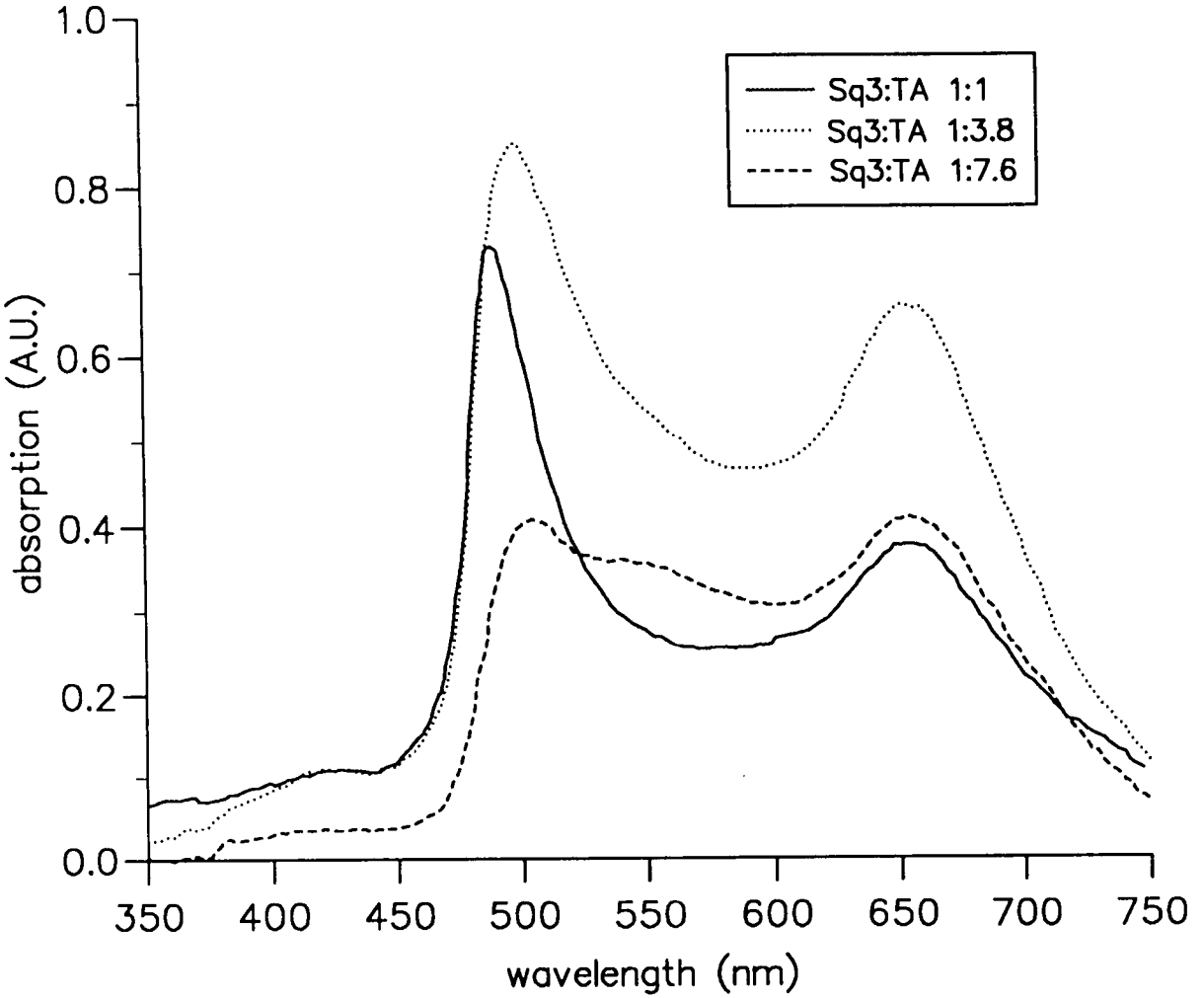

Figure 5.24 Absorption spectra of multilayers of Sq3:TA 1:1, 1:3.8 and 1:7.6.

When the molar ratio is increased to 1:7.6 Sq3:TA, the short-wavelength band is further red-shifted to 504 nm, making it identical to that band in the first condensed region spectrum. The relative intensity of the two bands also changes so that the long-wavelength band is fractionally larger, and the shoulder at 550 nm now becomes much clearer. As with Sq1, these changes in absorption with molar ratio indicate that aggregates are formed in the film when the molecules are in close proximity to each other. In section 5.3.4 a number of possible orientations were suggested for the molecules in the film at the above pressure. The a_m^0 for 1:1 was calculated to be 0.83 nm^2 and a tilting or stacking of the molecules was hypothesised. At ratios of 1:3.8 and 1:7.6 the a_m^0 was larger (1.2 nm^2 and 1.38 nm^2, respectively) and it was assumed that the molecules remained flat on the surface. These proposed changes in dye orientation might help to explain the observed absorption spectra. The intense band at 492 nm is probably due to the interaction between molecules when they are stacked or tilted such that their faces are in contact. Dilution of the mixture then results in a reduction in this interaction. The observed shift in the absorption maximum is therefore due to the formation of aggregates in the film. However, it is not possible to state with certainty how large these are, but from the size of the shift it is reasonable to assume that they are greater than dimers and may be H aggregates (described in chapter 3).

Authors who have reported broadened and red-shifted absorption bands in films compared to solution have attributed them to intermolecular charge transfer (CT) interactions between the donor (aniline) and acceptor (four-membered ring) groups in the squaraine. The blue-shifts observed for Sq1 and Sq3 indicate that such CT interactions are not taking place. Law and Chen[27] suggested that the C-O dipole-dipole interaction between the squaraine chromophores was responsible for these observations.

5.5 Polarized Optical Absorption

The polarized absorption measurements were made on glass slides which were coated with film on only one side. It has already been shown by Peterson and Russell[37] that LB films are composed of grains each of which may contain molecules with a common orientation. Thus, any dichroism observed in the film only indicates the average orientation of the molecules.

5.5.1 Perylene

The polarized absorption spectra of perylene:TA film of molar ratio 1:13 in figure 5.25 shows very pronounced dichroism when the slide is at 45 degrees to the incident beam. Table 5.6 shows the dichroic ratio ($\frac{A\parallel}{A\perp}$) of the film at different angles of incidence. The transition dipole moment for perylene responsible for the absorption in the visible was found by Fuke et al[18] to be polarized along the long molecular axis. From the dependence of the dichroic ratio with angle of incidence, it can be assumed firstly that the molecules are arranged predominantly with their long axis perpendicular to the substrate, and secondly that they are at an angle less than 90 degrees to the substrate. These assumptions are strengthened by the polarized absorption spectra in figure 5.26, which were both measured at 45 degrees with the polarizer parallel to the dipping direction but with the substrate reversed in each case, as illustrated in the inserted diagram. The greater absorption for the positive direction indicates that the molecules are preferentially oriented with their long axes perpendicular to the substrate and inclined at some angle, such that they are tilted upward relative to dipping. A schematic diagram showing a possible arrangement of the molecules is shown in figure 5.27.

Angle to beam (degrees)	$\frac{A\parallel}{A\perp}$
45	2.53
50	2.27
60	1.85
70	1.37
80	1.05
90	1.13

Table 5.6 Dichroic ratio of perylene:TA 1:13 at different angles of incidence

5.5.2 S120

Polarized absorption spectra of S120 sandwich films exhibited some dichroism when the slide was at 90° to the incident (figure 5.28) but not when it was at 45°. The electronic transition responsible for the absorption in the visible was found

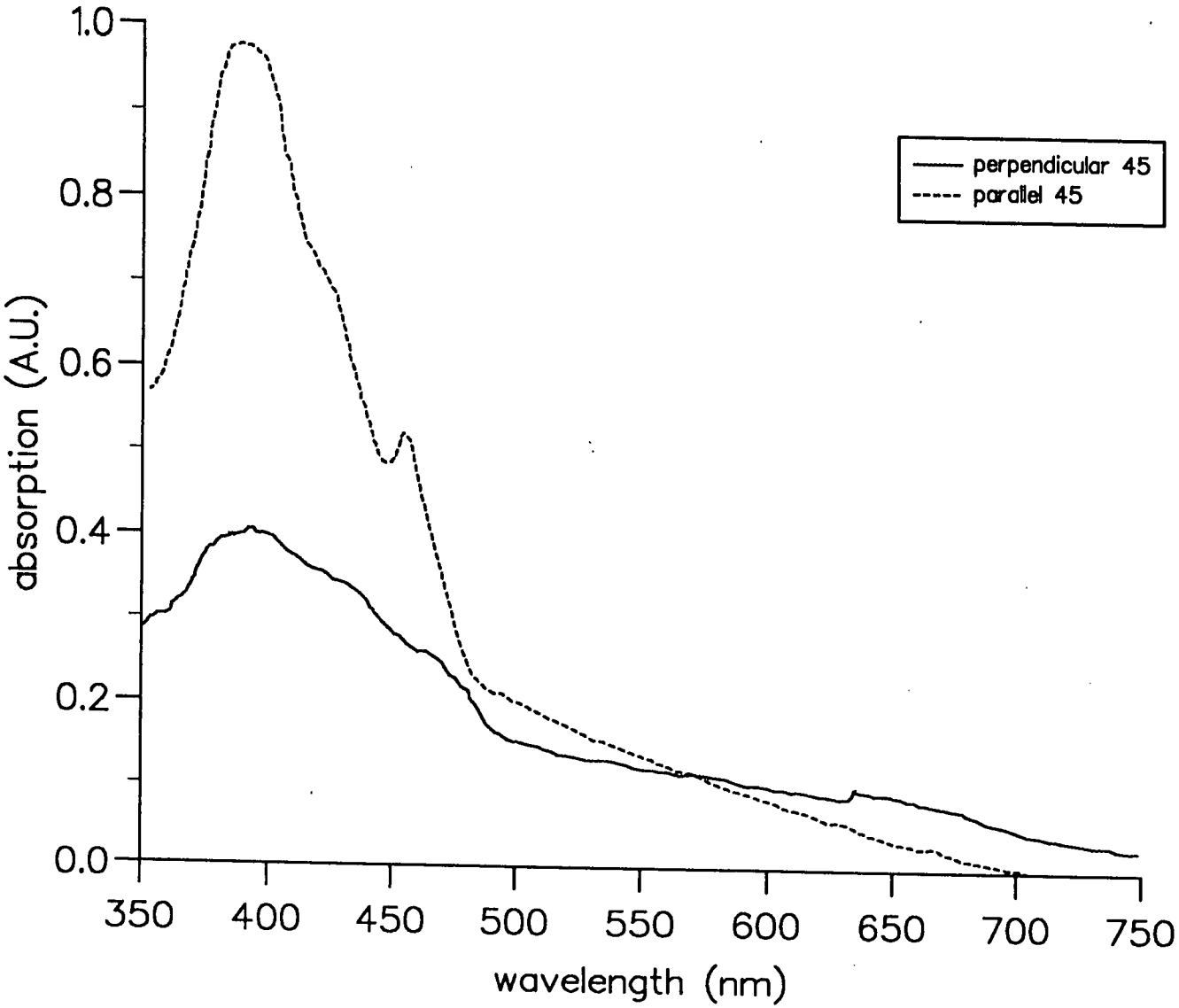

Figure 5.25 Polarized absorption spectra of 30 layers of 1:6 perylene:TA. With the slide at 45° to the beam, and the beam polarized perpendicular and parallel to the dipping direction.

Figure 5.26 Polarized absorption spectra of 30 layers of 1:6 perylene:TA on one side of the slide only. The slide is at 45° to the beam and the beam is polarized parallel to the dipping direction. The slide is rotated as illustrated in the inset diagram.

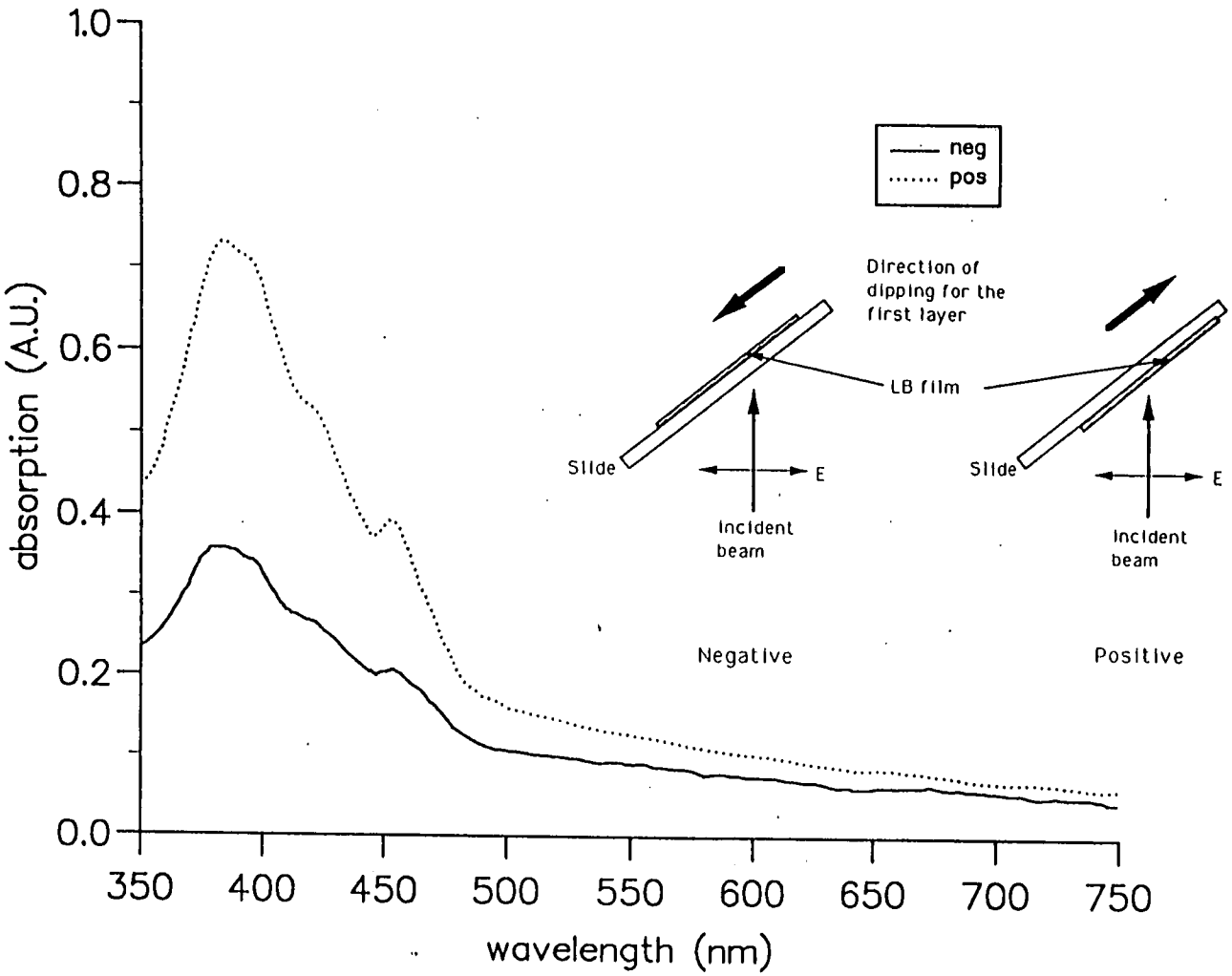

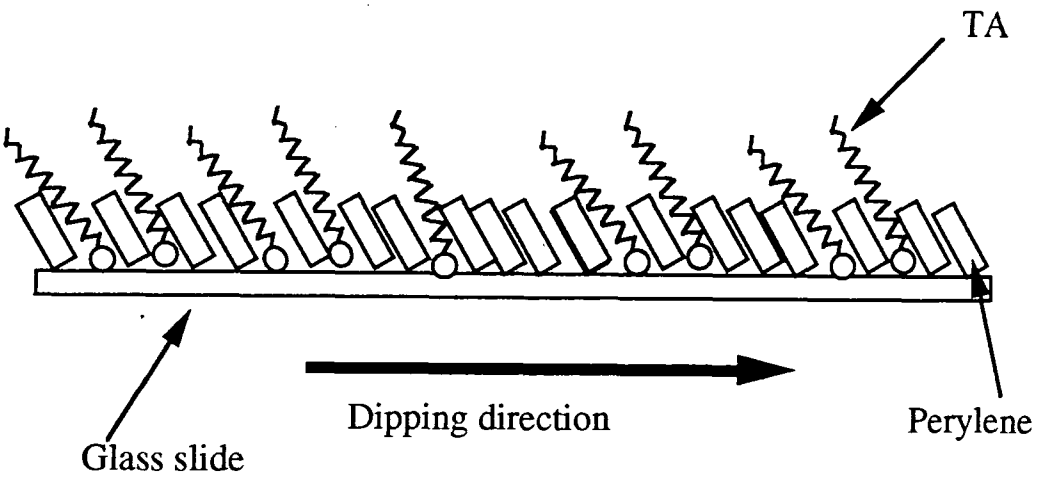

Figure 5.27 Possible orientation of molecules relative to the substrate and the direction of immersion.

Figure 5.28 Polarized absorption spectra for an S120 sandwich structure, with the beam at 90° to the substrate and polarized parallel and perpendicular to the dipping direction.

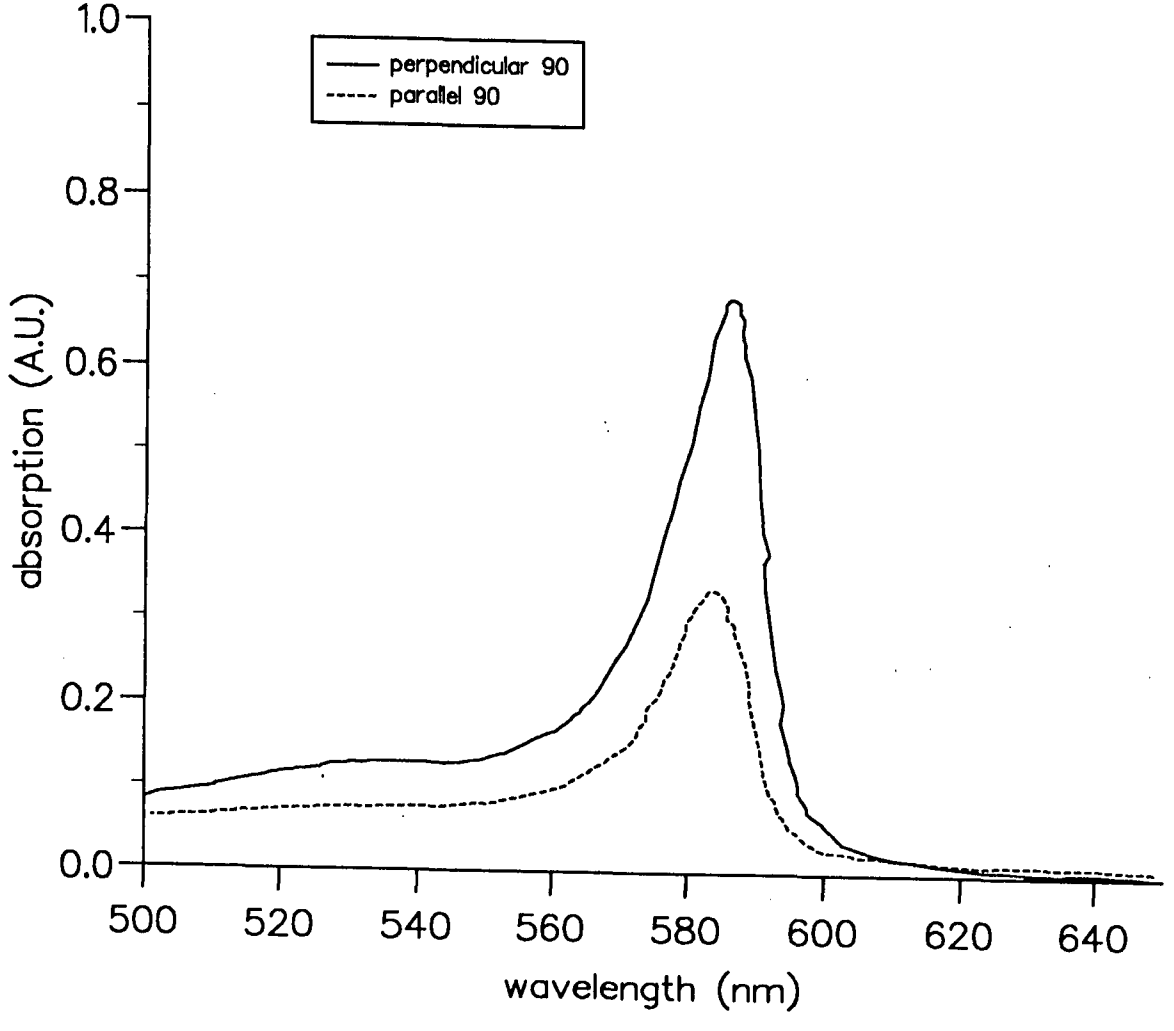

by Bücher and Kuhn[24] to be polarized along the long axis of the molecule. The molecules preferred orientation would appear to be with their long axes perpendicular to the dipping direction. However, it is difficult to explain why no dichroism is observed when the slide is at 45° to the incident beam.

5.5.3 Sq1 and Sq3

Both Sq1 and Sq3 LB films show some degree of dichroism when polarized absorption spectra were recorded; however, the shape of the absorption band remains the same. Films were dipped in both condensed regions and table 5.7 shows the results of the polarized absorption measurements. Tristani-Kendra et al[32] found that the electronic transition moment responsible for absorption in the visible for squaraines was polarized along the long axis of the molecule. From the results in table 5.7, it is difficult to draw any firm conclusions; however, a slightly preferred orientation perpendicular to the dipping direction is possible.

Material	$\frac{A\perp}{A\parallel}$ (90°)	$\frac{A\perp}{A\parallel}$ (45°)
Sq1 region 1	0.81	1.59
Sq1 region 2	1.03	1.23
Sq3 region 1	0.82	1.82
Sq3 region 2	1.75	1.18

Table 5.7 Dichroic ratio of squaraine LB films.

5.5.4 Sq2

Polarized absorption spectra for layers of Sq2:TA 1:7 on 2 layers of TA are shown in figures 5.29 and 5.30. With the slide at 90 degrees to the incident beam and the polarizer parallel to the dipping direction the spectrum resembles the unpolarized spectrum figure 5.23, but the peak at 550 nm is not flattened. When the plane of polarization is rotated so that it is perpendicular to the dipping direction the spectrum changes (figure 5.29), the intensity decreases and the short-wavelength band is shifted by 25 nm to 575 nm. The band at 730 nm disappears and is replaced by a broad shoulder between 650 and 800 nm. The unpolarized spectrum is therefore composed of both these features. When the slide is rotated

Figure 5.29 Polarized absorption spectra for 6 layers of Sq2:TA, with the beam at 90° to the substrate and polarized parallel and perpendicular to the dipping direction.

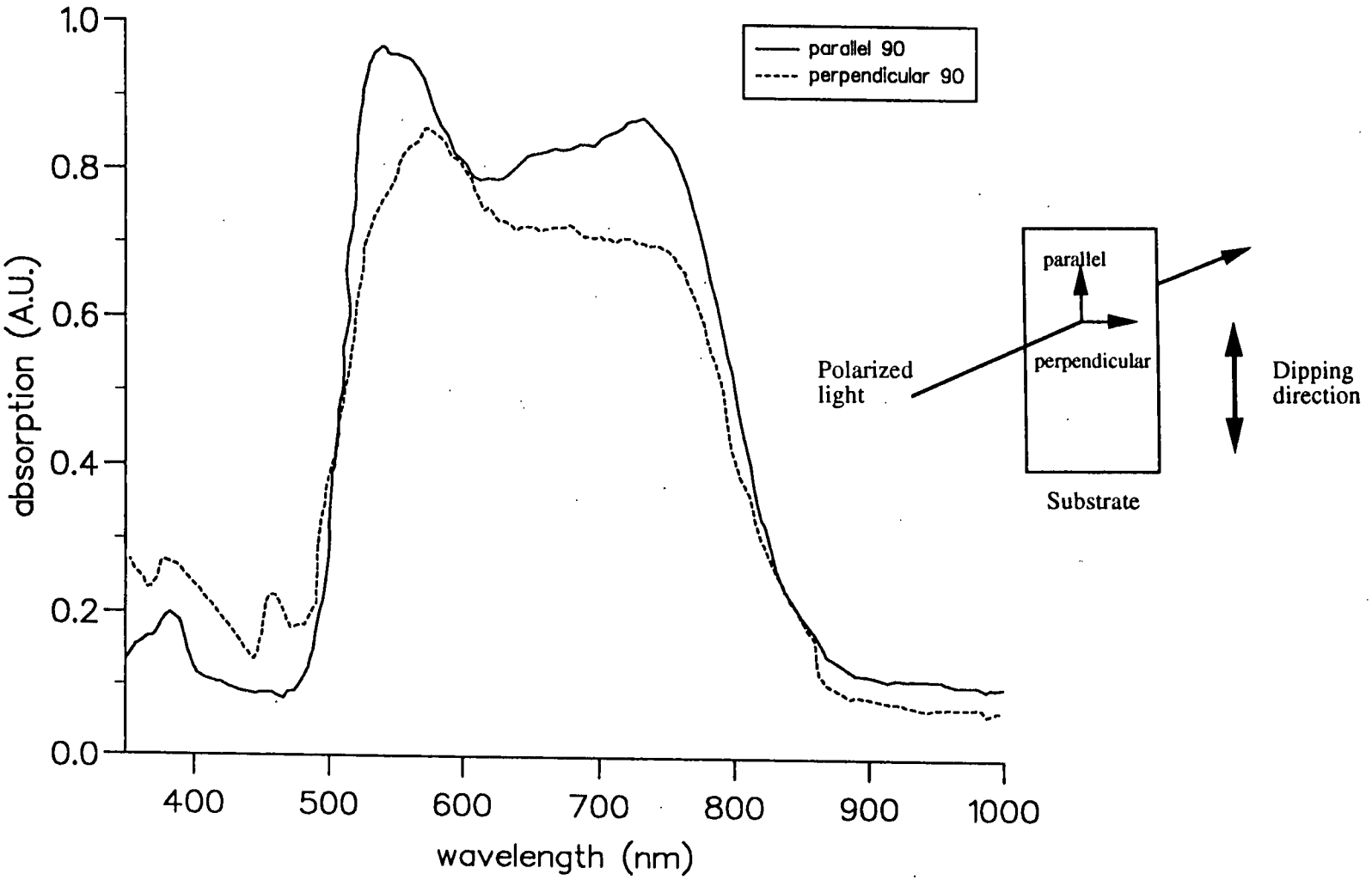

so that it is 45 degrees to the incident beam there is no significant change in the shape of the spectra (figure 5.30) but their relative intensity is now reversed. The spectra are clearly complex and are composed of many bands some of which are red-shifted relative to the solution absorption others which are blue-shifted. One possible explanation is that J- and H-aggregates coexist in the film. The shift in some of these bands when the plane of polarization is changed suggests that the dipoles which are responsible for these bands are at an angle to each other. The sample was selectively irradiated with parallel polarized light to bleach the blue shifted band but it was found that both spectra decreased in intensity indicating that only one complex exists. The observed absorption may therefore be due to Davydov splitting[5,36].

5.6 Fluorescence studies

5.6.1 Perylene at 293K

Comparison of the fluorescence spectrum of perylene solution (figure 5.31) and absorption spectrum (figure 5.12) reveals the mirror-image relationship often observed in aromatic hydrocarbons[15]. The fluorescence is intense and structured with maxima at 445 nm, 472 nm and 507 nm; these have been assigned to the monomer fluorescence singlet vibronic transitions. The fluorescence of microcrystals of perylene, in marked contrast to that of solution, shows no structure and is broad and red shifted with a maxima at 560 nm (figure 5.31).

Fluorescence spectra of perylene:TA films of molar ratios 2:1, 4:5, 1:4, 1:6 and 1:13 show two distinct emitters (figure 5.32). The first is unstructured and has a maximum at 546 nm; the second is structured and is clearly the perylene monomer, with maxima at 445 nm, 472 nm and 507 nm. The unstructured band is assigned to dimers. On increasing the perylene concentration, the emission spectrum changes from that of monomer to dimer as increased aggregation takes place.

The decay parameters were obtained by fitting to the fluorescence decay curves using two different decay models. A bi-exponential model was used for the emissions at 546 nm and a mono-exponential model was used for 445 nm, including solution spectra. The lifetimes obtained from this fitting are given in table 5.8. The value of 5 ns compares well with 4.9 ns reported by Birks and Dyson[15] for

Material	Molar ratio	τ_1 (ns)	τ_2 (ns)	B_1	B_2	χ^2
546 nm, 30 layers on glass	3:1	6.6	15.8	0.54	0.46	1.3
	3:2	6.5	15.9	0.55	0.45	1.1
	4:7	6.0	16.1	0.63	0.37	1.5
546 nm, 50 layers on glass	2:1	5.6	14.7	0.69	0.31	1.3
	4:5	5.2	14.8	0.67	0.33	1.3
	1:4	4.1	13.9	0.68	0.32	1.5
	1:6	4.1	14.2	0.64	0.36	1.5
560 nm, micro-crystals		34.2		0.31		1.6
445 nm, perylene in solution 10^{-4}M		5.4		0.26		1.1
445 nm, perylene in solution 10^{-2}M		4.9		0.31		1.2
445 nm, 50 layers on quartz	2:1	5.4		0.26		1.3
	4:5	5.1		0.31		1.2
	1:4	4.5		0.28		1.2
	1:6	4.4		0.25		1.3
	1:13	4.2		0.24		1.2

Table 5.8 The best-fit parameters for fluorescence decay of LB-films of perylene:TA at 293K. $I(t)=B_1\exp(-t/\tau_1)+B_2\exp(-t/\tau_2)$.

Figure 5.30 Polarized absorption spectra for 6 layers of Sq2:TA, with the beam at 45° to the substrate and polarized parallel and perpendicular to the dipping direction.

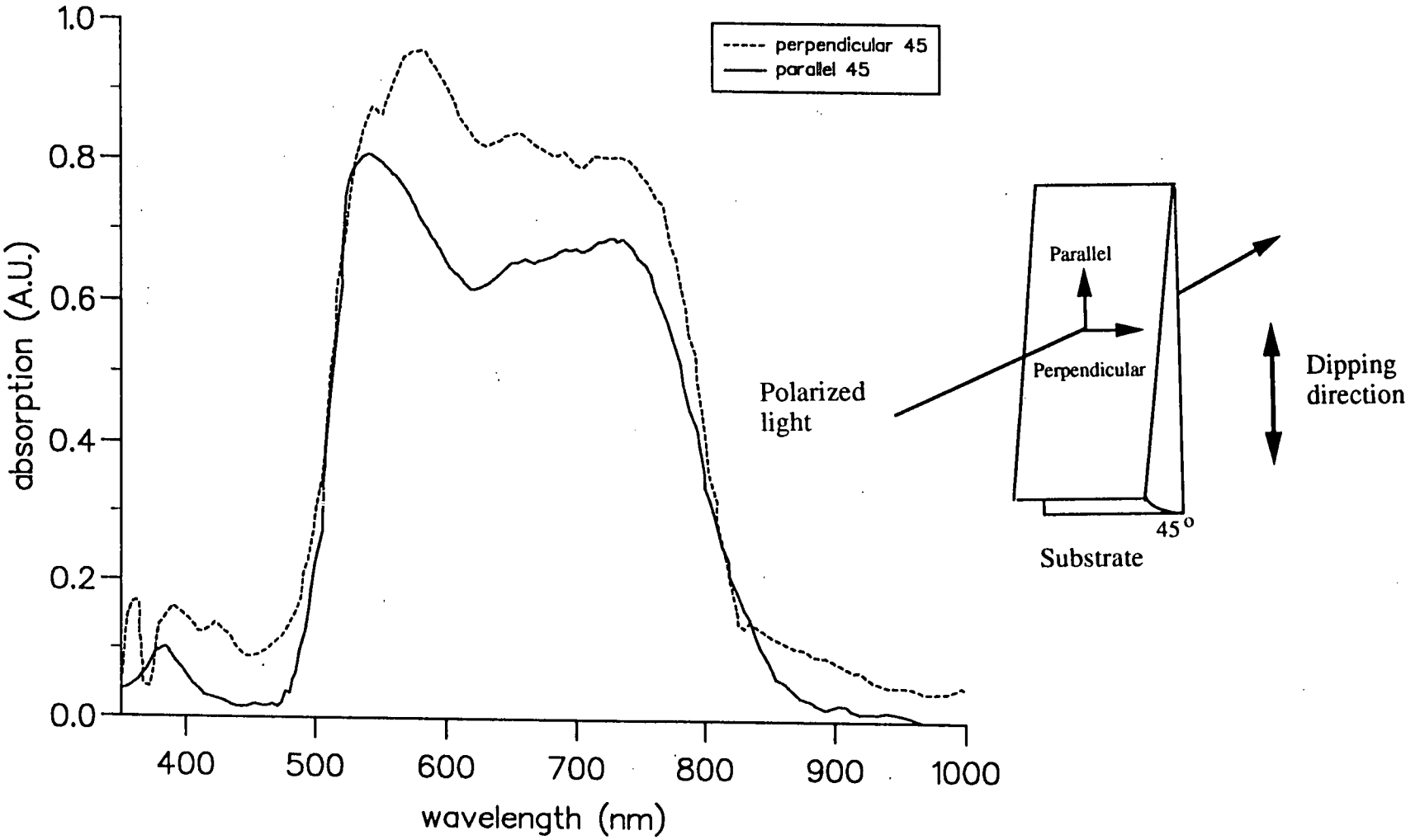

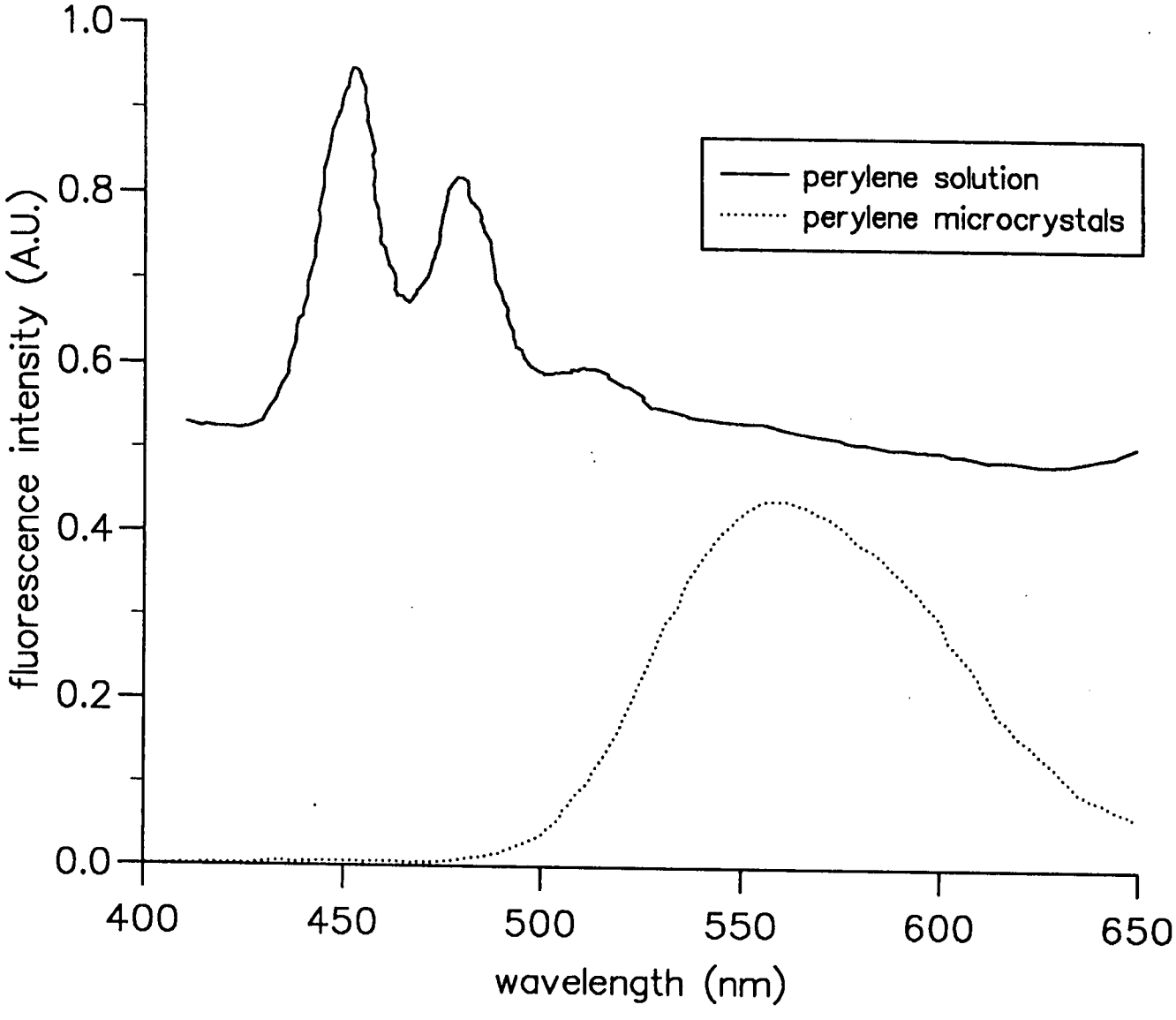

Figure 5.31 Fluorescence spectra of perylene microcrystals and a 10^{-5} M solution in chloroform.

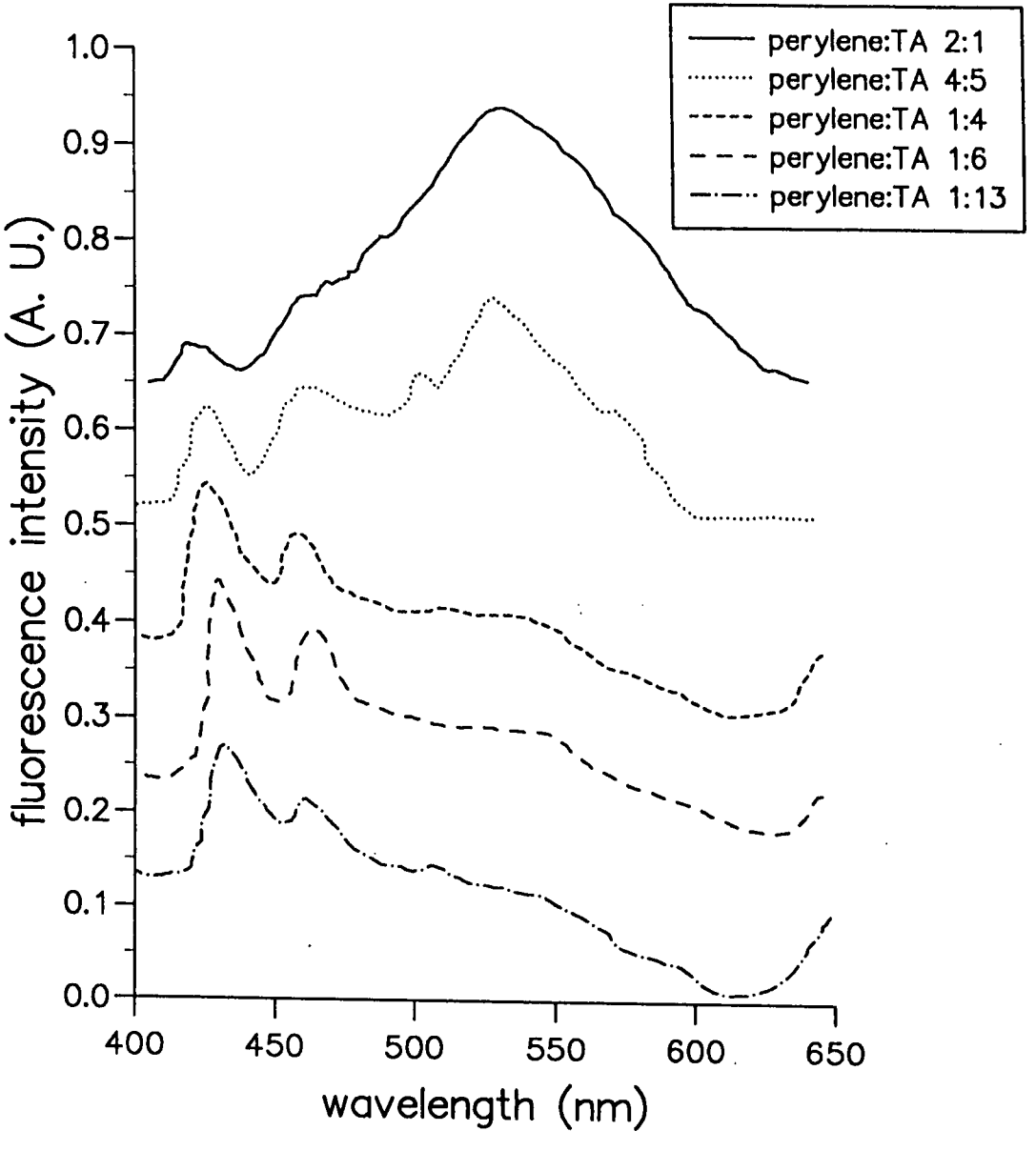

Figure 5.32 Fluorescence spectra of multilayers of perylene:TA 2:1, 4:5, 1:4, 1:6 and 1:13 at 293K.

perylene in solution and therefore can be attributed to monomer fluorescence. It is noticed that the lifetime of perylene in solution decreases with increasing concentration, due to concentration quenching. When the molar ratio of perylene to TA in the film decreases, the number of monomers relative to dimers increases causing a corresponding decrease in monomer lifetime due to concentration quenching. The lifetime of approximately 15 ns can be attributed to perylene dimers. The lifetime for microcrystals of 34.2 ns implies that the LB films are not microcrystalline in nature.

5.6.2 Perylene fluorescence at 110K

Further studies of perylene:TA LB films of molar ratios 2:1, 4:5, 1:4, 1:6 and 1:13 were undertaken at 110K. Emission spectra are shown in figure 5.33, with bands evident at 445, 480, 546, 580 and 600 nm. The first two can be associated with monomer fluorescence whilst the third, which appears as a shoulder, can be attributed to dimers as it is the mirror image of the broad absorption band at 374 nm. The origin of the fourth and fifth red-shifted bands may result from excimers. Similar spectra with excimer bands were reported by Ferguson[16] for a solvent glass of perylene. The emission spectrum becomes increasingly blue-shifted as the molar ratio of perylene to TA decreases. The unstructured emission finally disappears at a ratio of 1:13, leaving monomer and dimer bands only. These observations suggest that three emitters are present. Thus in order to determine the lifetimes from the fluorescence decay curves (figure 5.34) a tri-exponential model has to be used. The fluorescence decay curves show that the excimer (which emits from ~550-650 nm) is much longer-lived than the monomer (which emits from ~440-500 nm) and the dimer (which emits from ~500-600 nm). The results obtained from this fitting are shown in table 5.9. The film with a molar ratio of 1:13 has monomer emitters only with a lifetime of 5 ns, corresponding to monomers in solution. When the molar ratio is increased to 1:6 and 1:4, two lifetimes are obtained at an emission wavelength of 480 nm. These describe the isolated monomer (5 ns) and the quenched monomer (0.6 ns). The lifetimes of dimers and excimers are seen to decrease with decreasing fluorescence wavelength. This is in marked contrast with the constant fluorescence lifetime versus wavelength results for monomers in solution. The difference is explained by homogeneous broadening caused by the varied environment in which the perylene molecules exist.

λ_{fl} (nm)	Molar ratio	τ_1 (ns)	τ_2 (ns)	τ_3 (ns)	B_1	B_2	B_3	χ^2
		M→ E	E	D	M→ E	E	D	
600	2:1	0.5	77.7	12.0	-0.86	85.39	15.47	1.3
580		0.5	69.8	9.0	-1.67	79.59	22.09	1.6
546		0.4	54.8	8.2	-4.43	56.14	48.20	1.7
600	4:5	0.6	74.6	11.2	-1.19	86.85	14.34	1.2
580		0.6	69.8	9.9	-1.98	82.27	19.70	1.3
546		0.4	55.1	8.1	-6.25	61.91	44.35	1.7
600	1:4	0.6	72.5	10.1	-4.5	85.00	19.50	1.2
580		0.6	69.0	9.5	-7.1	81.97	25.13	1.4
546		0.5	54.2	8.1	-8.9	60.07	48.83	1.5
		M→ E	M		M→ E	M		
480		0.5	5.2		47.95	51.66		1.5
600	1:6	0.6	70.5	9.3	-5.52	86.63	18.88	1.1
580		0.5	68.4	9.3	-7.88	80.39	27.08	1.2
546		0.5	53.3	7.8	-9.7	58.98	50.72	1.5
		M→ E	M		M→ E	M		
480		0.7	5.0		47.95	52.05		1.3
		M						
480	1:13	5.1						1.6

Table 5.9 The best-fit parameters for fluorescence decay of LB-films of perylene:TA at 110K. $I(t)=B_1\exp(-t/\tau_1)+B_2\exp(-t/\tau_2)+B_3\exp(-t/\tau_3)$.

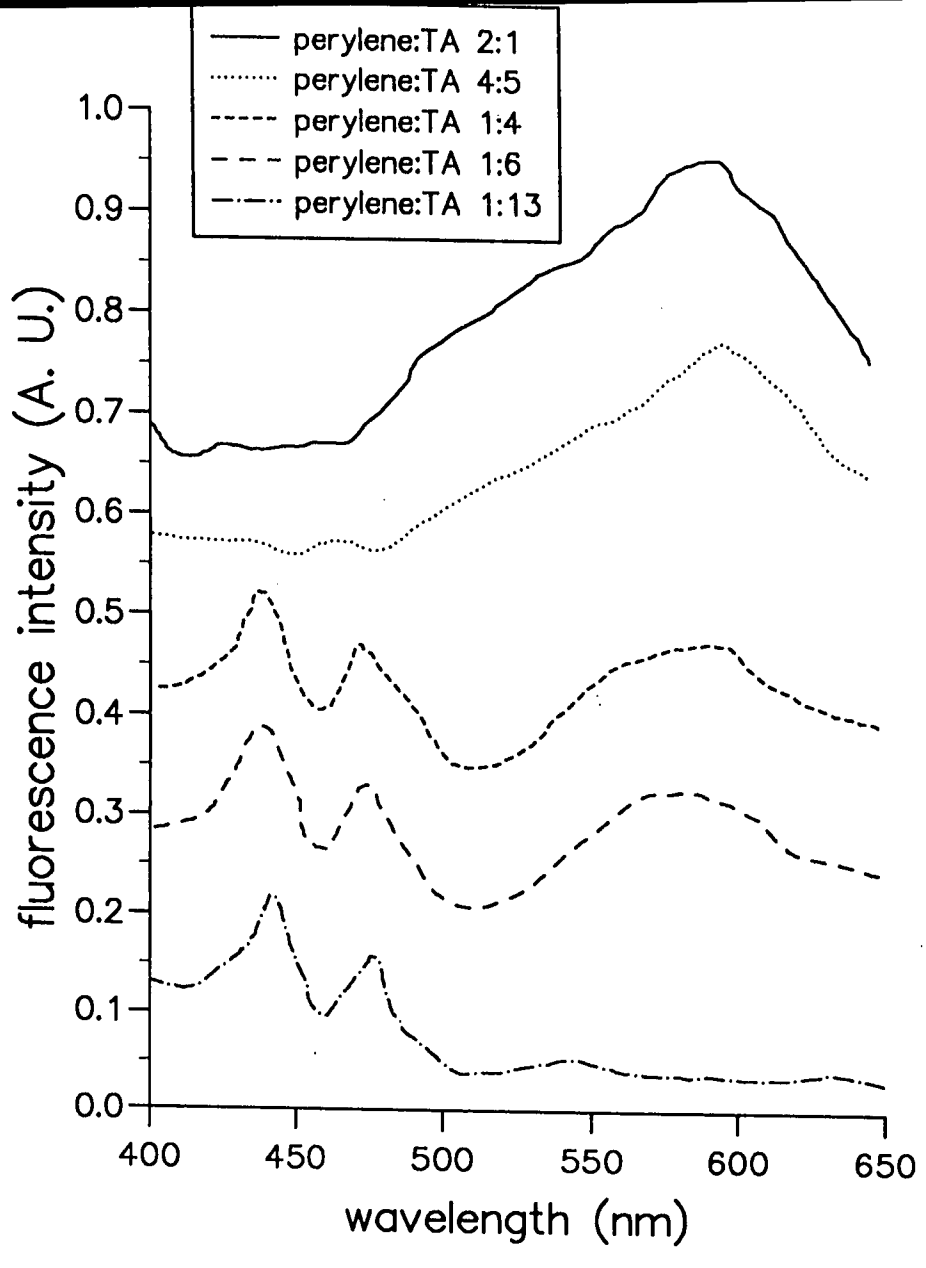

Figure 5.33 Fluorescence spectra of multilayers of perylene:TA 2:1, 4:5, 1:4, 1:6 and 1:13 at 110K.

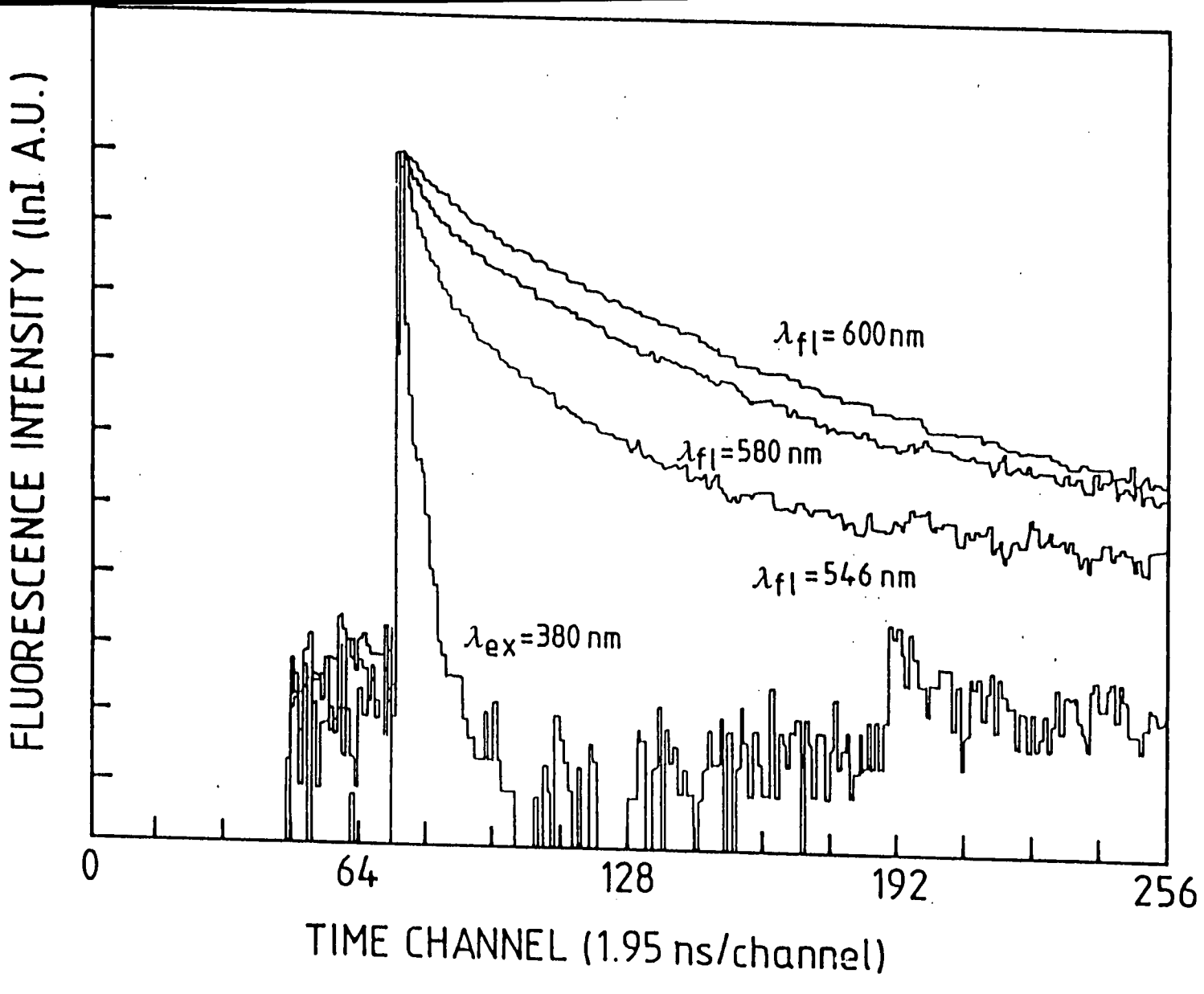

Figure 5.34 Fluorescence decay curves for perylene.

5.7 Ellipsometry

5.7.1 Sq1

The film thickness of 20 layers of Sq1 dipped on 2 layers of TA in the second condensed phase was measured by ellipsometry. The first two layers of TA were assumed to have a thickness of 5.6 nm, the remaining layers were then found to have an average thickness of 1.8 nm. This value might correspond to the long axis of the molecule. However, the polarized absorption measurements disagree with this because it was found that the dipole moments are in the plane of the substrate; this is also substantiated by the area per molecule results. Therefore the most probable orientation of the molecules is that they are stacked on their longest edge in the form of a bilayer.

5.7.2 Perylene:22TA

The thickness of stepped layers of perylene:22TA were measured by ellipsometry at a wavelength of 632.8 nm, where the film was least absorbing. The average thickness per layer is 2.8 nm, corresponding almost exactly to the layer thickness obtained for pure 22TA layers. It can therefore be concluded that either the perylene is not transferred onto the substrate or it is incorporated into the fatty acid matrix. As optical absorption studies have shown that perylene is present in the films the latter conclusion would appear to be correct. However, the perylene molecules may form domains within the fatty acid films.

5.8 X-Ray Diffraction

5.8.1 Perylene

X-ray low angle diffraction measurements were undertaken on a number of perylene:TA LB films and the results are given in table 5.10. These values of d-spacing obtained are consistent with TA molecules tilted by 28 degrees to the perpendicular. If squeezing out was taking place such that the perylene molecules were between the headgroups or the tails, two d-spacings would be obtained, corresponding to two different distances between the TA headgroups.

Perylene:TA	Spacing d(nm)
3:1	5.51
3:2	5.44
4:7	5.57

Table 5.10a X-ray d-spacings for 30 layers of perylene:TA on glass

Perylene:TA	Spacing d(nm)
2:1	5.55
4:5	5.47
1:4	5.58
1:6	5.56
1:13	5.48

Table 5.10b X-ray d-spacings for 30 layers of perylene:TA on quartz

As only one d-spacing is found which corresponds to that for a pure TA film it can be assumed that the perylene molecules are not squeezed out but are incorporated in the TA matrix. This is confirmed by ellipsometry of perylene/22TA films in section 5.8.

5.8.2 Sq3

The d-spacing for 76 layers of Sq3:22TA 5:1 was found to be 1.74 nm, giving a thickness per layer of 0.87 nm. From the dimensions of the molecule in section 5.3.4 this distance would correspond to the molecule lying on its longest edge. This is in agreement with the ellipsometry results for Sq1.

5.9 Electron Diffraction

RHEED studies are reported here for two dye:fatty acid LB systems. Sq3:TA was chosen for study because it was a high quality film and showed some anisotropy in polarized absorption studies. Perylene:TA was also selected for study because it showed significant dichroism. In both cases six layers of the mixed films were

deposited onto (111) Si.

5.9.1 RHEED of Sq3:TA

The RHEED pattern of 6 layers of Sq3:TA 1:6 (shown in figure 5.35) was taken with the electron beam parallel to the direction of dipping. The diffraction spots are smeared out to form arcs which are parallel to the shadow edge, indicating that the molecules are not tilted. This pattern is almost identical to a pattern of 22-tricosenoic acid obtained by Peterson and Russell[33], suggesting that there is very little contribution from the Sq3. Rotating the sample relative to the electron beam had no effect on the diffraction pattern indicating that there is no anisotropy with dipping direction.

5.9.2 RHEED of perylene:TA

The RHEED pattern obtained from 6 layers of 1:12 perylene:TA on hydrophobic (111) silicon (figure 5.36) is completely different from the previous pattern; the most striking observation is the profusion of diffraction spots and their sharpness. The spots are well defined and appear to form lines parallel to the central row of spots; a rectangular matrix of spots is almost visible. This quality of pattern is not obtained from simple fatty acid assemblies alone and has only been observed for an amido nitrostilbene[34] and C4 anthracene[35]. The central row of spots shows fine splitting which is expected of bilayer periodicity. The pattern is indicative of a material with preferred orientation and a high degree of structural order. This is in agreement with the results obtained from polarized absorption measurements.

5.10 Summary

In this chapter a variety of dyes have been investigated for their ability to form good quality LB films, with the desired spectroscopic properties required for SPR studies. It has been shown in section 5.3 that some of the dyes undergo reordering on the surface. In section 5.4, the optical absorption of these dyes is shown to be linked to the reorientation of the molecules. Comparison between spectra in sections 5.4 reveals the formation of aggregates. Fluorescence studies of perylene in section 5.6 show that the aggregates in these films to be dimers. In sections 5.7 and 5.8 layer thicknesses are determined which resolve the possible arrangement

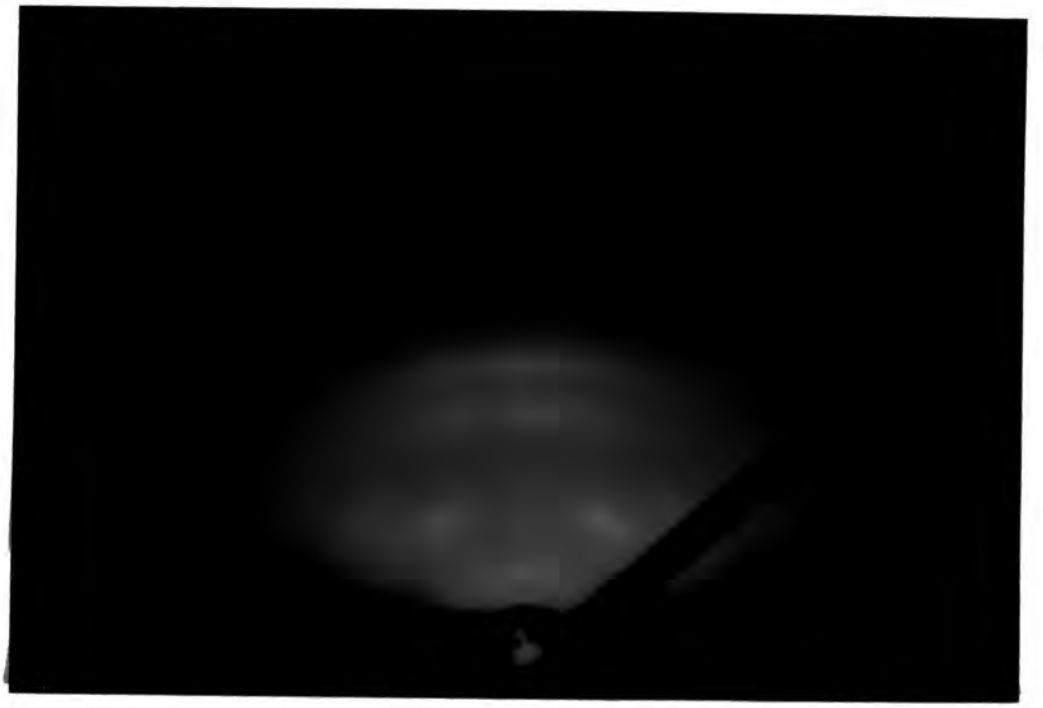

Figure 5.35 RHEED pattern for 6 layers of Sq3:TA 1:6.

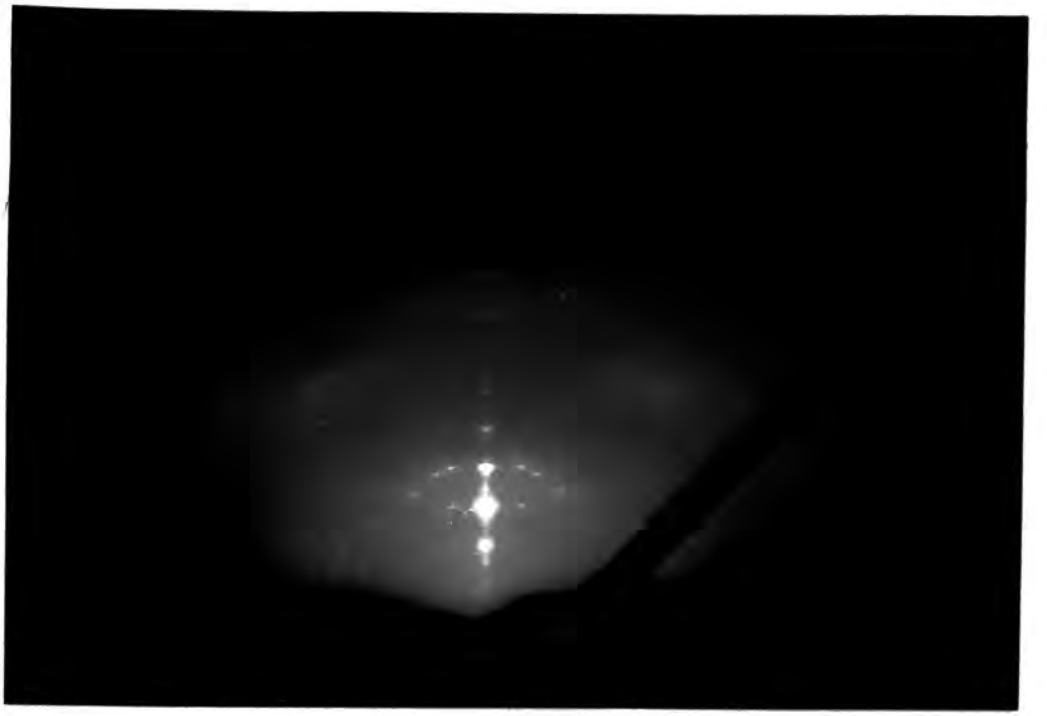

Figure 5.36 RHEED pattern for 6 layers of perylene:TA 1:12.

of the molecules. Finally, perylene:TA films are shown from RHEED studies to be highly ordered.

5.11 References

1. S. Baker *Phthalocyanine Langmuir-Blodgett Films and their Associated Devices* Ph.D. Thesis University of Durham (1985)

2. D.W. Kalina and S.W. Crane *Langmuir-Blodgett Films of Soluble Copper Octa(Dodecoxymethyl)Phthalocyanine* Thin Solid Films Vol 134 (1985) pp 109-119

3. K.A. Zachariasse and D.G. Whitten *Dimerization of Porphyrins in Highly Dilute Solution at Low Temperature and in Monomolecular Layers* Chem.Phys. Lett. Vol 22 (1973) pp 527-532

4. J.P. Li, R.H. Tredgold, R. Jones and P. Hodge *Interactions of Nitrogen Dioxide with Langmuir-Blodgett Films of a Copper Porphyrin* Thin Solid Films Vol 186 (1990) pp 167-176

5. W.S. Durfee, W. Storck, F. Willig and M. von Frieling *Davydov Splitting in 7-(2-Anthryl)-1-heptanoic Acid Langmuir-Blodgett Films* J.Am.Chem.Soc. Vol 109 (1987) pp 1297-1301

6. T. Yamazaki, N. Tamai and I. Yamazaki *Molecular Association of Pyrene in the Langmuir-Blodgett Monolayer Film: Analysis of Picosecond Time-Resolved Fluorescence Spectra* Chem.Phys.Lett. Vol 124 (1986) pp 326-330

7. A.H. Herz *Dye-Dye Interactions of Cyanines in Solution and at AgBr Surfaces* Photogr.Sci.Eng. Vol 18 (1974) pp 323-335

8. G. Biesmans, M. Van der Auweraer and F.C. De Schryver *Influence of Deposition Circumstances on the Spectroscopic Properties of Mixed Monolayers of Dioctadecyloxacarbocyanine and Arachidic Acid* Langmuir Vol 6 (1990) pp 277-285

9. P.M. Kazmaier, R. Burt, G. DiPaola-Baranyi, C.K. Hsiao, R.O. Loufty, T.I. Martin, G.K. Hamer, T.L. Bluhm and M.G. Taylor *The Photogenerating Properties of Unsymmetrical Squaraines and Squaraine Composites* J.Img.Sci. Vol 32 (1988) pp 1-4

10. V.B. Jipson and C.R. Jones *Infrared Dyes for Optical Storage* J.Vac.Sci. Technol. Vol 18 (1981) pp 105-109

11. R. Steiger *Studies of Oriented Monolayers on Solid Surfaces by Ellipsometry* Helvetica Chemica Acta Vol 54 (1971) pp 2645-2658

12. M. Aizawa, M. Matsuzawa and H. Shinohara *An Optical Chemical Sensor Using a Fluorophor-Embedded Langmuir-Blodgett Film* Thin Solid Films Vol 160 (1988) pp 477-481

13. P.L. Fan, D.C. Larson and M.M. Labes *Role of Substrate in Determining the Crystallinity of Organic Thin Films* Thin Solid Films Vol 12 (1972) S3-S7

14. A.B. Buckman and W.D. Bomberger *Optical Properties of Perylene Films in the Visible and Near UV* J.Opt.Soc.Am. Vol 63 (1973) pp 1432-1433

15. J.B. Birks and D.J. Dyson *The Relationship Between the Fluorescence and Absorption Properties of Organic Molecules* Proc.Roy.Soc. Ser. A275 (1963) pp 135-148

16. J. Ferguson *Absorption and Emission Spectra of the Perylene Dimer* J.Chem. Phys. Vol 44 (1966) pp 2677-2683

17. R.M. Hochstrasser *The Crystal Spectrum of Perylene* Can.J.Chem. Vol 39 (1961) pp 451-458

18. K. Fuke, K. Kaya, T. Kajiwara and S. Nagakura *The Polarized Reflection and Absorption Spectra of Perylene Crystals in Monomeric and Dimeric Forms* J.Mol.Spectr. Vol 63 (1976) pp 98-107

19. U. Lehmann *Aggregation of Cyanine Dyes at Langmuir-Blodgett Monolayers* Thin Solid Films Vol 160 (1988) pp 257-269

20. D.F. O'Brien *J-Aggregation in Monomolecular Layers of Cyanine Dyes* Photog.Sci.Eng. Vol 18 (1974) pp 16-21

21. Y.L. Hua, G.G. Roberts, M.M. Ahmad, M.C. Petty, M. Hanack and M. Rein *Monolayer Films of a Substituted Silicon Phthalocyanine* Phil.Mag.B Vol 53 (1986) pp 105-113

22. D.B Neal *Langmuir-Blodgett Films for Nonlinear Optics* Ph.D. Thesis University of Durham (1987)

23. M. Matsumoto, T. Nakamura, M. Tanaka, T. Sekiguchi, H. Komizu, S.Y. Matsuzaki, E. Manda, Y. Kawabata, M. Saito, S. Izima and M. Sugi *Structure Study of Supermonomolecular Layers in Langmuir-Blodgett Films. Surface Active Squarylium Dye-Fatty Acid Binary Mixed System* Bull.Chem.Soc.Jpn. Vol 60 (1987) pp 2737-2742

24. H. Bücher and H. Kuhn *Scheibe Aggregate Formation of Cyanine Dyes in Monolayers* Chem.Phys.Lett. Vol 6 (1970) pp 183-185

25. H.J. Nolte *A Model of the Optically Active Scheibe-Aggregate of Pseudoisocyanine* Chem.Phys.Lett. Vol 31 (1975) pp 134 139

26. S. Kim, M. Furuki, L.Y. Pu, H. Nakahara and K. Fukuda *Unique Monolayer Assembly of Squarylium Dye with Short Alkyl Chains* J.Chem.Soc.,Chem. Commun. (1987) pp 1201-1203

27. K.Y. Law and C.C. Chen *Squaraine Chemistry. Effect of Orientation on the Aggregation of Surfactant Squaraines in Langmuir-Blodgett Films* J.Phys. Chem. Vol 93 (1989) pp 2533-2538

28. R.O. Loufty, C.K. Hsiao and P.M. Kazamaier *Photoconductivity of Organic Particle Dispersions: Squaraine Dyes* Photo.Sc.Eng. Vol 27 (1983) pp 5-9

29. K.Y. Law *Effect of Dye Aggregation on the Photogeneration Efficiency of Organic Photoconductors* J.Phys.Chem. Vol 92 (1988) pp 4226-4231

30. M. Fujiki and H. Tabei *Preparation and Electrical Properties of Lightly Substituted Phthalocyanine Langmuir-Blodgett Films* Langmuir Vol 4 (1988) pp 320-326

31. I. Pockrand, A. Brillante and D. Möbius *Exciton-Surface Plasmon Coupling: An Experimental Investigation* J.Chem.Phys. Vol 77 (1982) pp 6289-6295

32. M. Tristani-Kendra, C.J. Eckhardt, J. Bernstein and E. Goldstein *Strong Coupling in the Optical Spectra of Polymorphs of a Squarylium Dye* Chem.Phys. Lett. Vol 98 (1983) pp 57-61

33. I.R. Peterson and G.J. Russell *An Electron Diffraction Study of ω-Tricosenoic Acid Langmuir-Blodgett Films* Phil.Mag.A Vol 49 (1984) pp 463-473

34. D.B. Neal, G.J. Russell, M.C. Petty, G.G. Roberts, M.M. Ahmad and W.J. Feast *A Highly Ordered LB Monolayer of an Amido Nitrostilbene* J.Mol.Elec. Vol 2 (1986) pp 135-138

35. I.R. Peterson, G.J. Russell, D.B. Neal, M.C. Petty, G.G. Roberts , T. Ginnai and R.A. Hann *An Electron Diffraction Study of LB Films Prepared from a Lightly Substituted Anthracene Derivative* Phil.Mag.B Vol 54 (1986) pp 71-79

36. K. Saito, K. Ikegami, S. Kuroda, M. Saito, Y. Tabe and M. Sugi *Davydov Splitting in Arachidic Acid-Cyanine Dye Complex Langmuir-Blodgett Films* J.Appl.Phys. Vol 68 (1990) pp 1968-1973

37. I.R. Peterson and G.J. Russell *The Deposition and Structure of Langmuir-Blodgett Films of Long-Chain Acids* Thin Solid Films Vol 134 (1985) pp 143-152

38. A.C. Tam *Optoacoustic Determination of Photocarrier Generation Efficiencies of Dye Films* App.Phys.Lett Vol 37 (1980) pp 978-981

39. V.Y. Morel and H.J. Hovel *Organic Solar Cells of Hydroxy-Squarylium* Appl. Phys.Lett. Vol 29 (1976) pp 414-415

40. V.Y. Morel, A.K. Gosh, T. Feng, E.L. Stogryn, P.E. Purwin, R.F. Shaw and C. Fishman *High-Efficiency Organic Solar Cells* Appl.Phys.Lett. Vol 32 (1978) pp 495-

41. V.Y. Merrit *Organic Photovoltaic Materials: Squarylium and Cyanine-TCNQ Dyes* IBM J.Res.Develop Vol 22 (1978) pp 353-371

Chapter VI

Surface Plasmon Studies

6.1 Introduction

The object of this chapter is to demonstrate how the surface plasmon technique can be used to probe organic layers deposited on a silver coated slide. Section 6.2 is concerned with the effect of silver parameters on the resonance curves and results from a theoretical model are compared to those obtained experimentally. The addition of absorbing and non-absorbing LB overlayers is studied in 6.3. In 6.4 results obtained from a variable wavelength experimental setup are given and discussed. Data are presented for a new dye system containing a derivative of squaraine. Values for the permittivity of a similar dye which has been reported in the literature are inserted into the model and the results obtained are compared to experiment in 6.5. Finally, the surface plasmon work is summarized in section 6.6.

6.2 Surface Plasmon Resonance on Silver Films

In Chapter 3 the theory of surface plasmon polaritons and the methods used to generate them were discussed in some detail; the importance of the evaporated silver layer was also noted. In this section the silver parameters are varied in a modelling program and the resonance curves obtained compared to experimental results. A qualitative explanation is made of the factors which affect the resonance conditions. The modelling program was written by J. Cresswell and solves Maxwell's equations to find the reflectivity at each interface (a schematic of the layer structure is shown in fig 6.1); more details are given in his thesis[1]. All the measurements were made using a HeNe laser which was tunable to four wavelengths: 632.8, 611.9, 594.1 and 543.0 nm.

A surface plasmon resonance (SPR) curve can be described by three features: the angular position at which the resonance minimum occurs (θ_{min}); the reflectivity

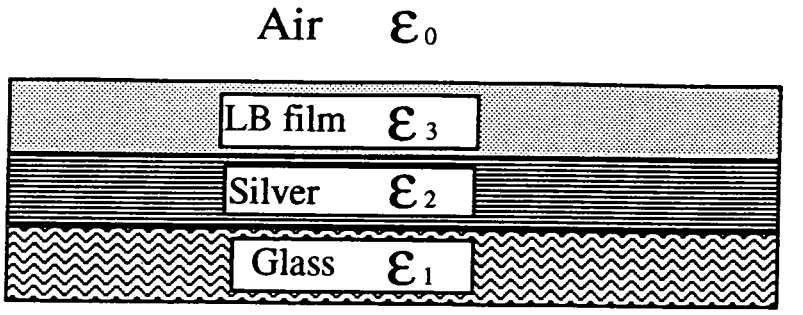

Figure 6.1 The layer structure used in the modelling program.

at this minimum (R_{min}); and the full width of the curve at half maximum (fwhm); these are shown on an ideal SPR curve (in figure 6.2). Values obtained from SPR curves for each of these parameters are presented as a function of either thickness (d) or wavelength (λ), in a graphical form; lines are drawn between points to indicate a trend in the results but this is not intended to show an absolute relationship.

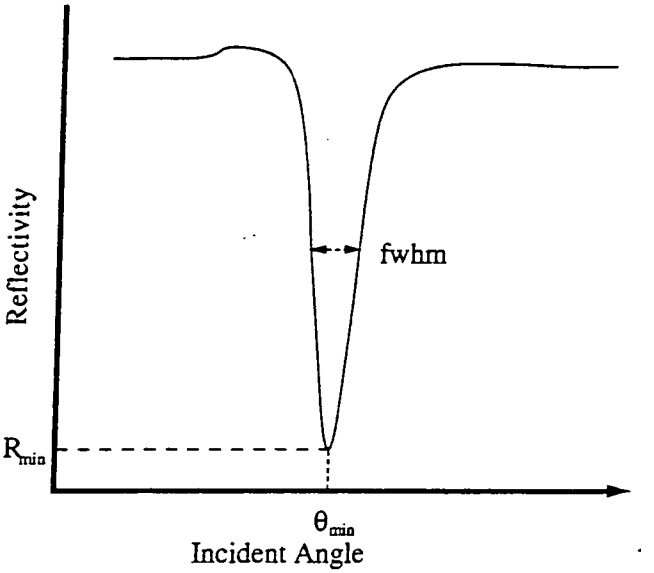

Figure 6.2 A typical SPR curve showing the important features.

6.2.1 Theoretically generated resonance curves

The values of silver permittivity used in the modelling program were obtained from a publication by Schröder[2] (determined from SPR measurements) and are listed in table 6.1.

$\lambda(nm)$	ϵ'	ϵ''
700	-22.4	0.91
690	-21.7	0.88
680	-21.0	0.85
670	-20.3	0.81
660	-19.7	0.77
650	-19.0	0.74
640	-18.3	0.69
630	-17.6	0.67
620	-16.9	0.65
610	-16.3	0.62
600	-15.6	0.59
590	-14.9	0.55
580	-14.3	0.52

$\lambda(nm)$	ϵ'	ϵ''
570	-13.6	0.49
560	-13.0	0.47
550	-12.4	0.45
540	-11.8	0.43
530	-11.2	0.41
520	-10.6	0.39
510	-10.0	0.38
500	-9.4	0.37
490	-8.9	0.35
480	-8.4	0.34
470	-7.7	0.33
460	-7.2	0.32
450	-6.6	0.31

Table 6.1 Silver real an imaginary values of dielectric constant (after Schröder).

The values for refractive index of the glass were taken from Melles Griot data for BK7 (borosilicate crown) glass and figures for ϵ_1 were then calculated and are listed in table 6.2. The dispersion of the glass was not considered to be significant. To see the effect of silver thickness on the resonance, the wavelength was kept constant at 543 nm and values for the silver thickness were changed in the model.

$\lambda(nm)$	Refractive index	Real permittivity ϵ'
660	1.5140	2.2922
640	1.5147	2.2943
620	1.5156	2.2967
600	1.5164	2.2995
580	1.5173	2.3022
570	1.5176	2.3031
560	1.5181	2.3046
550	1.5185	2.3058
540	1.5190	2.3074
530	1.5194	2.3086
520	1.5198	2.3108
510	1.5205	2.3119
500	1.5216	2.3153
480	1.5230	2.3195

Table 6.2 The refractive index and real part of permittivity for BK7 (Melles Griot data).

From the series of SPR curves (figure 6.3), the effect of silver thickness can be seen on θ_{min}, R_{min} and fwhm. The resonance angle θ is not influenced greatly by the silver thickness.

The change in silver thickness appears to have most effect on the reflectivity minimum. A plot of R_{min} versus thickness (fig 6.4) clearly shows that R_{min} passes through a minimum at 55 nm. Finally the width of the SPR curves decreases with increasing silver thickness. These observations fit well with the excepted behaviour of surface plasmon coupling[3,4]. The depth of the resonance minimum R_{min} is determined by the coupling efficiency of the system which is the ratio of two damping processes, inner and radiation damping. Inner damping is caused by

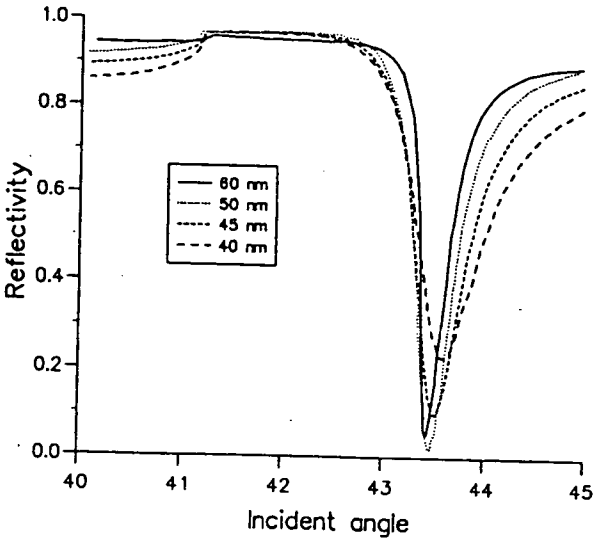

Figure 6.3 SPR curves at 543 nm for different values of silver thickness, from theory.

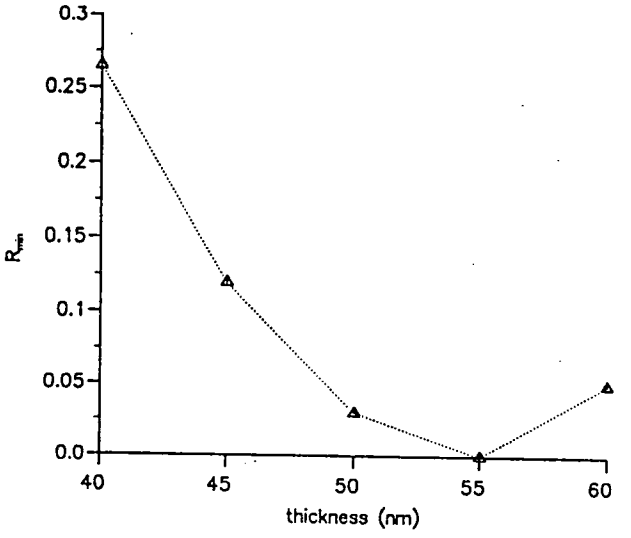

Figure 6.4 R_{min} versus thickness for silver from theory

absorption in the layer system, including the silver, and radiation damping results from back radiation into the halfspace (prism). Optimal coupling (R_{min}=0) is achieved when the two processes are of equal magnitude. When the silver layer is thin, radiation damping is dominant while inner damping becomes increasingly important as the layer is made thicker. Two thickness limits exist for the silver layer: the upper is where the silver is too thick for the evanescent field to penetrate and the lower is where the silver layer is too thin to support surface plasma waves. At 543 nm the optimal thickness from figure 6.4 is therefore approximately 55 nm; this value will of course be different at other wavelengths.

The effect of silver permittivity on the surface plasmon resonance curves can be determined by varying the real and imaginary parts of permittivity independently. A wavelength of 543 nm was chosen, and a constant value of -11.8 for the real part of permittivity ϵ_2' was used. There was no significant change in the SPR curves with the imaginary part of permittivity ϵ_2'' between 0.4 and 0.5. The resonance angle remained constant at 43.5°. The change in reflectivity minimum was virtually zero with increasing ϵ_2'' and the resonance width, fwhm, remained almost constant.

If ϵ_2'' was kept constant at 0.43 whilst ϵ_2' was varied the following trends were observed in the SPR curves: the angle at which the resonance occurs did not change significantly with increasing ϵ_2'; and the resonance minimum decreased slightly with decreasing ϵ_2'.

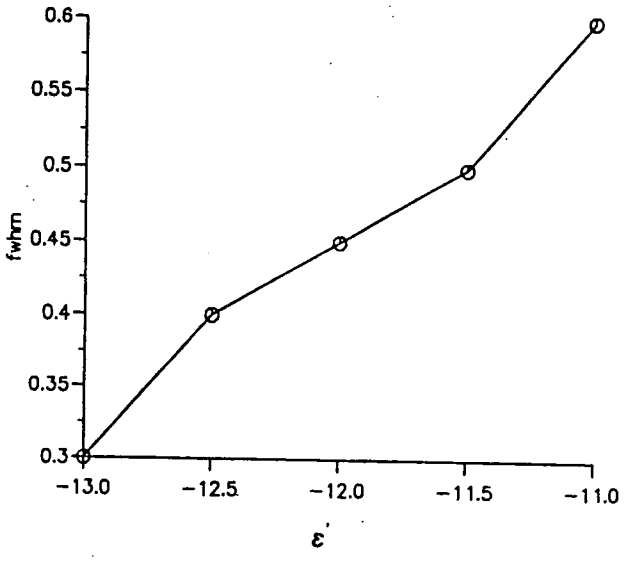

Figure 6.5 Fwhm versus ϵ_2', with ϵ_2''=0.43 from theory.

The resonance width fwhm decreases significantly with decreasing ϵ_2' (figure 6.5).

From these results it can be concluded that the imaginary part of the silver permittivity (associated with the damping) over a range between 0.4 and 0.5 has little effect on the resonance conditions. However, the real part of permittivity (associated with the refractive index) has a much greater influence, particularly on the resonance width.

The thickness of the silver layer was assumed to be 50 nm for all the theoretical modelling. However, this only gives optimum resonance conditions at a wavelength of 632.8 nm. This choice of thickness was convenient because the evaporator was set up specifically to deposit silver films of approximately 50 nm thick. Wavelengths of interest were taken as 632.8 nm, 611.9 nm, 594.1 nm and 543.1 nm (HeNe wavelengths). The values of θ_{min}, R_{min} and fwhm were observed to vary with λ. This is not surprising since the medium is dispersive. As λ increases, θ_{min} decreases, but the relationship is not linear (figure 6.6a); R_{min} decreases to zero at 611.9 nm (figure 6.6b); fwhm decreases with increasing λ but reaches a plateau (figure 6.6c).

6.2.2 Experimental silver resonances

Values obtained for θ_{min}, R_{min} and fwhm on two evaporated silver films (evaporated at different times and nominally 50 nm thick) are plotted alongside those predicted by the modelling program in figures 6.6a,b and c. The values for θ_{min} are larger, by approximately 0.3° for silver, but follow a similar relationship and the two sets of experimental points are in good agreement with each other. R_{min} also follows a similar relationship to theory but values for the experimental silver films are considerably larger and there is also a difference between the experimental curves. The widths of the resonance, fwhm, for the experimental data are greater than theory and follow a slightly different form; they also differ from each other.

The only two parameters which can give rise to the differences between experimental and theory are a difference in the real part of silver permittivity (only ϵ_2' has a significant effect on SPR) and the silver thickness. However, a variation in the silver thickness could not account for the difference in angle of 0.3°. Fitting has shown that the real part of the silver permittivity ϵ_2' would have to be smaller for the experimental silver value to explain the results. An alternative explanation is that the silver layer is not pure, ie it is covered by a thin oxide or sulphide layer. The tarnishing of the film according to Pockrand[5] is due to the formation of Ag_2S, but this worker only observed tarnishing 2h after depositing the silver. The formation of a sulphide layer is conceivable since the atmosphere during measurements was probably rich in sulphur compounds. In fact, a yellow deposit could clearly be seen on a silvered slide only partially coated with an LB

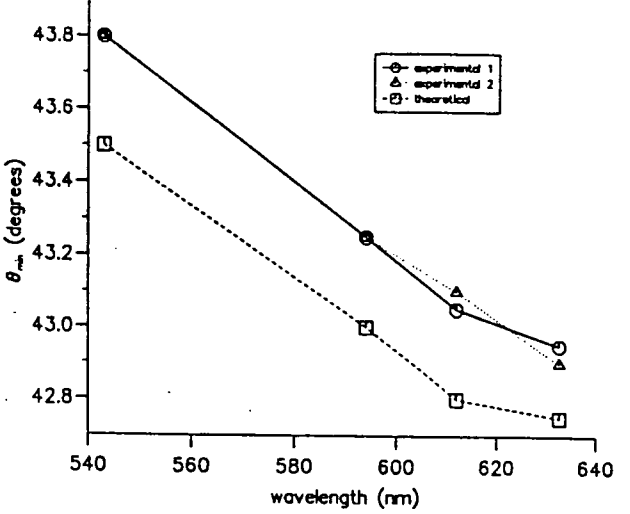

Figure 6.6a θ versus λ for silver theory and experimental where the silver thickness is 50 nm.

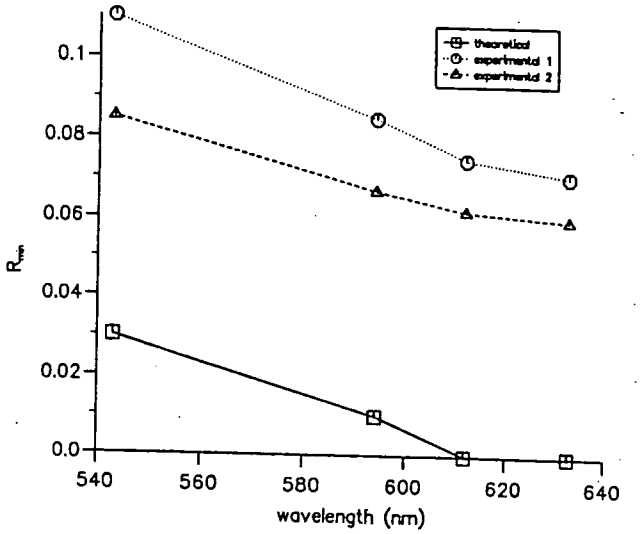

Figure 6.6b Rmin versus λ for silver theory and experimental where the silver thickness is 50 nm.

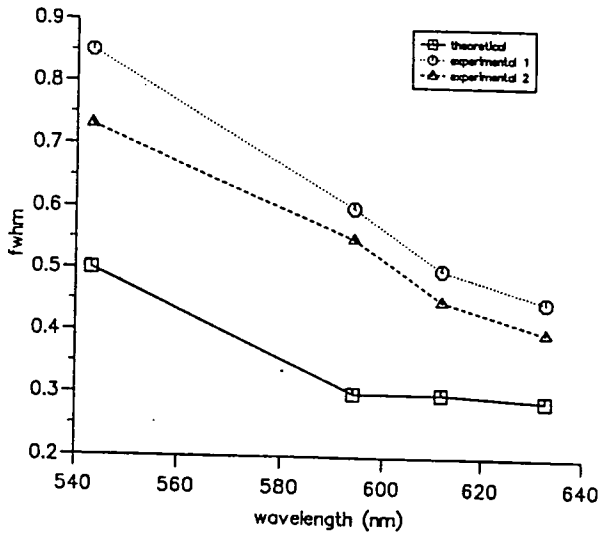

Figure 6.6c Fwhm versus λ for silver theory and experimental where the silver thickness is 50 nm.

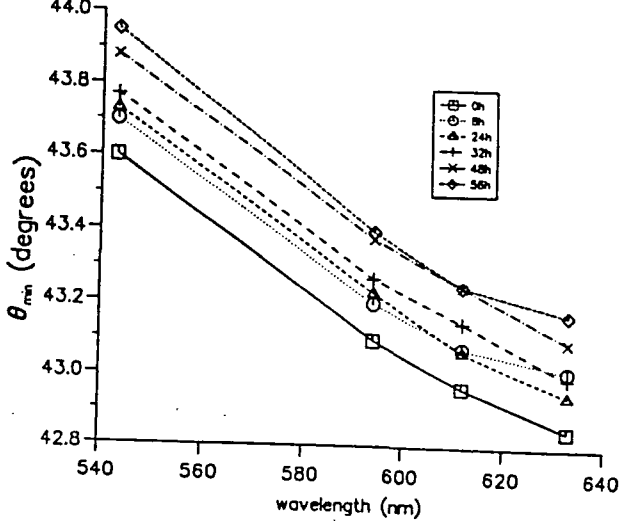

Figure 6.7a θ **versus** λ **for experimental curves measured over a 56h period. The silver thickness is 50 nm.**

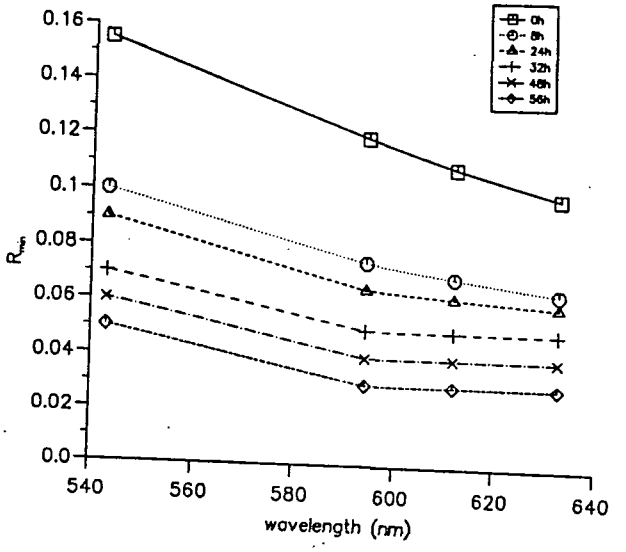

Figure 6.7b Rmin versus λ **for experimental curves measured over a 56h period. The silver thickness is 50 nm.**

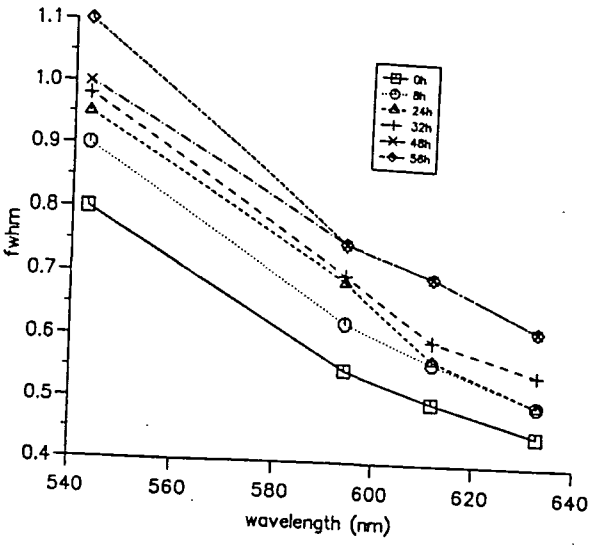

Figure 6.7c Fwhm versus λ **for experimental curves measured over a 56h period. The silver thickness is 50 nm.**

film. The differences between the two sets of experimental points might be due to variations in the evaporation conditions or different ages of the silver films.

A series of curves for θ_{min}, R_{min} and fwhm against λ were recorded for the same sample over a period of a couple of days (fig 6.7a,b and c). The time between the evaporation of the silver film and each measurement was 1) 0h 2) 8h 3) 24h 4) 32h 5) 48h 6) 56h. It is evident that the curves are shifted slightly with time. For example, at 543 nm, θ_{min} increases with time by 0.35° over the 56h period; R_{min} decreases, by approximately 1.05 at 543 nm; and fwhm increases, by approximately 0.3. These observations confirm the suggestion that an oxide or sulphide layer is formed on the metal surface. Silver films must be used immediately or stored carefully under nitrogen, but in either case it is difficult to avoid tarnishing completely.

6.3 The Effect of LB Overlayers

6.3.1 Non-absorbing layers

Figure 6.8 shows the theoretical curves for a non-absorbing layer, with permittivity ϵ_3= 2.5 + 0.002i, on silver 50 nm thick, at a wavelength of 543 nm. This value of permittivity was chosen to represent a typical fatty acid[3].

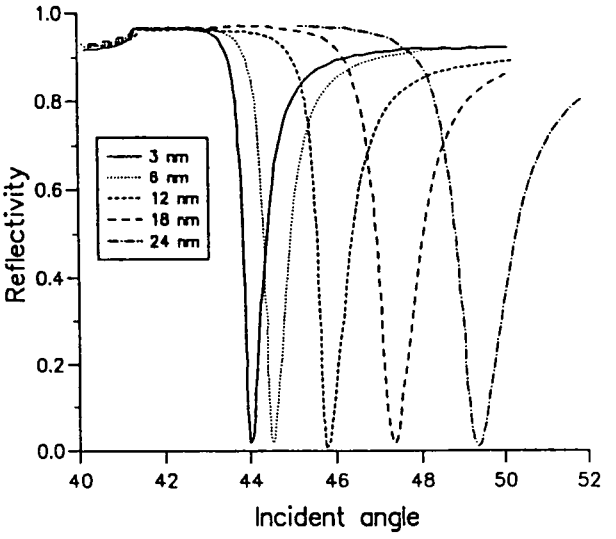

Figure 6.8 SPR curves, from theory, for a change in thickness of non-absorbing layers.

An almost linear relationship is seen between θ_{min} and the thickness of the layer. This is in excellent agreement with experimental data for a TA film (figure 6.9). R_{min}, from theory, remains constant with respect to the thickness, which is expected, since R_{min} has been shown to depend on loss in the overlayer. However, the experimental values for R_{min} (not shown) are larger than theory and are not constant with layer thickness. Both experimental and theoretical values of fwhm (not shown) are not constant but increase with thickness. The experimental values are again larger than for theory.

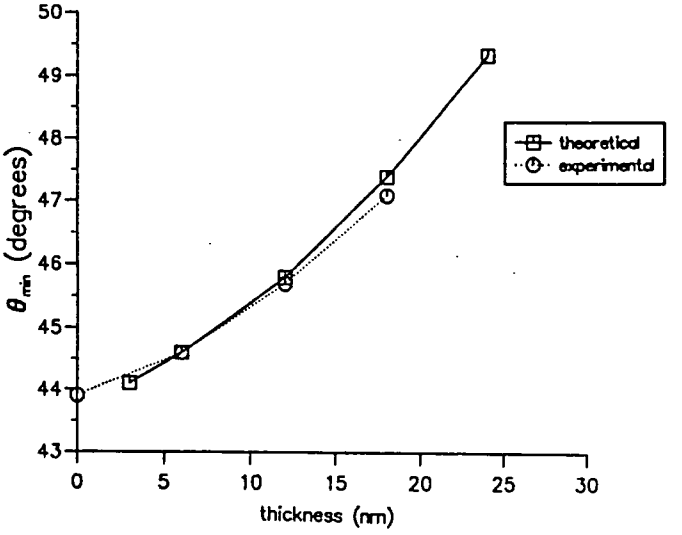

Figure 6.9 Theory and experimental results of θ_{min} versus d for a non-absorbing layer on 50 nm thick silver film.

The theoretical SPR curves at different wavelengths are shown in figure 6.10. The experimental values of θ_{min} for a TA film are in good agreement with this data (figure 6.11.). R_{min} values from theory are identical to those for silver only, which is not unexpected as the layer is non-absorbing. However, the experimental data for R_{min} (not shown) are greater than theory, but compare well with experimental values for silver only. The fwhm values for both experimental and theoretical curves bear little relation to the corresponding curves for silver (fig 6.6c), the latter values being much larger. The experimental values of fwhm are larger than theory and their relationship to the wavelength is slightly different in the long-wavelength region where the fwhm continues to decrease.

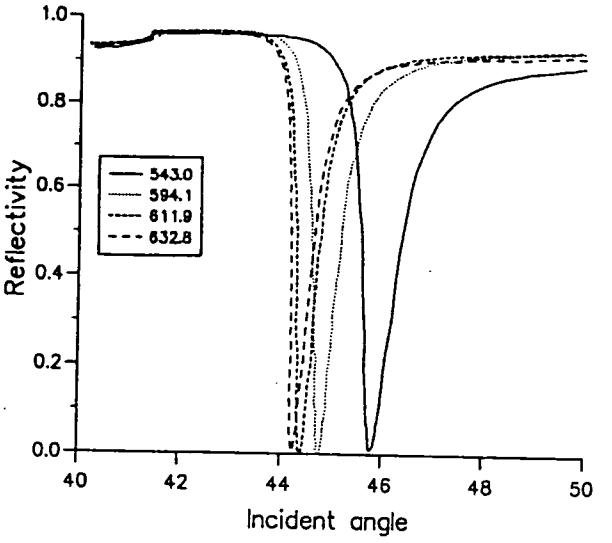

Figure 6.10 SPR curves from theory at different wavelengths for a 12 nm thick non-absorbing layer on 50 nm thick silver film.

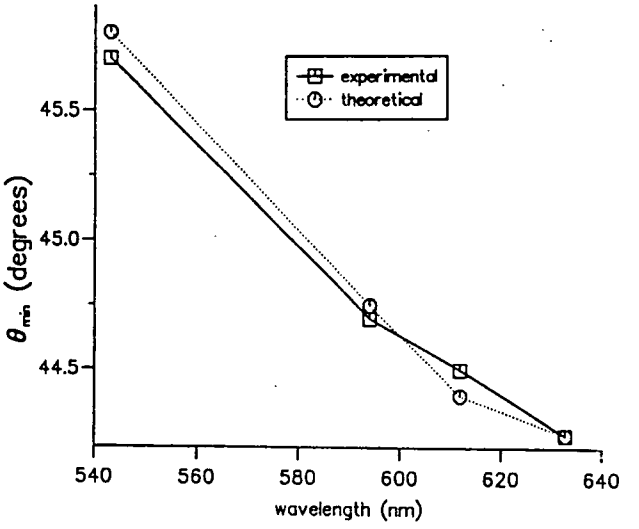

Figure 6.11 θ_{min} versus λ for a non-absorbing layer.

These differences between theoretical and experimental curves for TA can be explained in terms of surface roughness of the TA and changes in the refractive index of the layers with increasing thickness (due to non-uniform layer thickness). The damping of the surface plasmon oscillations caused by scattering of energy out of the plasmon mode into other surface modes and radiative fields results in a change in the halfwidth and resonance depth.

6.3.2 Absorbing layers

Figure 6.12 shows the effect of an absorbing overlayer on the SPR conditions using the model. The value of the film's permittivity was ϵ_3=2.3 + 0.5i; this was taken from an isotropic fit to an SPR curve of a squaraine dye by Pockrand[9]. The resonance angle increases with decreasing λ in the same way as for a non-absorbing layer, but the absolute values of θ_{min} are greater.

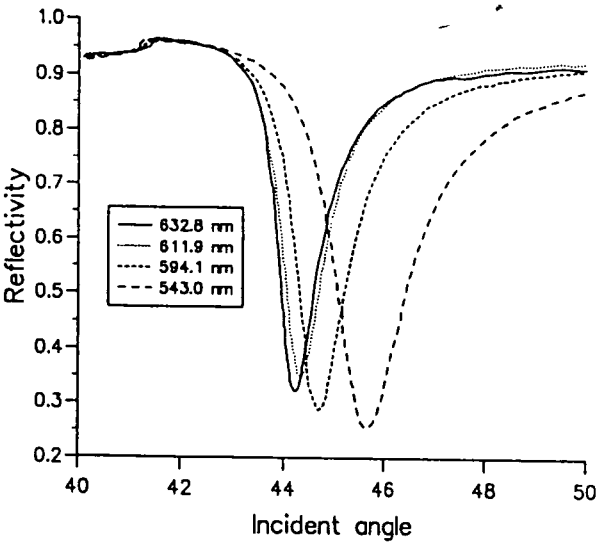

Figure 6.12 SPR curves at different wavelengths from theory for a 12 nm thick absorbing layer on 50 nm thick silver film.

R_{min}, which is evident from the diagram above, does not remain constant as in the non-absorbing case but increases with increasing wavelength, indicating that there is some absorption at higher wavelengths. The fwhm increases with decreasing λ but much more rapidly than for a non-absorbing film. A change in ϵ_3'' from 0.5 to 1 results in only a slight increase in the width but no change in θ_{min} and the R_{min} changes from 0.15 to 0.34.

Values for θ_{min}, R_{min} and fwhm increase monotonically but not linearly with thickness (figure 6.13). They follow a very similar pattern to those reported by Pockrand for a carbon coating[5].

Perylene:TA 1:6 was dipped in a stepped structure 2,4,6 layers (see figure 6.14) onto silver. θ_{min} versus λ for each step is shown in figure 6.15a and a similar graph

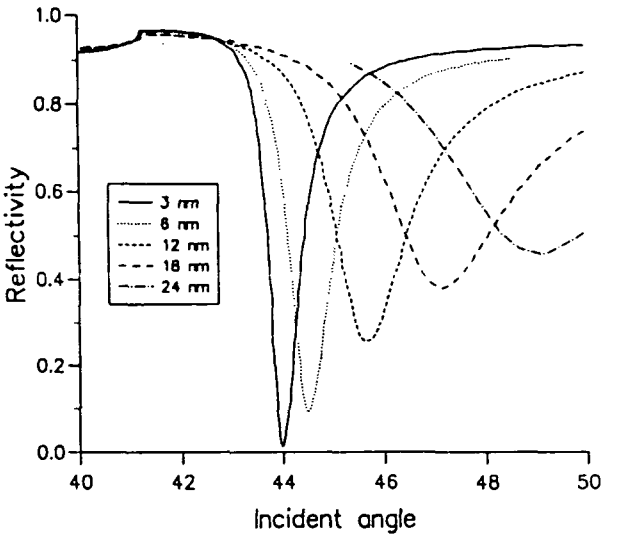

Figure 6.13 SPR curves at different thickness from theory for an absorbing layer at 543 nm on 50 nm thick silver film.

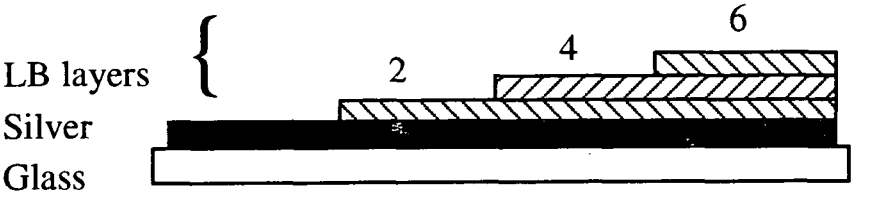

Figure 6.14 Schematic of stepped structure

of 2,4,6 layers of TA alone is shown in figure 6.15b. Both show similar trends in θ_{min} versus λ but the variation with thickness is greater for the perylene:TA than for the TA only. For the TA only, at 632.8 nm, there is an increase of approximately 0.4° per layer, each layer is approximately 3 nm thick for TA, and at 543 nm the increase is 0.55°. For perylene:TA there is an increase in θ_{min} of 1.5° at 632.8 nm and 3° at 543 nm. It is clear from these that there is a pronounced wavelength dependence for the angle shift in the case of the perylene:TA. There is also a

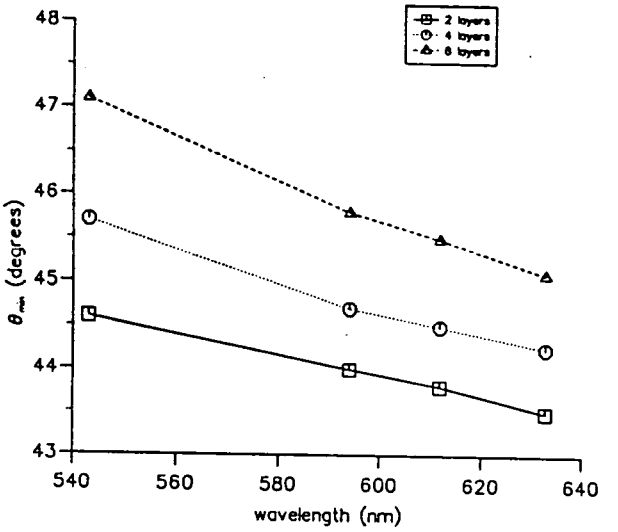

Figure 6.15b θ versus wavelength for 2,4 and 6 layers of TA.

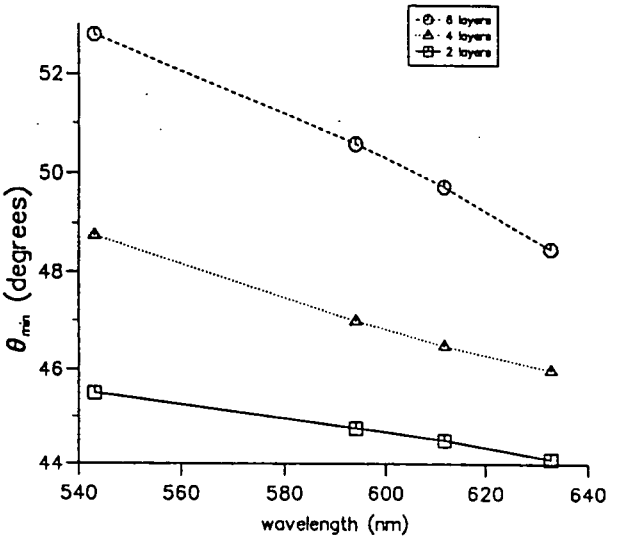

Figure 6.15a θ versus wavelength for 2,4 and 6 layers of perylene:TA 1:6.

significant difference between the θ_{min} shifts for TA and perylene:TA. If this shift is solely due to thickness it implies that the perylene:TA layers are thicker than the TA alone. However, the X-ray and ellipsometric results in Chapter 5 indicate that the perylene:TA has the same thickness as TA.

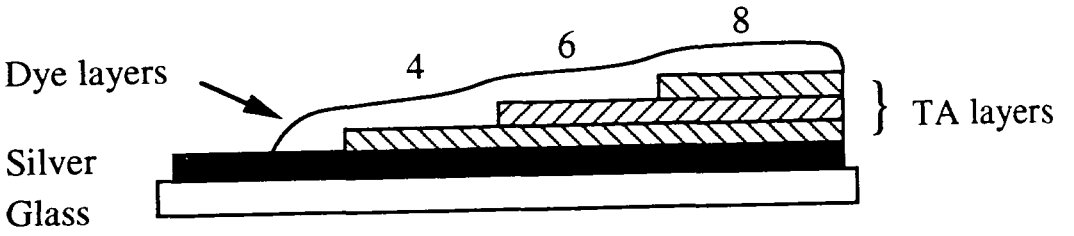

Figure 6.16 The structure of perylene:TA 1:6 on stepped TA layers.

The differences are more clearly illustrated in figure 6.17, where θ_{min} versus the number of layers is shown for three different multilayer structures a) TA, b) perylene:TA and c) 2 perylene:TA layers on a TA stepped structure (shown in figure 6.16), where λ is fixed at 632.8 nm.

As the thickness of structure b) (the perylene:TA) is increased the rate of change of θ_{min} becomes greater. For system c) (the perylene:TA on stepped TA) the shift in θ_{min} is fairly constant. The initial θ_{min} shift for curve c) may be due to perylene:TA layers but subsequently the only variable is the thickness of the TA spacer layers (as in curve a)). Since perylene only has absorption bands in the blue there should be no interaction between the dye and the surface plasmons. One possible explanation for the differences between curves b) and c) is that the dye has a different thickness to the TA. However, as noted above, the measurements discussed in Chapter 5 suggest that perylene:TA 1:6 has the same thickness as TA. Another possibility is that either the real or imaginary part of the permittivity (or both) are different for the dye. For example, it has been seen that varying ϵ_3'' has no effect on θ_{min} but ϵ_3' has a small effect. It can therefore be concluded

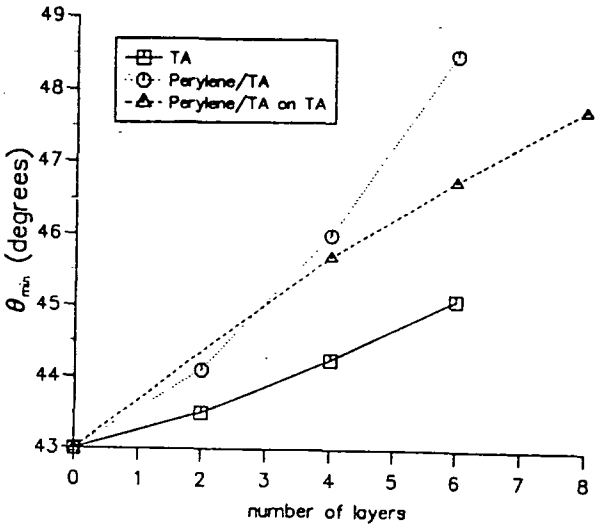

Figure 6.17 θ_{min} versus the number of layers for three different multilayer systems a) TA, b) perylene:TA 1:6 and c) 2 layers of perylene:TA on a stepped structure of TA.

that although perylene does not absorb at these wavelengths it has a significantly different ϵ_2' than TA.

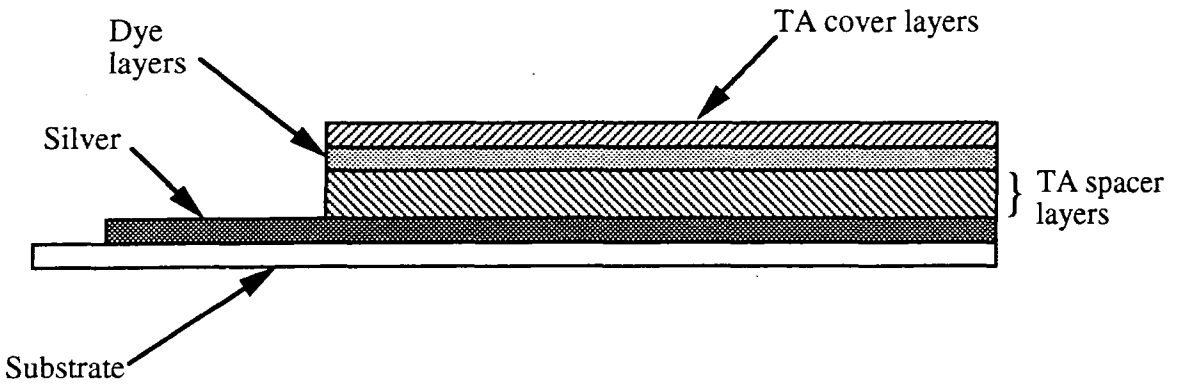

Figure 6.18 A schematic for the dye sandwich structure.

The SPR curves at four different wavelengths for an S120 sandwich are shown in figure 6.19. Figure 6.18 shows a schematic diagram of this structure, a bilayer of S120 sandwiched between layers of TA. Plots of θ_{min}, R_{min} and fwhm versus λ are

shown in figure 6.20a,b and c for the S120 sandwich structure and a 6 layer film of TA. In the plot of θ_{min} versus wavelength (fig 6.20a) the first obvious difference is that the resonance angles are much smaller for the S120 structure.

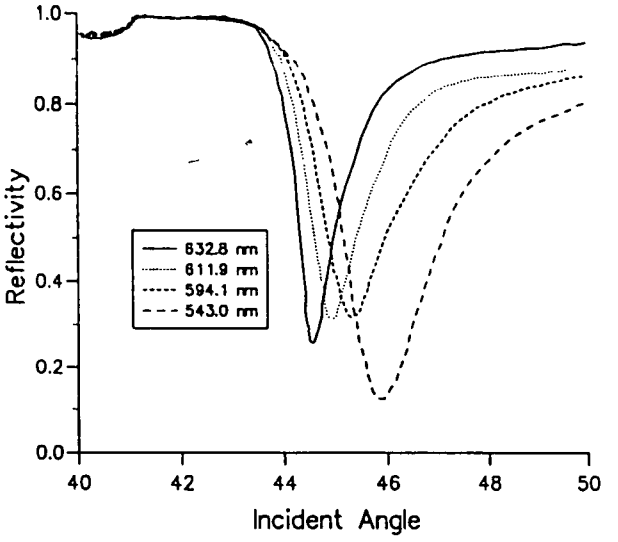

Figure 6.19 SPR curves at four wavelengths for an S120 sandwich structure.

Secondly, the slope of the S120 curve deviates slightly from the TA curve in the region below 595 nm. The R_{min} versus wavelength (fig 6.20b) plot is markedly different for the S120 structure, also in the below 595 nm. The observed difference in the angular position of the resonance for a given wavelength might well be due to the thickness of the sandwich structure or to a change in the layer's permittivity. There is no evidence for the former but the latter is almost certainly true. The dye layer is highly absorbing in the region of 580 nm due to the formation of J-aggregates, as was reported in section 5.5.2. Some care had to be taken with the sample because of photo-bleaching of the dye as described in section 5.5.2. The R_{min} versus λ curve for S120 sandwich is very different from that for the TA layers in the region above 580 nm, since the dye is highly absorbing here. Thus it is reasonable to assume that the surface plasma waves are being strongly damped. The value of fwhm deviates from that for TA in the region of 590 nm close to the absorption maximum of the dye, indicating a strong interaction resulting in a broadening of the SPR curve; this is also attributable to damping (increase in ϵ_3'').

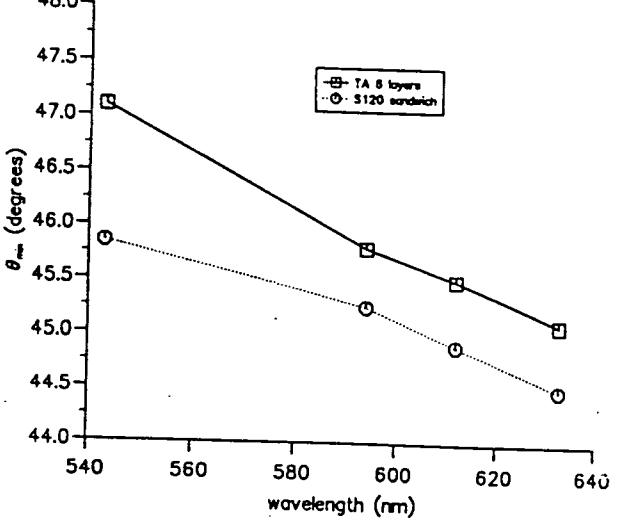

Figure 6.20a θ versus wavelength for an S120 sandwich and 6 layers of TA.

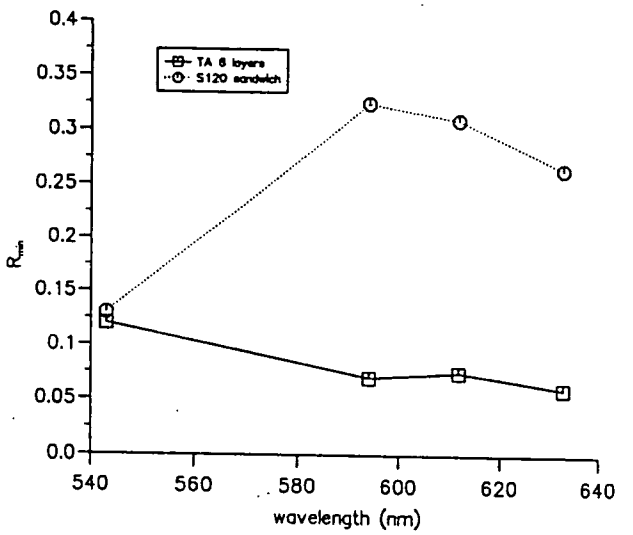

Figure 6.20b Rmin versus wavelength for an S120 sandwich and 6 layers of TA.

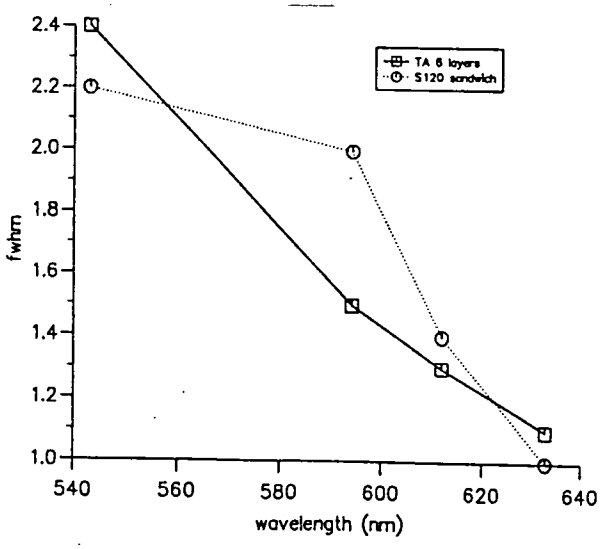

Figure 6.20c Fwhm versus wavelength for an S120 sandwich and 6 layers of TA.

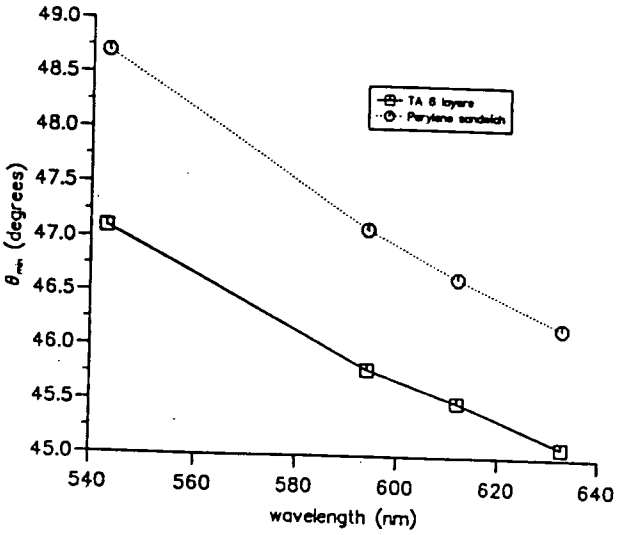

Figure 6.21a θ versus wavelength for a perylene sandwich and 6 layers of TA.

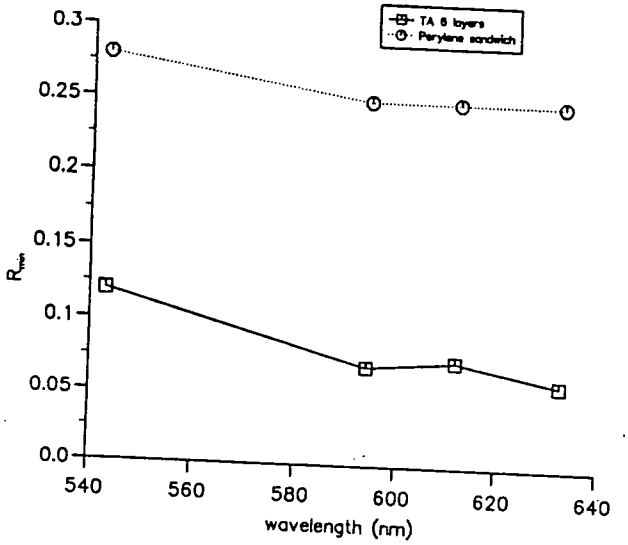

Figure 6.21b Rmin versus wavelength for a perylene sandwich and 6 layers of TA.

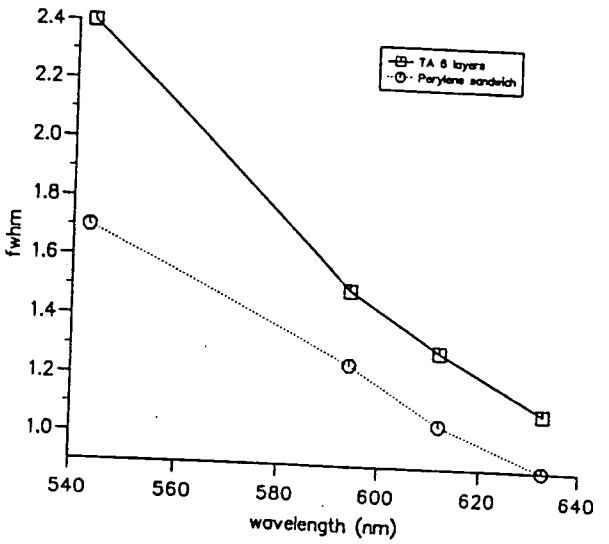

Figure 6.21c Fwhm versus wavelength for a perylene sandwich and 6 layers of TA.

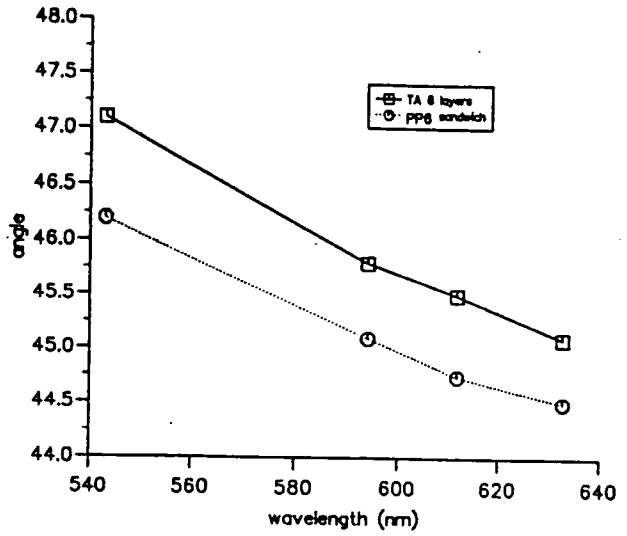

Figure 6.22a θ versus wavelength for a PP6 sandwich and 6 layers of TA.

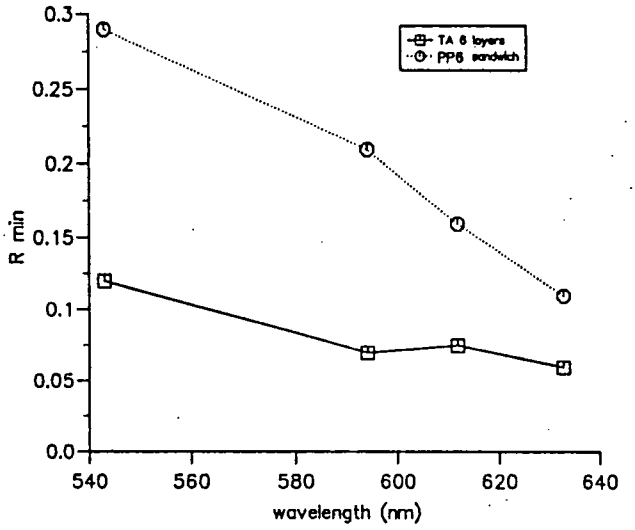

Figure 6.22b Rmin versus wavelength for a PP6 sandwich and 6 layers of TA.

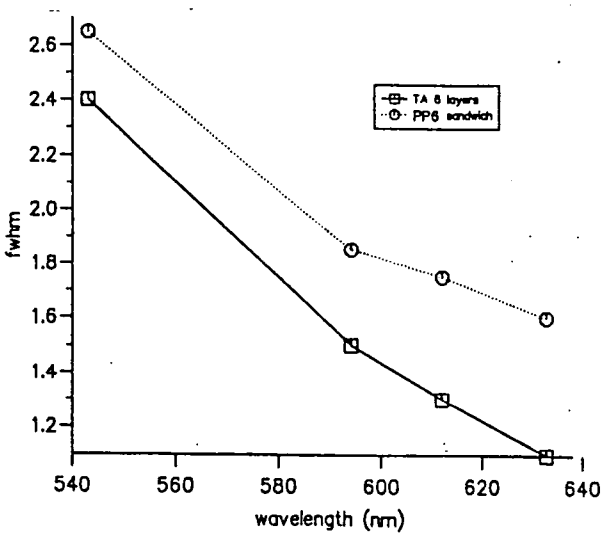

Figure 6.22c Fwhm versus wavelength for a PP6 sandwich and 6 layers of TA.

In contrast, perylene has no absorption bands in the red region of the spectrum, so no interaction between the chromophores and the surface plasmons would be expected. The first thing that is noticeable about the graph of θ_{min} versus λ for perylene when compared to TA is that the values of θ_{min} are greater, but their relationship with λ is essentially the same (figure 6.21a).

Values for R_{min} in figure 6.21b are also greater than those for a TA film, indicating that the film is lossy. In figure 6.21c, the values of fwhm are less for perylene than TA which is contradictory since it has been shown that ϵ'' has an influence on the fwhm.

The phthalocyanine dye PP6 also has an absorption band in the red, but it is broad and most intense in the range 600 nm to 750 nm. The plot of θ_{min} versus λ (fig 6.22a) for PP6 shows values for θ_{min} less than those for TA. So either the film is thinner or the permittivity of the film is smaller. In figure 6.22b, the values of R_{min} for the PP6 film are larger than for TA and diverge at shorter wavelength. There is an anomaly at 600 nm which may correspond to the known absorption band of the dye reported in section 5.4. Hence, the increase in R_{min} may result from an increase in ϵ_3''. The variation of fwhm with λ (fig 6.12c) is similar to that of TA but deviates slightly in the region of 600 nm. This subtle change may signify an interaction between the surface plasmons and the dye chromophores.

There is little doubt, however, in the case of the S120 system (figures 6.20a,b and c) that an interaction between the dye and the surface plasmon polaritons is observed, but owing to the limited number of wavelengths available from the laser it is not possible to obtain precise information about the phenomenon.

6.4 Variable Wavelength SPR

Two dyes, S120 and Sq1, which both possessed sharp absorption bands in the region 500 nm to 600 nm (see Chapter 5), were chosen for closer investigation using the variable wavelength system described in Chapter 4.

6.4.1 Angle scans

The reflectivity against angle was measured for a number of different wavelengths. The wavelengths selected covered the known absorption band of each dye

system. The experimental SPR curves of silver for ten different wavelengths are shown in figure 6.23. It is evident that each curve is shifted to a higher angle as the wavelength is increased.

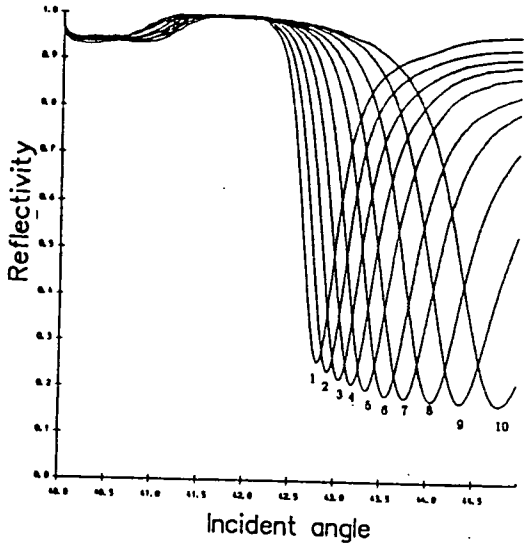

Figure 6.23 Surface plasmon resonance curves for a 50 nm silver film at wavelengths of 1) 660 nm 2) 640 nm 3) 620 nm 4) 600 nm 5) 580 nm 6) 560 nm 7) 540 nm 8) 520 nm 9) 500 nm and 10) 480 nm.

This SPR progression was expected since it had been previously observed for the curves recorded with the laser and is a result of the dispersion of the silver film. A feature of the curves in figure 6.23, which is not seen in those recorded with the laser or from the theoretical model, is the decrease in R_{min} with decreasing wavelength. One explanation may be a variation in linewidth of the monochromator with wavelength. At 700 nm the fwhm is 15 nm but at 400 nm it is only 10 nm; this increase in resolution at lower wavelengths will improve the coupling conditions, hence the decreased reflectivity.

The SPR curves at four selected wavelengths are shown in figures 6.24 for two layers of S120 which are separated from the silver surface by two layers of TA and coated by a further two layers to give a total film thickness of 6 layers (see sandwich structure figure 6.18). The resonance angle increases for curves at 620 nm to 600 nm but at 580 nm the angle is less than expected. This shifting backwards of the resonance curve corresponds with the absorption band of the

dye and signifies that an interaction is occurring between the dye and the surface plasmon polaritons (SPPs). When the wavelength reaches 550 nm, the resonance curve returns to its expected position.

Figure 6.24 Surface plasmon resonance curves for an S120 sandwich structure spaced at 2 layers from a silver surface, at four different wavelengths.

When the spacing is increased to 12 nm (4 spacing layers of TA), so that there are a total of 8 layers, the resonance angle is shifted to higher angle as expected due to the increase in film thickness (figure 6.25). In addition, some of the curves are more clearly damped than for the 2-layer spaced sample. The depth is reduced and the width increased of the 600 nm curve, and at 580 nm the curve is shifted back so that it occurs at almost the same angle as the curve recorded at 620 nm. Again, the resonance curve resumes its normal angular position at 550 nm. It is evident that at 580 nm there is a very strong interaction between the dye chromophores and the surface plasmons.

Four curves for Sq1:TA separated by 6 nm (2 spacing layers of TA) were recorded at 660 nm, 600 nm, 540 nm and 520 nm. This range of wavelengths covers the absorption band for the dye in LB film (figure 6.26). In section 5.4.4 there was shown to be maximum at 535 nm and a shoulder at 650 nm. The SPR curves at 660 nm and 600 nm follow the expected progression but at 540 nm the

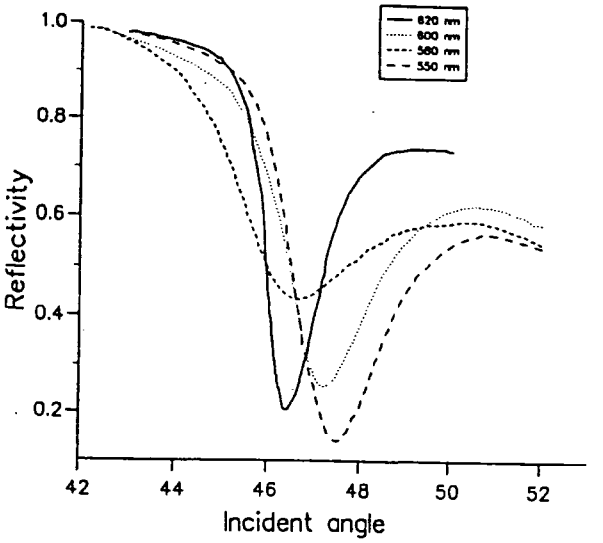

Figure 6.25 Surface plasmon resonance curves for an S120 sandwich structure spaced at 4 layers from a silver surface, at different wavelengths.

curve is broader, shallower and slightly shifted to a smaller angle. This indicates that there is a significant interaction between the surface plasmons and the dye molecules at 540 nm. Again, by 520 nm the resonance curve has returned to its expected position.

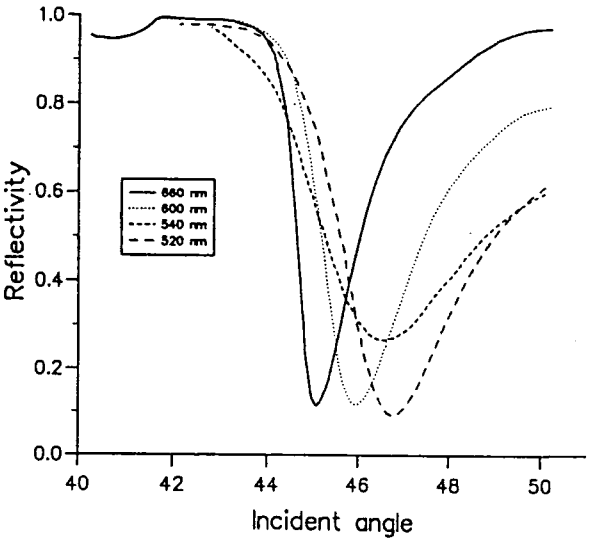

Figure 6.26 Surface plasmon resonance curves for an Sq1:TA 1:1 sandwich structure spaced at 2 layers from a siver surface, at four different wavelengths.

Four SPR curves for Sq1:TA, at a separation of 12 nm (4 spacing layers of TA) are shown in figure 6.27; the wavelengths selected are the same as for the previous example. The curves at 660 nm and 600 nm occur at higher angles than before but this is expected owing to an increase in thickness of the layers The curves are also broader which suggests a more absorbing film; this is not surprising when the absorption spectrum of the dye is examined. The curve at 540 nm is much shallower, broader and shifted to shorter angle (by about the same amount as for the 2 layer spaced sample), again indicating a strong interaction between the surface plasmons and the dye layer. Finally the curve at 520 nm resumes the form and position expected.

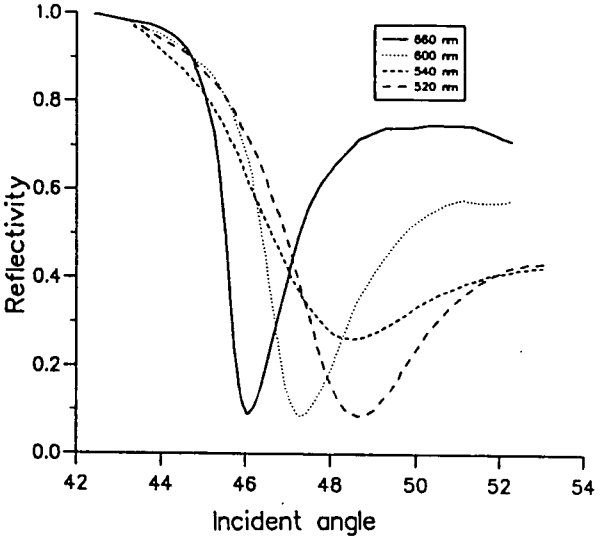

Figure 6.27 Surface plasmon resonance curves for an Sq1:TA 1:1 sandwich structure spaced at 4 layers from a silver surface, at four different wavelengths

6.4.2 Wavelength scans

The curves in this section are generated by a different method to the previous ones. In this case the angle of the prism is kept constant and the wavelength is varied. The wavelength scan recorded for uncoated silver at an angle of 44° is shown in figure 6.28. Since there is a relationship between the angle and wavelength scans, a vertical line can be drawn on the angle scan curves (figure 6.23) corresponding to an angle of 44° and values of reflectivity read off where each SPR curve crosses

the line; these values are also plotted in figure 6.28. This angle scan curve should correspond exactly to the wavelength scan. It is evident from the diagram that it does not, it is shifted to longer wavelength by approximately 10 nm. Thus, either there is an error in the angles or the wavelengths differ. The latter could be due to the increased linewidth of the monochromator. Apart from the shift in position the shape and width of the curves are identical. Both the curves for angle and wavelength scans are quite broad confirming that the linewidth of the light source is large.

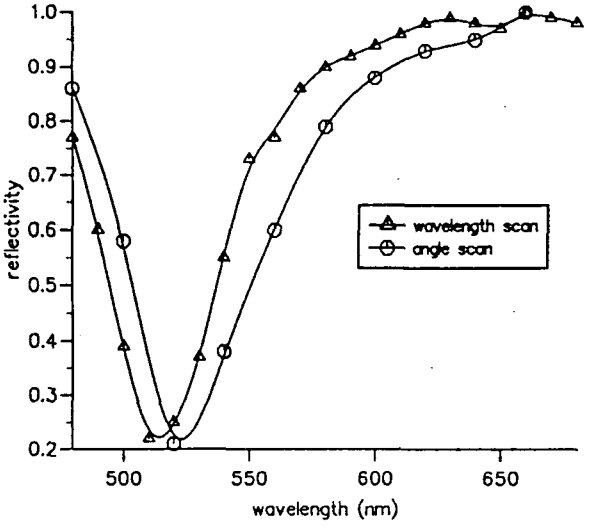

Figure 6.28 Reflectivity versus wavelength, for λ scan and points derived from the angle scans, for 50 nm of silver.

Similar plots to the above were made for S120 (6.29 and 6.30) and Sq1 (6.31 and 6.32) dye systems. When the dye silver spacing is only two layers (6.29 and 6.31) the agreement between angle and wavelength scans is quite good. However, when the separation is increased to four layers (6.30 and 6.32) the angle scan curve is shifted to longer wavelength, by approximately 10 nm, as in the case of silver. The most prominent feature of these curves is the double dip in the reflectivity; these only occur in the wavelength scans and their relative intensities depend on the angle of incidence at which the scan was recorded. From the theory in Chapter 2 it was shown that these minima arise due to the splitting of the dispersion curve into two branches on either side of a transition frequency (see figure 2.8). The λ scan for the S120 dye system, separated by 2 layers from the silver surface, and

recorded at an angle of 45.5° is shown in figure 6.29. Two minima are visible but they are both quite shallow. The long wavelength minimum is slightly deeper than the short wavelength indicating that the lower branch of the dispersion curve is dominant.

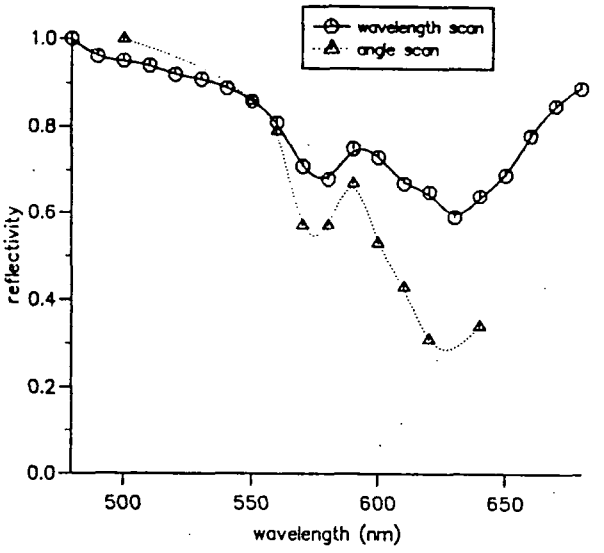

Figure 6.29 Reflectivity versus wavelength, for λ scan and points derived from the angle scans, for an S120 sandwich structure spaced 2 layers from 50 nm of silver

The 4 layer spacing of S120, figure 6.30, recorded at an angle of 47° gives two much deeper resonances, with the short wavelength one being deeper than the long wavelength, indicating the upper branch of the dispersion curve is now dominant.

The Sq1 sandwich system separated from the silver by 2 layers of TA is shown in figure 6.31. It was recorded at an angle of 48°. There are two distinct dips in the reflectivity curve, one deep one at 500 nm and a shallower one at 575 nm. This again indicates that the upper branch of the dispersion curve is dominant.

When the spacing is increased to 4 layers and the angle at which the curve is recorded is 49° (figure 6.32), two dips are observed but their relative depths change and the position of the short wavelength is shifted to 510 nm. These changes suggest that lower branch of the dispersion curve is having more influence.

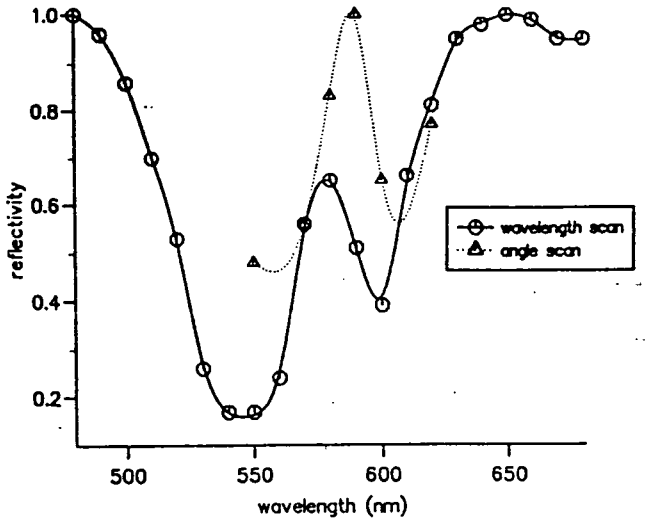

Figure 6.30 Reflectivity versus wavelength, for λ scan and points derived from the angle scans, for an S120 sandwich structure spaced 4 layers from 50 nm of silver.

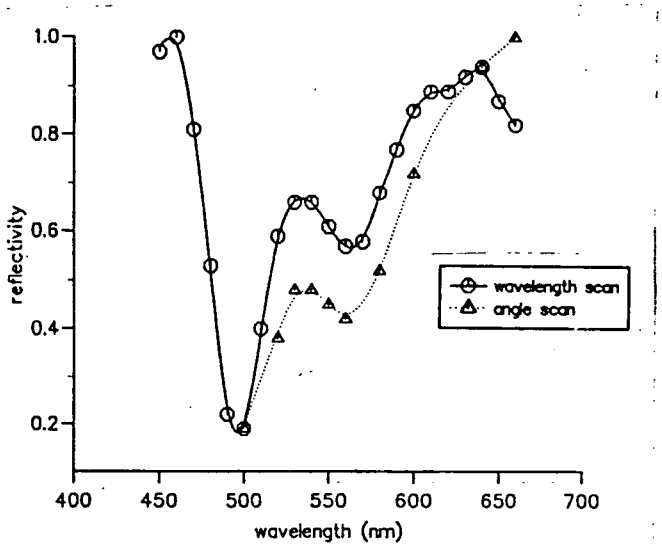

Figure 6.31 Reflectivity versus wavelength, for λ scan and points derived from the angle scans, for an Sq1:TA 1:1 sandwich structure spaced 2 layers from 50 nm of silver.

If the angle of the resonance minimum is plotted against the wavelength (from the angle scans), a dispersion curve can be obtained, since λ and θ are directly related to ω and k, respectively. The curve for silver is single valued in angle as expected but is not a straight line since there is some dispersion; however, the

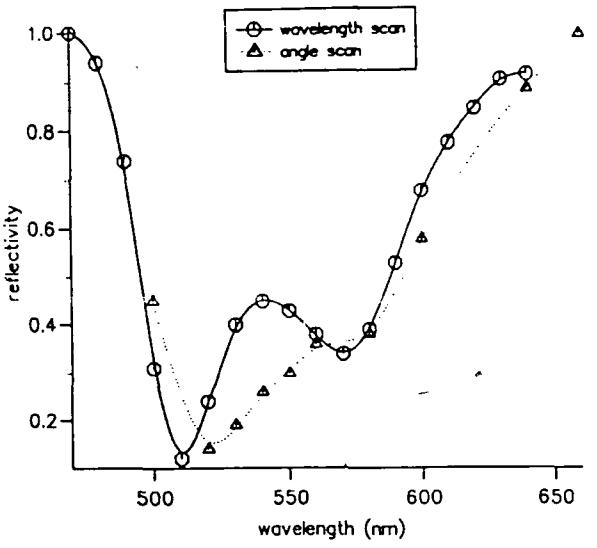

Figure 6.32 Reflectivity versus wavelength, for λ scan and points derived from the angle scans, for an Sq1:TA 1:1 sandwich structure spaced 4 layers from 50 nm of silver.

dispersion curves for the S120 layers are multi-valued in angle and are said to exhibit anomalous dispersion. The point of inflection for each curve occurs at 580 nm, corresponding to the transition frequency (which is the maximum between the two dips in the wavelength scan). It is also the point where absorption in the dye is a maximum. The transition is from one branch where excitation of surface waves is of pure surface plasmon polariton character to a second branch which is due to excitation of transverse excitons with a mixture of SPPs (see figure 2.8).

A comparison of the dispersion curves for S120 (fig 6.33) reveals the sample which is spaced by 4 layers to have more pronounced 'backbending' than the 2 layer spaced sample. This is in accordance with Pockrand's findings[7]. He suggests that the exciton states of the transition layer become increasingly damped as the proximity of the dye to the silver surface is reduced.

A similar set of dispersion curves for Sq1 is shown in figure 6.34. There is also a difference in the degree of backbending between the two separations, and it is not as pronounced in the case of S120. Indicating that the proximity of the dye to the silver is not so influential.

The dielectric function of a film, ϵ_f, may be related to the frequency of the

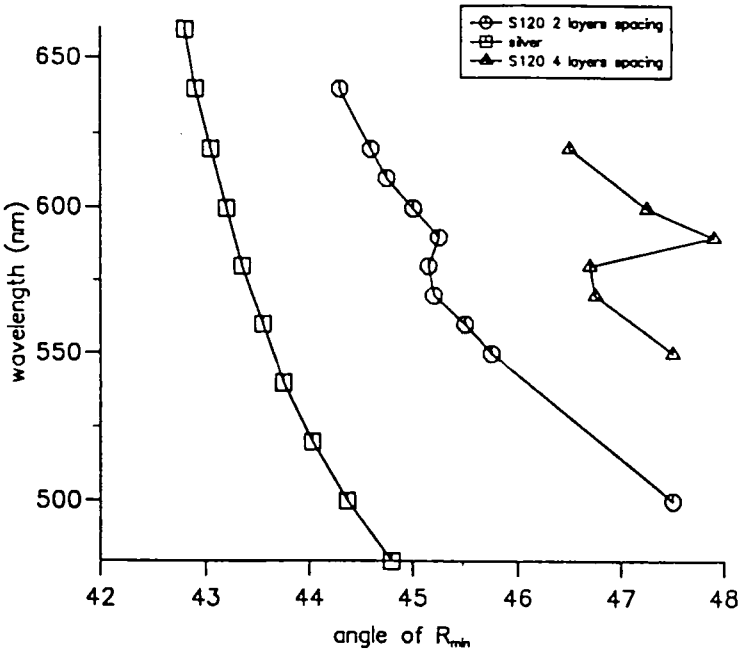

Figure 6.33 Dispersion curves for 50 nm of silver, S120 sandwich structure spaced by 2 layers of TA and S120 sandwich structure spaced by 4 layers of TA.

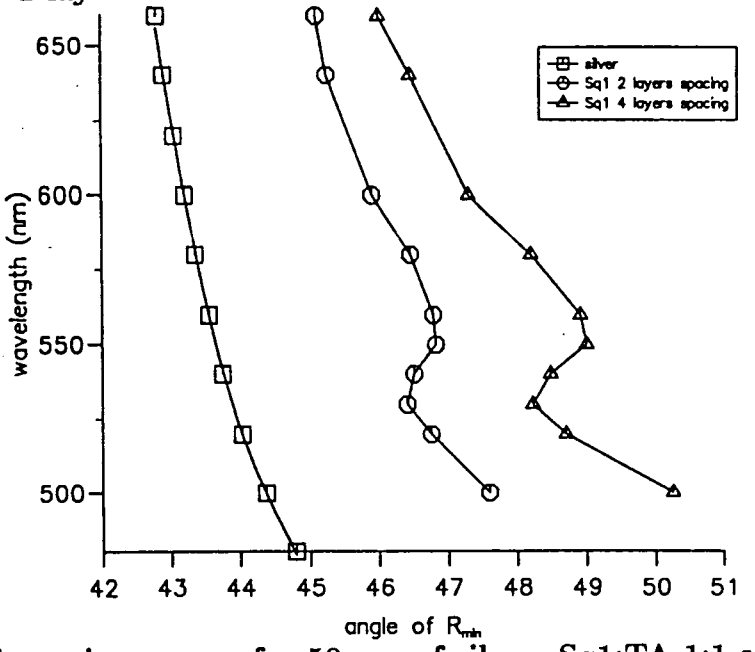

Figure 6.34 Dispersion curves for 50 nm of silver, Sq1:TA 1:1 sandwich structure spaced by 2 layers of TA and Sq1:TA 1:1 sandwich structure spaced by 4 layers of TA

surface exciton, ω_s, by the following equation derived from the Drude-Lorentz formula

$$\epsilon_f = \epsilon_\infty + \frac{\omega_p^2 f}{\omega_s^2}[1 - (\frac{\omega}{\omega_s})^2 - i(\frac{1}{\omega_s \tau}\frac{\omega}{\omega_s})]^{-1}$$

τ is the relaxation time (lifetime of the excited state), ω_p is the plasma frequency,

f is the reduced oscillator strength, ω is the frequency of excitation and ϵ_∞ is the background dielectric function.

The dielectric function of the film (ϵ_f) can be anisotropic or uniaxially isotropic in the x ($\epsilon_{||}$) or z ($\epsilon_\perp$) directions. If the transition moments of the dye are orientated parallel to the substrate, $\epsilon_{||}$ is equal ϵ_f in the above equation and $\epsilon_\perp$ is real and constant. Only a single backbending is observed giving rise to a structure at long wavelength (transverse exciton mode ω_T).

If the transition moments are orientated perpendicular to the substrate, $\epsilon_\perp$ is described by the above equation and $\epsilon_{||}$ is real and constant. This also gives rise to a single backbending but it occurs at a shorter wavelength (longitudinal exciton mode ω_L). Therefore isotropy leads to double backbending and anisotropy to single backbending.

Anomalous dispersion is most pronounced for long relaxation times (τ) [6]. Anomalous dispersion and the large shift in θ_{min} occur close to the λ values where ϵ'=0. To be precise, they occur where the real part of the permittivity ϵ' crosses the zero axis to become negative. There are two such points (see figure 6.35), the first crossing occurs where the imaginary part of the permittivity ϵ'' is a maximum. This corresponds to the frequency of the transverse exciton mode (ω_T), which is also the maximum measured in the absorption spectrum. The second zero crossing point occurs at the frequency of the longitudinal exciton mode ω_L, which is the point where $(\epsilon'')^{-1}$ is a maximum.

For small damping (large $\omega_s\tau$) we approach the *resonance* case where the exciton removes energy from the plasmon surface polariton in a narrow frequency range and radiates the energy back, hence reducing the reflectivity minimum. *Quenching* occurs at larger damping (small $\omega_s\tau$) for a transition with stronger oscillator strength and the overlayer extracts energy over a wide frequency range from the surface polariton, which is damped by dissipative mechanisms.

According to Pockrand[8], the minimum at the longitudinal mode ω_L is larger than at the transverse mode ω_T because the z component of the electromagnetic field strength of the plasmon surface polariton is larger by approximately $(\epsilon_1')^{\frac{1}{2}}$ than the x component. Therefore, a larger coupling between surface plasmons and

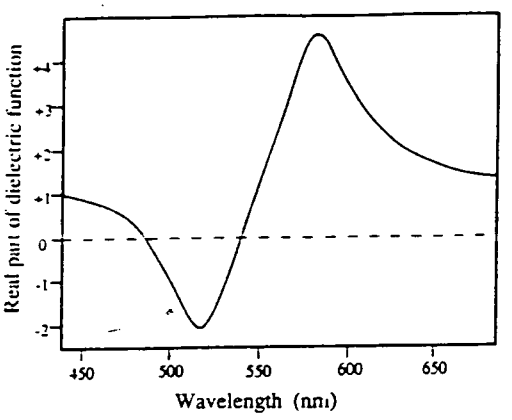

Figure 6.35 The real part of permittivity versus wavelength, showing the zero crossing points.

exciton transitions polarized perpendicular to the surface should be observed. No backbending at ω_L was observed for any of the films studied in this work.

If there is a perpendicular component of the exciton transition in the films studied it might be masked out by damping. However, it may be difficult to resolve the perpendicular exciton interaction due to the increased linewidth of the light source and the limited number of points measured. Alternatively no perpendicular component of the exciton transition suggests that the film is completely anisotropic. Polarized absorption measurements in section 5.5.3 show that there is a degree of anisotropy associated with the films, but that it is not complete.

Plots of R_{min} versus λ from the angle scans for S120 and Sq1 are shown in figures 6.36 and 6.37. These plots are related to the absorption, k, and hence the imaginary part of the permittivity ϵ_3''. The maximum values of R_{min} coincide with the absorption peak. Plots of θ_{min} versus λ are related to the refractive index n, and hence the real part of the permittivity ϵ_3'.

6.5 Backbending Predictions from Theoretical Curves

Values obtained for the permittivity of a squaraine dye, similar to Sq1, were taken from a paper by Pockrand[9] and were inserted into the modelling program to obtain a series of SPR curves at different wavelengths. The R_{min} values are

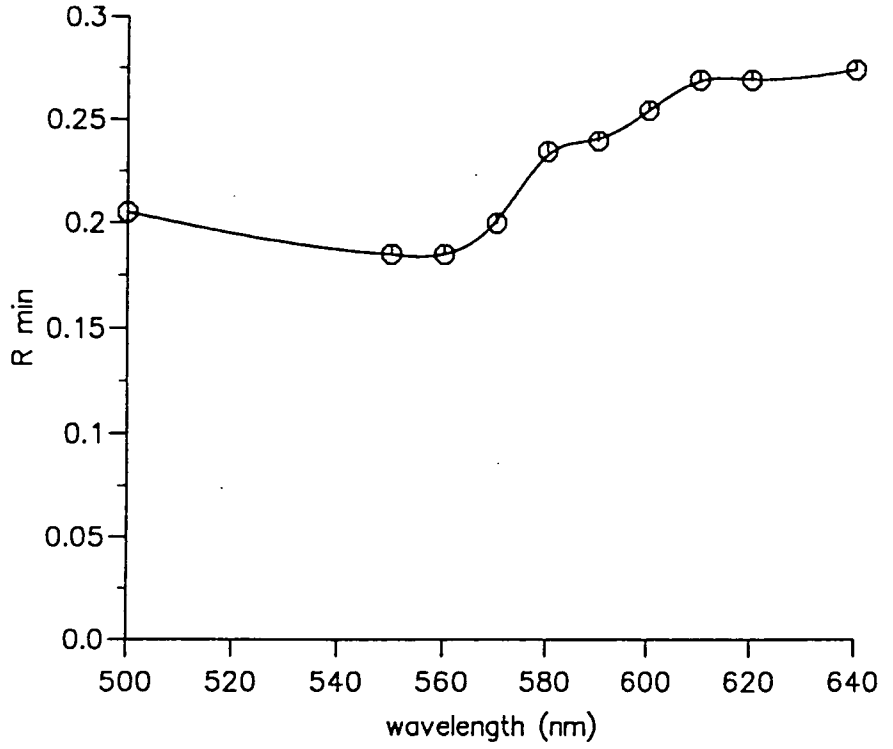

Figure 6.36a Rmin versus wavelength from angle scans for S120 sandwich structure spaced by 2 layers of TA.

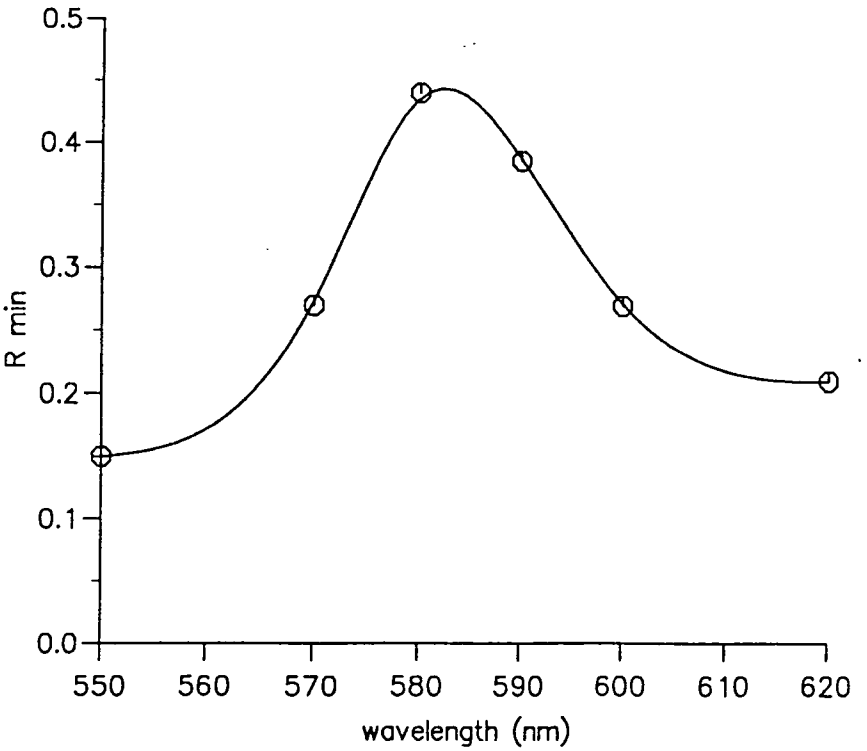

Figure 6.36b Rmin versus wavelength from angle scans for S120 sandwich structure spaced by 4 layers of TA.

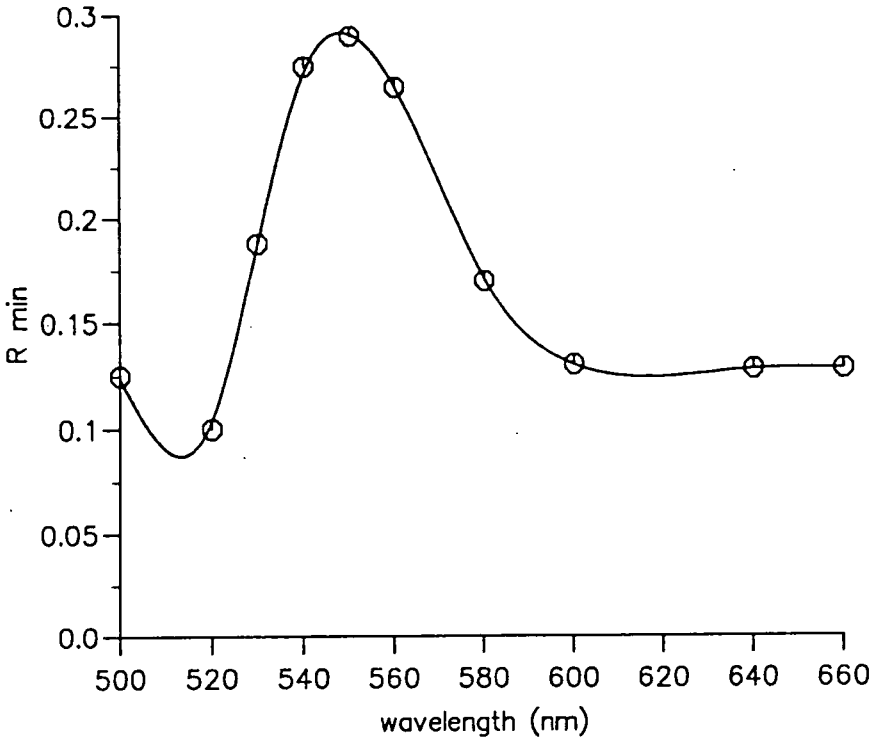

Figure 6.37a Rmin versus wavelength from angle scans for Sq1/TA 1:1 sandwich structure spaced by 2 layers of TA.

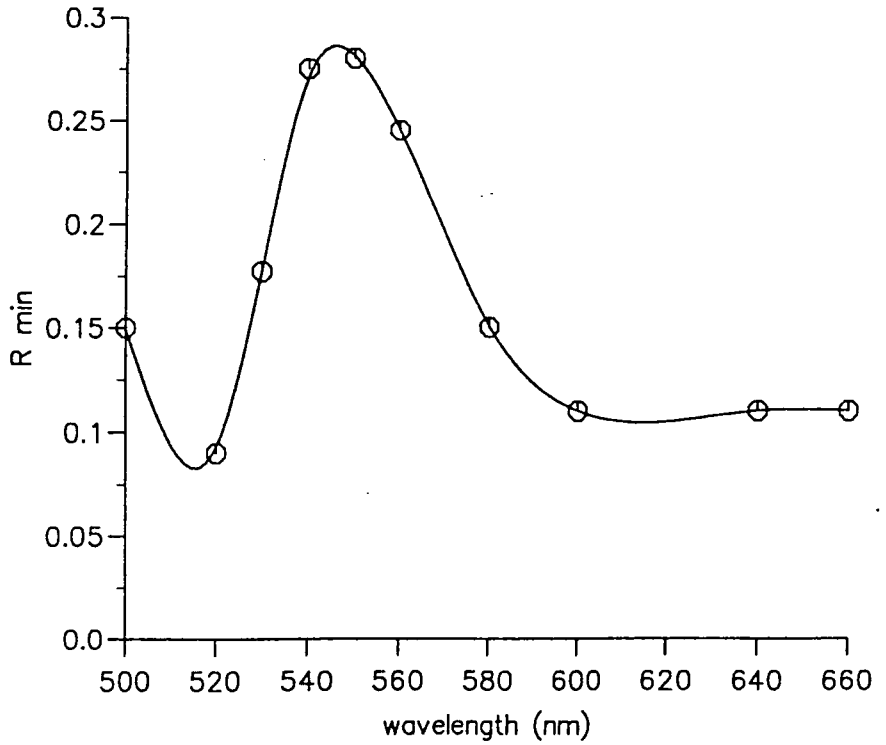

Figure 6.37b Rmin versus wavelength from angle scans for Sq1/TA 1:1 sandwich structure spaced by 4 layers of TA.

plotted against λ and are compared to experimental values for Sq1. Although the transition point is different, (530 nm as opposed to 540 nm for Sq1) there are some similarities. The values from the isotropic fit ($\epsilon_{||}$ and $\epsilon_{\perp}$ are varied) match best with the 2 layer spaced Sq1 sample. Whilst the anisotropic fit (only $\epsilon_{||}$ varied) curve coincides with the 4 layer spaced sample. However, it is not possible to draw any definite conclusions from these observations.

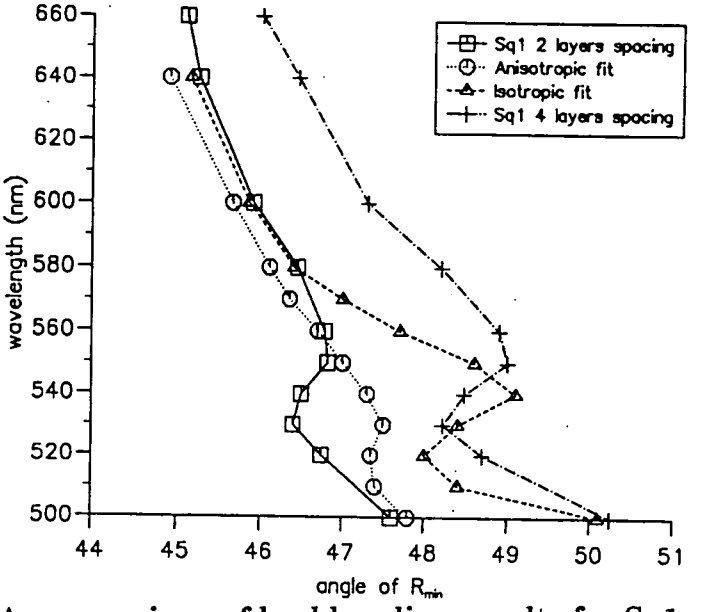

Figure 6.38 A comparison of backbending results for Sq1 and theoretical ones obtained from published values of permittivity. After Pockrand.

6.6 Summary

In this chapter the SPR technique has been shown to be a sensitive method for studying the properties of a metal surface. In section 6.1 the effect on the SPR resulting from changes in the silver parameters was demonstrated using a modelling program. These were then compared to real silver results and the effect of tarnishing was seen to be important. A non-absorbing overlayer was introduced in section 6.3.1, theory and experimental results were shown to have some similarities. Theoretical curves were obtained in section 6.3.2 for an absorbing overlayer and compared well with results by Pockrand; however, it was not possible to compare these directly to experimental results since the dyes in question had absorptions which changed with wavelength. These dye systems were investigated for dye-plasmon interactions but the limited choice of wavelengths available from the laser

made this difficult. Two dye systems were selected in section 6.4 for further investigation using a monochromated source. Angle scans were made in section 6.4.1 and wavelength scans were recorded in section 6.4.2. The results of these two different measurements were compared and were shown to have important similarities and differences. In both cases clear interactions were observed between dye and surface plasmons. The form of these interactions was shown to have a relationship to the transition dipole orientation of the molecules. Good agreement was found between the results for S120 and Pockrand's results, especially in respect to the damping effect of the silver. Backbending was observed for the first time in the Sq1 squaraine derivative. Finally, in section 6.5, backbending results for the Sq1 dye system were compared to dispersion curves generated from permittivity values published by Pockrand for a very similar squaraine dye.

6.7 References

1. J. Cresswell *Waveguiding in electrooptic Langmuir-Blodgett films* PhD Thesis Durham University (1992).

2. U. Schröder *Der Einfluss dünner metallischer decshichten auf die dispersion von oberfläschen plasmuschngungen in gold-silber schichtsystemen* Surface Science vol 102 (1981) pp118-130

3. W. L. Barnes and J. R. Sambles *Guided optical waves in Langmuir-Blodgett films of 22-Tricosenoic acid* Surf.Sci. Vol 177 (1986) pp399-416

4. G. Wähling, H. Raether and D. Möbius *Studies of organic monolayers on thin silver films using the attenuated total reflection method* Thin Solid Films Vol 58 (1979) pp391-395

5. I. Pockrand *Surface plasma oscillations at silver surfaces with thin transparent and absorbing coatings* Surf.Sci. Vol 72 (1978) pp577-588

6. I. Pockrand and J.D. Swalen *Anomalous dispersion of surface plasma oscillations* J.Opt.Soc.Am. Vol 68 No 8 (1978) pp1147-1151

7. I. Pockrand, A. Brillante and D. Möbius *Exciton-surface plasmon coupling: An eperimental investigation* J.Chem.Phys. Vol 77 No 12 (1982) pp6289-6295

8. I. Pockrand, J.D. Swalen, J.G. Gordon and M.R. Philpott *Exciton-surface plasmon interactions* J.Chem.Phys. Vol 70 No 7 (1979) pp3401-3408

9. I. Pockrand, J.D. Swalen, R. Santo, A. Brillante and M.R. Philpott *Optical properties of organic dye monolayers by surface plasmon spectroscopy* J.Chem. Phys. Vol 69 No 9 (1978) pp4001-4011

Chapter VII

Conclusions and Suggestions for Further Work

7.1 Summary

The LB technique has been sucessfully used to form organized dye multilayers. The effects of dye concentration on the absorption spectra were studied. The orientation of dye chromophores in pure films and those mixed with fatty acid were investigated. The sensitivity of the SPR technique to changes in the surface conditions was demonstrated. When dye multilayers with sharp absorption bands coated the silver, a resonant interaction was observed between the chromophores and the surface plasmons; this was referred to as "backbending".

The optical behaviour of dyes in solution, cast films and Langmuir-Blodgett films have been investigated. A comparison of cast and LB films is particularly revealing. The materials studied were: porphyrins and phthalocyanines (PP), a cyanine derivative S120, three squaraine derivatives Sq1, Sq2 and Sq3 and an aromatic hydrocarbon perylene.

A variety of studies were undertaken on the films, these could be divided into three groups.

7.1.1 Structural studies

It was clear from isotherms that the phthalocyanine and porphyrin materials did not form ordered films. Perylene, however, produced good quality films when mixed with a fatty acid. A series of isotherms for different molar ratios of perylene to tricosanoic acid suggested that the perylene molecules reside in the space between the fatty acid chains and are not squezzed-out as has been reported by Steiger. Ellipsometric and X-ray measurements confirmed that the mixed layers were indeed the same thickness as TA only. Further evidence for the orientation of the perylene molecules was obtained by optical dichroism, which revealed that the molecules are probably tilted with their large face at some angle between 45° and

90° to the substrate. This order was also shown by RHEED studies. Isotherms of the cyanine derivative S120 indicated that the molecules lay on their longest edge on the water surface. No change in this orientation was observed when S120 was mixed with TA. A small amount of dichroism, compatible with the molecules assumed orientation, was detected. Sq1 and Sq3 squaraine derivatives underwent a significant phase change in their isotherms which was attributed to the molecules moving from one orientation to another on the water surface. Sq2 did not exhibit any such changes. Dichroic measurements of Sq1 and Sq3 indicated only a slight preference in the molecules orientation. There was no obvious order in the RHEED of Sq3. Significant optical dichroism was observed for Sq2:TA films marked by a splitting of the bands (possibly Davydov).

7.1.2 Optical studies

All the dyes studied had sharp absorption bands in solution, characteristic of monomers. The extinction coefficients measured compared well with reported values. The cast spectra of the dyes were broad and featureless with one exception Sq3, which had a spectra with two bands similar to those for its LB film spectrum. The absorption spectrum of perylene:TA LB films was broad and red shifted relative to the solution. No change in the spectrum was observed with molar ratio of perylene:TA. Pure S120 deposited onto TA had a sharper absorption band than in solution, due to the formation of J-aggregates. When mixed with TA, however, this band becomes much broader. The squaraine derivatives Sq1 and Sq3 were deposited in both high and low pressure phases; the spectra were similar for both phases and dyes. Both dyes had a band at the wavelength of the monomer and a more intense blue-shifted band. Mixing Sq1 and Sq3 with TA to different molar ratios had a significant effect on the spectra; increasing the TA concentration caused the blue-shifted band to decrease and the monomer band to increase. The blue shifted band is probably due to aggregates, possibly H-aggregates. Pure Sq2 LB films had a broad absorption band, but on mixing wth TA this band appeared to split into red-shifted and blue-shifted bands. This behaviour suggests the formation of aggregates with orthogonal dipoles (Davydov splitting), which is supported by the optical dichroism observed.

Fluorescence studies of perylene:TA LB films at 293 K revealed that two strong

7.2 Suggestions for Further Work

Use of a dye laser as the source would improve the resolution and increase the wavelength range, this may make it possible to observe ω_L. This work could easily be extended to investigate other more complex dye systems with overlapping absorption and fluorescence bands, where energy transfer might be possible. Different optical arrangements, such as pumping the dye from the sample side and monitoring the fluorescence back into plasmon modes could provide additional information about dye-plasmon interactions. An application may be found for the phenomena of backbending. Ultimately a bio-sensor may be constructed based on absorption or fluorescence quenching.

7.3 Conclusions

Finally, to conclude the work presented in this thesis, there follows a brief evaluation of the LB and SPR techniques. The LB technique can be used to create ordered dye systems with unique optical features arising from the orientation of the aggregated dye molecules. However, the behaviour of these multi-component systems is not fully understood and further studies are required to fully characterize them. Although LB films suffer from a lack of mechanical strength, they offer an excellent system for the study of energy transfer and other physical processes such as nonlinear optical effects.

SPR is a very sensitive measuring technique. However, it is significantly affected by deposits on the metal layer and a large number of interelated parameters are responsible for changes in the resonance conditions. Therefore, it cannot easily provide absolute values and can only accurately detect changes.

Allowing for these drawbacks, there are sufficient advantages in both techniques to make further investigation into the development of SPR based sensors worthwhile.

Appendix A

Publications

1. J.G.Warren, J.P.Cresswell, M.C.Petty, J.P.Lloyd, A.Vitukhnovsky and M.I.Sluch *Optical Properties of Highly Ordered Perylene Multilayers* Thin Solid Films Vol 179 (1989) pp515-520

2. A.Vitukhnovsky, M.I.Sluch, J.G.Warren and M.C.Petty *The Fluorescence of Perylene-Doped Langmuir-Blodgett Films* Chem.Phys.Lett Vol 173 (1990) pp425-429

3. A.Vitukhnovsky, M.I.Sluch, J.G.Warren and M.C.Petty *Observation of Perylene Excimers in Langmuir-Blodgett Films* Chem.Phys.Lett Vol 184 (1991) pp235-238

4. M.I.Sluch, A.Vitukhnovsky, J.G.Warren and M.C.Petty *Dye Fluorescence Kinetics of Langmuir-Blodgett Films* Thin Solid Films Vol 210/211 (1992) pp211-212

5. A.Vitukhnovsky, M.I.Sluch, J.G.Warren and M.C.Petty *Two-Dimensional Energy Transfer in Langmuir-Blodgett films* To be published.